Universidad del País Vasco
Euskal Herriko Unibertsitatea

Calpain 3 in skeletal muscle regeneration: Potential role in satellite cells and in the myogenic differentiation of iPSC-derived muscle progenitors

Alba Judith Mateos Aierdi

2017

A dissertation submitted to the Neuroscience Department (Faculty of Medicine and Nursing) of the University of the Basque Country, in partial fulfillment of the requirements for the degree of Doctor of Philosophy.

Amari, aitari eta Xabiri

Eskerrak - agradecimientos - acknowledgements

Lehenik eta behin, nire eskerrik beroenak eman nahi dizkiet ezagutzeko aukera izan dudan LGMD2A-dun paziente guztiei eta beren familiartekoei, eta baita ezagutu ez ditudanei ere, egiten dugun lana baloratu eta beraien babesa erakusteagatik aukera izan duten bakoitzean. Primeramente, me gustaría dar las gracias a todos los pacientes con LGMD2A y a los familiares que he tenido la oportunidad de conocer, y también a los que no he llegado a conocer, por valorar el trabajo que realizamos y mostrarnos su apoyo cada vez que han tenido la oportunidad de hacerlo.

Mi más sincero agradecimiento a Adolfo, por darme la oportunidad de incorporarme a este equipo y de realizar esta tesis en un momento en el que tanto me hacía falta, por tu confianza y apoyo, por guiarme durante estos años y poner a mi disposición todos los recursos que me han hecho falta, por los consejos profesionales y personales, y por las risas, ¡que no han sido pocas!

Gracias de todo corazón a María, por tu apoyo constante, por aceptar ser la codirectora de esta tesis con el esfuerzo que ha conllevado, por las risas, los cafés y las charlas interminables, ¡y por las gaupasas! Gracias a ti y a Ana, por formar ese genial tándem, por enseñarme tantas cosas y con tantísima paciencia, por cuidarme y preocuparos de la peque del equipo, y por hacer a veces de jefas, otras veces de madres, otras veces de hermanas mayores, y siempre de amigas. Ha sido un verdadero placer y una inmensa suerte teneros a mi lado durante estos años.

Era berean, eskerrik beroenak eman nahi dizkiet bost urte hauetan bidelagun izan ditudan bi altxorrei, Neiari eta Leireri, erraz ahaztuko ez ditudan horrenbeste momentu txiki eta handiengatik, brainstorming eta unpothesiengatik, arratsaldeetako kantengatik, eta abar amaiezin batengatik. Eta nola ez, Jaioneri, eskainitako laguntza eta prestutasunagatik, lereleengatik eta tartengatik, besteak beste.

Halaber, eskerrak eman nahi dizkiet kalpaina 3-ren erregintzat ditudan Ametsi eta Oihaneri, talde hau sortzeko lehen pausuak eman eta zuen jakinduria partekatzeagatik.

Si hay una persona que se empeña en hacernos la vida más fácil en el laboratorio, y además, lo hace con una sonrisa de oreja a oreja, esa es Karmele. Muchísimas gracias por ser así y por toda tu ayuda durante estos años. ¡Así da gusto! Y a Leyre, por el trabajo realizado y por tu amabilidad.

También quiero dedicarle un especial agradecimiento a Belén, por transmitirme tus ganas de investigar y por el gran apoyo que me ofreciste al principio de esta etapa.

Han sido muchas las personas a las que he acudido durante estos años para pedirles su ayuda, opinión o consejo. Gracias a todos ellos y en especial a Nahikari, Roberto, Iván, Garazi y Haizpea, Ander, Estefania y Paula, David, Maider, Matías y Haritz, Goros y Pili, Ander y Haizea. También me gustaría mostrar mi agradecimiento a las últimas incorporaciones: Mónica, Anabel, Garazi y Martxel, y a los investigadores y personal de Biodonostia, por crear este microambiente en el que da gusto trabajar. También quiero mostrar mi agradecimiento a esas personas que hacen que Biodonostia y el área de

Neurociencias funcionen día a día, destacando la labor de José, Marisabel, Puy, y Miren. ¡Muchas gracias!

Quiero agradecer a Ángel Raya y a Antonella Consiglio el haberme acogido en su laboratorio, poniendo a mi disposición sus conocimientos y medios que han posibilitado el inicio de este proyecto. Y como no, a los investigadores de sus grupos, en especial a Yvonne y Senda, por enseñarme los misterios de la reprogramación celular con mucha paciencia y risas, y a Juan y Dalel, por hacer tan amenos aquellos meses.

Likewise, I would like to thank Rita Perlingeiro for giving me the opportunity to join her lab and learn novel techniques that have improved so much this project, as well as her lab members, especially Sridhar, Jim, Alessandro, Tania and Robert, for their patience and kindness in teaching, and for spending their time to help me improve this project.

También quiero dar las gracias a las chicas del FACS de Inbiomed: a Paz, Ariane, Idoia y Lorea, por su ayuda y profesionalidad a la hora de diseñar los experimentos y realizar las separaciones celulares.

Azkenik, nire eskerrik goxoenak amari, aitari eta Xabiri, urte guzti hauetan emandako babesagatik eta momentu ez hain onetan beti aurrera bultzatzeagatik. Era berean, etxeko guztiei, lagunei, Xabiren etxekoei eta kaliforniako familiari, ikerketaren mundu hau ulertzen saiatzeagatik, ama zelulek asteburuetan ere *jan* egiten dutela onartzeagatik, eta nola ez, momentuoro erakutsitako babesagatik.

Eskerrik asko guztioi!! ¡¡Gracias a todos!! Gràcies a tots!! Thank you all!!

Ikerlan hau Biodonostia Osasun Ikerketa Institutuko Neurozientzien Departamentuan, Kataloniako Bioingenieritza Institutuko Ángel Raya doktorearen laborategian eta Minnesotako Unibertsitateko Lillehei Heart Institutuko Rita Perlingeiro doktorearen laborategian garatu da, Adolfo López de Munain eta Maria Goicoechea doktoreen gidaritzapean. Ikerlana, Eusko Jaurlaritzako Hezkuntza, Unibertsitate eta Ikerketa Sailaren ikertzaileak prestatzeko doktoretza-aurreko beka bati esker eta Ilundain Fundazioaren, Isabel Gemio Fundazioaren, Fundació La Caixaren, Gipuzkoako Foru Aldundiaren, Eusko Jurlaritzaren eta Espainiako Gobernuaren hainbat diru laguntzei esker burutu ahal izan da.

Este proyecto de investigación ha sido realizado en el Departamento de Neurociencias del Instituto de Investigación Sanitaria Biodonostia, en el laboratorio del doctor Ángel Raya situado en el Instituto de Bioingeniería de Cataluña y en el laboratorio de la doctora Rita Perlingeiro, en el Instituto Lillehei Heart de la Universidad de Minnesota, bajo la dirección de los doctores Adolfo López de Munain y María Goicoechea. El proyecto ha sido realizado gracias a una beca para la Formación de Investigadores predoctorales del Departamento de Educación, Universidades e Investigación del Gobierno Vasco, y a varias ayudas concedidas por la Fundación Ilundain, la Fundación Isabel Gemio, Fundació La Caixa, la Diputación Foral de Guipúzcoa, el Gobierno Vasco y el Gobierno de España.

This research project has been conducted at the Neuroscience Department at Biodonostia Health Research Institute, at doctor Ángel Raya's laboratory at the Institute for Bioengineering of Catalonia and at doctor Rita Perlingeiro's laboratory located at the Lillehei Heart Institute of the University of Minnesota, under the guidance of doctors Adolfo López de Munain and María Goicoechea. The project has been funded by a predoctoral fellowship given by the Department of Education, Universities and Research of the Basque Government, and several grants conceded by Ilundain Foundation, Isabel Gemio Foundation, Fundació La Caixa Provincial Council of Gipuzkoa, the Basque Government and the Spanish Government.

INDEX

INDEX **17**
INDEX OF FIGURES **19**
INDEX OF TABLES **20**
ABBREVIATIONS AND ACRONYMS **21**

LABURPENA **27**

RESUMEN **35**

INTRODUCTION **43**

1. MUSCLE TISSUE **45**
1.1 SKELETAL MUSCLE **45**
1.1.1 STRUCTURE 46
1.1.2 MUSCLE CONTRACTION 48
1.1.3 FIBER TYPES 51
1.2 MUSCLE GENERATION **52**
1.2.1 REGULATION OF MYOGENESIS 52
1.2.2 SKELETAL MUSCLE DEVELOPMENT 53
1.3 MUSCLE REGENERATION **56**
1.3.1 SATELLITE CELLS 56
1.3.2 MUSCLE REGENERATION AFTER INJURY 58
1.3.3 REGULATION OF SATELLITE CELL PERFORMANCE 59
1.3.4 OTHER CELL TYPES WITH SKELETAL MUSCLE REGENERATIVE POTENTIAL 61
2. MUSCULAR DYSTROPHIES, LGMD2A AND CALPAIN 3 ..... **62**
2.1 MUSCULAR DYSTROPHIES **62**
2.1.1 MUSCLE REGENERATION AND SATELLITE CELLS IN MUSCULAR DYSTROPHIES 63
2.2 LIMB-GIRDLE MUSCULAR DYSTROPHY TYPE 2A **64**
2.2.1 EPIDEMIOLOGY 64
2.2.2 CLINICAL FEATURES 65
2.2.3 HISTOPATHOLOGICAL FEATURES 66
2.2.4 GENETIC CAUSE OF LGMD2A 67
2.2.5 EXPERIMENTAL APPROACHES TO TREAT LGMD2A 69
2.3 CALPAIN PROTEASES AND CALPAIN 3 ..... **69**
2.3.1 THE CALPAIN SUPERFAMILY 69
2.3.2 CALPAIN 3 71
2.3.2.1 STRUCTURE 71
2.3.2.2 EXPRESSION AND ISOFORMS 72
2.3.2.3 ACTIVATION MECHANISM 73
2.3.2.4 ROLE OF CALPAIN 3 IN THE PATHOGENIC MECHANISM 74
2.3.2.4.1 Calpain 3 and NFkB-mediated apoptosis 77
2.3.2.4.2 Calpain 3, titin and sarcomere remodeling 78

2.3.2.4.3 Calpain 3 and signal transduction 79
2.3.2.4.4 Calpain 3 in the regulation of the cytoskeleton 80
2.3.2.4.5 Calpain 3 and calcium homeostasis 81
2.3.2.4.6 Calpain 3 and mitochondria 82
2.3.2.4.7 Calpain 3 and maintenance of muscle stem cells 82
2.3.2.4.8 Capain 3 and control of cell cycle 83

GOALS AND HYPOTHESES 85

CHAPTER 1 89

BACKGROUND AND HYPOTHESIS 91
MATERIALS AND METHODS 93
RESULTS 111
DISCUSSION 144

CHAPTER 2 163

BACKGROUND AND HYPOTHESIS 164
MATERIALS AND METHODS 166
RESULTS 172
DISCUSSION 181

FINAL DISCUSSION 185

CONCLUSIONS 189

APPENDIX I: PRODUCT REFERENCES CHAPTER 1 193
APPENDIX II: PRODUCT REFERENCES CHAPTER 2 197
APPENDIX III: PUBLICATIONS 199
BIBLIOGRAPHY 201

INDEX OF FIGURES

Figure 1. Optical microscopy images of different muscle types 45
Figure 2. Structure of skeletal muscle..... 46
Figure 3. Structure of sarcomeres..... 47
Figure 4. Muscle contraction..... 48
Figure 5. The sarcoplasmic reticulum 49
Figure 6. Timing of muscle contraction..... 50
Figure 7. Muscle generation and regeneration in mice 54
Figure 8. Schematic representation of the initial stages of myogenesis in mouse embryo 55
Figure 9. Schematic representation of the location of a satellite cell 56
Figure 10. Sequential MRF and myogenic gene expression in differentiating satellite cells... 58
Figure 11. Representation of a myofiber section 63
Figure 12. Magnetic resonance and *scapula alata*...... 66
Figure 13. Hematoxylin-eosin staining of muscle sections of LGMD2A patients..... 67
Figure 14. Schematic representation of the structure of human calpains. 70
Figure 15. Schematic representation of conventional calpains and calpain 3 72
Figure 16. Distribution of pathogenic mutations in *CAPN3* reported in LGMD2A patients 75
Figure 17. Representation of the sarcomeric proteins and signaling molecules 80
Figure 18. Workflow for the generation of patient-specific iPSC-derived cellular models 93
Figure 19. Workflow of reprogramming..... 96
Figure 20. Schematic representation of the characterization workflow..... 98
Figure 21. Maps of the plasmids comprising the doxycycline-inducible *PAX7* system..... 104
Figure 22. Schematic representation of the myogenic induction protocol..... 106
Figure 23. Schematic representation of *CAPN3* exons and calpain 3 protein..... 113
Figure 24. Representative picture of an AP-stained colony from each cell line..... 115
Figure 25.a. Expression rates of transgenic and endogenous pluripotency genes 116
Figure 25.b. Expression rates of transgenic and endogenous pluripotency genes 117
Figure 25.c. Expression rates of transgenic and endogenous pluripotency genes..... 118
Figure 26. Southern blot images show bands corresponding to *cMYC* 119
Figure 27. Southern blot images show bands corresponding to *OCT4*..... 119
Figure 28. Multiple immunofluorescence images of pluripotency markers 120
Figure 29. Multiple immunofluorescence images of lineage-specific markers..... 122
Figure 30. Methylation pattern of CpG islands in the *OCT4* promoter region 123
Figure 31. Methylation pattern of CpG islands in the *NANOG* promoter region 124
Figure 32. Representative karyotype images for each of the reprogrammed cell lines..... 125
Figure 33. Representative histograms showing the infection efficiencies..... 127
Figure 34: Representative light microscopy images during the induction process..... 128
Figure 35. FACS plots corresponding to the isolation of GFP-positive cells 129
Figure 36. Effect of transient GSK3β inhibition 131
Figure 37. Immunofluorescence detection of sarcomeric myosin..... 132
Figure 38. Assessment of myogenic terminal differentiation..... 133
Figure 39. Immunofluorescence images at day 5 of differentiation..... 134
Figure 40. Immunofluorescence detection in cell cultures at day 5 of differentiation..... 135
Figure 41. Gene expression of myogenic markers in differentiated cultures 136

Figure 42. Analysis of *PAX7* mRNA and PAX7 protein expression 138
Figure 43. *CAPN3* expression and Calpain 3 levels in iPSC-derived myogenic cultures 140
Figure 44. Study of total *CAPN3* expression and its isoforms 141
Figure 45. *DMD* expression in iPSC-derived cultures 142
Figure 46. Expression of extracellular protein-coding genes in iPSC-derived cultures 142
Figure 47. SERCA2 protein levels in iPSC-derived cultures 143
Figure 48. Analysis of the *in vivo* regenerative potential of iPSC-derived progenitor cells ... 144
Figure 49. Experimental outline of the gene expression study 167
Figure 50. Experimental outline of colony assay 168
Figure 51. SC isolation strategy 172
Figure 52. Plots corresponding to FMO controls 173
Figure 53. SC isolation 175
Figure 54. Expression of *Pax7* and *Myod1* in satellite cells 176
Figure 55. Expression of *Myh3*, *Myog* and *Ryr1* in satellite cells 177
Figure 56. *Capn3* expression in satellite cells 178
Figure 57. Expression of *Dmd* and *Myh2* in satellite cells 179
Figure 58. SC isolation fror colony assay 179
Figure 59. Example of processing colony images with the G-tool software 180
Figure 60. Colony assay results 180

INDEX OF TABLES

Table 1. Fiber types 52
Table 2. Overview of cell surface markers used to isolate mouse satellite cells 57
Table 3. Expression preference of calpain genes 71
Table 4. Modified Vignos and Archibald Scale 94
Table 5. Classification of LGMD2A patients phenotype 94
Table 6. Primers used during gene expression analysis of pluripotency genes 99
Table 7. Primers used to generate probes against the indicated targets 100
Table 8. Antibody combinations and dilutions for pluripotency markers 101
Table 9. Antibody combinations for lineage-specific markers in reprogrammed cells 102
Table 10. Primers used to amplify the promoter region of *OCT4* and *NANOG* genes 103
Table 11. Primary and secondary antibodies for protein detection through Western blot .. 109
Table 12. Primary and secondary antibodies used for immunofluorescence analysis 109
Table 13. Primary and secondary antibodies used for immunofluorescence analysis 110
Table 14. Summary of clinical and molecular data available from sample donors 112
Table 15. Antibodies for SC isolation 169

ABBREVIATIONS AND ACRONYMS

ADP	Adenosine diphosphate
AFP	Alpha-1-fetoprotein
AHNAK	AHNAK nucleoprotein
AldoA	Aldolase A
AP	Alkaline phosphatase
Asn	Asparagine
ATP	Adenosine triphosphate
α-SMA	Alpha-2-smooth muscle actin
bHLH	Basic helix-loop-helix
BMD	Becker muscular dystrophy
bp	Base pair
BSA	Bovine serum albumin
Ca^{2+}	Calcium ion
Calpain	Calcium-dependent papain-like protease
CAPN1	Calpain 1, micro-calpain
CAPN2	Calpain 2, milli-calpain
CAPN3	Muscle-specific calcium-activated neutral protease 3 large subunit
CAPNS1	Calcium-activated neutral proteinase small subunit
CBSW	Calpain-type beta-sandwich domain
CD106/VCAM1	Vascular cell adhesion molecule 1
CD11b	Integrin alpha-M
CD133	Prominin1
CD31	Platelet endothelial cell adhesion molecule
CD34	Hematopoietic progenitor cell antigen
CD45	Receptor type tyrosin-protein phosphatase C
c-FLIP	Caspase-like apoptosis regulatory protein / cellular FLICE inhibitory protein
CHIR	CHIR99021, GSK3β inhibitor
CK	Creatine kinase
c-MET/HGFR	Mesenchymal/epithelial transition factor / Hepatocyte growth factor receptor
cMYC	MYC proto-oncogene / Avian myelocytomatosis viral oncogene homolog
CO_2	Carbon dioxide
CRIPTO	Teratocarcinoma-derived growth factor 1
CRISPR	Clustered regularly interspaced short palindromic repeats
Cys	Cysteine
CysPc	Calpain-like protease domain
CXCR4	C-X-C chemokine receptor factor

C1	Control 1
C2	Control 2
C2	Protein C conserved domain 2
C3KO	Calpain 3 knockout
DAPI	4',6-diamino-2-phenylindole
Delta1	Delta like non-canonical Notch ligand 1
DHPR	Dihydropyridine receptor
DIG	Digoxigenin
DM	Myotonic dystrophy
DM1	Myotonic dystrophy type 1
DMD	Duchenne muscular dystrophy
DMD	Dystrophin-coding gene
DMPK	Dystrophia myotonica protein kinase
DMSO	Dimethyl sulfoxide
DNA	Deoxyribonucleic acid
DOXY	Doxycycline
DPBS	Dulbecco's phosphate-buffered saline
DTT	1,4-Dithiothreitol
EB	Embryoid body
EDL	*Extensor digitorum longus*
EDTA	Ethylenediaminetetraacetic acid
EMT	Epithelial-mesenchymal transition
Endo-	Endogenous
ES	Embryonic stem
E-64	trans-Epoxysuccinyl-L-leucylamido(4-guanidino)butane
F	Fibroblasts
FACS	Fluorescence-activated cell sorting
FBS	Fetal bovine serum
FGF_2	Fibroblast growth factor 2
FMO	Fluorescence minus one
FOXA2	Forkhead box A2
FRZB	Frizzled related protein
FSC-A	Forward-scatter-area
FSC-H	Forward-scatter-height
FSC-W	Forward-scatter-width
GAPDH	Glyceraldehyde 3-phosphate dehydrogenase
GATA4	GATA-binding factor 4
GFAP	Glial fibrillary acidic protein
GFP	Green fluorescent protein
GR	Glycine-rich domain
GSK3β	Glycogen synthase kinase 3 beta

Gy	Gray
HCl	Hydrochloric acid
HEPES	4-(2-hydroxyethyl)-1-piperazineethanesulfonic acid
hES	Human embryonic stem
HFF	Human foreskin fibroblast
HGF	Hepatocyte growth factor
His	Histidine
HLA	Human leucocyte antigen
HS	Horse serum
IACUC	Institutional Animal Care and Use Committee
IBM	Inclusion body myositis
IGF1	Insulin like growth factor 1
IkB	Inhibitor of NFkB
IkBα	Inhibitor of NFkBα
IL-6	Interleukin 6
IPTG	Isopropyl β-D-1-thiogalactopyranoside
iPS	Induced pluripotent stem
iPSC	Induced pluripotent stem cell
IS1	Insertion site 1
IS2	Insertion site 2
IQ	Calmodulin (CaM) – interacting motif
JAK/STAT	Janus kinase / Signal transduced and activator of transcription
KCl	Potassium chloride
kDa	Kilodalton
KLF4	Kruppel like factor 4
KO-DMEM	KnockOut - DMEM
KOSR	KnockOut serum replacement
LB	Luria Bertani
LGMD	Limb-girdle muscular dystrophy
LGMD2B	Limb-girdle muscular dystrophy type 2B
LGMD2D	Limb-girdle muscular dystrophy type 2D
LGMD2H	Limb-girdle muscular dystrophy type 2H
LGMD2I	Limb-girdle muscular dystrophy type 2I
LiCl	Lithium chloride
M	Molar
mA	Milliamp
MAC-1	Macrophage-1 antigen
MADSC	Multipotent adipose-derived stem cells
MAPK	Mitogen-activated protein kinase
MARP	Muscle ankyrin repeat protein
MARP2/Ankrd2	Muscle ankyrin repeat protein 2/Ankyrin repeat domain 2

MEF	Murine embryonic fibroblast
mg	Milligram
MIT	Microtubule interacting and transport motif
ml	Milliliter
mM	Millimolar
MRF	Myogenic regulatory factor
MRF4/MYF6	Myogenic factor 6
MURF	Muscle RING finger protein
mV	Millivolt
MVA	Modified Vignos and Archibald
MYF5	Myogenic factor 5
MYF6	Myogenic factor 6
MyHC	Myosin heavy chain
MYH2	Myosin heavy chain 2, adult
MYH3	Myosin heavy chain 3, embryonic
MYOD1	Myoblast determination protein 1
MYOG	Myogenin
N	Newton
N	N-terminus domain
NaCl	Sodium chloride
NADH-TR	NADH-tetrazolium reductase
NANOG	Homeobox transcription factor nanog
NaPi	Sodium phosphate buffer
NCAM1	Neural cell adhesion molecule 1
NEAA	Non-essential amino acids
ng	Nanogram
NFkB	Nuclear factor kappa B
NS	N-terminus sequence
NSC	Neural stem cell
O.C.T.	Optimum Cutting Temperature
OCT4	Octamer-binding transcription factor 4
PABP2	Polyadenine binding protein 2
PAX3	Paired box protein 3
PAX7	Paired box protein 7
PBS	Phosphate-buffered saline
PC1	Protease core subdomain 1
PC2	Protease core subdomain 2
PCr	Phosphocreatine
PCR	Polymerase chain reaction
PE	Phycoerythrin
PE-Cy7	Phycoerythrin-Cy7

PFA	Paraformaldehyde
PFKM	Phosphofructose kinase muscle type
PITX2	Pituitary homeobox 2
PLEIAD	Platform element for inhibition of autolytic degradation
PMSF	Phenylmethanesulfonyl fluoride
POGLUT1	Protein O-glucosyltransferase 1
POMT1	Protein O-mannosyltransferase 1
POMT2	Protein O-mannosyltransferase 2
P1	Patient 1
$p16^{Ink4a}$	Cyclin-dependent kinase inhibitor 2A
$p19^{Arf}$	Cyclin-dependent kinase inhibitor 2D
P2	Patient 2
$p27^{kip1}$	Cyclin-dependent kinase inhibitor 1B
P3	Patient 3
P4	Patient 4
P5	Patient 5
qPCR	Quantitative polymerase chain reaction
Rb	Retinoblastoma protein / RB transcriptional corepressor 1
REX	RNA exonuclease 1 homolog
RNA	Ribonucleic acid
ROCK	Rho associated coiled-coil containing protein kinase
rpm	Revolutions per minute
RyR	Ryanodine receptor
RyR1	Ryanodine receptor type 1
RyR2	Ryanodine receptor type 2
SC	Satellite cell
SCA-1	Stem cell antigen-1
SDS	Sodium dodecyl sulfate
SERCA	Sarcoplasmic/endoplasmic reticulum calcium ATPase
SMAD-3	Mothers against decapentaplegic homolog 3
SOD1	Superoxide dismutase 1
SOL	Small optic lobes product homology domain
SOX2	SRY-box 2
SP	Side population
SSC-A	Side-scatter-area
SSEA-3	Stage-specific embryonic antigen 3
SSEA-4	Stage-specific embryonic antigen 4
TA	*Tibialis anterior*
TAE	Tris-acetate-edta
TALEN	Transcription activator-like effector nucleases
TBP	TATA-box binding protein

TBS	Tris-buffered saline
TBST	Tris-buffered saline with tween
TBX1	T-box transcription factor 1
TGF-β	Transforming growth factor beta
TNF-α	Tumor necrosis factor alpha
TRA-1-60	Keratan-sulfated transmembrane protein (podocalyxin) carbohydrate epitope 1-60
TRA-1-81	Keratan-sulfated transmembrane protein (podocalyxin) carbohydrate epitope 1-81
Trans-	Transgenic
TUJ1	Neuron-specific class III beta-tubulin
TUNEL	Terminal deoxynucleotidyl transferase dUTP nick-end labeling
U	Unit (enzyme activity)
USA	United States of America
UTR	Untranslated region
VCAM1	Vascular cell adhesion molecule 1
VSV-G	Vesicular stomatitis virus g protein
WT	Wild type
ZFN	Zinc finger nuclease
Zn	Zinc-finger motif
µl	Microliter
µg	Microgram
µM	Micromolar
Δ	delta
#	Clone

LABURPENA

Muskulu distrofiak, muskulu eskeletikoaren degenerazio progresiboa eragiten duten jatorri genetikoko gaixotasun multzo bat dira. Hauen artean, gerrietako muskulu distrofiek (LGMD, ingelesezko *Limb-Girdle Muscular Dystrophy* izenetik) osatzen duten azpitaldean kokatzen dira gerri pelbikoko eta eskapularreko muskuluen eta muskulu proximalen ahultasuna eragiten duten gaixotasunak. Herentzia ereduen arabera, bi talde nagusitan banatzen dira: LGMD1 izenez ezagutzen dira herentzia gainartzailea dutenak, eta LGMD2 izenez herentzia azpirakorra dutenak.

Azken hauen artean, 2A motako gerri distrofia (LGMD2A), *CAPN3* genean kokatzen diren mutazioen ondorioa da. Gene honek, batik bat muskuluan espresatzen den kalpaina 3 izeneko proteasa ez lisosomala kodetzen du. Gaixoei, orokorrean nerabezaroan agertzen zaizkie lehenengo sintomak. Hala ere, badira kasu goiztiarrak, 2 urterekin gaixotasunari hasiera eman diotenak, edota beste muturrean 50 urterekin hasitakoak ere. Gaixotasunaren hasieran, ohikoak dira eskailerak igo, korrika egin, pisua jaso edota aulkitik altxatzeko zailtasunak. Gaixotasunak aurrera egin ahala, muskuluen ahultasuna areagotuz joaten da eta gaixoek ibiltzeko zailtasunak izaten dituzte, gurpil-aulki baten beharra izatera iritsiz. Degenerazioak ez die muskulu guztiei berdin eragiten. Gorputz enborreko eta izterretako atzeko konpartimentuetako muskuluak dira endekapen handiena jasaten dutenak, beste muskuluen ahuldura txikiagoa edo hautemanezina izanik.

Histologiari dagokionez, muskulu biopsietan distrofia agerikoa da. Gune nekrotikoak zein erregeneratiboak ageri dira, baita diametro aldakorreko zuntzak eta nukleo zentralizatuak ere. Gaixotasunaren hasieran, gaixoa ia asintomatikoa denean, ohikoa da muskuluetan zein odolean eosinofiloak agertzea; gaixotasuna aurrera doan heinean hauek desagertuz joaten dira. Hala, zuntz lobulatuak eta mitokondrioen kokapen anomaloa agertzen dira, azkenik fibrosiak eta ehun adiposoak muskulua ordezkatzen dutelarik.

LGMD2A-ren oinarri genetikoa aztertzerako orduan, mutazio aniztasun handia deskribatu da gaixoen artean. Gaur egun, gaixotasunaren eragile diren 450 mutazio baino gehiago aurkitu dira *CAPN3* genearen baitan. Mutazio hauek aldaera desberdinak eragiten dituzte kalpaina 3 proteinarengan: aminoazido baten ordezkapena, irakurketa arauaren aldaketa, exoi berrien sorrera, eta abar eraginez. Ondorioz, sortzen den proteinaren funtzioa eraldatua egon daiteke, edota aldaera hauek proteinaren degradazioa bultzatu dezakete.

Fenotipoari dagokionez, azpimarratzekoa da gaixoen artean ikusten den aldakortasuna, baita familia bereko kideen artean ere. Aldakortasun hau histologikoki ere agerikoa da. Saiakerak egin diren arren, ezin izan da mutazio desberdinen eta gaixoen larritasunaren arteko korrelazio zuzenik finkatu. Hala ere, orokorrean, proteinaren desagertzea eragiten duten bi mutazio (*null* erako mutazioak) dituzten gaixoek fenotipo larriagoa

garatu ohi dute, gutxienez proteinaren galtzea ez dakarren mutazio bat (*missense* erako mutazioa) daramaten gaixoekin alderatuz.

Gaixotasunaren jatorri genetikoa garbi ezagutzen den arren, oraindik ez da ongi ulertzen zein den kalpaina 3 proteinaren funtzioa muskulu eskeletikoan. Bereziki, ez da ezagutzen kalpaina 3-ren gabeziak zergatik muskulu espezifiko batzuei eragiten dien, ezta endekapen hau adin jakin batetik aurrera garatzearen arrazioa ere.

Gaixoen muskulu biopsiak eta berauetatik lortutako mioblastoen hazkuntzak tresna baliagarri bilakatu dira LGMD2A-ren fisiopatologia eta kalpaina 3-ren funtzioa ikertzerako orduan. Hala ere, gaixotasun arraroa izateak eta gaur egun diagnostiko genetikoa odol lagin baten bidez egiteak asko murriztu ditu ikerketarako erabilgarri izango liratekeen biopsien kopurua. Muga hauek gainditu nahian, gaixotasunaren sagu ereduak sortu dira, bai saguari *CAPN3* genea isilaraziz, baita proteinaren zentro aktiboaren aktibitatea eragozten dion mutazioa sortuz ere. Sagu hauen azterketek kalpaina 3-ren ezagutzarako informazio baliagarria eman duten arren, ez dute gaixoek pairatzen duten muskulu-endekapen progresiboa jasaten. Hau, saguek kalpaina 3-ren gabeziak sortutako kalteak konpentsatzeko beste mekanismo batzuk dituztelako izan daiteke. Aipaturiko zailtasun hauek direla eta, gaixoetatik eratorritako eredu zelular ezberdinak lortzea interesgarri gerta daiteke, berauek muskulua ez den beste ehun batean badute ere jatorria.

Esan bezala, bai gaixoetatik lortutako mioblastoek, baita sagu ereduek eta bestelako *in vitro* sistemek ere, kalpaina 3-k burutu ditzakeen zenbait funtzio argitu dituzte. Ikerketa hauen arabera, 1) kalpaina 3-k NFkB seinalizazio bidezidorrean parte har lezake, eta gaixoetan kalpaina 3-ren gabeziak seinalizazioa eten lezake, bere funtzio antiapoptotikoa galaraziz. Bestalde, 2) kalpaina 3-k muskuluko proteina estruktural erraldoia den titina molekulekin bat egiten du gune desberdinetan, eta honi esker sarkomeroaren egituraren eraldaketan parte har lezake. Era berean, 3) kalpaina 3-k bai sarkomeroko gune jakin batzuetan, baita mintz zelularraren inguruan beste proteina batzuekin konplexuak osatuz, hautemate mekanikoan eta honen erantzunean parte har lezake. 4) *In vitro* burututako esperimentuek frogatu dute kalpaina 3-k zitoeskeletoko proteina desberdinak proteolizatu ditzakeela, eta honen ondorioz, zitoeskeletoaren birmoldaketan ere parte har lezakeela. 5) Kalpaina 3-ren gabeziak mitokondrioengan ere eragina izan lezake, gaixoen biopsietan ikusten den kokapen ezohikoak erakusten duen bezala. Organulu hauetan ATParen sintesia murriztua eta estres oxidatzailea areagotuak aurkitu dira, beste proteinetan aldaketak eraginez. 6) Azkenaldian, kalpaina 3-k kaltzioaren homeostasiaren mantenuan izan dezakeen parte-hartzea garrantzia hartuz joan da. Ikusi denez, muskuluaren uzkurketa eragiteko erretikulu sarkoplasmikotik zitoplasmara doazen kaltzio isuriak murriztuta daude kalpaina 3-ren *knockout* sagu ereduan. Gainera, uzkurketaren ondoren kaltzio hau berriro ere erretikulu sarkoplasmikora eramaten duten SERCA garraiatzaileak ere murriztuta daude LGMD2A gaixoen biopsietan. 7) Azkeneko hamarkadan kalpaina 3-k muskuluko ama zeluletan

(zelula sateliteetan) nahiz zelula tumoralen ziklo zelularraren kontrolean izan lezakeen funtzioa aztergai izan da, batez ere muskulu zelulen hazkuntzetan eta baita minbiziak erasandako zeluletan ere.

Aurrekari hauek kontuan hartuta, LGMD2A-ren fisiopatologiaren ulermenean aurrera pauso bat eman ahal izateko, ikerlan honen helburua kalpaina 3-k muskuluko zelula sateliteetan nahiz miogenesiaren lehenengo faseetan izan dezakeen funtzioa aztertzea izan da. Helburu hau betetzeko bi estrategia desberdin erabili ditugu. Alde batetik, gaixoen eta pertsona osasuntsuen azaleko fibroblastoak birprogramatu eta muskulura desberdinduz, hauen *in vitro* ereduak sortu ditugu, bertan kalpaina 3-ren funtzioa aztertzeko. Bestalde, saguen zelula sateliteak isolatu eta berauetan gene adierazpena eta kalpaina 3-ren gabeziak sortutako fenotipoak aztertu ditugu, jarraian azaltzen diren emaitzak lortuz.

Lehenengo atalean, Donostiako Ospitale Unibertsitarioan artatzen diren LGMD2A gaixoen taldearen ordezkari bezala, 5 gaixo hautatu ziren ikerketa honetan parte hartzeko, *CAPN3* genean zeramatzaten mutazioetan eta beraien gaixotasunaren larritasun mailan oinarrituz. Hauen azaleko zelulak, adin eta sexuz parekatutako bi kontrol osasuntsuren azaleko fibroblastoekin batera, birprogramatuak izan ziren. Horretarako, *OCT4, SOX2, KLF4* eta *cMYC* faktoreen adierazpena bultzatzen duten bektore retrobiralak erabili ziren. Ondoren, horrela lortutako zelula lerroen pluripotentzia egiaztatzeko, karakterizazio frogak egin ziren: a) fosfatasa alkalinoaren aktibitatea baieztatzea, b) birprogramatzeko erabilitako transgeneen adierazpena isiltzea eta pluripotentzia gene endogenoen adierazpenaren aktibazioa frogatzea, c) zelula lerro bakoitzaren genoman integratutako transgene bakoitzaren kopurua zehaztea, d) pluripotentzia markatzaileak antzematea, e) zelula hauek enbrioiko hiru lerro germinaletatik sortutako zelula motetara desberdintzea *in vitro,* f) pluripotentzia gene espezifiko batzuen promotoreetan aldaketa epigenetikoak eman direla frogatzea eta g) prozesu guzti honetan kariotipoa egonkor mantendu dela egiaztatzea.

Honen ondoren, birprogramatutako zelula lerroak, zelula sateliteen markatzaile den *PAX7* faktorearen aldi baterako adierazpena ahalmentzen duen sistemarekin transduzitu ziren. Zelula hauek zazpi egunez suspentsioan eta beste zazpi egunez itsatsita hazi ziren eta azken lau egunetan *PAX7* transkripzio faktorearen adierazpena aktibatuz, zelula lerro pluripotenteetatik muskuluko zelula progenitoreak lortu ziren. Azkenik, progenitoreen diferentziazio terminala eraginez, miotubo hazkuntzak sortu ziren.

Sortutako zelula lerroek miotuboak garatzeko ahalmen desberdina erakutsi zuten. Desberdintasun hauek ez ziren gaixo edo kontrol izatearen menpeko, hau da, *CAPN3* genean zituzten mutazioen ondorio. Emaitza hauek, eta karakterizazio prozesuan lortutakoek, sortutako zelula lerroen pluripotentzia maila ez dela lerro guztietan berdina

pentsarazi digute. Karakterizazio froga sakonagoak baliagarriak izan daitezke hipotesi hau egiaztatzeko.

Diferentziatzeko ahalmen desberdina izan arren, lerro zelularrek diferentziatzean, *CAPN3* genearen adierazpena aktibatu zuten, eta kalpaina 3 proteina ere aurkitu zen diferentziatutako kontrolen hazkuntzetan eta baita gaixo batzuenetan ere. Gainera, kontrolen diferentziazioan, *CAPN3*-k muskuluaren garapenean eta birsorpenean burutzen duen isoforma heldugabeetatik helduetarako trantsizioa ere ikus zitekeen progenitoreak diferentziatu ahala. Trantsizio hau behagarria izan zen ongi diferentziatzen ziren zelula lerroetan, baina ez okerrago diferentiatzen zen lerro batean.

Bestalde, birprogramatutako zeluletatik sortutako muskuluko progenitoreen erregenerazio gaitasuna neurtzeko, progenitore hauek saguen muskuluetan transplantatu ziren, eta hilabetera, transplantatutako zelulen kopurua eta hauek sortutako zuntz berrien kopurua aztertu ziren. Bai gaixo batetik eta bai kontrol osasuntsu batetik lortutako progenitoreek muskulua birsortzeko ahalmena azaldu zuten. Hala ere, *in vitro* hazkuntzetan ikusitako zelula lerroen arteko desberdintasunak zirela eta, transplantearen ondoren berauen artean aurkitutako desberdintasunak ez ziren aintzakotzat hartu.

Beraz, proiektu honi esker ondorioztatu dezakegu *CAPN3* ez dela beharrezkoa zelulen birprogramaziorako, eta birprogramatutako zelulak erabil ditzakegula kalpaina 3-ren funtzioa ikertzeko miogenesian. Hala ere, zelula lerro desberdinen arteko konparaketak egin ahal izateko hobekuntzak egitea beharrezko litzateke, *CAPN3* geneari atxiki ezin zaizkion lerroen arteko desberdintasunak gutxitu edo desagertarazteko. Arazo honi aurre egiteko modu bat zelula lerro isogenikoak sortzea izango litzeteke, gaixoen zeluletako mutazioak ezabatuz edota kontrol osasuntsuen zelula lerroetan *CAPN3* genearen adierazpena isilaraziz, horretarako gaur egun eskuragarri diren edizio genikoko teknikak erabiliz.

Bigarren atalean, *Capn3* genearen adierazpena eta bere funtzio hipotetikoa saguen zelula sateliteetan aztertzeari ekin genion. Zelula sateliteak, muskulua birsortzeaz arduratzen diren ama zelulak dira. Egoera basalean (muskuluko minik ez denean), zelula hauek kieszentzian aurkitzen dira. Muskuluak min bat jasotzen duenean ordea, aktibatu, ugaritu, eta zelulen gehiengoak diferentziazio miogenikoari ekiten dio, ehuna erregeneratuz. Aktibatutako zelulen gutxiengo bat ordea berriro ere kieszentziara bueltatzen da, aurrerago egon litezkeen minei erantzun ahal izateko. Prozesu guzti hauen erregulazio zorrotza beharrezkoa da muskuluak bere erregenerazio ahalmena denboran zehar mantendu dezan.

Gure hipotesiari jarraituz, kalpaina 3-k zelula sateliteetan funtziorik izan dezakeen aztertzeko, lehenik eta behin, *Capn3* genearen adierazpena aztertu genuen saguetatik

isolatutako zelula sateliteetan, bai kieszentzian, baita kardiotoxina bidez eragindako minaren ondorioz aktibatutakoetan ere. Gene adierazpen zein zitometria bidezko analisien emaitzen arabera ondorioztatu genuen zelulen aktibazio maila altuena mina egin eta 3 egunetara lortu genuela, eta ondoren, 5 eta 7 egunetara, aktibatutako zelulen kopurua progresiboki murriztuz zihoala. Kalpaina 3-ren adierazpenik altuena zelula aktibatuetan lortu zen, mina egin eta 3 egunetara, eta bere adierazpena murriztuz joan zen hurrengo egunetan.

Emaitza honek kalpaina 3-k zelula sateliteetan izan lezakeen funtzioa haratago aztertzeko oinarri bat ezartzen du. Jarraian, beharrezkoa litzateke kalpaina 3 proteina mailan ere adierazten dela frogatzea zelula hauetan. Kontuan hartuta zelula sateliteen isolatze prozesuaren iraupena eta kalpaina 3-ren autolisi azkarra, ezinezkotzat jo genuen proteina hau *Western blot* bidez antzematea. Aukeran, sagu osasuntsuen eta C3KO (*Capn3 knockout*) saguen zelula sateliteak isolatu eta berauen artean desberdintasun funtzionalak aztertzeari ekin genion. Horretarako, *colony assay* izeneko froga gauzatu genuen, eta honi esker, zelula sateliteen ugaritze ahalmena, diferentziazio miogenikoa zein fusio ahalmena aztertu genituen zelula hazkuntzetan, *G-tool* programa informatikoa erabiliz.

Ez zen desberdintasunik antzeman sagu osasuntsuetatik eta C3KO saguetatik isolatutako zelula sateliteen ugaritze ahalmenean, ezta beraien diferentziazio miogeniko nahiz fusio ahalmenean ere. Zelula sateliteak *soleus* eta *tibialis anterior* muskuluetatik isolatu ziren, sagu zein gizakietan muskulu hauek degenerazio handia eta txikia jasaten dituztelako, hurrenez hurren. Hauen artean ere ez zen desberdintasunik antzeman. Desberdintasunik ikusi ez izanaren arrazoia esperimentuetan erabilitako saguen adin txikia izan daiteke. Lehenago esan bezala, saguetan muskuluaren degenerazioa oso arina da gaixoenarekin alderatuz, eta gainera, gaixotasun progresiboa izanik, baliteke sagu gazteen zelula sateliteetan oraindik desberdintasunik ez egotea.

Beraz, emaitza guztiak kontuan hartuta, *Capn3* genea zelula sateliteetan adierazten dela frogatu dugu, berauen aktibazioarekin bat datorren adierazpen eredua jarraituz. Sagu helduagoekin esperimentu funtzional, proteomiko zein transkriptomikoak burutzeak, kalpaina 3-k zelula sateliteetan eta orokorrean muskuluen erregenerazioan izan lezakeen funtzioa argituko du, LGMD2A distrofiaren fisiopatologia hobeto ulertzeko ezagutza eskainiz.

Laburbilduz, proieku honetan, LGMD2A duten gaixoen azaletik abiatuta eredu zelular miogenikoak sortu ditugu, kalpaina 3-ren funtzioa eta LGMD2A-ren fisiopatologia ikertzeko baliagarri diren zelula ereduak lortuz. Eredu hauek hobetu beharra dago beraien artean alderagarriak izan daitezen. Garrantzitsua da eredu hauek *CAPN3* genearen adierazpena aktibatu eta beronen heltze transkripzionala eragiten dutela ongi diferentziatzen diren zelula lerroetan, eta kalpaina 3 proteina mailan ere antzematen

dela kontrol osasuntsuen hazkuntzetan eta baita gaixo batzuenetan ere. CRISPR/Cas9 bezalako aldaketa genetikoak eragiteko ahalmena duten teknikak erabiliz zelula lerro isogenikoak lortuz gero, azaldutako zailtasunak gainditzea espero da. Bestalde, saguetan, *Capn3* genearen adierazpena zelula sateliteetan antzeman izanak, kalpaina 3-ren funtzioa zelula hauetan eta muskuluaren erregenerazioan aztertzen jarraitzeko abiapuntua eman digu. Funtzio hau frogatuko balitz, LGMD2A gaixotasunaren fisiopatologiaren ulermenean aurrerapauso bat emango litzateke eta zelula sateliteak gaixotasunari aurre egiteko tratamenduen helburu bilakatuko lirateke.

RESUMEN

Las distrofias musculares constituyen un grupo de enfermedades de origen genético que causan la degeneración progresiva del músculo esquelético. Entre estas enfermedades, las distrofias de cinturas o LGMD (de sus siglas en inglés *Limb-Girdle Muscular Dystrophy)* forman un subgrupo de enfermedades que causan la debilidad de los músculos de las cinturas pélvica y escapular y los músculos proximales. De acuerdo con su patrón de herencia, las distrofias de cinturas se clasifican en dos grupos: las de herencia dominante, que se denominan LGMD1, y las de herencia recesiva, conocidas como LGMD2.

Dentro de este último subgrupo, la distrofia de cinturas de tipo 2A (LGMD2A) se desarrolla como consecuencia de mutaciones en el gen *CAPN3*. Este gen codifica la calpaína 3, una proteasa no lisosomal que se expresa mayoritariamente en el músculo esquelético. El inicio de los síntomas se da generalmente en la adolescencia, aunque se conocen casos extremos en los que se ha desarrollado tan pronto como a los 2 años de edad, o en el otro extremo, a los 50. Al principio de la enfermedad, los pacientes comienzan a tener dificultades para subir escaleras, correr, elevar peso o levantarse de la silla. A medida que la debilidad muscular aumenta, los pacientes presentan dificultades para caminar, acabando en silla de ruedas. La debilidad muscular no afecta de la misma forma a todos los músculos. Los músculos del tronco y del compartimento posterior de los muslos son los más afectados, mientras que los demás músculos presentan una debilidad menor o incluso ausente.

En lo que respecta a la histología, las biopsias musculares presentan un aspecto distrófico con zonas necróticas y otras regenerativas, un diámetro de fibra variable y núcleos centralizados. Al inicio de la enfermedad es común la presencia de infiltraciones eosinofílicas, que también son detectables en sangre periférica, y que van desapareciendo a medida que progresa la enfermedad. También son frecuentes las fibras lobuladas y la presencia de mitocondrias desorganizadas. En fases más avanzadas, el tejido fibrótico y adiposo sustituyen progresivamente al tejido muscular.

A la hora de estudiar la causa genética de la LGMD2A, se ha descrito una extensa variedad de mutaciones como causantes de la enfermedad. Hoy en día se conocen más de 450 mutaciones patogénicas en el gen *CAPN3*. Estas mutaciones afectan de distinta forma a la proteína que sintetizan, pudiendo dar lugar al cambio de un aminoácido, a un cambio del marco de lectura, a la creación de neo-exones, etc. modificando la funcionalidad de la proteína o favoreciendo su degradación.

Es de destacar la gran variabilidad fenotípica existente entre los pacientes, incluso entre los afectados de una misma familia. Esta variabilidad también es visible a nivel histológico. Aunque varios estudios han intentado correlacionar las distintas mutaciones en el gen *CAPN3* y la gravedad del fenotipo que presentan los pacientes, ha sido imposible establecer correlaciones directas. En general, los pacientes que presentan dos mutaciones *null* (que dan lugar a la pérdida de la proteína) tienden a desarrollar

fenotipos más graves, en comparación con los pacientes que presentan al menos una mutación *missense* (que sí que da lugar a una proteína diferente pero completa).

Se desconoce cuál es la función principal de la calpaína 3 en el músculo esquelético, y por qué su ausencia o pérdida de función da lugar a la LGMD2A. También se desconoce el motivo por el que la deficiencia de calpaína 3 afecta a unos músculos más que a otros, y por qué la degeneración muscular está ausente en los recién nacidos, y se desarrolla a partir de la infancia tardía, en la adolescencia o incluso en edades más tardías.

Las biopsias musculares de pacientes y los cultivos de miotubos derivados de ellos se han convertido en una herramienta muy valiosa para el estudio de la función de la calpaína 3 y la fisiopatología de la LGMD2A. Sin embargo, el hecho de que la LGMD2A sea una enfermedad rara y que en la actualidad su diagnóstico se pueda realizar de manera directa mediante estudios moleculares a partir de muestras de sangre, ha minimizado el número de biopsias disponibles para investigación.

Para hacer frente a estas limitaciones y estudiar la fisiopatología de la enfermedad, se han generado varios modelos murinos de calpainopatía, tanto bloqueando la expresion de *Capn3* en estos animales como introduciendo mutaciones que bloquean su actividad proteolítica. Estos modelos, a pesar de que han aportado información valiosa para el conocimiento de las funciones de la calpaína 3, no desarrollan la degeneración muscular causada por la enfermedad tal y como sucede en los pacientes, probablemente porque los ratones poseen otros mecanismos que compensan el efecto de la deficiencia de calpaína 3. Como alternativa, se podrían generar modelos celulares derivados de tejidos no musculares de pacientes que permitirían estudiar *in vitro* la enfermedad.

Los estudios realizados con las biopsias de pacientes y los cultivos derivados de los mismos, así como los modelos murinos y los sistemas de expresión *in vitro*, han atribuido distintas funciones a la calpaína 3. De acuerdo a estos estudios, 1) la calpaína 3 podría participar en la vía de señalización NFkB, por lo que esta vía de señalización estaría desregulada en los pacientes, impidiendo que lleve a cabo su función antiapoptótica. 2) Por otro lado, se ha demostrado que la calpaína 3 interacciona en varias localizaciones con la titina, una proteína gigante del músculo con función estructural, y que a través de estas interacciones podría participar en el remodelado del sarcómero. 3) A su vez, la calpaína podría participar en la transducción de señales mediante su interacción con proteínas del sarcómero y de la membrana celular. 4) También se ha demostrado que la calpaína 3 es capaz de proteolizar numerosas proteínas del citoesqueleto *in vitro*, por lo que se espera que podría participar en el remodelado del citoesqueleto. 5) La calpaína 3 podría jugar un papel en las mitocondrias, las cuales se encuentran desorganizadas en algunas fibras musculares de pacientes de LGMD2A, lo que se correlaciona con una capacidad reducida de síntesis de ATP y un aumento del estrés oxidativo que se refleja en las modificaciones protéicas. 6) La calpaína 3 también podría participar en el mantenimiento de la homeotasis del calcio. A este respecto, se ha visto que las

corrientes del calcio que se dan desde el retículo sarcoplásmico hacia el citoplasma para activar la contracción muscular, están disminuidas en el ratón *knockout* de calpaína 3. A su vez, también están reducidos los niveles de la proteína SERCA en biopsias de pacientes de LGMD2A, la cual se encarga de recaptar el calcio hacia el retículo sarcoplásmico para terminar la contracción. 7) Por último, en la última década se han publicado estudios que sugieren que la calpaína 3 podría ejercer alguna función en las células madre musculares, conocidas como células satélite, y en el control del ciclo celular en células tumorales.

Basándonos en estos útimos estudios, nos hemos propuesto estudiar el papel que la calpaína 3 podría ejercer en las células satélite o en las fases tempranas de la miogénesis, para de esta manera contribuir al conocimiento de la fisiopatología de la LGMD2A. Para ello, se han diseñado dos estrategias. Por un lado, hemos establecido modelos miogénicos *in vitro* a partir de muestras de piel de pacientes de LGMD2A y de controles sanos. Por otro lado, hemos aislado células satélite de los músculos de ratones y hemos estudiado la expresión génica en ellas, así como el fenotipo al que podría dar lugar la falta de calpaína 3 en estas células, obteniendo los resultados que se detallan a continuación.

En el primer capítulo, se seleccionaron 5 pacientes para participar en este estudio en representación de los pacientes de LGMD2A atendidos en el Hospital Universitario Donostia. La selección se realizó en base a la gravedad de su fenotipo y las mutaciones que albergaban en el gen *CAPN3*. Los fibroblastos de la piel de estos pacientes y de dos controles sanos pareados por edad y sexo, fueron reprogramados mediante vectores retrovirales que sobreexpresan los factores de transcripción *OCT4, SOX2, KLF4* y *cMYC*. Como resultado, se establecieron líneas de células reprogramadas (iPSCs), cuya pluripotencia fue verificada mediante las siguientes pruebas de caracterización: a) comprobación de la actividad de la fosfatasa alcalina, b) silenciamiento de los transgenes utilizados para reprogramar las muestras e inducción de la expresión de genes endógenos de pluripotencialidad, c) determinación del número de inserciones de cada uno de los transgenes en el genoma de las líneas establecidas, d) detección de marcadores de pluripotencia, e) diferenciación *in vitro* hacia tipos celulares derivados de las tres líneas germinales embrionarias, f) detección de cambios epigenéticos en el patrón de metilación de los promotores de genes de pluripotencialidad, y g) comprobación del mantenimiento de la estabilidad del cariotipo.

Tras ello, las células pluripotentes o iPSCs fueron transducidas con un sistema de sobreexpresión inducible de *PAX7*, y cultivadas en condiciones de inducción miogénica siguiendo un protocolo de siete días de cultivo en suspensión y agitación y otros siete días de cultivo en adherencia. Mediante la activación transitoria de la expresión de *PAX7* durante los cuatro últimos días del protocolo de inducción, se establecieron cultivos de progenitores miogénicos. La activación de la diferenciación terminal de estos progenitores dio lugar a cultivos de miotubos.

Las líneas pluripotentes generadas mostaron una capacidad variable de diferenciación miogénica. Estas diferencias no se dieron entre las líneas derivadas de pacientes y de controles, sino de forma general, y por tanto no fueron atribuidas a las mutaciones en el gen *CAPN3*. Estos resultados, junto con los indicios obtenidos de los resultados de la caracterización de las líneas pluripotentes, sugieren que las líneas reprogramadas adquirieron un estado de pluripotencia diferente. En este sentido, una caracterización más detallada de las líneas estabecidas podría corroborar dicha hipótesis.

Sin embargo, las líneas establecidas fueron capaces de activar la expresión de *CAPN3* al diferenciarse, y también se detectó calpaína 3 a nivel protéico en los cultivos derivados de controles sanos y en el de algunos pacientes. Además, a lo largo de la diferenciación miogénica de las líneas de controles sanos, fue posible observar la sustitución de tránscritos inmaduros de *CAPN3* por las forma madura correspondiente, tal y como sucede durante el desarrollo miogénico y en modelos celulares de mioblastos. Es de destacar que esta sustitución se dio de forma notable en las líneas que mostraron un potencial de diferenciación contundente, mientras que no se dio en la línea que mostró una capacidad de diferenciación reducida.

Por otro lado, con el objetivo de estudiar la capacidad regenerativa de los progenitores miogénicos derivados de las iPSCs, dichos progenitores fueron trasplantados en ratones mediante inyecciones intramusculares. Al mes, se analizó la cantidad de células trasplantadas que permanecían en los músculos y el número de fibras derivadas de dichos progenitores. Tanto los progenitores derivados de un paciente de LGMD2A como los derivados de un control sano mostraron capacidad regenerativa. Sin embargo, dadas las diferencias detectadas anteriormente en la capacidad de diferenciación de dichas líneas celulares, no se consideraron relevantes las comparaciones realizadas entre dichas líneas.

Por tanto, concluímos que la *CAPN3* no es esencial en el proceso de reprogramación celular, y que las células reprogramadas y los modelos derivados de ellas pueden ser utilizados para estudiar la función de la calpaína 3 en la miogénesis, dado que estos cultivos activan la expresión de *CAPN3* y calpaína 3 durante su diferenciación miogénica. Sin embargo, es necesario optimizar el modelo para poder reducir o eliminar la variabilidad no atribuible a la *CAPN3* y así poder realizar comparaciones entre las distintas líneas celulares generadas. Una opción consistiría en establecer líneas isogénicas, mediante la corrección de mutaciones en las líneas derivadas de pacientes o mediante el silenciamiento de *CAPN3* en líneas de controles sanos, empleando técnicas de edición génica disponibles en la actualidad, como es el CRISPR/Cas9.

En el siguiente apartado estudiamos la expresión de *Capn3* y su hipotética función en las células satélite murinas. Las células satélite son las células madre musculares encargadas de la regeneración muscular. En condiciones basales (ausencia de daño muscular), estas células se encuentran en quiescencia. Cuando el músculo sufre un

daño, estas células se activan, proliferan, y la mayoría de ellas activan la diferenciación miogénica, regenerando el tejido muscular. A su vez, una pequeña parte de las células vuelve a quiescencia, para de esta manera poder hacer frente a daños musculares que pudieran ocurrir más adelante. Por ello, estos procesos requieren una estricta regulación para poder preservar la capacidad regenerativa del músculo.

Para ahondar en nuestra hipótesis y determinar si la calpaína 3 podría ejercer alguna función en las células satélite, en primer lugar estudiamos la expresión génica de *Capn3* en las células satélite en quiescencia y tras su activación tras el daño inducido por la inyección intramuscular de cardiotoxina. Tanto los resultados de expresión de genes miogénicos como los resultados de la citometría nos permitieron concluir que el punto de mayor activación de células satélite se alcanzó a los 3 días tras la inyección de cardiotoxina, y que después, a los 5 y 7 días, dicha activación se fue reduciendo de forma progresiva. La mayor expresión de *CAPN3* se detectó en las células satélite aisladas de las patas inyectadas con cardiotoxina a los 3 días post inyección, y su expresión se redujo de forma progresiva en días posteriores.

Este resultado establece una base para seguir profundizando en el estudio de la función de la calpaína 3 en las células satélite. Sin embargo, para ello sería necesario corroborar la expresión de calpaína 3 a nivel protéico en estas células. Teniendo en cuenta la extensa duración del protocolo de aislamiento de células satélite y la rápida autolisis de la calpaína 3, se consideró inviable la detección de esta proteína mediante *Western blot*. En su lugar, se aislaron células satélite de ratones sanos y deficientes en capaína 3 (C3KO) y se estudiaron las posibles diferencias funcionales entre ambas poblaciones mediante el ensayo *colony assay*. En concreto, este ensayo evaluó la capacidad de proliferación, diferenciación y fusión de las células satélite sanas y C3KO mediante el programa informático *G-tool*.

No se encontraron diferencias funcionales entre las células satélite derivadas de ratones sanos y C3KO en cuanto a su capacidad proliferativa, potencial de diferenciación y fusión *in vitro*. Tampoco se encontraron diferencias entre las células satélite extraídas de músculos que tanto en ratones C3KO como en pacientes de LGMD2A se encuentran bastante afectados (soleo) y levemente afectados (*tibialis anterior*). La ausencia de diferencias fenotípicas puede deberse a la edad temprana de los ratones. Tal y como se ha mencionado anteriormente, la degeneración muscular es muy leve en ratones C3KO comparado con los pacientes de LGMD2A, y además, el hecho de que sea una enfermedad de caracter progresivo podría hacer que las células satélite de estos ratones no presentaran ningún fenotipo en edades tempranas.

Por tanto, considerando estos resultados, se puede concluir que la *Capn3* se expresa en células satélite, siguiendo un patrón dependiente de su activación. La realización de experimentos funcionales, proteómicos y transcriptómicos en células satélite aisladas

de ratones de edades más avanzadas esclarecerá el papel de la calpaína 3 en las células satélite, y en general, en el proceso de regeneración muscular, proporcionando conocimientos que permitan avanzar en el entendimiento de la fisiopatología de la LGMD2A.

En conclusión, se han establecido modelos celulares miogénicos a partir de fibroblastos de la piel de pacientes con LGMD2A, que serán de utilidad para estudiar la función de la calpaína 3 y la fisiopatología de la LGMD2A. Es necesario optimizar estos modelos para que se puedan realizar comparaciones entre las distintas líneas celulares generadas. Estos modelos son capaces de activar la expresión de *CAPN3* y su maduración transcripcional en las células que se diferencian de forma eficiente, detectándose calpaína 3 a nivel protéico en los cultivos derivados de controles sanos y de algunos de los pacientes. La obtención de líneas isogénicas mediante el empleo de técnicas de edición génica como el CRISPR/Cas9 prevendría gran parte de los problemas derivados de la variabilidad existente entre las distintas líneas celulares.

Por otro lado, la detección de la expresión de *Capn3* en células satélite de ratones establece una base para seguir estudiando la función que podría ejercer la calpaína 3 en estas células y en la regeneración muscular. Si se demostrara esta función, este descubrimiento supondría un avance en la comprensión de la fisiopatología de la LGMD2A y situaría a las células satélite como potencial diana para futuros tratamientos.

INTRODUCTION

1. MUSCLE TISSUE

Muscle tissue is involved in all kinds of body movements due to its ability to contract. This tissue can be classified into two categories based on the structure of its cells: **striated muscle,** which includes tissues showing transversal lines visible under a light microscope, and **smooth muscle,** where transversal striations are absent. According to its location and function, this tissue can be further classified into three categories (figure 1):

a. **Skeletal muscle:** Comprised of striated and multinucleated cells. It is attached to bones, and voluntarily performs movements of axial and appendicular skeletons, as well as maintaining body posture.

b. **Cardiac muscle:** Comprised of striated cells that bind to each other through intercalated discs, creating long fiber-like structures. This tissue is only found in the heart, where it induces spontaneous and continuous contraction.

c. **Smooth muscle:** Does not show striations since muscle proteins do not achieve a high enough organizational level required to build these structures. This tissue is found coating several body parts, such as blood vessels, urinary bladder, kidneys, esophagus and small intestines. Induces spontaneous and sustained contraction.

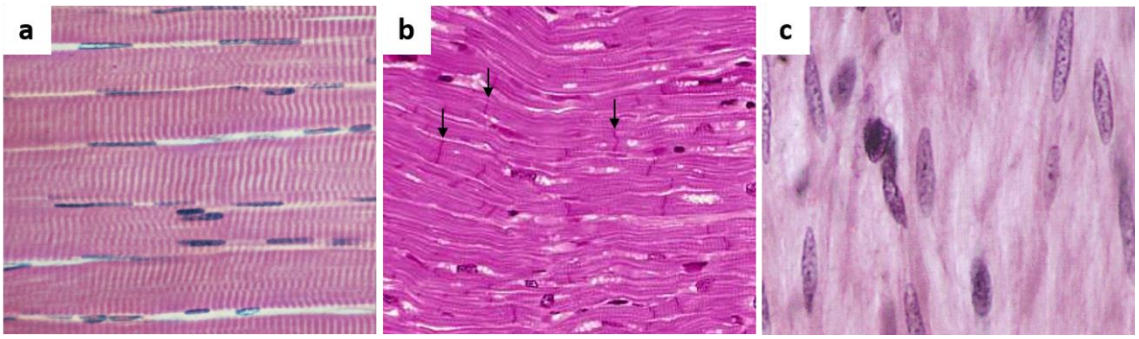

Figure 1. Optical microscopy images of different muscle types. a) Microphotography of a longitudinal section of skeletal muscle, where nuclei are purple-stained and fibers are a pink color. Striations can be observed as slightly darker pink vertical lines. (From: *Eric Grave, Getty Images*). b) Microphotography of a longitudinal section of cardiac muscle. Arrows indicate intercalated disks (From: *Dr. Gladden Willis, Getty Images*). c) Microphotography of smooth muscle from colon tissue. (From: Ross and Pawlina, 2013).

1.1 SKELETAL MUSCLE

Approximately 40% of body weight in humans corresponds to skeletal muscles (reviewed by Frontera and Ochala, 2015). More than 600 different skeletal muscles are found in the human body, each one with specific size, shape and contractile properties that allow them to perform specific roles (Dumont *et al.,* 2015a). This tissue has a remarkable adaptive potential. For example, resistance training can induce muscle

hypertrophy, increasing muscle size and strength, as well as modifying the fiber type composition of muscles. Moreover, several diseases, such as cancer and dystrophies, can cause muscle atrophy and loss of function (Angelini *et al.*, 2014; Kazior *et al.,* 2016).

1.1.1 STRUCTURE

The skeletal muscle cell, or **myofiber,** is a multinucleated structure built by mononuclear muscle cells known as **myoblasts** that fuse with each other. In these myofibers, **sarcomeres**, which are the contractile units formed by several muscle proteins, account for most of the cytoplasmic space and the nuclei tend to locate right below the cell membrane, the **sarcolemma**. The sarcolemma is covered by a layer of glycoproteins and extracellular proteins, such as collagens and laminins, known as the **basal lamina**, which is the external coat of the myofiber. Lastly, each myofiber is surrounded by an outer sheath of conjunctive tissue known as **endomysium**. This tissue contains numerous blood vessels and nerves and extends beyond the muscles, creating tendons and similar structures that generally bind the muscles to the bones. Subsequently, muscle fibers converge forming **fascicles** that are surrounded by another layer of conjunctive tissue known as **perimysium**. Several fascicles are coated by a thick layer of conjunctive tissue called **epimysium**, leading to different skeletal muscles (figure 2).

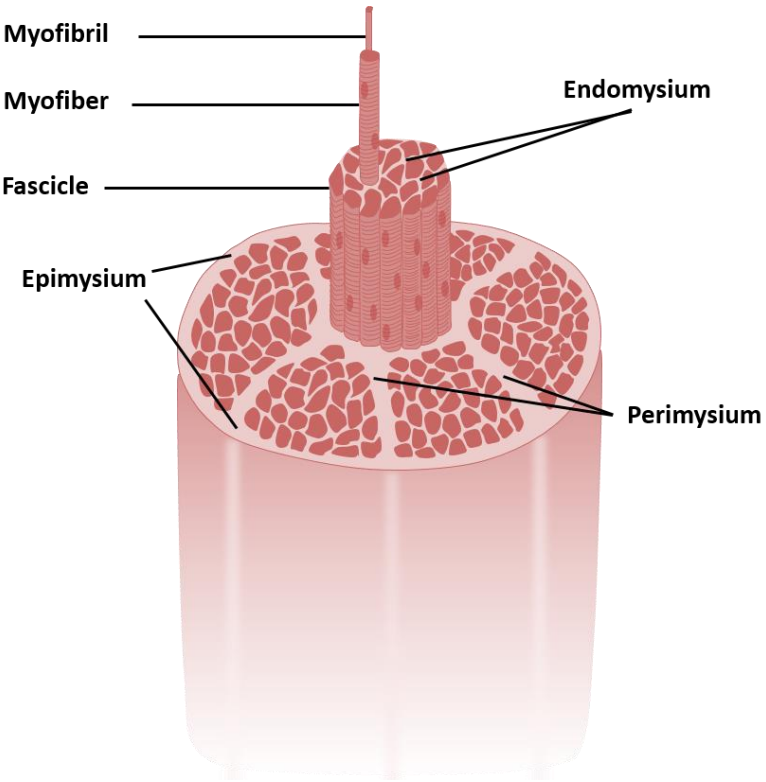

Figure 2. Structure of skeletal muscle. Myofibers are surrounded by endomysium and packed in groups, forming fascicles. Fascicles are surrounded by perimysium, and different fascicles are finally surrounded together by the epimysium.

As previously mentioned, sarcomeres are the contractile units of the muscles. They consist of thick myosin type II filaments and thin actin filaments, which connect to

several other muscle proteins to build the contractile units. These myofilament bundles, named **myofibrils**, are surrounded by highly developed smooth endoplasmic reticulum, also known as **sarcoplasmic reticulum**, which encloses the myofibers and plays a key role in the muscle contraction process by controlling calcium influxes.

Transversal striations formed by these myofilaments can be observed in longitudinal sections of skeletal muscle tissue. Electron microscopy images of these sections show dark **A bands** and light **I bands.** A bands are the regions where thick and thin filaments locate together, and they show a clearer middle region known as **H band**, where thin filaments are absent. The **M line** is located in the middle of the H band, and it corresponds to the region where thick filaments come together. I bands contain exclusively thin filaments and they are divided by a darker line known as the **Z disk**, where thin filaments of consecutive sarcomeres join together through α-actinin (figure 3).

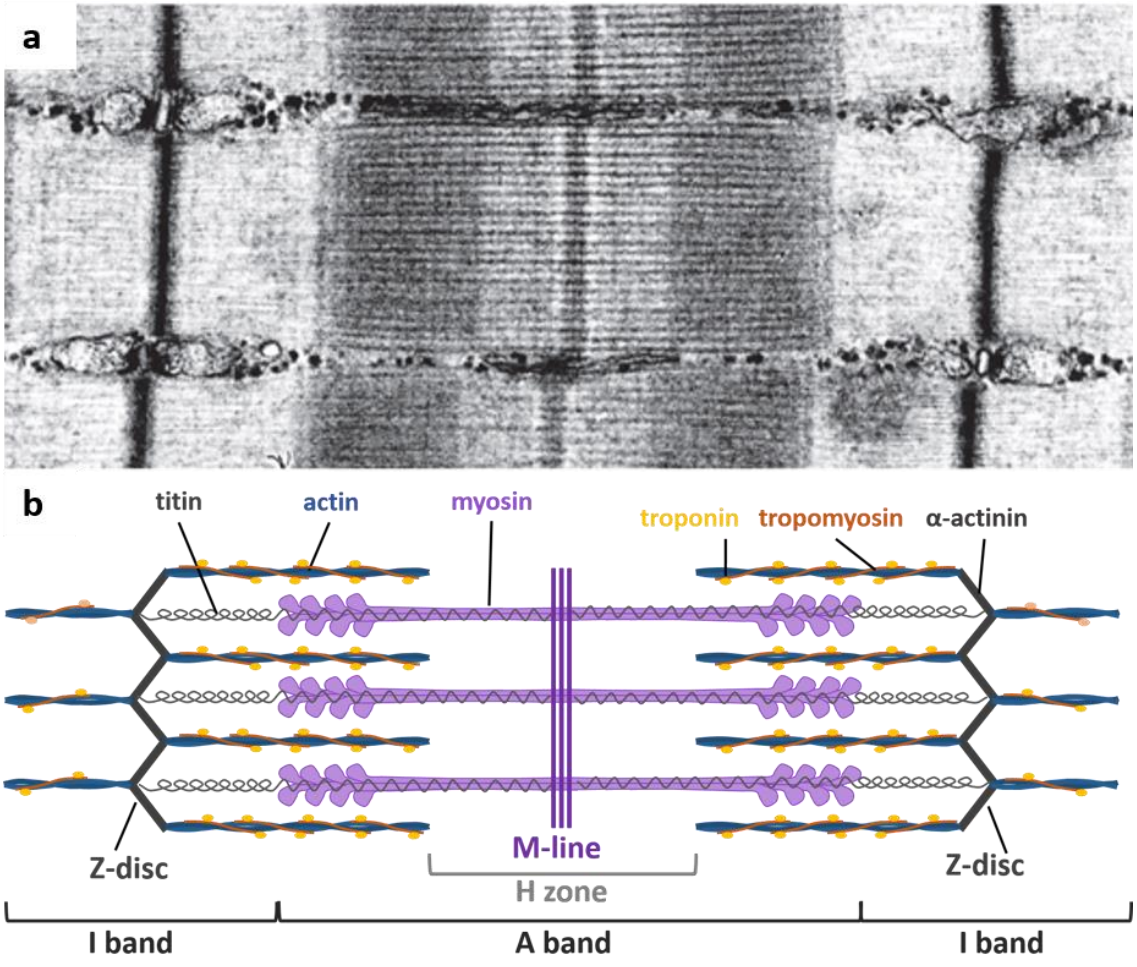

Figure 3. Structure of sarcomeres. a) Electron microscopy image of striated muscle, where different bands of the sarcomere are visible. From: *http://www.ks.uiuc.edu/~ericlee/Telethonin/.* b) Simplified representation of the sarcomere, showing the protein composition of different bands.

Skeletal muscle is a highly vascularized tissue. Medium-size arterioles and veins are visible between the muscle fascicles, while small capillaries are observed within the

fascicles, close to myofibers. Although less frequently than vasculature, nerves and neuromuscular junctions are also found in muscle biopsies, but specific immunohistochemical reactions are often required in order to visualize them properly.

1.1.2 MUSCLE CONTRACTION

Calcium flows between the sarcoplasmic reticulum and the sarcoplasm control muscle contraction. At a molecular level, this process occurs as follows: Actin filaments are associated with tropomyosin and troponin molecules (figure 4.c). In resting muscles, these molecules block the interactions between myosin and actin. When calcium is released from the sarcoplasmic reticulum to the sarcoplasm, calcium ions bind troponin, inducing conformational changes that enable the interaction between actin and myosin filaments. Contractions begin with myosin tightly binding actin, in the absence of adenosine triphosphate (ATP) (figure 4.c1). When a myosin head binds ATP, it separates from actin (figure 4.c2). Hereafter, the ATP molecule is hydrolyzed into adenosine diphosphate (ADP) and inorganic phosphate, and consequently the head of the myosin molecule moves along the actin filament (figure 4.c3). Finally, the phosphate group is released, and myosin and actin molecules bind strongly to each other (figure 4.c4). Next, the ADP molecule is released, and subsequently the head of the myosin molecule returns to its original position, inducing the movement of the actin molecule along the myosin filament (figure 4.c5). Actin and myosin filaments are packed, shortening the length of the I band and therefore, the length of the entire sarcomere, which results in muscle contraction (figure 4.a and figure 4.b). Despite the central role of myosin and actin filaments in the contraction process, titin potentially binds to calcium ions, increasing filament stiffness (Herzog, 2014).

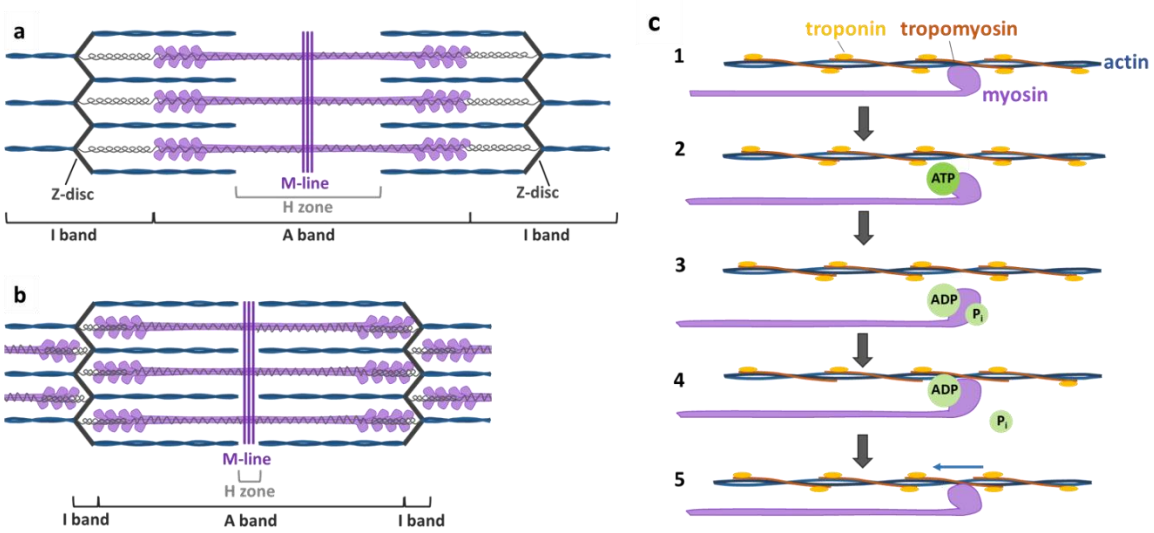

Figure 4. Muscle contraction. a) Structure of sarcomere, relaxed. b) Structure of sarcomere, contracted. c) Contraction mechanism, where myosin and actin filaments interact through an ATP-dependent mechanism that induces the movement of actin filaments along myosin filaments.

As previously mentioned, calcium ions activate the contraction process by interacting with troponin. Therefore, calcium release and uptake by the sarcoplasmic reticulum, which acts as an intracellular calcium storage, directly regulates this process.

The sarcoplasmic reticulum embraces the myofibrils, creating structures that resemble a net. Each net surrounds an I band or an A band, forming a **terminal cisternae** exactly where the A and I bands join together (figure 5.a). These cisternae work as calcium storages and include a high number of channels that are able to release calcium ions to the cytosol when required. Numerous mitochondria and glycogen molecules are also observed close to the sarcoplasmic reticulum, which provide the energy required for the contraction process. In these regions, the sarcolemma creates invaginations known as **T tubules**, which are located between the terminal cisternae, transversely to the fiber, and are rich in voltage-sensitive proteins. The complex formed by the T tubule and the two adjacent terminal cisternae is known as the **triad** (figure 5.b).

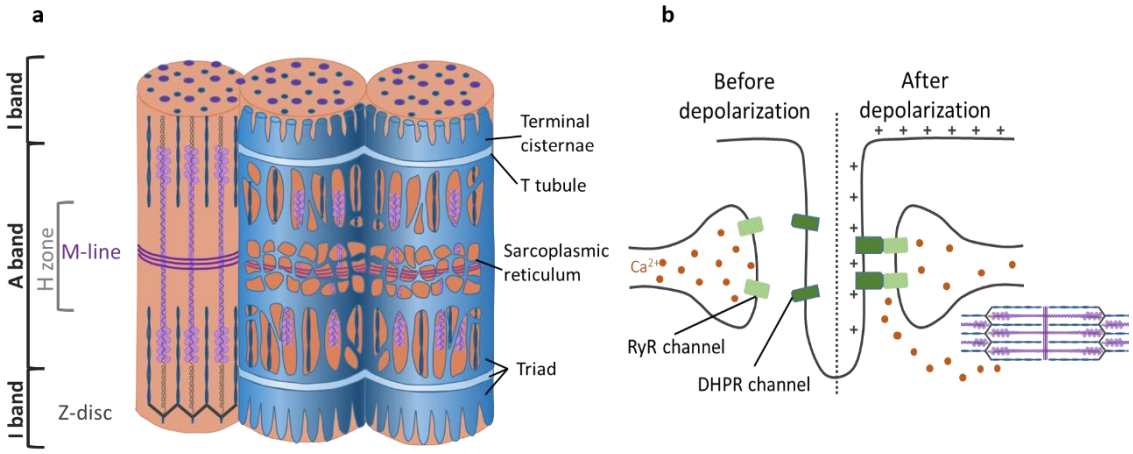

Figure 5. The sarcoplasmic reticulum. a) Structure of sarcoplasmic reticulum (in blue), surrounding myofibrils. The figure shows the location of triads with regard to the sarcomeres. b) Structure of the triad, representing calcium release following membrane depolarization.

When a nerve impulse reaches a neuromuscular junction, acetylcholine is released, inducing a localized depolarization of the sarcolemma. As a result of this depolarization, voltage-sensitive sodium channels are activated, allowing Na^+ to flow from the extracellular space to the sarcoplasm. Consequently, the depolarization is quickly extended over the muscle cell and when it reaches a T tubule, voltage-sensitive dihydropyridine receptor (DHPR) channels activate and couple with the ryanodine receptor (RyR) channels located in the membrane of the sarcoplasmic reticulum, inducing a large calcium release from the terminal cisternae to the sarcoplasm (figure 5.b). As a result of the cytoplasmic calcium increase, Ca^{2+} ions bind to troponin and activate the previously detailed contraction process (figure 4.c). At the same time, ATP-dependent Ca^{2+} pumps located in the sarcoplasmic reticulum (SERCA pumps) are activated and reuptake Ca^{2+} ions to the terminal cisternae, reducing the sarcoplasmic calcium concentration and therefore ending the muscle contraction. An example of the

timing of the nerve impulse, calcium release and reuptake and muscle contraction is represented in figure 6.

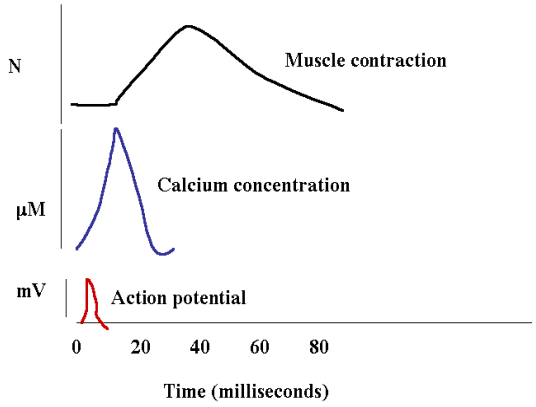

Figure 6. Timing of muscle contraction. Example of the timing (in milliseconds) of the nerve impulse (red line, in millivolts, mV), variation of sarcoplasmic calcium concentration (blue line, micromolar concentration, µM) and muscle contraction (black line, in newtons, N). The process takes milliseconds and the muscle contraction lasts longer than the variation in calcium levels that cause it. Similarly, cytoplasmic calcium increase lasts longer than the action potential that induces it. From: http://www.ucl.ac.uk/~sjjgsca/MuscleControl.html

The force generated by the sarcomere contraction is transmitted to the sarcolemma and the extracellular matrix through the **costameres**, which are protein complexes that bridge the Z-disks of the sarcomeres with the membrane and the extracellular components of the skeletal muscle. Several proteins found in these complexes, as well as sarcomeric proteins, play an essential role in muscle contraction and functioning, since mutations in these protein-coding genes often lead to a wide spectrum of muscle pathologies (reviewed by Jaka *et al.*, 2015).

Muscle contractions require an important energy supply, because SERCA pumps and myosin heads consume ATP molecules during the contraction process. This energy arises from anaerobic as well as aerobic metabolic pathways, depending on the contraction type. Fast, short and high intensity contractions use anaerobic energy sources, whereas energy for low intensity and prolonged contractions is from aerobic pathways.

Anaerobic pathways comprise two main catabolic reactions to generate ATP: the degradation of phosphocreatine (PCr), which is catalyzed by creatine kinase, and the breakdown of muscle glycogen to lactate. As for **aerobic metabolism**, oxidation of carbohydrates and lipids is the principal source of ATP. Among the carbohydrates, muscle glycogen and extracellular glucose are the main substrates, whereas free fatty acids stored in skeletal muscle and adipose tissue provide energy through lipid oxidation pathways. In specific situations, muscle protein degradation can potentially contribute to ATP production through aerobic metabolism, although the energy provided is very limited (reviewed by Westerblad *et al.,* 2010).

According to the main energy source used by muscle fibers, they have been classified into different fiber types, which can be studied based on their specific biochemical features.

1.1.3 FIBER TYPES

Most skeletal muscles contain a combination of different fiber types, which are classified according to their metabolic activity, the speed of contraction and the myosin heavy chain isoforms they express. The categories are:

a. **Type I fibers or slow oxidative fibers.** These small fibers are reddish and they contain large amounts of mitochondria and high levels of myoglobin and cytochrome complexes. These fibers twitch slowly since their myosin ATPase activity is the lowest of the three fiber types, and they do not generate considerable force, although they are highly resistant to exhaustion.

   In humans, dorsal muscles that contribute to the maintenance of body posture show a high type I fiber content, and these muscles perform slow and long-lasting contractions.

b. **Type IIa fibers or fast oxidative glycolytic fibers.** These intermediate-size fibers also contain a large number of mitochondria and show high myoglobin content. However, contrary to type I fibers, type IIa fibers contain elevated amounts of glycogen and they are able to perform anaerobic glycolysis. These fibers contract rapidly, generating an intense peak strength, and they are also resistant to fatigue. In immunohistochemical analyses, both type IIa and IIb fibers specifically react with antibodies against fast myosin heavy chain.

c. **Type IIb fibers or fast glycolytic fibers.** These large fibers appear whitish and have lesser amounts of mitochondria and myoglobin when compared to type I and type IIa fibers. They have a low oxidative enzymatic rate, but possess considerable anaerobic enzymatic activity, besides storing glycogen. Type IIb fibers contract rapidly and are able to perform intense contractions, although they become exhausted easily due to the production of lactic acid.

   Therefore, these fibers are suitable for quick and precise contractions, such as the ones that control the movement of the fingers and some eye muscles. They also express fast myosin heavy chain.

   In humans, type IIb fibers have been reclassified as type IIx/d fibers due to their similarity to type IIx/d fibers found in small mammals, which also have very fast type IIb fibers that are absent in humans. However, they are still named as type IIb fibers (Scott *et al.,* 2001).

d. **Type IIc fibers or immature fibers.** These fibers are rare in adult human muscles, but are commonly found in developing muscles and in some pathological conditions.

Moreover, along with the mentioned features (reviewed in table 1, upper part), several immunohistochemical reactions are performed regularly to determine the fiber type composition of skeletal muscle sections. These reactions are indicated in the lower portion of the following table (table 1):

	Type I	Type IIa	Type IIb	Type IIc
Color	Red	White	White	
Twitch speed	Slow	Fast	Fast	
Fatigability	Resistant	Resistant	Sensitive	
Metabolic activity	Oxidative	Oxidative and Glycolytic	Glycolytic	
Fast MyHC	-	+++	+++	++/+++
Slow MyHC	+++	-	-	-/+/++
SERCA pump type	Type 2	Type 1	Type 1	
SERCA pump density	Low	High	High	
ATPase pH 9.4	+	+++	+++	+++
ATPase pH 4.6	+++	-	++	+++
ATPase pH 4.3	+++	-	-	++/+++
NADH-TR	+++	++	+	++/+++
Cytochrome oxidase	+++	++	+	+
Succinic dehydrogenase	+++	++	+	++

Table 1. Fiber types. Summary of skeletal muscle fiber type-specific features (upper part) and immunohistochemical reactions regularly used to identify each fiber type (lower part). -/+/++/+++ represent the intensity of each staining. (Adapted from: Dubowitz and Sewry, 2007; Westerblad *et al.,* 2010).

The fiber-type composition of muscles varies among people, and even in different parts of a specific muscle. Factors such as innervation, hormones, exercise and disuse, drugs or age can influence fiber typing (Pette and Staron, 2000). For example, marathon runners generally have a higher percentage of type I fibers in the majority of their muscles, whereas intermediate distance runners and swimmers usually have a higher percentage of type IIa fibers. Further, sprinters and weight lifters tend to have more type IIb fibers, compared to the average population. Fiber typing has also been observed to be altered in several muscular dystrophies (Reviewed by Beedle, 2016).

1.2 MUSCLE GENERATION

1.2.1 REGULATION OF MYOGENESIS

Mammalian skeletal muscle formation and regeneration have generally been studied using murine transgenic models. These studies have shown that both processes are

tightly regulated by specific transcription factors. Muscle stem cell specification is driven by paired box protein 3/paired box protein 7 (PAX3/PAX7) transcription factors in the trunk and T-box transcription factor 1/pituitary homeobox 2 (TBX1/PITX2) in the head muscles, whereas four transcription factors known as myogenic regulatory factors (MRFs), control the determination of muscle stem cells and the myogenic differentiation process: myogenic factor 5 (MYF5), myogenic factor 6 (MYF6 or MRF4), myoblast determination protein 1 (MYOD1) and myogenin (MYOG) (Reviewed by Comai and Tajbakhsh, 2014).

Generally, PAX3 plays an important role in the embryonic development of trunk and limb muscles, whereas PAX7 is critical for perinatal muscle growth and for the maintenance of muscle stem cells in adult muscles, also known as satellite cells (Seale *et al.,* 2000; Oustanina *et al.,* 2004; Relaix *et al.,* 2005; Kuang *et al.,* 2006; Relaix *et al.,* 2006). Several transgenic mouse models have provided vital information about this process. For example, depletion of *Pax3*-expressing cells in postnatal muscles does not impair muscle regeneration in adult mice (Relaix *et al.,* 2004). Further, depletion of *Pax7* in embryos has very mild effects, but it definitively blocks satellite cell formation in adult mice. Moreover, *Pax7*-null mice progressively lose satellite cells and demonstrate important deficiencies in muscle regeneration, leading to death quickly after birth (Seale *et al.,* 2000; Oustanina *et al.,* 2004; Kuang *et al.,* 2006; Relaix *et al.,* 2006; von Maltzahn *et al.,* 2013).

MRFs regulate the progression of muscle PAX3/PAX7+ stem cells across the myogenic differentiation program. Among the four MRFs, MYF5, MRF4 and MYOD1 determine skeletal muscle cell identity during embryogenesis. In this regard, it has been observed that a double *Myf5:MyoD1* mutant mouse model neither generates myoblasts nor muscle fibers but has plenty of muscle stem cells (Rudnicki *et al.,* 1993; Kassar-Duchossoy *et al.,* 2004). The last MRF, myogenin, is required for muscle differentiation (Hasty *et al.,* 1993; Nabeshima *et al.,* 1993), as well as MRF4 and MYOD1, which control the differentiation of myoblasts into skeletal muscle fibers (Reviewed by Moncaut *et al.,* 2013).

1.2.2 SKELETAL MUSCLE DEVELOPMENT

Skeletal muscle development and its regeneration following trauma involve common regulatory pathways and transcription factors, such as the previously mentioned MRFs. However, there are notable differences between both processes.

Embryonic myogenesis has been primarily studied in mouse and avian models. However, it is necessary to highlight that considerable differences in the myogenic process may potentially exist among species and therefore, data is required to be carefully considered when applying this knowledge to human myogenesis.

Skeletal muscle development is a regulated, sequential process. Founder stem cells are specified and allocated to the lineage during prenatal development. These stem cells differentiate into myoblasts, which proliferate and further differentiate, fusing to each other and generating multinucleated muscle fibers (Biressi *et al.,* 2007; Sambasivan and Tajbakhsh, 2007; Tajbakhsh, 2009).

Skeletal muscle in the mouse is established from embryonic day 8.5/9 to 18.5 (birth at day 19), and it continues maturing during the first 3-4 weeks after birth. The long-term Pax7+ satellite cells are not found in the early stages of the embryo. They show up only after an anlage of differentiated cells is established during mid-embryogenesis. Next, primary embryonic fibers are formed in the anlage, and finally these fibers act as a scaffold allowing the formation of secondary fetal fibers, which subsequently fuse and enlarge to form adult muscles (figure 7).

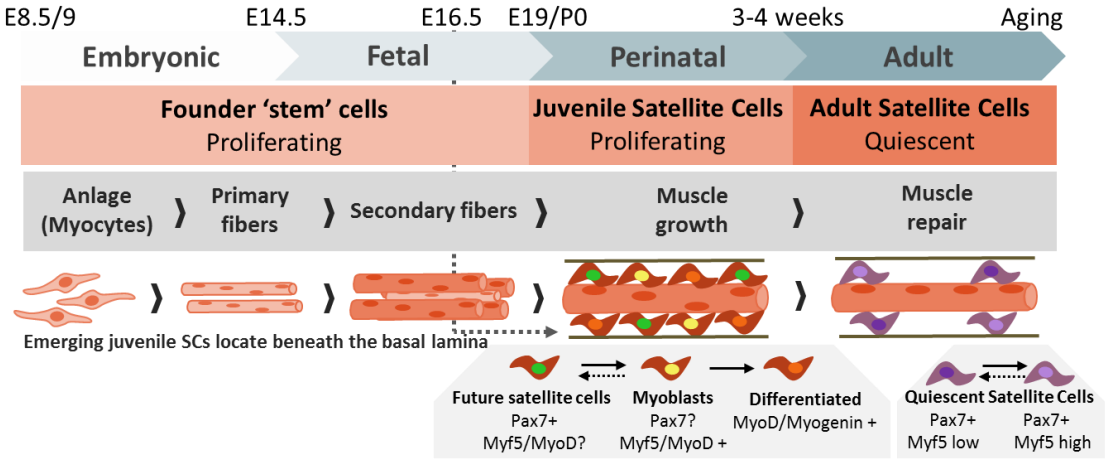

Figure 7. Muscle generation and regeneration in mice during embryonic, fetal, perinatal and adult stages. (Adapted from: Tajbakhsh, 2009).

In humans, primary fiber formation occurs at approximately 7 weeks of gestation. At this point, post-mitotic myoblasts fuse to form centrally nucleated myotubes. At the initiation, these myotubes are clustered together, surrounded by a common basal lamina, but as differentiation proceeds, they become separated and surrounded individually by the basal lamina. Next, secondary myotubes arise on the surface of primary fibers. Similar to primary myotubes, they are initially surrounded by the same basal lamina, but get separated and individually coated as differentiation progresses forward. The number of fibers can keep increasing until four months after birth. Thereafter, muscle growth only occurs as a result of the addition of myoblasts to the end of the fibers.

It has been shown that fetal fibers cannot be classified into regular type 1 and type 2 fibers until 18 weeks of gestation, and thus, they are named as type 2C fibers or immature fibers. Between 20 and 28 weeks, type 1 fibers begin appearing, and only after 28 weeks of gestation type 1 and type 2 fibers can be distinguished. At birth, there are

still 15-20% of type 2C fibers, but in one year these fibers are reduced to 3-5%, being 60-65% type 1 fibers and 30-35% type 2 fibers (Dubowitz and Sewry, 2007).

Muscle development in the mouse embryo occurs differently, depending on whether the cells are going to give rise to trunk muscles, limb muscles or head muscles. Trunk and limb muscles originate from somites, which are derived from the segmentation of the paraxial mesoderm on either sides of the neural tube, following an anterior-posterior gradient (Sambasivan and Tajbakhsh, 2007) (figure 8). In contrast, head muscles are derived from the cranial mesoderm, which is non-segmented.

The ventral side of the somites contains sclerotomal precursors that lead to the axial skeleton and ribs, whereas the dorsal side of the somites gives rise to the epithelial dermomyotome that over time leads to all skeletal muscles of the body, the tongue and some neck muscles, besides several other non-muscle cell types. Myogenesis is initiated in the somites when *Myf5* is expressed in the epaxial domain first, and later in the hypaxial domain. *Mrf4* is induced after *Myf5*, although later in the developmental process it is only expressed in differentiating cells. *MyoD1* expression is also activated after *Myf5*. These cells rapidly constitute the first skeletal muscle (anlage) of the embryo.

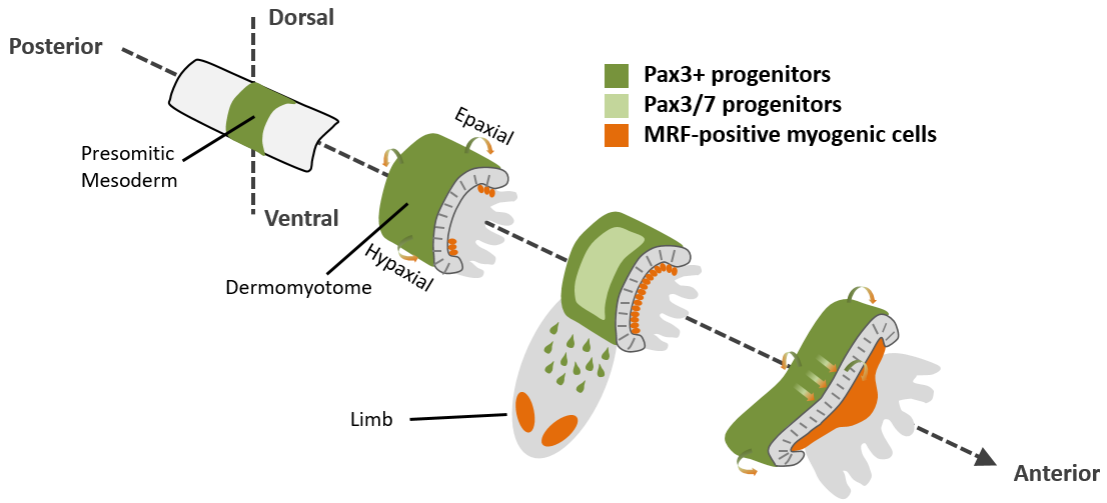

Figure 8. Schematic representation of the initial stages of myogenesis in the mouse embryo. (Adapted from: Buckingham and Rigby, 2014; Tajbakhsh,2009).

Once this anlage is established, *Pax3/Pax7+* stem cells migrate from the center of the dermomyotome to form the underlying myotome, which is comprised of MRF-expressing cells that will continue proliferating to build the muscles of the trunk. *Pax3+* cells that do not express any MRF and are located in the hypaxial lip of the dermomyotome undergo epithelial to mesenchymal transition (EMT) and migrate to the forming limb buds, where they start expressing *Myf5* and *MyoD1* (Kassar-Duchossoy *et*

al., 2005). Hepatocyte growth factor (HGF) and its receptor c-Met are critical to induce this EMT transition (Brand-Saberi *et al.,* 1996).

Regulation of head myogenesis differs from trunk and limb myogenesis. The previously mentioned MRFs participate in the development of these muscles, but contrary to trunk and limb muscle development, where PAX3 plays a central role, TBX1 and PITX2 transcription factors guide head muscle myogenesis (Kelly *et al.,* 2004; Sambasivan *et al.,* 2009).

1.3 MUSCLE REGENERATION

1.3.1 SATELLITE CELLS

In addition to their high plasticity, skeletal muscles possess an enormous regenerative potential. Muscle regeneration relies on muscle stem cells, also known as satellite cells (Reviewed by Dumont *et al.*, 2015a). These are mononuclear cells located between the sarcolemma and the basal lamina of muscle fibers (Mauro, 1961) (figure 9). Only 2 to 10% of cell nuclei found in skeletal muscles correspond to satellite cells. However, this proportion in greatly influenced by factors such as age (Gibson and Schultz, 1983), muscle type and specie. For example, a study performed in rats demonstrated that slow oxidative fibers contain more satellite cells when compared to fast glycolytic fibers, likely due to the high repair demand of postural muscles, which contain an important percentage of type I fibers (Schmalbruch and Hellhammer, 1977). In humans, aging induces a reduction of the cross-sectional area of type II fibers, as well as a progressive decrease of type II fiber-associated satellite cells, whereas the cross-sectional area and the number of satellite cells remains relatively constant in type I fibers (Verdijk *et al.,* 2014).

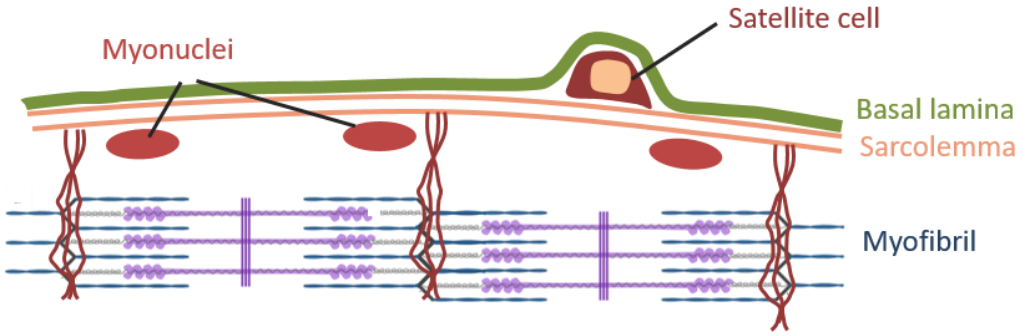

Figure 9. Schematic representation of the location of a satellite cell, between the sarcolemma and the basal lamina.

In addition to their anatomic location, satellite cells are also detected based on the expression of specific intracellular and membrane proteins. In adult muscles, PAX7 transcription factor is the principal satellite cell marker, which is ubiquitously expressed in all satellite cells, both in a quiescent and active state, and in a wide range of species.

Pax7 expression is essential to generate and maintain the satellite cell pool (Seale *et al.,* 2000; von Maltzahn *et al.,* 2013). *Myf5* and *MyoD1* are highly expressed in activated satellite cells, but not in quiescent satellite cells. As for surface proteins, no satellite cell-specific markers have been reported. However, several combinations of markers have been used to detect and isolate satellite cells through fluorescence-activated cell sorting (FACS) (Reviewed by Tedesco *et al.*, 2010). For example, M-cadherin, integrin α-7, Integrin β-1, hepatocyte growth factor receptor (c-MET), C-X-C chemokine receptor factor 4 (CXCR4), syndecan-3 and syndecan-4, hematopoietic progenitor cell antigen CD34 (CD34), vascular cell adhesion protein 1 (VCAM1) and neural cell adhesion molecule 1 (NCAM1) have been described as satellite cell markers in mice, and have been used in FACS-based satellite cell isolation in combination with the negative selection of hematopoietic and endothelial cells. The negative markers include receptor-type tyrosine-protein phosphatase C (CD45), integrin α-M (CD11b), platelet endothelial cell adhesion molecule (CD31), or stem cell antigen-1 (SCA-1) (table 2) (Liu *et al.,* 2015; Maesner *et al.,* 2016). Of note, some of these markers, such as CD34, are expressed in mouse satellite cells but not in human satellite cells (Péault *et al.,* 2007).

Positive markers	Negative markers	SCs isolated	Starting muscles	References
VCAM1	CD31, CD45, SCA-1.	Quiescent and activated	Hind limb muscles, diaphragm	(Liu *et al.,* 2013)
SM/2.6	CD45.	Quiescent	Hind limb muscles	(Fukada *et al.,* 2007)
CXCR4 Integrin-β1	CD45, MAC1, SCA-1.	Quiescent	Hind limb muscles	(Sherwood *et al.,* 2004)
CD34	CD45, SCA-1.	Quiescent	Hind limb muscles, diaphragm	(Montarras *et al.,* 2005)
CD34	CD31, CD45, SCA-1.	Quiescent	Hind limb muscles	(Joe *et al.,* 2010)
Integrin-α7	CD31, CD45, SCA-1.	Activated	Hind limb muscles	(Joe *et al.,* 2010)
CD34 Integrin-α7	CD31, CD11b, CD45, SCA-1.	Quiescent	*Tibialis anterior*	(Sacco *et al.,* 2008; Pasut *et al.,* 2012).

Table 2. Overview of cell surface markers used to isolate mouse satellite cells, types of satellite cells isolated and tissue of origin. (From: Liu *et al.,* 2015).

1.3.2 MUSCLE REGENERATION AFTER INJURY

Skeletal muscle contains an enormous regenerative potential in adults, even after a massive injury that demolishes muscle structure. As previously indicated, satellite cells control this regeneration process. These cells are quiescent under resting conditions, but following muscle injury they activate, migrate to the site of the injury, proliferate and differentiate into skeletal muscle, regenerating the damaged tissue. This process is tightly controlled through the sequential expression of MRFs (figure 10). Importantly, a subset of activated satellite cells returns to quiescence, replenishing the satellite cell pool (Kuang *et al.,* 2007). This way, skeletal muscle is able to retain its regenerative potential to confront subsequent muscle injuries.

Quiescent satellite cells express *Pax7* and *Myf5* (except for the *Myf5*-negative satellite stem cell population, referred below). Once activated, most satellite cells commit to differentiation, and they express *Pax7* and *MyoD1*, with variable expression of *Myf5*. These cells are known as myoblasts, which later exit the cell cycle to become myocytes. At this stage of the differentiation, expression of *Pax7* and *Myf5* is reduced whereas *Mrf4* and myogenin are induced. Finally, these myocytes fuse to each other or to damaged fibers, downregulating *MyoD1*, while sarcomeric proteins such as myosin heavy chain (MyHC) are expressed in terminally differentiated myotubes (Reviewed by Dumont *et al.*, 2015a). The balance between *Pax7* and *MyoD1* levels seems to importantly impact satellite cell fate. Thus, high *Pax7*:*MyoD1* ratios appear to promote satellite cell quiescence and medium ratios allow satellite cell proliferation, while low *Pax7*:*MyoD1* ratios induce their differentiation (Olguin *et al.,* 2007).

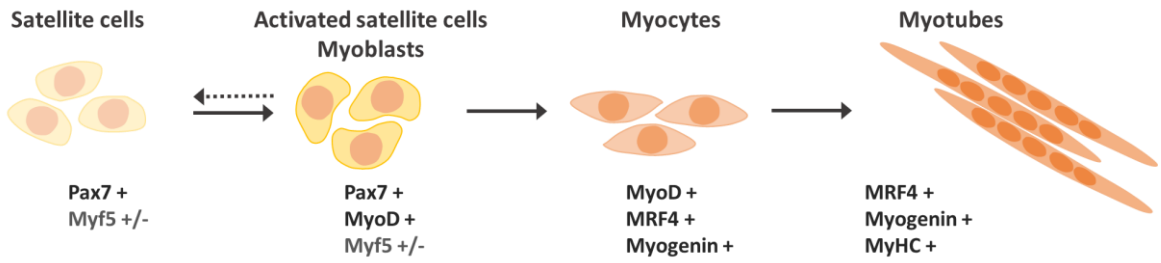

Figure 10. Sequential MRF and myogenic gene expression in terminally differentiating satellite cells. (Adapted from: Dumont *et al.,* 2015).

Although all adult satellite cells can be detected based on *Pax7* expression, different satellite cell types have been identified based on MRF expression patterns and their role during muscle regeneration. Among them, a subset of satellite cells has been described as *satellite stem cells*, characterized by the lack of *Myf5* expression both during development and after birth. This population, which has been estimated as 10% of the total satellite cell pool in mice, possesses higher self-renewal and engraftment potential and a lower tendency to differentiate into skeletal muscle, compared to *Myf5*-

expressing satellite cells. Importantly, these *Myf5*-negative cells exert a key role in the maintenance of the muscle regenerative capacity, due to their ability to perform asymmetric divisions, leading to a *Myf5*-positive committed satellite cell and a *Myf5*-negative satellite stem cell (Kuang *et al.,* 2007).

1.3.3 REGULATION OF SATELLITE CELL PERFORMANCE

Satellite cell quiescence and activation are tightly regulated processes, due to their impact in the maintenance of the muscle regenerative capacity. Although the overall RNA content of quiescent satellite cells is notably reduced when compared to activated satellite cells, more than 500 genes have been shown to be upregulated in quiescent satellite cells (Fukada *et al.,* 2007). Many of these genes are involved in common processes such as inhibition of cell cycle, proliferation and myogenesis, or they encode proteins participating in cell to cell adhesion, formation of extracellular matrix, copper and iron homeostasis, and lipid transportation (Fukada *et al.,* 2007). Moreover, these and other studies have identified proteins specifically expressed in quiescent satellite cells but not in activated satellite cells, such as calcitonin receptor (Fukada *et al.,* 2007; Gnocchi *et al.,* 2009).

It is worth noting the role of broadly expressed proteins, such as the proteins of the Notch pathway and the retinoblastoma tumor suppressor protein (Rb), in the regulation of satellite cell quiescence and activation. The Notch pathway is active in quiescent satellite cells (Bjornson *et al.,* 2012; Philippos *et al.,* 2012), likely due to the interaction of Notch receptors found in the satellite cell membrane with the Notch ligand delta1 expressed at the fiber membrane. Importantly, loss of Notch signaling in quiescent satellite cells induces their activation and differentiation (Kuang *et al.,* 2007; Bjornson *et al.,* 2012; Philippos *et al.,* 2012), whereas sustained activation of Notch signaling prevents satellite cell activation (Wen *et al.,* 2012). Additionally, Rb is highly expressed in quiescent satellite cells, but it is phosphorylated and inactivated in proliferating satellite cells. Next in the myogenic differentiation process, Rb is dephosphorylated again, inducing the cell cycle withdrawal required for terminal myogenic differentiation (Hosoyama *et al.,* 2011). Additional proteins involved in the regulation of the cell cycle, such as the negative regulator of the fibroblast growth factor 2 (FGF_2) signaling pathway sprouty-1 and the cyclin-dependent kinase inhibitor $p27^{kip1}$, are also enriched in quiescent satellite cells (Chakkalakal *et al.,* 2012).

As previously mentioned, there are several proteins that prevent satellite cell activation during homeostasis. Similarly, a quiescent satellite cell's determination to activate is affected by numerous extracellular and intracellular factors. For example, several factors released following muscle injury induce satellite cell activation. Among them, FGF_2 induces satellite cell proliferation (Kastner *et al.,* 2000; reviewed by Fu *et al.,* 2015) by activating the p38-MAPK pathway (Jones *et al.,* 2005). Similar to FGF_2, other factors such as hepatocyte growth factor (HGF) (Tatsumi *et al.,* 1998) and tumor necrosis factor

α (TNF-α)(Li, 2003) are released following muscle injury and induce satellite cell activation.

Recently, several studies have attempted to determine if the age-dependent loss of regenerative capacity of muscular tissue is due to the progressive reduction of satellite cells' intrinsic regenerative potential or due to age-dependent changes in the satellite cell niche that directly affect their performance. It remains unclear whether the number of satellite cells declines with aging *(*Shefer *et al.,* 2006) or remains relatively constant (Brooks *et al.,* 2009). Importantly, satellite cells in aged organisms seem to have increased cycling activity in resting conditions, likely due to their reduced capacity to return to quiescence following activation and self-renewal (Chakkalakal *et al.,* 2012).

Age-dependent changes in the satellite cell microenvironment clearly affect satellite cell performance. Conboy and colleagues (Conboy *et al.,* 2005) demonstrated this with heterochronic parabiosis experiments. The results demonstrated that exposure of aged satellite cells to young serum rescues their regenerative potential. Similarly, age-dependent increases of certain circulating factors appear to act on these cells. For example, reduced self-renewal capacity of satellite cells in aged organisms is potentially caused by increased amounts of FGF_2 in their microenvironment. p38, which is activated by FGF_2 signaling and localizes asymmetrically in committed progenitor cells, is also elevated in aged satellite cells (Bernet *et al.,* 2014), leading to increased myogenic differentiation and reduced self-renewal of the satellite cell pool. Importantly, pharmacological inhibition of p38 effectively rescues the regenerative potential of aged satellite cells (Cosgrove *et al.,* 2014; Bernet *et al.,* 2014). Additionally, the JAK/STAT pathway is involved in the age-dependent reduction of satellite cell self-renewal. This signaling pathway is more active in aged satellite cells when compared to young satellite cells, perhaps due to increased serum IL-6 levels in aged organisms (Tierney *et al.,* 2014). Overactivation of JAK/STAT signaling pushes satellite stem cells to undergo asymmetric divisions instead of symmetric divisions, thereby decreasing the satellite stem cell self-renewal (Price *et al.,* 2014). Similarly, age-dependent increases of muscle transforming growth factor beta (TGF-β) levels activate mothers against decapentaplegic homolog 3 (*Smad3*), which in turn inhibits Notch signaling, impairing satellite cell self-renewal (Carlson *et al.,* 2008). Age-dependent increases of Wnt signaling in aged satellite cells could also impact muscle regeneration since it antagonizes Notch signaling in satellite cells (Brack *et al.,* 2008) and favors the conversion of myogenic cells into fibrotic cells (Brack *et al.,* 2007).

As previously mentioned, there is evidence demonstrating the activation of cell-intrinsic age-dependent mechanisms that induce the loss of regenerative capacity. Sousa-Victor and colleagues (Sousa-Victor *et al.,* 2014) reported that satellite cells in 30 month-old mice retain a reduced regenerative capacity since quiescent satellite cells switch to irreversible senescence, losing their ability to activate following injury. The cell cycle inhibitors $p16^{INK4a}$ and $p19^{Arf}$ were highly expressed in these senescent satellite cells,

which were not able to recover their regenerative potential even when exposed to a young microenvironment (Sousa-Victor *et al.,* 2014).

Therefore, both cell intrinsic factors and environmental changes seem to contribute to the age-dependent loss of muscle regenerative potential.

1.3.4 OTHER CELL TYPES WITH SKELETAL MUSCLE REGENERATIVE POTENTIAL

Besides satellite cells, several other cell types found outside of the basal lamina have been shown to have *in vitro* myogenic potential, as well as the ability to contribute to muscle regeneration *in vivo*. These cells have attracted the attention of the scientific community, which has tested their potential for the development of cell transplantation-based therapies to treat muscle pathologies.

One of these cell types are neural stem cells (NSC), which are able to differentiate into skeletal muscle *in vitro* when cocultured with myoblasts, as well as *in vivo* following intramuscular transplantation (Galli *et al.,* 2000). Similarly, it has been shown that bone marrow-transplanted cells also contribute to muscle regeneration following muscle injury in mice (Ferrari *et al.,* 1998). This fact has been confirmed in humans through the detection of donor-derived cells in the muscles of bone marrow-transplanted Duchenne muscular dystrophy (DMD) patients (Gussoni *et al.,* 2002). Additionally, therapeutic approaches have been tested by concentrating this myogenic progenitor-enriched fraction, termed *side population* (SP), prior to transplantation (Gussoni *et al.,* 1999; Ferrari *et al.,* 2001). The myogenic potential of pericytes has also been tested for the treatment of DMD (Dellavalle *et al.,* 2007). Likewise, CD133-positive circulating stem cells have been shown to express early myogenic markers. CD133-positive cells have also been isolated from muscle, and their therapeutic potential has been tested for the treatment of DMD (Torrente *et al.,* 2004; Benchaouir *et al.,* 2007). However, each of these therapeutic approaches have failed to translate into treatments for affected humans since the frequency of the myogenic contribution of these cells is not high enough to functionally benefit the patients. Additional cell types have also shown myogenic potential, such as mesoangioblasts (Sampaolesi *et al.,* 2003), bone marrow stromal cells (Dezawa *et al.,* 2005) and myoendothelial cells (Zheng *et al.,* 2007). Multipotent adipose-derived stem cells (MADSCs) also have myogenic potential that can be enhanced by the transient expression of *MYOD1* (Goudenege *et al.,* 2009).

During the last decade, embryonic stem (ES) cells and induced pluripotent stem (iPS) cells have been investigated and appear promising for future cell-transplantation therapies for muscular dystrophies. Numerous protocols have been published describing the myogenic induction of these pluripotent stem cells, both *in vitro* and *in vivo* (Awaya *et al.*, 2012; Darabi *et al.*, 2012; Chal *et al.*, 2015, 2016; Maffioletti *et al.*, 2015; Shoji *et al.,* 2015; Iovino *et al.*, 2016), which involve culturing the cells in specific

conditions, selection of myogenic cells through FACS and/or transient expression of exogenous genes (reviewed by Kodaka *et al.,* 2017).

2. MUSCULAR DYSTROPHIES, LGMD2A AND CALPAIN 3

2.1 MUSCULAR DYSTROPHIES

Muscular dystrophies are a heterogeneous group of inherited disorders affecting skeletal muscle (Emery, 2002). From a clinical point of view, these diseases induce a progressive muscular degeneration that leads to muscle weakness. Each type of muscular dystrophy shows a specific pattern of predominantly affected muscles, progression rate and age of onset of the symptoms. Importantly, respiratory, cardiac and facial muscles may also be affected in some specific muscular dystrophies.

Myotonic dystrophy (DM), or *Steinert's Disease,* is the most common form of muscular dystrophy in adults. DM1, the most frequent form of DM, is caused by a pathological (CTG) triplet expansion in the 3' untranslated region (UTR) of the dystrophia myotonica protein kinase (DMPK) gene. These patients suffer a progressive muscular weakness, atrophy and myotonia, as well as other clinical manifestations such as cardiomyopathy, cognitive decline, insulin resistance and cataracts, resembling an accelerated aging phenotype (Reviewed by Mateos-Aierdi *et al.,* 2015).

As for muscular dystrophies affecting children, Duchenne muscular dystrophy (DMD) and its more benign form known as Becker muscular dystrophy (BMD), are the most common and severe forms of dystrophy. These diseases are caused by mutations in the dystrophin-coding gene located in the X chromosome. DMD symptoms appear in the early childhood and muscle degeneration progresses fairly quickly. Cardiac abnormalities and respiratory difficulties lead to problems to the affected patients. Although there is no cure for these diseases, palliative care such as physiotherapy and assisted ventilation have effectively increased the life expectancy of patients from the teen years up to the 40's or 50's (Carter *et al.,* 2012).

To date, the genetic origin of most muscular dystrophies has already been elucidated (Kaplan and Hamroun, 2014). However, further investigation is still required to understand the pathogenic mechanism of many of these diseases. The disease-causing mutated genes encode proteins involved in a wide range of biological processes, such as dystrophin, which binds the sarcomere with the sarcolemma (Hoffman *et al.,* 1987), emerin (Bione *et al.,* 1994) and lamin A/C (Bonne *et al.,* 1999), located in the nuclear envelope, mannosiltransferases POMT1 (D'Amico *et al.,* 2006) and POMT2 (Biancheri *et al.,* 2007), which perform post-translational glycosylation, and RNA-binding proteins, such as Poly(A)-binding protein PABP2 (Brais *et al.,* 1998). Noticeably, these mutations affect both ubiquitously expressed and muscle-specific genes. The following figure (figure 11) represents proteins that lead to muscular dystrophies when mutated.

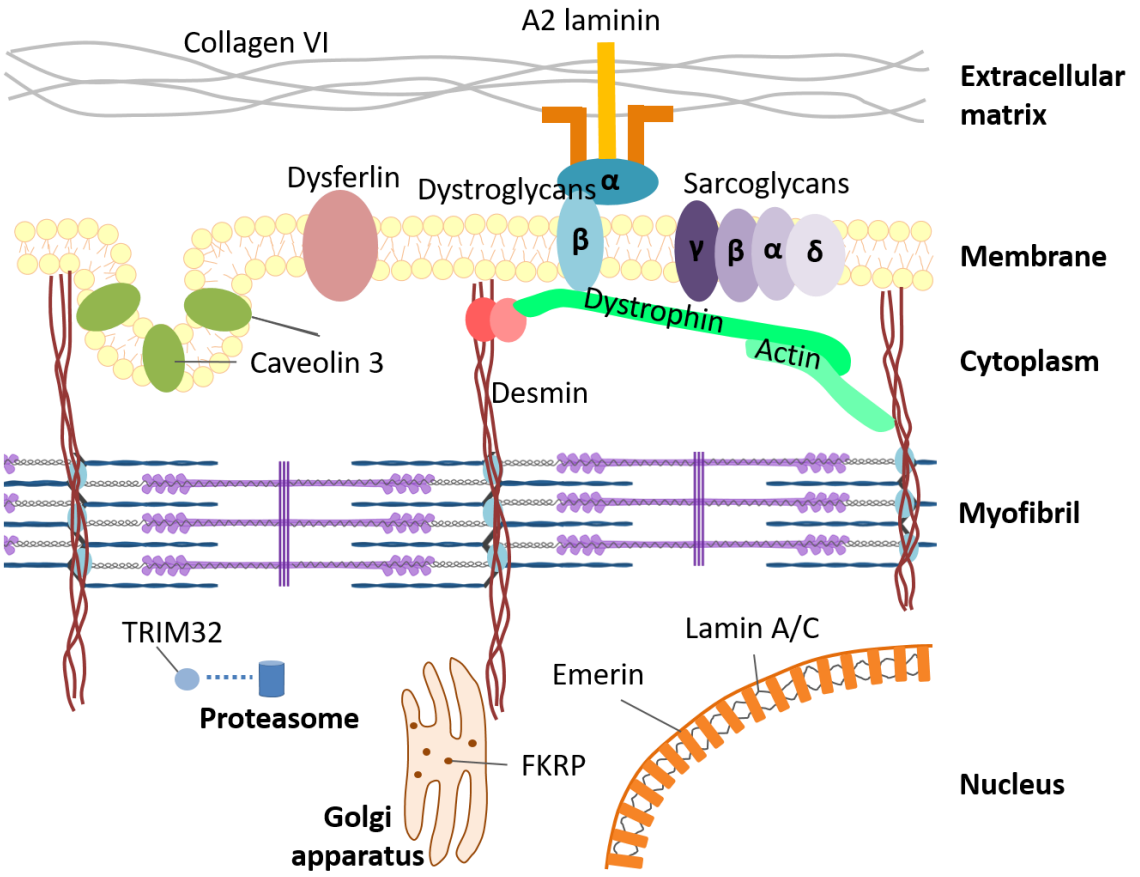

Figure 11. Representation of a myofiber section, where different dystrophy-related proteins are indicated. (Adapted from: www.afm-telethon.com).

2.1.1 MUSCLE REGENERATION AND SATELLITE CELLS IN MUSCULAR DYSTROPHIES

It is evident that muscle regeneration mechanisms are not sufficient to repair the muscle wasting in patients with muscular dystrophy. Several studies have shown that satellite cells are involved in the pathophysiology of various muscular dystrophies (reviewed by Randolph and Pavlath, 2015). One of the most evident cases was described by Sacco and colleagues (Sacco *et al.,* 2010), who demonstrated that muscle stem cells in a DMD mouse model lose their regenerative potential due to their exhaustion. Next, it was shown that the number of satellite cells is increased in young *mdx* mice (a DMD mouse model), but however, as the disease progresses, loss of Notch signaling leads to the depletion of the satellite cell population, impairing the muscle regenerative potential (Jiang *et al.,* 2014). *In vitro* studies have also reported that DMD patient-derived myoblasts have a considerably shortened lifespan (Webster and Blau, 1990). However, contrary to what is expected, some authors have reported increased satellite cell number in DMD patients (Kottlors and Kirschner, 2010). Similar defects have also been described in satellite cells in other dystrophies, such as LGMD2H (Kudryashova *et al.,* 2012) and myotonic dystrophy (Thornell *et al.,* 2009).

Overall, this deficient satellite cell performance in muscular dystrophies may derive from two different causes. On the one hand, the chronic muscle degeneration occurring in muscular dystrophies could induce satellite cells to be constantly activated to confront the sustained regenerative demands of the affected tissues, leading to satellite cell exhaustion. On the other hand, satellite cell-intrinsic defects could emerge if the mutated genes that cause the dystrophy are expressed in these cells, playing a specific role (Morgan and Zammit, 2010).

One example of this second cause of satellite cell impairment has been described in a recent study (Servián-Morilla *et al.,* 2016), which has identified the first case of muscular dystrophy due to mutations in the *POGLUT1* gene. This disease presents an autosomal recessive inheritance pattern with late onset and has been classified as limb-girdle muscular dystrophy (LGMD). The genetic mutation induces a dramatic reduction of Notch signaling in muscle satellite cells, causing their defective self renewal and increased differentiation that ultimately leads to satellite cell depletion. Loss of adequate Notch signaling in satellite cells is also implicated in the physiopathology of DMD (Jiang *et al.,* 2014). Importantly, overexpression of the Notch activator protein Jagged1 in dystrophin-deficient dogs has been shown to notably ameliorate dystrophic symptoms (Vieira *et al.,* 2015).

Since both the regenerative requirements, as well as satellite cell performance, appear to differ among different muscles (Ippolito *et al.,* 2012; reviewed by Randolph and Pavlath, 2015), the implication of satellite cells in muscular dystrophies could partially clarify why each muscular dystrophy affects a specific subset of muscles (Reviewed by Randolph and Pavlath, 2015).

2.2 LIMB-GIRDLE MUSCULAR DYSTROPHY TYPE 2A

Limb-girdle muscular dystrophy type 2A (LGMD2A) or calpainopathy (OMIM: 253600) is a genetically defined muscular dystrophy that presents an autosomal recessive inheritance pattern. LGMD2A patients develop a slowly progressive muscular weakness affecting both scapular and pelvic girdles, as well as proximal lower limb muscles (Fardeau *et al.*, 1996a; Fardeau *et al.*, 1996b; Kawai *et al.*, 1998). Strickingly, two recent studies have reported a dominant form of calpainopathy with a similar but milder phenotype compared to LGMD2A (Vissing *et al.,* 2016; Martinez-Thompson *et al.,* 2017). This fact potentially impacts the study of calpainopathies, as well as the understanding of the role of calpain 3 in skeletal muscle.

2.2.1 EPIDEMIOLOGY

LGMD2A is one of the most frequent recessive LGMD forms, globally accounting for approximately 30% of all recessive LGMD cases (Dinçer *et al.,* 1997; Richard *et al.,* 1997; Topaloglu *et al.,* 1997; Chae *et al.,* 2001; de Paula *et al.,* 2002; Zatz and Starling, 2005).

It is worth noting that this prevalence is considerably higher in specific regions, such as some Amish communities in the USA (Allamand *et al.,* 1995), the Reunion Island, where 95% of LGMDs correspond to calpainopathies (Fardeau *et al.*, 1996b), and the province Gipuzkoa in Spain, where 79% of LGMDs are type 2A (Urtasun *et al.,* 1998). Moreover, frequencies in these regions are also the highest ones known across the world, with 48 cases per million inhabitants in the Reunion Island (Fardeau *et al.*, 1996b), 69 cases per million in Gipuzkoa (Urtasun *et al.,* 1998) and 40 cases out of 3000 inhabitants in an Amish population (reviewed by Gallardo, *et al.,* 2011).

2.2.2 CLINICAL FEATURES

Considerable heterogeneity is observed in LGMD2A disease outcomes, both among affected members of the same family and among unrelated patients (Fardeau *et al.*, 1996a; Fardeau *et al.*, 1996b; Pénisson-Besnier *et al.*, 1998; Zatz *et al.,* 2000; de Paula *et al.*, 2002). Initial symptoms usually appear during the second decade of life, although some cases report the beginning of symptoms as early as 2 years and as late as 50 years of age (Reviewed by Gallardo *et al.,* 2011). Muscle degeneration is progressive and patients may show a staggering or tip toe walking. Difficulties to lift weight, climb stairs, run and/or get up from a chair or from the floor keep increasing during the progression of the disease (Urtasun *et al.,* 1998; Pollitt *et al.,* 2001). Affected individuals become wheelchair-bound approximately one or two decades after the beginning of the symptoms, depending on the progression rate and age of onset (Fardeau *et al.*, 1996a; Fardeau *et al.*, 1996b; Urtasun *et al.*, 1998). To date, there are no effective treatments for this disease, and only palliative care, such as physiotherapy, can exert beneficial effects in the affected patients.

Muscle weakness predominantly affects shoulder and pelvic girdles, as well as proximal limb muscles. In the majority of patients, weakness begins in the pelvic girdle. However, in some cases shoulder girdle muscles are firstly affected, or both girdles suffer a simultaneous weakness. Trunk muscles and posterior thigh muscles suffer a prominent atrophy, being the *adductor magnus* and *semimembranous muscle* two of the predominantly affected muscles. A recent study has reported that *soleus*, *vastus intermedius* and *biceps femoralis* also suffer a pronounced decline in affected patients (Richard *et al.,* 2016). Moreover, magnetic resonance imaging (MRI) has shown that some distal muscles, such as the *soleus*, are also affected in the early stages of the disease (Mercuri *et al.,* 2005). Distal lower limb hypertrophy has been described in a Brazilian LGMD2A population, although this feature is not shared by most European patients (de Paula *et al.,* 2002). Affected individuals may often experience contractures in the hips, knees, elbows, fingers, Achilles tendon and backbone area, and they might develop shoulder bone protrusions known as *scapula alata* (Pollitt *et al.,* 2001) (figure 12).

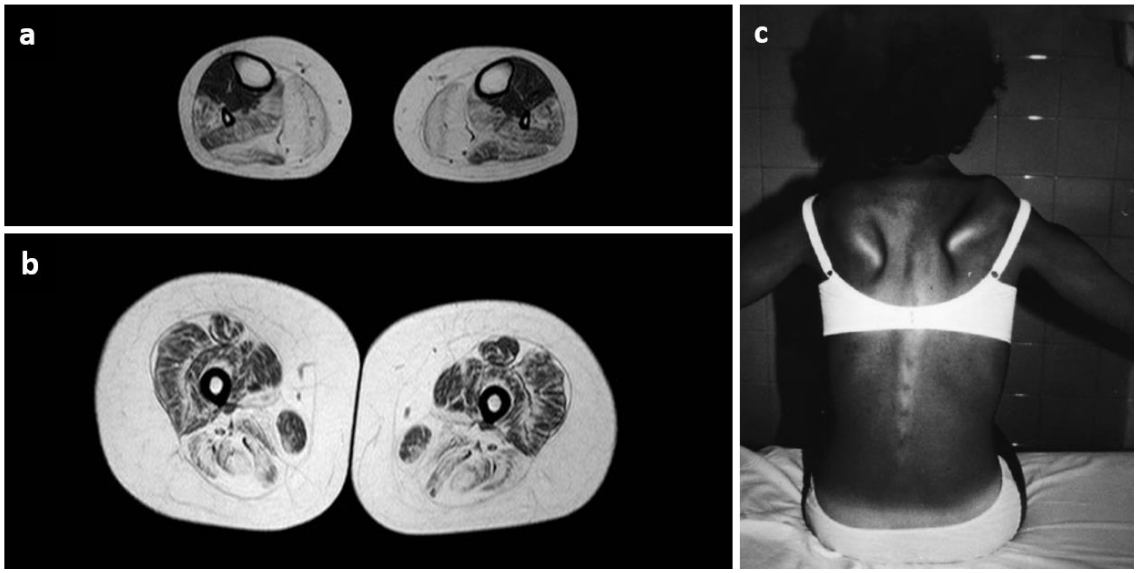

Figure 12. Magnetic resonance images and *scapula alata*. Magnetic resonance images of a) calves and b) thighs of an ambulant LGMD2A patient (kindly provided by Dr. Fernández-Torrón). c) Scapular winging in a LGMD2A patient. (From: Urtasun *et al.,* 1998).

It is worth noting that contrary to some other muscular dystrophies, cardiac and facial muscles are not affected in LGMD2A, and patients do not show mental retardation (Dinçer *et al.,* 1997; Topaloglu *et al.,* 1997). Some patients may experience mild respiratory insufficiency in advanced stages of the disease as a result of abdominal muscle weakness (Urtasun *et al.,* 1998). Muscular impairment is slightly more significant in men than in women (Richard *et al.,* 2016).

Patients with the previously described dominant form of calpainopathy show clinical symptoms that resemble those of LGMD2A patients, although with an overall milder phenotype. Of note, these patients manifest myalgia and back pain as predominant symptoms in addition to the LGMD2A-like muscle affectation (Vissing *et al.,* 2016).

Blood tests show that similar to other muscular dystrophies, patients experience a marked increase of their serum creatine kinase (CK) levels (5-80 times increased) in the early stages of the disease, but it progressively decreases to normal levels in wheelchair-bound patients (Urtasun *et al.,* 1998). However, unaltered serum CK levels have been reported in several affected members of the same family with various severity (Starling *et al.,* 2003). Overall, these CK increases are moderate compared to other muscular dystrophies such as DMD, dysferlinopathies and LGMD2I (Gallardo *et al.,* 2011).

2.2.3 HISTOPATHOLOGICAL FEATURES

Similar to the clinical features of LGMD2A, muscle biopsies of these patients are greatly variable, even among different patients with the same mutations (Chae *et al.,* 2001; Fanin *et al.,* 2003). These biopsies display common dystrophic features, such as necrotic areas with regenerative regions, fiber size variability and disorganized myofibrils, as well

as a variable degree of fibrosis that increases as the disease progresses (figure 13) (Fardeau *et al.*, 1996b; Chae *et al.*, 2001; Keira *et al.*, 2007). During the early stages of the disease, eosinophilic infiltrations are observed in these biopsies as well as in peripheral blood, although they tend to diminish and disappear as the disease progresses (Krahn *et al.,* 2006; Amato, 2008; Krahn *et al.,* 2011; Rosales *et al.,* 2013). An increased number of apoptotic nuclei compared to other muscle dystrophies have also been reported (Baghdiguian *et al.,* 1999). It is remarkable that the amount of satellite cells continues to increase as the disease progresses (Rosales *et al.,* 2013).

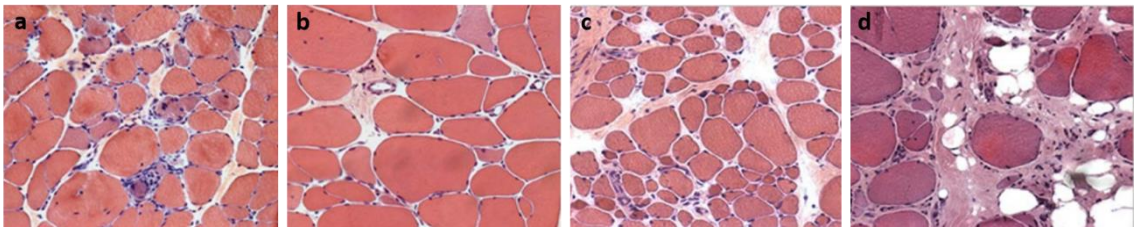

Figure 13. Hematoxylin-eosin staining of muscle sections of LGMD2A patients at different stages of the disease. Images show a) degenerating fibers and blood cell infiltrations, indicative of inflammation, b) fiber size variability, centrally nucleated regenerating fibers and fibrosis, c) considerable connective tissue (fibrosis) and d) adipose tissue infiltrations. Original magnification (200x) (From: Fanin and Angelini, 2015).

Staining of muscle sections to detect oxidative enzymatic activity demonstrated that lobulated fibers are often found in these biopsies (Guerard *et al.,* 1985; Kawai *et al.,* 1998; Chae *et al.,* 2001; Hermanová *et al.,* 2006; Keira *et al.,* 2007), as it happens in other muscular dystrophies (Guerard *et al.,* 1985; Figarella-Branger *et al.,* 2002). This is potentially caused by disorganized mitochondria and myofibrils found in affected fibers (Chae *et al.,* 2001). Biopsies of patients with the dominant form of calpainopathy show similar, but milder, histological traits with central nucleation and fiber size variability, sporadic cell necrosis, ring fibers and increased fibrosis (Vissing *et al.,* 2016).

As for the differential fiber type-specific affectation, muscle biopsies display different outcomes depending on the study sample. For example, a cohort of Japanese patients had an increased proportion of type I fibers, but also increased atrophy of these fibers, (Chae *et al.,* 2001), whereas a cohort of Czech patients displayed a type II fiber atrophy and loss as well as type I lobulated and hypertrophic fibers (Hermanová *et al.,* 2006). Other authors have also reported an increased number of type I fibers in muscles of patients in advanced disease stages (Fardeau *et al.,* 1996b; Rosales *et al.*, 2013).

2.2.4 GENETIC CAUSE OF LGMD2A

Many LGMD forms are caused by mutations in genes that encode structural muscle proteins. LGMD2A is caused by mutations in *CAPN3* gene, which encodes an enzyme known as calpain 3 or p94 (Richard *et al.,* 1995). This non-lysosomal protease is highly expressed in skeletal muscles and, despite its protease activity, structural roles have also been attributed to this protein.

Calpain 3 was first described in 1989, when Sorimachi and colleagues (Sorimachi *et al.,* 1989) detected the expression of a skeletal muscle-specific transcript that showed high homology with the ubiquitously expressed calpain 1 and calpain 2. *CAPN3* gene is a 53Kb sequence located in chromosome 15q15.1-q21.1. It contains 24 exons of variable length, ranging from 12 to 309 nucleotides (Richard *et al.,* 1995). To date, several transcript variants have been described, which are generated as a result of the alternative splicing of the gene and due to different promoters that can activate its transcription in different tissues (Herasse *et al.,* 1999; Kawabata *et al.,* 2003). Among them, the longest and most common isoform leads to an 821 amino acid calpain 3 protein.

Since 1995, when the genetic cause of LGMD2A was discovered, more than 450 pathogenic mutations have been reported in *CAPN3* gene (Reviewed by Kramerova *et al.,* 2007; Richard *et al.,* 2016). This includes point mutations that lead to premature stop codons, mutations that affect splice sites, mutations that alter the reading frame, or even bigger insertions and deletions (http://www.dmd.nl). These mutations induce various protein outcomes, such as loss of the protein or the impairment of its enzymatic activity (Ono *et al.,* 1998; Fanin *et al.,* 2003). Other mutations do not alter the enzymatic activity, but they affect its titin-binding affinity (Ono *et al.,* 1998; Kramerova *et al.,* 2004), which suggests that calpain 3 is a multifunctional protein. Interestingly, 20-30% of LGMD2A patients present normal muscle calpain 3 levels in Western blot analysis. Besides the wide range of pathogenic mutations described, some of them are highly prevalent, such as the c.2362_2363delinsTCATCT, also known as the “Basque mutation” due to its high prevalence in this population.

As previously mentioned, LGMD2A phenotypes are variable among different patients regarding their severity, age of onset and progression rate. Currently, there are several studies aimed to establish a relationship between the mutations observed in *CAPN3* gene in LGMD2A patients and their disease outcomes. Nevertheless, it has not been possible to directly correlate the mutations found in different patients and their disease severity (Urtasun *et al.,* 1998; de Paula *et al.,* 2002; Sáenz *et al.,* 2005). However, it is worth noting that in general, patient with two null mutations in their *CAPN3* alleles appear to develop a more severe phenotype of the disease with an earlier onset, compared to patients that harbor at least one missense mutation (Fardeau *et al.,* 1996a; Fardeau *et al.,* 1996b; Chae *et al.,* 2001; de Paula *et al.,* 2002; Sáenz *et al.,* 2005; Hermanová *et al.,* 2006; Fanin *et al.,* 2007a). Intermolecular complementation could also partially explain this weak genotype:phenotype correlation (Sáenz *et al.,* 2011; Ono *et al.,* 2014). As previously mentioned, an autosomic dominant form of calpainopathy caused by a 21 bp in-frame deletion has recently been reported, demonstrating a comparable, but milder, phenotype than LGMD2A patients. The authors suggest that the mutated *CAPN3* allele in these patients potentially leads to calpain 3 proteins that exert a dominant negative effect (Vissing *et al.,* 2016; Martinez-Thompson *et al.,* 2017).

2.2.5 EXPERIMENTAL APPROACHES TO TREAT LGMD2A

The development of novel therapeutic approaches to treat muscular dystrophies is progressing rapidly. A majority of these experimental treatments consist of cell transplantation approaches as well as gene therapies aimed at restoring the expression of the wild type version of the disease-causing gene in affected tissues. However, many of these approaches have failed to reproduce the beneficial effects observed in laboratory animals when transferred to humans, primarily due to the great difficulty of delivering the treatment (cells, viruses, short oligonucleotide sequences, etc.) to the large amount of skeletal muscle tissue found in humans.

As for calpainopathy, efficacy of adeno-associated virus-mediated gene transfer of calpain 3 was tested in an animal model of the disease (Bartoli *et al.,* 2006). The therapy induced the expression of a functionally active calpain 3 in the sarcomere, although the clinical improvement was modest. Dose increases led to cardiac toxicity, but this undesired effect was circumvented when calpain 3 expression was restricted to skeletal muscle, preventing cardiac toxicity (Roudaut *et al.,* 2013).

In an alternative attempt, gene therapy has been studied to halt the progression of muscle dystrophy by transferring genes that do not cause the disease if mutated, but can still exert a positive effect in this tissue. Myostatin, a negative regulator of muscle mass, was inhibited in a mouse model of calpainopathy by overexpressing a mutated version of the gene (Bartoli *et al.,* 2007). Blockage of myostatin was able to ameliorate the dystrophic phenotype in this animal model. However, this gene therapy was not successful to treat α-sarcoglycan deficiency (Bartoli *et al.,* 2007). To date, none of these therapeutic approaches have been tested in LGMD2A patients.

2.3 CALPAIN PROTEASES AND CALPAIN 3

2.3.1 THE CALPAIN SUPERFAMILY

Calpains (calcium-dependent papain-like proteases) are a group of non-lysosomal proteases whose activity depends on the intracellular calcium ion level (Guroff, 1964; reviewed by Goll *et al.*, 2003). Calpains are found in a wide range of species, from prokaryotic organisms to mammals. Currently, 15 different calpains have been identified in humans, some of them ubiquitously expressed, whereas others show tissue specificity (table 3).

Calpain 1 (CAPN1 or μCL) and calpain 2 (CAPN2 or mCL) are the best understood members since they were the first calpains to be discovered and they are both ubiquitously expressed. Each of them comprises two subunits: an 80 kDa subunit, where the active site is located, and the 28 kDa subunit known as CAPNS1, which regulates the activity of the 80 kDa subunit and provides stability to the protein structure, acting as a chaperone (reviewed by Goll *et al.*, 2003; Kramerova, *et al.,* 2007; Ono *et al.*, 2016).

The study of the protein structure has revealed that the big subunit of calpains comprises at least 4 domains whereas the small subunit has at least 2 domains (Moldoveanu *et al.*, 2002; Reviewed by Campbell and Davies, 2012). The domains in the big subunit are the following:

Domain I: the propeptide domain.
Domain II: the catalytic domain, named CysPc, is divided into two subdomains; PC1 (or domain IIa) and PC2 (or domain IIb). Both subdomains harbor calcium-binding sites, as well as amino acids that constitute the catalytic triad.
Domain III: this is the calcium-binding and phospholipid-binding C2 domain (Tompa et al., 2001), nowadays named as CBSW (Calpain-type Beta-SandWich domain).
Domain IV: it is the C-terminal calcium-binding domain, which harbors five EF sequences (penta-EF, PEF).

The small subunit consists of two domains:

Domain V: a glycin- and proline-rich domain.
Domain VI: an EF sequence-containing region similar to domain IV.

Although the small subunit of calpains is ubiquitously expressed, only calpain 1 and calpain 2 bind this subunit *in vivo* (Ono and Sorimachi, 2012). Both subunits bind non-covalently to each other through the EF domains located in their C-terminal region (reviewed by Goll *et al.*, 2003; Kramerova *et al.,* 2007; Ono *et al.*, 2016).

Some members of the calpain superfamily contain domains I to IV and therefore, are known as *classical calpains*, whereas other calpains that lack one or more of these domains are termed *non-classical* calpains (figure 14).

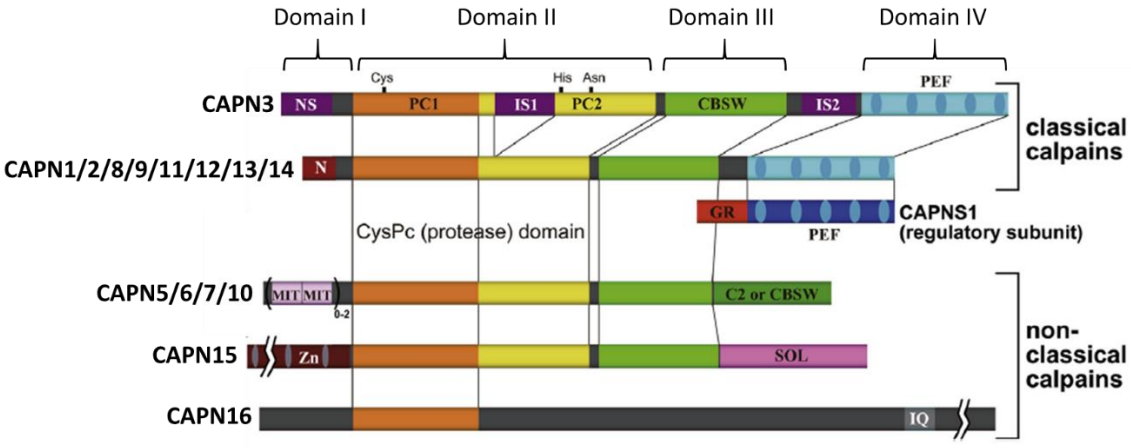

Figure 14. Schematic representation of the structure of human calpains. NS, N-terminus sequence; IS1, Insertion Site 1; IS2, Insertion Site 2; *N*, N-terminus domain; GR, Gly-rich domain; MIT, microtubule interacting and transport motif; *C2*, protein C conserved domain 2; Zn, zinc-finger motif; SOL, small optic lobes product homology domain; IQ, calmodulin (CaM)-interacting motif. (Adapted from: Ono *et al.,* 2016).

Activity of calpains is implicated in multiple pathologies, such as cataracts (Biswas *et al.,* 2004) and brain ischemia (Bartus *et al.,* 1994). Similarly, calpain deficiency can lead to pathological conditions, known as calpainopathies. Table 3 summarizes the expression preference of calpain genes and the phenotypes derived from its deficiency.

Gene	Expression preference	Deficiency phenotype
Capn1	Most cells	Platelet dysfunction
Capn2	Most cells	Embryonic lethal
CAPN3, Capn3	Skeletal muscle	Muscular dystrophy
CAPN5, Capn5	Most cells	Vitreoretinopathy
Capn6	Embryonic muscle	Hypergenesis
Capn7	Most cells	Under investigation
Capn8	Gastrointestinal tract	Gastric ulcer
Capn9	Gastrointestinal tract	Gastric ulcer
CAPN10	Most cells	Type 2 diabetes
Capn11	Testis	Under investigation
Capn12	Hair follicle	Under investigation
Capn13	Most cells	No information
CAPN14	Esophagus	Eosinophilic esophagitis
CAPN15/SOLH	Most cells	No information
Capn16/Adgb/C6orf103	Testis	Under investigation

Table 3. Expression preference of calpain genes in humans (genes in capital letters) and mice (genes in lower case) and the phenotypes derived from their deficiency. (From: Ono and Sorimachi, 2012).

2.3.2 CALPAIN 3

2.3.2.1 STRUCTURE

Calpain 3 contains the four domains found in *classical calpains*. Domains I-IV show more than 50% homology with other calpains. Importantly, calpain 3 also harbors three unique sequences named (1) NS, a 47 amino acid sequence located in the N-terminal domain, (2) IS1, a 48 amino acid sequence in domain II, and (3) IS2, a 77 amino acid sequence between domains III and IV, which contains a nuclear localization motif (figure 15). Among them, IS1 and IS2 sequences are only found in calpain 3, which suggests that these two regions could perform calpain 3-specific roles. In particular, it has been shown that IS1 contains the autocatalytic activity of the enzyme (Kinbara *et al.,* 1998).The three key amino acids that constitute the active site are located adjacent to IS1: Cys-105 (located in PC1), His-262 and Asn-286 (located in PC2) (Sorimachi and Suzuki, 2001; Moldoveanu et al., 2002). This region itself could block the active site of calpain 3 until it is proteolyzed, avoiding substrates to access the active site (García-Diaz *et al.,* 2004). Conversely, IS2 enables the interaction between calpain 3 and titin in the cytoplasm (Sorimachi *et al.,* 1995) and it could also control the subcellular localization of calpain 3

since it contains a nuclear localization signal (Sorimachi *et al.,* 1993, 1995), as well as exerting fodrinolytic activity (Herasse *et al.,* 1999).

Contrary to conventional calpains, which associate with the smaller subunit CAPNS1, calpain 3 molecules potentially bind in pairs through their penta-EF domains, forming homodimers (Kinbara *et al.,* 1998; Ravulapalli *et al.,* 2005; Partha *et al.,* 2014). However, homodimerization of full-length calpain 3 molecules has not been reported yet, likely because this dimerization might be sensitive to calcium ion levels (Ono *et al.,* 2016).

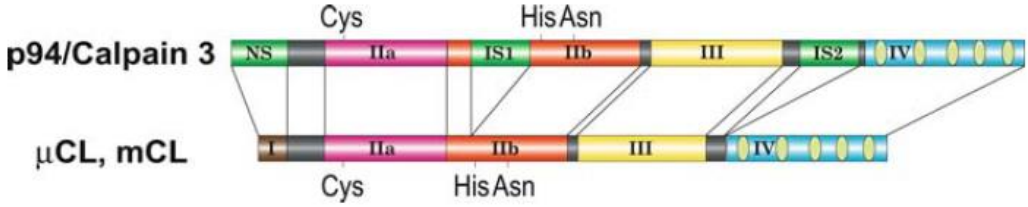

Figure 15. Schematic representation of the structure of conventional calpains and calpain 3 (From: Ojima *et al.,* 2005).

2.3.2.2 EXPRESSION AND ISOFORMS

CAPN3 is basally expressed in almost all tissues. Nonetheless, this gene is predominantly expressed in skeletal muscle tissue, where its expression level is ten times higher than that of the ubiquitous calpains (Sorimachi *et al.,* 1989). Of note, calpain 3 levels appear to be higher in type IIa and type IIb fibers compared to type I fibers in porcine muscle extracts (Jones *et al.,* 1999).

Different calpain 3 isoforms have been detected in several tissues, such as the lens (Ma *et al.,* 2000), retina (Azuma *et al.,* 2000), cornea (Nakajima *et al.,* 2001), brain and smooth muscle (Herasse *et al.,* 1999), which lack one or more of the mentioned unique domains. Alternative promoters may also activate the transcription of calpain 3 in specific tissues, leading to different calpain 3 isoforms (Kawabata *et al.,* 2003).

Similarly to tissue-specific isoforms, different splicing variants of calpain 3 have been detected during embryonic muscle development, some of them lacking the exons that encode the IS1 region (exon 6) and/or the IS2 sequence (exons 15 and 16), or variants including a newly generated exon located in intron 16 (Herasse *et al.,* 1999). These "immature" calpain 3 isoforms are found during embryonic development and the perinatal stage. However, in adult mice, they are only found in regenerating skeletal tissue, which suggests that IS1 and IS2 exert specific roles during adulthood (Herasse *et al.,* 1999). Importantly, overexpression of the calpain 3 variant lacking IS1 region (encoded by exon 6) in adult mice induces centrally nucleated fibers with variable diameter. This phenotype has been linked to lack of proper maturation of the fibers rather than a defect in the regenerative process, since skeletal muscles in these mice do not show regenerative areas, elevated serum CK levels, or cell membrane damage (Spencer *et al.,* 2002).

These immature isoforms are more stable than the full-length calpain 3, which is rapidly autolyzed both following *in vitro* overexpression and in muscle homogenates (Sorimachi *et al.,* 1993; Kinbara *et al.,* 1998; Guyon *et al.,* 2003). This increased stability could be due to reduced sensitivity to calcium. Importantly, calpain 3 can also be activated through a calcium-independent mechanism (Kinbara *et al.,* 1998).

CAPN3 expression has also been studied in human embryos by *in situ* hybridization. It has been reported that this gene is also expressed in cardiac tissues at early developmental stages, but later, its expression is limited to skeletal muscle (Fougerousse *et al.,* 1998). Immature *CAPN3* isoforms are detected in fetal muscles beginning at 10-12 weeks, which follow specific distribution patterns (Fougerousse *et al.,* 1998). This differential splicing of *CAPN3* during the embryonic development, postnatal growth and adulthood suggests that *CAPN3* isoforms play specific roles during muscle development and regeneration (Kramerova *et al.,* 2007).

2.3.2.3 ACTIVATION MECHANISM

The fact that full-length calpain 3 is extremely unstable in muscle extracts as well as in most cell lines has hampered the study of its structure and its activation mechanism (Sorimachi *et al.,* 1993). Therefore, more stable mutant versions and isoforms lacking one or several exons have been expressed using *in vitro* gene expression systems and cell cultures to elucidate its enzymatic mechanism (Federici *et al.,* 1999; Herasse *et al.,* 1999, Ono *et al.,* 2006, 2007).

The rapid calpain 3 degradation could be caused by its sensitivity not only to calcium ions, but also to sodium ions (Ono *et al.,* 2010). Using *in vitro* expression systems, it has been determined that calpain 3 is activated at 100 mM sodium ion concentration, and at 0.01 mM calcium ion level. Nevertheless, these activation concentrations decrease substantially when both ions are added at the same time, making calpain 3 a very unstable protein (Ono *et al.,* 2010). However, these values can differ in skeletal muscle tissue, where binding of calpain 3 to myogenic proteins could make it more resistant to activation. In this regard, is has also been reported that calpain 3 is only activated after prolonged periods of increased cytosolic calcium levels, but not after normal exercise, which only causes short calcium increases (Murphy and Lamb, 2009).

Based on these and other experimental evidence, a two-step activation mechanism for calpain 3 has been suggested. According to this mechanism, binding of calcium ions to calpain 3 causes a conformational change in the proteolytic domain. Consequently, the three key amino acids, known as the catalytic triad, move closer to each other, forming the active site (García-Díaz *et al.,* 2006). This step is known as *intramolecular activation*. Next, calpain 3 is autolyzed at the IS1 region. As a result, the three key amino acids of the active site are distributed in the two resulting 31 kDa and 58 kDa fragments, but calpain 3 retains its enzymatic activity as long as these two fragments remain together. Subsequently, proteolysis of the IS2 region leads to enzymatic inactivation. Binding of

calpain 3 to muscle proteins, such as titin, through its IS2 region appears to prevent its activation (Ono *et al.,* 2006). Recently, a protein named PLEIAD has also been found to interact with calpain 3, suppressing its protease activity (Ono *et al.,* 2013). Phosphorylation of the IS2 region might also prevent calpain 3 autolysis in differentiated muscle cells, allowing calpain 3 to perform a structural role (Ojima *et al.,* 2014).

Importantly, Ono and colleagues have reported that calpain 3 activity of two mutated versions of the protein can be rescued when the two mutations are distributed in both protein fragments derived from IS1 autolysis. This is attributed to the *intermolecular complementation* of the two wild type fragments of the proteins (Ono *et al.,* 2014). This phenomena could contribute to understanding the weak genotype:phenotype correlations observed among LGMD2A patients (Sáenz *et al.,* 2011; Ono *et al.,* 2014).

2.3.2.4 ROLE OF CALPAIN 3 IN THE PATHOGENIC MECHANISM

Currently, the pathogenic mechanisms that explain how mutations in *CAPN3* gene cause LGMD2A are still unknown. Since calpain 3 potentially proteolyzes a wide range of proteins *in vivo*, it could participate in several cellular processes, such as apoptosis (Baghdiguian *et al.,* 1999), myogenic differentiation and sarcomere formation (Kramerova *et al.,* 2004) and maintenance of calcium homeostasis (Toral-Ojeda *et al.,* 2016). The fact that calpain 3 has been detected in several subcellular compartments, such as the M line and the Z disk of the sarcomere (Kramerova *et al.,* 2004, 2005), subsarcolemmal membrane (Huang *et al.,* 2005, 2008), the triad-associated protein complex (Kramerova *et al.,* 2008), or the nucleus (Sorimachi *et al.,* 1993; Baghdiguian *et al.,* 1999; Richard *et al.,* 2000; Benayoun *et al.,* 2008), reinforces its multifunctionality.

As previously mentioned, calpain 3 comprises several domains and each of them contributes one or more specific roles to this protein: autolytic activity, proteolytic activity, calcium and/or sodium sensitivity, dimerization ability, etc. It is striking that mutations in *CAPN3* gene found in LGMD2A patients are distributed all along the entire gene (figure 16), and thus, each mutation would theoretically disrupt one or more functions of calpain 3 depending on its location and the effect (e.g., protein modification, protein degradation) of each specific mutation on the protein outcome. For example, it has been shown that the proteolytic activity of calpain 3 is normal in 32% of LGMD2A patient-derived biopsies (Milic *et al.,* 2007). Therefore, alterations of additional calpain 3-specific functions that do not implicate its proteolytic activity also lead to LGMD2A.

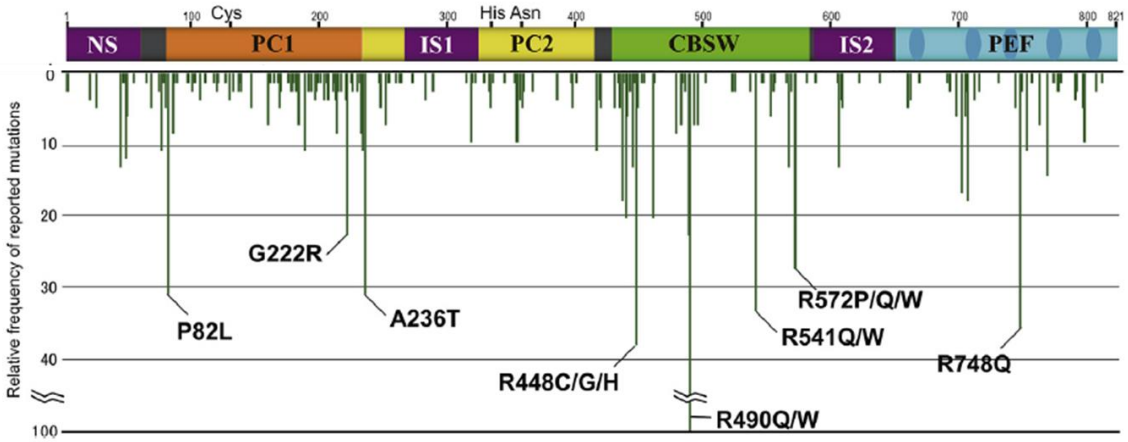

Figure 16. Distribution of pathogenic mutations in *CAPN3* reported in LGMD2A patients, and their relative frequency. (From: www.calpain.org and Ono *et al.,* 2016).

In addition to all the information provided by patients' biological samples and *in vitro* systems, several mouse models of calpainopathy have been created to determine the role of calpain 3 in muscle biology and muscular dystrophy.

The first knockout mouse model was developed by Richard and colleagues (Richard *et al.,* 2000). The authors replaced exons 2 and 3 of the *Capn3* gene with a neomycin resistance cassette. As a result, mRNA of *Capn3* gene was nearly undetectable in skeletal muscles of these animals, and calpain 3 protein was absent. However, *in vitro* studies demonstrated that the neomycin resistance cassette was eliminated during the maturation of *Capn3* mRNA, and the resulting recombinant protein preserved the titin-binding ability in the N2A region, although contrary to wild type calpain 3, it was not able to perform autolysis nor fodrin proteolysis. The knocked *Capn3* gene was preserved in the pure 129Sv mouse background, as well as in a mixed C57BL/6 - 129Svter background. Both mice displayed a similar dystrophic affectation observed as centrally nucleated fibers, necrotic and regenerative areas, inflammatory cell infiltrates and splitted fibers. Importantly, this phenotype was muscle-specific; *psoas*, *soleus*, and *deltoid* were predominantly affected, whereas *tibialis anterior* (TA) and *biceps* showed a mild phenotype and the *quadriceps*, *gastrocnemius*, and *triceps brachii* did not seem to be affected. Furthermore, these dystrophic signs were evident at two months of age in the 129Sv background, whereas the mixed-background strain did not develop the phenotype until 6 months of age. This strongly suggests that additional genetic traits play a role in the genotype:phenotype correlation in calpainopathy (Richard *et al.,* 2000b).

Four years later, Kramerova and colleagues (Kramerova *et al.,* 2004) developed a full *Capn3* knockout (C3KO) mouse model. These mice were smaller than their wild type counterparts and had reduced muscle mass. C3KO mice developed a muscle-specific phenotype with reduced fiber size, inflammation and necrotic and regenerative areas were observed in cross-sections of *gastrocnemius*, *soleus*, TA and *diaphragm*. The *soleus*

and the *diaphragm* were the most affected muscles. The authors also discovered that lack of calpain 3 led to delayed myofibrillogenesis and reduced maturity of the fibers.

Another knockout model of calpain 3 was developed by Laure and colleagues by targeting the exon 1 of *Capn3* gene with an *IRES-LacZ-Lox-PGK-Hygro-lox* cassette that prevented its expression (Laure *et al.,* 2009). *Soleus* and *psoas* were the most affected muscles in this C3-null mouse model at 7-8 months of age, whereas *extensor digitorum longus* (EDL) and TA were slightly affected and the *quadriceps* was unaffected.

In combination with knockout models of the disease, in 2000 Tagawa and colleagues published a transgenic mouse model of calpainopathy, which ubiquitously expressed a mutant version of the *Capn3* gene that led to a calpain 3 protein containing a single amino acid substitution (C129S). This mutation turned calpain 3 into a proteolytically inactive molecule, despite preserving its structure. Importantly, this mouse model also expressed the wild type calpain 3. Mutant calpain 3 expression increased with aging, while muscle strength decreased progressively. However, histological abnormalities were essentially absent in EDL and *soleus* muscles at 40 weeks of age, and only some slight dystrophic features were observed in muscles of 2 year-old transgenic mice (Tagawa *et al.,* 2000). Thus, accumulation of the mutated calpain 3 might exert a toxic gain of function effect in skeletal muscles of this mouse model.

In 2010, Ojima and colleagues developed a knockin model of calpainopathy (Ojima *et al.,* 2010), in which the endogenous *Capn3* was replaced with the previously described proteolitically inactive calpain 3 (C129S). This strain developed several dystrophic features that were detected in histological analyses, such as centrally nucleated fibers and necrotic and regenerative areas. This phenotype was exacerbated with aging and exercise.

Each of these animal models of calpainopathy has provided valuable data to determine the role of calpain 3 in skeletal muscle. However, lack of functional calpain 3 in these mice leads to minor phenotypic traits that are far from representing the muscle degeneration observed in LGMD2A patients.

Despite these mouse models of calpainopathy, *Capn3* overexpression models have been created to assess the toxicity of calpain 3 in potential gene therapies. In this regard, Spencer and colleagues established three mouse models overexpressing wild type *Capn3*, as well as the developmental isoforms lacking exon 6 or exon 15, under the control of the skeletal muscle-specific promoter α-actin (Spencer *et al.,* 2002). These models proved that wild type calpain 3 had no toxic effects when overexpressed *in vivo* in these animals. Importantly, overexpression of the developmental isoforms led to immature muscles, suggesting that wild type calpain 3 might play a role in the maturation of skeletal muscle.

Numerous studies have been performed to decipher the physiopathology of LGMD2A. These studies involve the mentioned mouse models of calpainopathy, cellular models, patient-derived samples and *in vitro* overexpression systems. Based on the results, multiple roles have been attributed to calpain 3, which are described below.

2.3.2.4.1 Calpain 3 and NFkB-mediated apoptosis

One of the earliest attempts to decipher the pathophysiology of LGMD2A associated the lack of calpain 3 with an altered nuclear factor kappa B (NFkB) signaling pathway, leading to myonuclear apoptosis (Baghdiguian *et al.,* 1999). The common NFkB protein comprises two subunits known as p65 and p50, which tend to locate in the cytoplasm of cells due to their interaction with inhibitors of kappa B (IkB) (Baldwin, 1996). Upon activation by a wide range of signals, IkB proteins are degraded, allowing the translocation of p65 to the nucleus, which activates the expression of anti-inflammatory genes and cell survival genes. Therefore, this is considered as an anti-apoptotic signaling pathway.

Immunofluorescence analysis of deltoid muscle sections of LGMD2A patients and healthy subjects revealed that IkBα tends to accumulate in patients' fibers, retaining NFkB in the cytoplasm of the cells. This suggests that lack of functional calpain 3 in patients could prevent the degradation of this inhibitor, leading to its accumulation and therefore, steadily inhibiting the NFkB signaling pathway (Baghdiguian *et al.,* 1999). In parallel, the number of apoptotic myonuclei observed in LGMD2A biopsies was 100 times higher when compared to healthy controls and other muscular dystrophies. These TUNEL-positive cells also accumulated high IkBα levels. Therefore, the study concluded that inhibition of NFkB, caused by a lack of functional calpain 3, prevented the expression of antiapoptotic genes activated by the NFkB pathway, increasing cellular apoptosis (Baghdiguian *et al.,* 1999). Indeed, a subsequent study demonstrated that mRNA and protein levels of the anti-apoptotic factor cellular-FLICE inhibitory protein (c-FLIP), which is induced by the NFkB signaling pathway, were downregulated in LGMD2A biopsies (Benayoun *et al.,* 2008). However, the overall number of apoptotic nuclei in LGMD2A muscle sections, besides being significantly higher than in other dystrophies, remained lower than 0.5% of total myonuclei (Baghdiguian *et al.,* 1999), which casts doubts about this apoptosis rate being causative of the muscle degeneration seen in LGMD2A patients.

One year later, Richard and colleagues (Richard *et al.,* 2000) tested this hypothesis in their newly generated knockout mouse model of calpainopathy. The study detected some apoptotic myonuclei that colocalized with IkBα. NFkB displayed a subsarcolemmal localization in half of the fibers, whereas the other half showed a normal pattern in the myonuclei. Thus, the authors concluded that calpain 3 deficiency alone was not sufficient to induce an abnormal localization of NFkB, suggesting that an activator signal, such as oxidative or mechanical stress, might be necessary to clearly visualize the

phenotype derived from calpain 3 deficiency. Importantly, c-FLIP expression was also reduced in affected muscles of these mice (Benayoun *et al.,* 2008). Apoptotic TUNEL-positive nuclei were also detected in the C3KO mouse model (Kramerova *et al.,* 2004), but contrary to previous findings, these cells were located outside of the sarcolemmal membrane and co-stained for CD11b, indicating that the apoptotic cells were, in fact, immune cells instead of myogenic cells (Kramerova *et al.,* 2004).

The role of the NFkB signaling pathway in calpainopathy remains controversial, since its constitutive activation in mice leads to muscle degeneration (Cai *et al.,* 2004), whereas its inactivation in transgenic mice makes these animals resistant to atrophy (Mourkioti *et al.,* 2006). In accordance with this, Rajakumar and colleagues (Rajakumar *et al.,* 2013) determined that oxidative stress and protein ubiquitinylation were increased in calpainopathic muscles, potentially leading to the activation of the NFkB that was represented as nuclear translocation of the p65 subunit in patient-derived biopsies but not in control samples (Rajakumar *et al.,* 2013). Consequently, these authors suggest that inhibition of NFkB signaling might be beneficial for LGMD2A patients.

2.3.2.4.2 Calpain 3, titin and sarcomere remodeling

Titin or connectin is a giant protein found in the sarcomeres, connecting the Z disks to the M lines, as shown in figure 3. Yeast two-hybrid studies performed in the nineties showed that calpain 3 was able to bind titin in two different sites, the N2 region and the C-terminal region of titin, which is located in the M line of the sarcomeres (figure 17) (Sorimachi *et al.,* 1995; Kinbara *et al.,* 1997).

Since calpain 3 is highly stable in muscular tissue, but is rapidly proteolyzed in muscle homogenates and *in vitro* cellular models, it has been suggested that binding of calpain 3 to titin potentially stabilizes this protein in its inactive state, preventing its degradation (Haravuori *et al.,* 2001; Garvey *et al.,* 2002). Titin would also directly control calpain 3 activity by limiting its access to different substrates. It is worth noting that during myogenesis, titin is one of the first proteins to be synthesized, even before myosin, actin and nebulin (Fürst, 1989). This could be important for the quick stabilization of calpain 3 during myogenic differentiation.

To determine the relevance of calpain 3 binding to titin in the pathophysiology of LGMD2A, Ono and colleagues tested the titin-binding ability of several mutant calpain 3 proteins harboring missense mutations found in LGMD2A patients (Ono *et al.,* 1998). Interestingly, it was reported that even though each of the mutations affected the fodrinolytic activity of calpain 3, some of them did not alter its titin-binding ability, suggesting that loss of titin binding ability does not play a crucial role in the muscle wasting. However, Ermolova and colleagues demonstrated that calpain 3 mutants that preserve proteolytic activity, but lack titin-binding ability, were extremely unstable and caused muscle dystrophy (Ermolova *et al.,* 2011). Thus, the interaction between

calpain 3 and titin appears necessary, but is not sufficient to prevent muscle degeneration.

Along with titin-binding ability, it has been found that calpain 3 is able to cleave titin *in vitro*. Therefore, calpain 3 may participate in sarcomere remodeling by cleaving titin molecules when required. This is supported by the fact that C3KO mice display abnormal sarcomere organization in affected muscles, although titin molecules are correctly distributed in the sarcomeres (Kramerova *et al.,* 2004). In addition, overexpression of the calpain 3 isoform lacking IS1 (exon 6) or IS2 (exon 15) prevents the correct maturation of the myofibers (Spencer *et al.,* 2002), supporting that calpain 3 participates in myofiber architecture. Moreover, *in vivo* induced sarcomere remodeling in C3KO mice shows ubiquitination deficiencies during remodeling, consistent with the formation of protein aggregates that presumably exert a cytotoxic effect in calpain 3-deficient muscles (Kramerova *et al.,* 2005). Altered *in vitro* differentiation has also been reported in LGMD2A patient-derived myotubes, consistent with an inefficient replacement of integrin β1A expression by integrin β1D expression that occurs during regular myogenic differentiation (Jaka *et al.,* 2017). Importantly, deficient induction of integrin β1D in patient-derived myotubes is rescued by silencing frizzled-related protein (FRZB), as well as following pharmacological administration of LiCl, indicating a basis for a potential treatment for LGMD2A patients (Jaka *et al.,* 2017).

Taken together, the data suggests that calpain 3 is necessary for sarcomere remodeling and myogenic maturation.

2.3.2.4.3 Calpain 3 and signal transduction

Numerous studies suggest that proteins located in the sarcomeres, as well as in the sarcolemma, actively participate in mechanical sensing and response of myofibers (Granzier and Labeit, 2004). Calpain 3 likely participates in this signal transduction process since it is located in both subcellular locations.

As for sarcomeric proteins, calpain 3 has been detected in three different locations: in the N2 region and the M-line, interacting with titin as previously indicated, and also in the Z-disks, associated with α-actinin (figure 17) (Ojima *et al.,* 2010). These three sites are the regions where signaling molecules, such as muscle RING finger proteins (MURFs) and muscle ankyrin repeat proteins (MARPs), interact with structural sarcomeric molecules. Therefore, calpain 3 could participate in this signal transduction via its interaction with signaling proteins found in these locations (Ojima *et al.,* 2005).

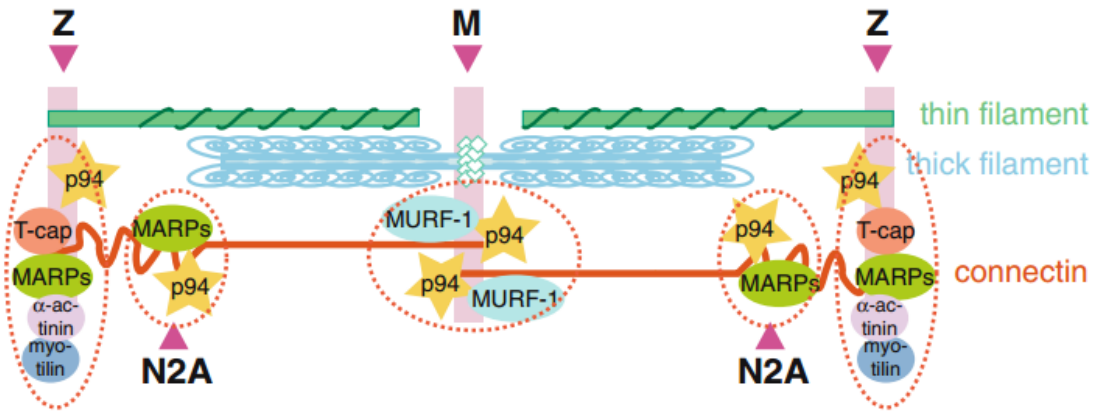

Figure 17. Representation of the sarcomeric proteins and signaling molecules found in the M line, Z disks and N2A regions. (From: Ojima *et al.,* 2005).

Indeed, these interactions have been reported in the N2A region, where MARP2/Ankrd2 competes with calpain 3 for binding titin in this site. Interestingly, calpain 3 also proteolyzes these signaling proteins (Hayashi *et al.,* 2008).

As for membrane proteins, calpain 3 directly interacts with the transmembrane protein dysferlin *in vitro* (Huang *et al.,* 2005). Dysferlin participates in vesicle transportation and cell membrane repair. An interaction between calpain 3 and dysferlin is presumed since some LGMD2B patients (caused by mutations in the dysferlin-coding gene) display a secondary calpain 3 deficit (Anderson *et al.,* 2000), whereas secondary dysferlin deficiency has been detected in some LGMD2A patients (Chrobáková *et al.,* 2004). However, C3KO mice do not develop membrane alterations, which excludes the participation of calpain 3 in membrane repair processes. The link between calpain 3 and dysferlin seems to involve AHNAK, a member of the dysferlin protein complex that participates in the subsarcolemmal architecture of the cytoskeleton and membrane repair processes. AHNAK is a substrate of calpain 3 and once it is proteolyzed, it is not able to interact with dysferlin. Moreover, AHNAK is accumulated in muscles of LGMD2A patients, which could explain secondary deficiencies of calpain 3 and dysferlin found in LGMD2B and LGMD2A patients, respectively (Huang *et al.,* 2008).

Calpain 3 is additionally able to degrade alternative membrane proteins, such as M-cadherin and membrane-associated β-catenin, which are accumulated in C3KO fibers (Kramerova *et al.,* 2006). However, it is still unknown whether these protein interactions contribute to LGMD2A physiopathology.

2.3.2.4.4 Calpain 3 in the regulation of the cytoskeleton

In vitro assays have shown that calpain 3 is able to proteolyze several cytoskeletal components, such as filamin C (Guyon *et al.,* 2003), filamin A (Taveau *et al.,* 2003; Ono *et al.,* 2007), talin, vinexin and erzin (Taveau *et al.,* 2003). Therefore, calpain 3-mediated proteolysis might be necessary to modify the structure of muscle fibers. However,

despite all the efforts, it has not been confirmed that any of these and other cytoskeletal proteins are proteolyzed *in vivo* by calpain 3.

2.3.2.4.5 Calpain 3 and calcium homeostasis

As previously mentioned, calcium released from the sarcoplasmic reticulum to the cytosol of the fibers activates muscle contraction. The signal for calcium release comes from motor neurons, which induce a membrane depolarization that activates DHPRs that couple with RyR1 in skeletal muscle. These RyR1 channels are able to rapidly transport millions of calcium ions from the sarcoplasmic reticulum to the cytosol of the fibers. Following contractions, muscles are relaxed due to the SERCA pumps that reuptake calcium into the sarcoplasmic reticulum. This mechanism ensures the maintenance of calcium homeostasis in skeletal muscle tissue, which has been found altered in several muscular dystrophies (Reviewed by Vallejo-Illarramendi *et al.*, 2014).

Calpain 3 was found to proteolyze RyR1 in skeletal muscle (Shoshan-Barmatz *et al.*, 1994). This cleavage was thought to enhance calcium ion effluxes from the sarcoplasmic reticulum to the cytosol. However, contrary to the expectations, RyR1 was already cleaved in calpain 3-deficient myotubes (Dayanithi *et al.*, 2009), which suggests that ubiquitous calpains may also cleave RyR1 in skeletal muscle (Verburg *et al.*, 2009). Calcium release from the sarcoplasmic reticulum showed significant impairment in calpain 3-deficient myotubes following caffeine-induced RyR1 activation (Dayanithi *et al.*, 2009). Additionally, it was significantly reduced in C3KO mouse-derived myotubes (Kramerova *et al.*, 2008) and isolated fibers (Difranco *et al.*, 2016). These authors reported that calpain 3 interacts with the glycolytic enzyme aldolase A (AldoA) and with RyR1 in the triads. Therefore, calpain 3-deficiency leads to inefficient recruitment of AldoA and RyR1 to the triads, consistent with reduced calcium effluxes (Kramerova *et al.*, 2008). Calpain 3 was described in the triad in the knockin mouse model of calpain 3 (Ojima *et al.*, 2011). In line with previous results, calpain 3 interacted with RyR, calsequestrin, SERCA1a and phosphofructose kinase muscle type (PFKM), although none of these were proteolyzed by calpain 3. Moreover, calcium effluxes were regular in these mice, which indicates that calpain 3 performs a non-proteolytic role in the sarcoplasmic reticulum (Ojima *et al.*, 2011).

Importantly, a recent study has shown that calpain 3 interacts with SERCA proteins, which suggests that calcium impairment in LGMD2A patients does not only derive from deficiencies in RyR-related calcium release from the sarcoplasmic reticulum, but also from altered calcium reuptake to sarcoplasmic reticulum by SERCA pumps. Involvement of SERCA proteins in LGMD2A pathophysiology is supported by diminished amounts of SERCA2 and small ankyrin 1 (a SERCA1-binding protein) in LGMD2A muscle extracts, while they remain unaltered in other muscular dystrophies (Toral-Ojeda *et al.*, 2016). Considerably reduced calpain 3 mRNA and protein levels in inclusion body myositis (IBM)

muscles, which also show altered calcium levels, reinforce the idea that calpain 3 plays a critical role in calcium homeostasis (Amici *et al.*, 2017).

Absence of calpain 3 in skeletal muscle also alters the calcium-calmodulin protein kinase-II signaling pathway, which in healthy mice promotes the expression of the slow form of myosin following exercise. Therefore, C3KO mice do not show this adaptive switch of fiber types, which could partially explain the fiber type-specific affectation of muscles in LGMD2A patients and mouse models of calpainopathy (Kramerova *et al.*, 2012). Recently, this adaptive failure has been correlated with a defective induction of genes involved in lipid metabolism and energy production after exercise, suggesting that calpain 3 deficiency leads to defective oxidative metabolism (Kramerova *et al.*, 2016). Altered oxidative metabolism following exercise has also been reported in a small cohort of LGMD2A patients (Siciliano *et al.*, 2015), and studies have suggested a correlation between *CAPN3* variants and serum lipid content in specific populations (Guo *et al.*, 2017).

2.3.2.4.6 Calpain 3 and mitochondria

Lack of calpain 3 in skeletal muscles correlates with abnormal structure and distribution of mitochondria in C3KO mice, besides reduced ATP production in mitochondria and elevated oxidative stress, leading to increased protein modifications by free radicals (Kramerova *et al.*, 2009). These abnormalities have been confirmed in LGMD2A patient muscles, which also show deficient levels of mitochondrial antioxidant enzymes such as superoxide dismutase 1 (SOD1) protein, as well as increased lipid peroxidation (Nilsson *et al.*, 2014). Therefore, mitochondrial dysfunction seems to be involved in LGMD2A pathophysiology.

2.3.2.4.7 Calpain 3 and maintenance of muscle stem cells

Only a few studies have suggested that calpain 3 participates in the maintenance of muscle stem cells. Using a murine cellular model of myogenesis, *CAPN3* expression was observed to be upregulated in *reserve cells* (a population of undifferentiated and quiescent satellite cell-like cells found in myoblast cultures) compared to proliferating myoblasts (Stuelsatz *et al.*, 2010). Importantly, authors report that calpain 3 reduced the transcriptional activity of MYOD1, although a direct MYOD1 proteolysis by calpain 3 was not expected due to the different subcellular location of both proteins (Stuelsatz *et al.*, 2010). If this regulation of MYOD1 activity by calpain 3 is also consistent in human muscle progenitors, lack of functional calpain 3 in LGMD2A patients would lead to an inefficient maintenance of the quiescent satellite cell population due to an increased MYOD1 activity. However, the number of PAX7-positive cells in LGMD2A muscle biopsies increases as the disease progresses, and it is the highest in fibrotic tissues (Rosales *et al.*, 2013). Therefore, these authors suggested that satellite cells in LGMD2A patients may have difficulties switching from proliferation to differentiation, leading to

inefficient muscle regeneration (Rosales *et al.,* 2013). Of note, the number of type II fiber-associated satellite cells is reduced with aging (Verdijk *et al.,* 2014), but this tendency is reversed in LGMD2A patients, who show increased Pax7-positive cell numbers primarily associated with type II fibers (Rosales *et al.,*2013). Considering this experimental data, satellite cells might be implicated in the pathophysiology of LGMD2A, although a direct role of calpain 3 in satellite cells has not been reported to date.

2.3.2.4.8 Capain 3 and control of cell cycle

Several studies have implicated calpain 3 in control of the cell cycle progression in different cell types. For example, it has been reported that calpain 3 participates in the differentiation of myeloid precursor cells into granulocytes by cleaving cyclin A (Welm *et al.,* 2002). Calpain 3 isoforms have been implicated in the development of different tumors. For example, calpain 3 is downregulated in very aggressive and metastatic melanoma cells compared to treatment-responding melanoma cells, suggesting that calpain 3 potentially exerts a pro-apoptotic effect over these tumor cells (Moretti *et al.,* 2009). Contrarily, Roperto and colleagues suggested that activated calpain 3 could promote the proliferation of tumor cells in urothelial tumors in cattle (Roperto *et al.,* 2010). Indeed, calpain 3 appears to regulate the amount of the tumor suppressor protein p53 by promoting its degradation (Tao *et al.,* 2013; Guan *et al.,* 2016). However, overexpression of the calpain 3 isoform hMp84 in melanoma cells may induce p53 stabilization and reduce cell proliferation (Moretti *et al.,* 2015). Therefore, different calpain 3 isoforms potentially exert antagonistic roles in a wide range of cell types with regard to the regulation of cell cycle progression.

Currently, it is unknown whether calpain 3 participates in the regulation of the cell cycle in skeletal muscle cells. Since this tissue is predominantly constituted by post-mitotic cells, this hypothetical role may be performed in muscle satellite cells, which require a strict proliferative control to retain their regenerative potential over time.

GOALS AND HYPOTHESES

This project aims to explore the potential role of calpain 3 in the early stages of muscle regeneration and myogenesis, in order to contribute to the understanding of the pathophysiology of LGMD2A. This project will test the following hypotheses:

I. It is possible to establish LGMD2A patient-specific iPSC-derived cellular models of the disease.

II. *In vitro* modeling of LGMD2A through myogenic differentiation of patient-specific iPSCs will allow investigation into the role of calpain 3 in different stages of the myogenic differentiation process.

   a. iPSC-derived *PAX7*-expressing muscle progenitor cells, similar to activated satellite cells, can be used to study the role of calpain 3 in the early stages of myogenesis.

   b. Terminal differentiation of PAX7-expressing muscle progenitor cells will lead to myotube cultures, which may be used to study the role of calpain 3 in more advanced, or even terminal, stages of myogenesis.

   c. Comparative study of LGMD2A- and healthy control-derived cultures will establish calpain 3-specific phenotypes at different stages of the myogenic differentiation process.

III. Mutations in *CAPN3* will affect the regenerative potential of iPSC-derived *PAX7*-expressing myogenic progenitors upon intramuscular transplantation.

IV. *CAPN3* is expressed in murine satellite cells.

V. Calpain 3 plays a role in the activation, proliferation, differentiation and/or return to quiescence of murine satellite cells.

CHAPTER 1

In vitro modeling of LGMD2A through patient-specific iPSC-derived cultures

BACKGROUND AND HYPOTHESIS

The study of the physiopathology of LGMD2A endures several challenges due to multiple features of this disease. One of the difficulties originates from its rare condition. Consequently, the number of patients providing clinical data is reduced compared to other diseases. Moreover, currently its genetic diagnosis is performed in blood samples (Blázquez *et al.,* 2008). Therefore, the amount of muscle biopsies that were originally performed with diagnostic purposes and then used for research purposes has dramatically reduced in recent years. Thus, patient-derived muscle samples are limited and greatly appreciated to study the physiopathology of the disease.

An additional difficulty when studying the role of calpain 3 in skeletal muscle lies on its autolytic activity, which makes it a highly unstable protein with a very short half-life (Fanin *et al.,* 2007b). As a result, it has not been possible to crystalize the entire protein to determine its three-dimensional structure. Lack of calpain 3-specific antibodies suitable for immunodetection has also slowed the study of calpain 3.

As previously reviewed, a considerable number of roles have been attributed to calpain 3 in skeletal muscle tissue (Kinbara *et al.,* 1997; Baghdiguian *et al.,* 2001; Taveau *et al.,* 2003; Kramerova *et al.,* 2004; Ojima *et al.,* 2005, 2010; Stuelsatz *et al.,* 2010; Rosales *et al.,* 2013; Nilsson *et al.,* 2014; Toral-Ojeda *et al.,* 2016;). Nevertheless, to date none of these functions appear to explain how mutations in the calpain 3-coding gene lead to the muscle degeneration observed in LGMD2A patients, which predominantly affects a specific subset of muscles and induces progressive muscle wasting that is not evident in newborns, but appears in the teen years. In this regard, the large range of mutations observed in affected patients along with the lack of a clear genotype:phenotype correlation makes it more difficult to elucidate the role of calpain 3 in skeletal muscle.

To evade some of these obstacles in the study of the physiopathology of LGMD2A, several mouse models of calpainopathy have been generated (Richard *et al.,* 2000; Kramerova *et al.,* 2004; Laure *et al.,* 2009; Ojima *et al.,* 2010). These mice, despite providing valuable information about the role of calpain 3 in skeletal muscle, fail to reproduce the muscle wasting that occurs in LGMD2A patients. This fact suggests that these mouse models have compensatory mechanisms that alleviate the muscle degeneration caused by a lack of calpain 3 in humans. Each of these hurdles led to the idea that a patient-derived *in vitro* model of LGMD2A would be highly useful to study the physiopathology of the disease and to elucidate the role of calpain 3 during myogenesis.

Patient-derived myoblasts, as well as healthy donor-derived myoblasts, have been broadly used to study the physiopathology of muscular dystrophies as well as to test the efficacy of molecules with possible therapeutic potential (Delaporte *et al.,* 1990; Volonte *et al.,*2003; Petrov *et al.,* 2006; Bou Saada *et al.,* 2016). However, a muscle biopsy is

required to get this patient-specific material, which is usually uncomfortable for the donors and can negatively affect their daily life for several weeks following the biopsy. Moreover, these biopsies offer a limited amount of cells. Thus, in order to maximize this material, several authors have chosen to immortalize myoblasts, despite the fact that this process can slightly alter their properties (Mamchaoui *et al.,* 2011; Yoon *et al.,* 2013).

Alternatively, researchers have been investigating for other easy-access cell types with myogenic potential to establish patient-specific cellular models. In this regard, skin-derived fibroblast transdifferentiation into myotubes through exogenous *MYOD1* expression has been very useful to establish myogenic *in vitro* models of a wide range of muscular dystrophies (Choi *et al.,* 1990; Cooper *et al.,* 2007).

The development of mouse (Takahashi and Yamanaka, 2006) and human (Takahashi *et al.,* 2007) induced pluripotent stem (iPS) cell lines from somatic cells has been one of the most important recent breakthroughs in regenerative biology and medicine. In 2006, the Nobel Prize winner Shinya Yamanaka and his colleague Kazutoshi Takahashi, described a protocol to reprogram differentiated somatic cells into an undifferentiated state (induced Pluripotent Stem Cells or iPSCs) via the induced expression of four transcription factors, referred to as Yamanaka factors: OCT4, SOX2, KLF4 and cMYC. Cell reprogramming provides subject-specific undifferentiated cells with unlimited proliferative capacity, as well as with differentiation potential to practically any cell type. Therefore, despite their considerable applicability to cell therapies, iPSCs are additionally being used to establish patient-specific cellular models of diseases (Ravulapalli *et al.,* 2005; Campbell *et al.,* 2015; Hashimoto *et al.,* 2015; Torrent *et al.,* 2015; Mungenast *et al.,* 2016; Ueki *et al.,* 2017). These iPSC-derived patient-specific cellular models are useful to study the physiopathology of the diseases, as well as to test the efficacy of potential therapies.

Thus, we pursued to establish patient-specific iPSC-derived myogenic cellular models of LGMD2A, in order to determine the role of calpain 3 during the myogenic differentiation process, as well as to investigate how different mutations found in LGMD2A patients alter this process. In particular, we wanted to study 1) the differential myogenic potential of healthy donor- and LGMD2A patient-derived iPSCs, 2) expression of *CAPN3* during myogenic differentiation of iPSCs and 3) *in vitro* and *in vivo* phenotypes caused by mutations in *CAPN3* gene.

To accomplish this, LGMD2A and healthy control-derived fibroblasts were reprogrammed to pluripotency. These newly established cell lines were subjected to a battery of characterization tests in order to assess their pluripotency. Myogenic differentiation was achieved following a protocol that involved the transient expression of exogenous *PAX7*, which drives pluripotent cells into muscle progenitor cells that afterward can be terminally differentiated into multinucleated myotubes (Darabi *et al.,*

2012), leading to patient-specific myogenic cultures. Intramuscular transplantations of muscle progenitor cells into immunosuppressed mice were also performed to assess the role of calpain 3 in the *in vivo* regenerative potential of muscle progenitor cells (figure 18).

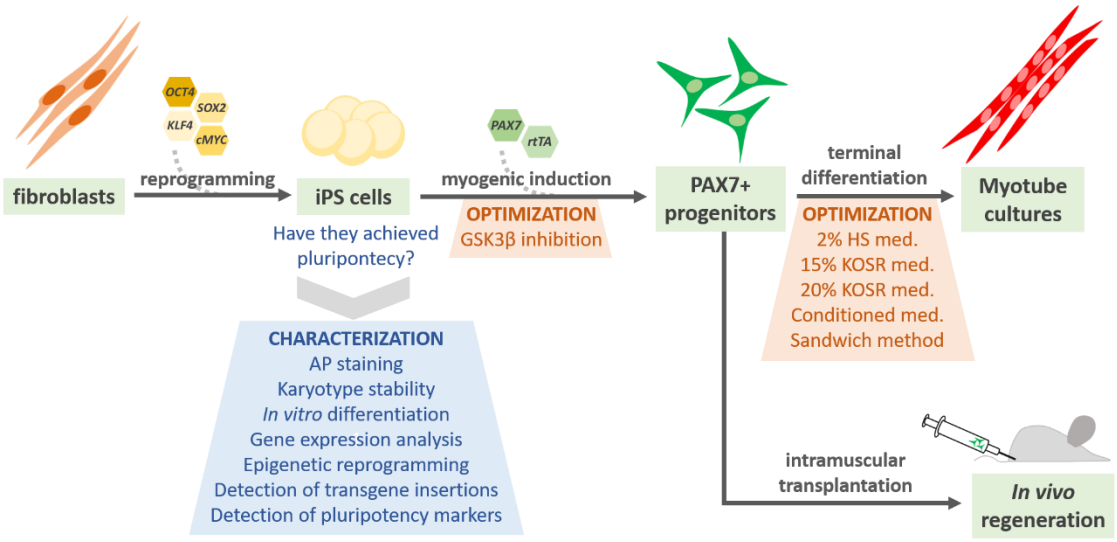

Figure 18. Workflow for the generation of patient-specific iPSC-derived cellular models of LGMD2A, and assessment of the *in vivo* regenerative potential of healthy and calpain 3-deficient muscle progenitor cells. Med.: medium.

The previously mentioned difficulties to obtain patient muscle biopsies, as well as the lack of optimized protocols to isolate human satellite cells, challenges the study of the potential role of calpain 3 in human satellite cells and/or during early myogenesis. Therefore, we considered that these patient-specific iPSC-derived muscle progenitors, which express surface markers described in murine satellite cells (CD56, M-cadherin, integrin-α7, integrin-β1) and mesenchymal stem cells (CD105, CD90, and CD13) (Darabi *et al.,* 2012), and their subsequent terminal differentiation may potentially contribute to understanding the role of calpain 3 during myogenesis.

MATERIALS AND METHODS

Selection of samples to be reprogrammed. Five LGMD2A patients evaluated at the Neurology Service of the Donostia University Hospital were selected to participate in this study. Inclusion was based on the mutations in *CAPN3* gene and their disease phenotype, classified as mild, intermediate, advanced or severe by the physicians that examined these patients. Patients were graded according to an adapted version of the Vignos and Archibald Scale, as indicated in table 4 (From: Walton, 1981).

Hereafter, patients were classified into different phenotypes according to their clinical grade and age, as shown in table 5.

Genetic diagnosis was performed by the Neurogenetics research group of the Experimental Unit located at the Donostia University Hospital, under the supervision of Dr. López de Munain and Dr. Amets Sáenz. Additionally, the theoretical effects of the mutations in the protein outcomes were determined by the same experts. Two age- and sex-matched healthy donor derived fibroblasts were obtained from the Basque Biobank and used as controls for this study. Absence of mutations in the *CAPN3* gene was ascertained in these two samples.

Grade	Clinical data
0	hyperCKemia, all activities normal.
1	Normal gait, unable to run freely, myalgia.
2	Incapacity to walk on tiptoes, wadding gait.
3	Evident muscular weakness, steppage and climbing stairs with banister.
4	Difficulty to rise from the floor, Gowers' sign.
5	Incapacity to rise from the floor.
6	Medical incapacity to climb stairs.
7	Incapacity to rise from a chair.
8	Unable to walk unassisted.
9	Unable to eat, drink or sit without assistance.

Table 4. Modified Vignos and Archibald Scale (MVA) (From: Walton, 1981).

	Age <24	Age 24-34	Age 35-44	Age >44
Mild	0-1	0-2	0-3	0-4
Intermediate	2	3	4	5
Advanced	3	4	5	6
Severe	4 or more	5 or more	6 or more	7 or more

Table 5. Classification of LGMD2A patients into mild, intermediate, advanced or severe phenotypes according to their age and grade of disability assessed using the modified Vignos and Archibald Scale.

Establishment of patient-specific fibroblast cultures. Selected patients were invited to participate in this study. Following acceptance, participants signed an informed consent prior to the sample collection. Skin samples were obtained with a punch biopsy and processed by the Cell Culture Platform at Biodonostia Research Institute. Skin was collected in RPMI 1640 medium containing 200 U/ml penicillin and 200 µg/ml streptomycin. Once in the cell culture hood, fatty tissue was removed from the biopsy using a sterile scalpel. The remaining tissue was washed with fresh medium, chopped into 2-3mm^3 pieces and placed in culture flasks previously rinsed with MEM medium supplemented with 13% of newborn calf serum, 40 U/ml penicillin, 40 µg/ml streptomycin and 2mM L-glutamine. Flasks were incubated vertically for three hours in a cell incubator to favor the attachment of biopsy pieces to the flasks, and then placed horizontally. The medium was replaced twice a week until fibroblasts were observed in

the flasks. Fibroblasts were cultured in DMEM medium containing 10% FBS, 100 U/ml penicillin and 100 µg/ml streptomycin, and expanded for 3-4 passages using 0.25% trypsin.

Cell reprogramming: production of retroviruses expressing the 4 reprogramming factors. pMSCV-based retroviral vectors expressing FLAG-tagged *OCT4, SOX2, KLF4* and *cMYC^{T58A}* were packaged using *Phoenix Amphotrophic* cells. A GFP-expressing vector was used as a positive control. The day prior to the transfection, 4.5 million cells were plated in each of the five P100 dishes. The following day, 9 µg of each plasmid were diluted in Optimem together with X-tremeGene9 DNA Transfection reagent. Following a 25- minute incubation at room temperature, each of these cocktails was spread, drop by drop, in one of the plates containing the *Phoenix Amphotrophic* cells, and incubated overnight at 37°C. The following day, the medium of the plates was replaced with 10.5 ml of DMEM supplemented with 10% FBS, 100 U/ml penicillin and 100 µg/ml streptomycin and cells were incubated at 32°C to favor retroviral production. The following day, supernatants were collected and filtered through a low protein-binding 0.45 µm pore filter, and used for the first fibroblast infection. An additional 10.5 ml of medium were added to each of the retrovirus-producing plates and these were incubated at 32°C for a second round of retroviral production. The next day, the supernatants were collected and filtered as indicated previously and culture dishes used for retroviral production were discarded. The workflow is illustrated in figure 19.

Cell reprogramming: infection of fibroblasts with retroviral vectors. One day prior to the first infection, 100 000 fibroblasts of the selected samples were plated in a well of a six well plate. The day of the infection, cell supernatants containing retroviruses carrying *OCT4*, *SOX2*, *KLF4* and *cMYC* genes were collected and filtered, as previously mentioned. Polybrene was added to the supernatants at a final concentration of 1 µg/ml, and these were combined by mixing equal volumes of each or them, which led to the infectious supernatant containing the four reprogramming retroviruses. In parallel, an additional 100 000 fibroblasts from each sample were infected with the GFP-expressing retroviral vector and used as a positive control. Fibroblasts were spin-infected at 700 x *g* for 45 minutes at 32°C. Finally, cells were incubated at 37°C for 24 hours. The following day, fibroblasts were infected for the second time, following the same protocol described for the first infection. The workflow is illustrated in figure 19.

Cell reprogramming: cell culture during the reprogramming process. Three days following the second infection, the infected fibroblasts were seeded on top of non-proliferating (irradiated) human foreskin fibroblasts (HFFs), also known as *feeder cells*. These feeder cells were previously generated by expanding CRL-2429 cells in DMEM medium supplemented with 10% FBS, 100 U/ml penicillin and 100 µg/ml streptomycin for three passages (up to passage 12), then irradiated with ionizing radiation at a dose of 40 Gy and frozen in 90% FBS/10% DMSO. Irradiated feeder cells were thawed and seeded in matrigel-coated dishes in DMEM medium supplemented with 10% FBS,

100 U/ml penicillin and 100 µg/ml streptomycin at a density of 65 000 cells/cm^2, two days prior to seeding the infected fibroblasts on top of them. Two days after seeding the infected fibroblasts on top of feeder cells, the medium was switched to human embryonic stem cell medium (hES medium), which consisted of knockOut DMEM medium supplemented with 20% knockOut Serum Replacement, 2 mM GlutaMAX, 1x non-essential amino acids (NEAA) solution, 50 µM 2- mercaptoethanol, 100 U/ml penicillin, 100 µg/ml streptomycin and 10 ng/ml FGF_2. This medium was replaced daily until colonies of reprogrammed cells appeared on top of the feeder cell layer. The workflow is illustrated in figure 19.

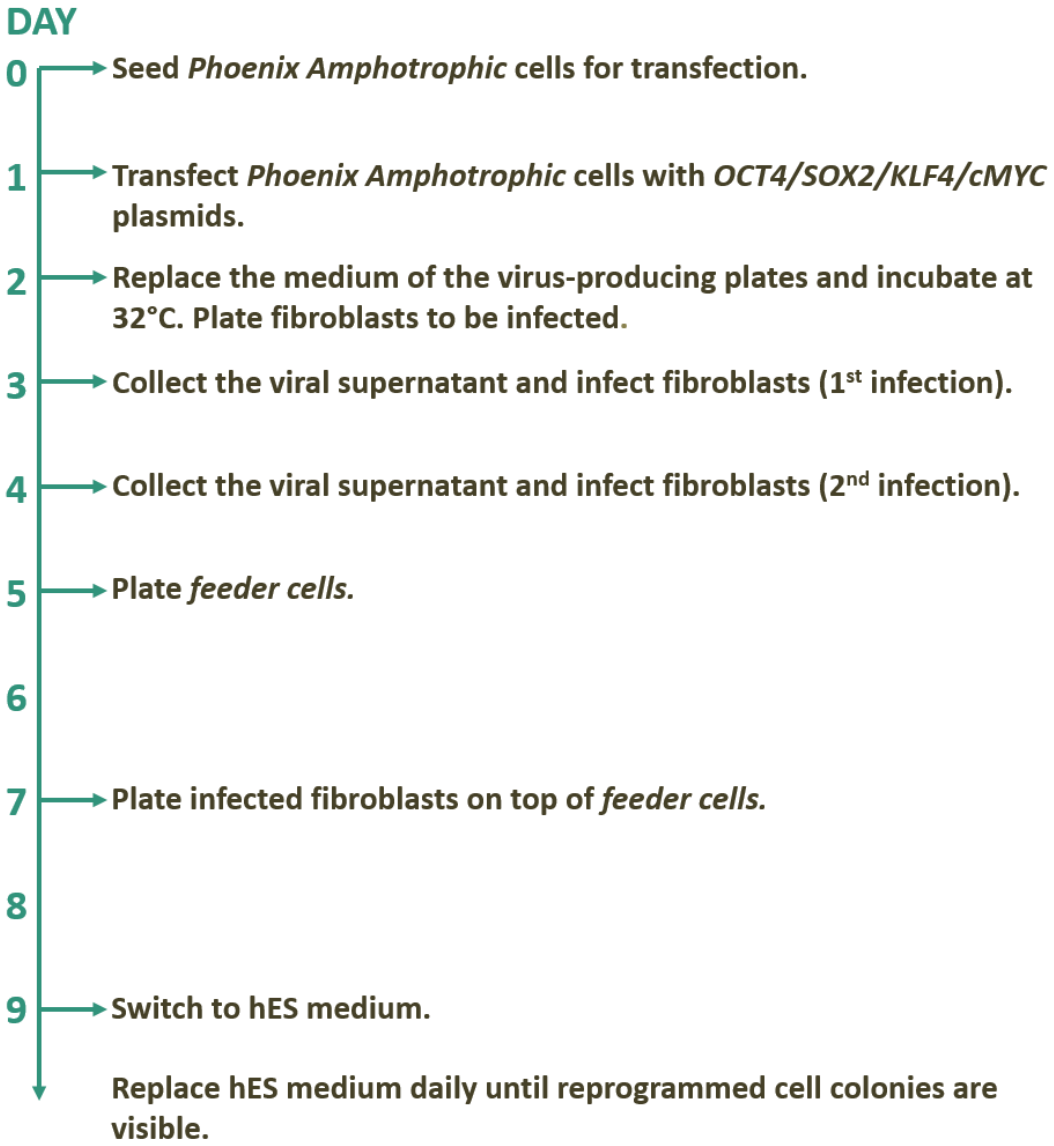

Figure 19. Workflow of retroviral production, infection of donor-derived fibroblasts and culture during reprogramming.

Cell reprogramming: establishment of iPSC clones, culture and expansion. In order to establish different reprogrammed cell lines (i.e., clones) from each sample, up to 6 colonies from each reprogramming plate were independently picked, seeded, cultured

in feeder cell-coated dishes and expanded on hES medium. Feeder cells were seeded two days prior to passaging the reprogrammed cells, in matrigel-coated wells using DMEM medium supplemented with 10% FBS, 100 U/ml penicillin and 100 µg/ml streptomycin, at a density of 65 000 cells/cm^2. The following day, culture medium was switched to hES medium. Cell passages were performed mechanically, using a stripper pipette with 100 µm tips. Reprogrammed cells at early passages were mechanically detached and frozen in freezing medium (90% FBS/10% DMSO) to generate a frozen stock of the newly generated cell lines.

***Cell reprogramming: establishment and maintenance of pure (feeder-free) reprogrammed cell cultures*.** Reprogrammed cells growing over feeder cells at passage 6 or higher were mechanically picked and seeded on matrigel-coated wells. These cells were cultured in hES medium that had been previously exposed to irradiated CD1-murine embryonic fibroblasts (CD1-MEFs) for 24 hours (known as *conditioned medium*). A stock of irradiated MEFs was created following the same steps previously described for generating feeder cells. Alternatively, matrigel-adapted reprogrammed cells were cultured using the commercially available mTeSR1 medium supplemented with 100 U/ml penicillin and 100 µg/ml streptomycin. Cell medium was replaced daily. Cells proliferated and formed colonies. Colonies were passaged using Trypsin-EDTA 0.05%, ReLeSR reagent or StemPro Accutase, depending on the purpose. Cells were seeded in culture medium supplemented with 5 µM Y-27632 rock inhibitor for 24 hours to improve cell survival following passaging. Similar to feeder-dependent reprogrammed cells, a stock of frozen matrigel-adapted reprogrammed cells was generated for future experiments.

Characterization of reprogrammed cell lines. Once a stock of reprogrammed cells was created for each of the established cell lines, characterization tests were performed to assess their pluripotency.

As summarized in figure 20, the characterization process began by testing alkaline phosphatase (AP) activity in each of the clones established per reprogrammed sample. Cell lines that positively stained for AP activity were further characterized by analyzing the gene expression rates of reprogramming transgenes and a set of endogenous pluripotency genes. Based on transgene silencing criteria and the induction of pluripotency genes, two cell lines per sample were chosen for further characterization. Thereafter, Southern blot analysis of transgenes allowed to verify the clonal independence of each pair of cell lines analyzed per sample, and one of them was selected for final characterization tests. These final characterization tests consisted of the detection of pluripotency markers, *in vitro* differentiation into cell types derived from the three embryonic germ layers, epigenetic reprogramming and verification of karyotype stability. In the case of karyotype abnormalities detected in a subpopulation of cells, these cell lines were subcloned and karyotyped again to ensure the absence of

genomic alterations. Following these characterization tests, cell lines that met all the characterization criteria were used for following differentiation experiments.

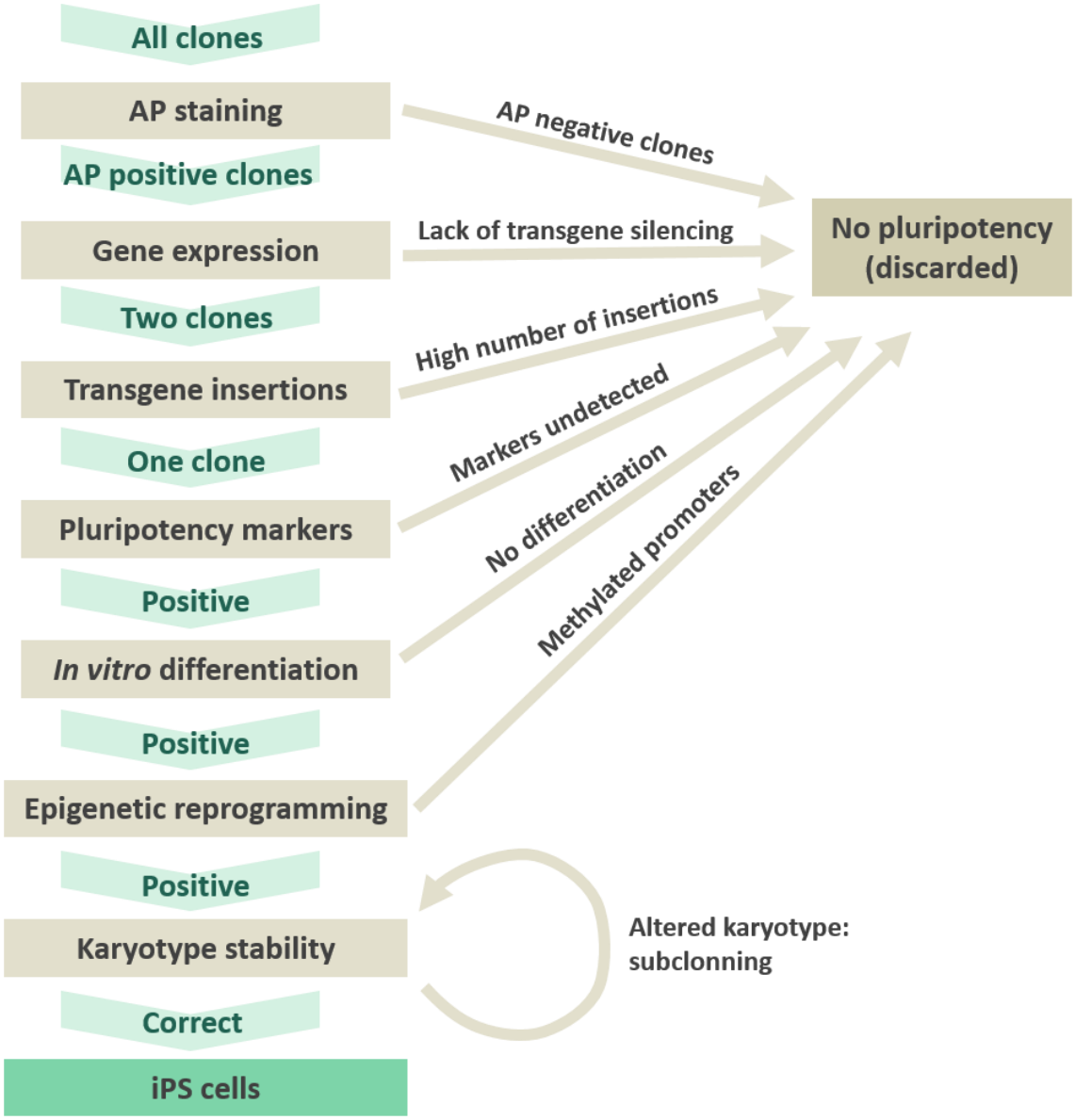

Figure 20. Schematic representation of the characterization workflow.

Characterization: detection of alkaline phosphatase activity. AP activity was assessed using the alkaline phosphatase blue membrane substrate solution kit. Reprogrammed cell colonies grown over feeder cells were fixed by incubating them in 3.7% formaldehyde for 2.5 minutes. Following fixation, cells were washed twice with PBS and incubated in a mixture of substrate A and B (1:1) from the staining kit for 25 minutes at room temperature, protected from light. After the incubation, the staining solution was replaced with PBS and AP-expressing colonies were observed as blue colonies under an optic microscope.

Characterization: gene expression analysis of pluripotency markers through qPCR. RNA was extracted from reprogrammed cell lines (clones) following the classical trizol-

chloroform protocol. 1 µg of RNA was retrotranscribed using the SuperScript III kit, following manufacturer's instructions. Expression of endogenous *OCT4, SOX2, KLF4, cMYC, NANOG, CRIPTO* and *REX1,* and transgenic *OCT4, SOX2, KLF4* and *cMYC* pluripotency genes was determined through qPCR, using specific primer pairs for each of the genes (Aasen *et al.,* 2008) (table 6) and SYBR green real-time master mix, in an Applied Biosystems StepOnePlus Real-Time PCR Machine.

Target	Forward primer	Reverse primer
Trans-*OCT4*	5'-TGGACTACAAGGACGACGATGA-3'	5'-CAGGTGTCCCGCCATGA-3'
Trans-*SOX2*	5'-GCTCGAGGTTAACGAATTCATGT-3'	5'-GCCCGGCGGCTTCA-3'
Trans-*KLF4*	5'-TGGACTACAAGGACGACGATGA-3'	5'-CGTCGCTGACAGCCATGA-3'
Trans-*cMYC*	5'-TGGACTACAAGGACGACGATGA-3'	5'-GTTCCTGTTGGTGAAGCTAACGT-3'
Endo-*OCT4*	5'-GGGTTTTTGGGATTAAGTTCTTCA-3'	5'-GCCCCCACCCTTTGTGTT-3'
Endo-*SOX2*	5'-CAAAAATGGCCATGCAGGTT-3'	5'-AGTTGGGATCGAACAAAAGCTATT-3'
Endo-*KLF4*	5'-AGCCTAAATGATGGTGCTTGGT-3'	5'-TTGAAAACTTTGGCTTCCTTGTT-3'
Endo-*cMYC*	5'-CGGGCGGGCACTTTG-3'	5'-GGAGAGTCGCGTCCTTGCT-3'
NANOG	5'-ACAACTGGCCGAAGAATAGCA-3'	5'-GGTTCCCAGTCGGGTTCAC-3'
CRIPTO	5'-CGGAACTGTGAGCACGATGT-3'	5'-GGGCAGCCAGGTGTCATG-3'
REX1	5'-CCTGCAGGCGGAAATAGAAC-3'	5'-GCACACATAGCCATCACATAAGG-3'
GAPDH	5'-GCACCGTCAAGGCTGAGAAC-3'	5'-AGGGATCTCGCTCCTGGAA-3'

Table 6. Primers used during gene expression analysis of pluripotency genes. In order to distinguish endogenous and transgenic expression of reprogramming genes, gene names are indicated with trans- (transgenic) and endo- (endogenous) prefixes.

Characterization: detection of transgene insertions through Southern blot. Genomic DNA from two clones of each sample was isolated using the QIAamp DNA mini kit, and concentrated following a classical sodium acetate and ethanol-based protocol. 10 µg of each DNA sample were digested overnight with 50 U of *HindIII* and an additional 10 µg with 50 U of *PstI,* in a final volume of 50 µl. The following day, 3 µl of the digestion product were run on a small 1% agarose gel to verify complete digestion. If the digestion was incomplete, additional 20 U of the corresponding restriction enzyme were added to the samples and digestion was hold for 3 more hours. Once the digestion was successful, samples were electrophoresed in a large 1% agarose gel using fresh TAE buffer, denaturalized in 1.5 M NaCl/0.5 M NaOH solution for 30 minutes, washed once with distilled water, neutralized in 1.5 M NaCl/0.5 M Tris/0.001 EDTA, pH 6.9, for 30 minutes, washed once with distilled water and incubated again in neutralizing solution for 15 minutes, washed in distilled water and transferred to a hybond nylon membrane overnight through capillarity.

The next day, the membrane was washed in 1.5 M NaCl/0.17 M sodium citrate, pH 7.0, for 5 minutes, dried using whatman paper, and DNA was cross-linked by incubating the membrane for 75 seconds under UV light. Then, membranes were placed in hybridization tubes, wet with milliQ water, prehybridized with preheated CHURCH buffer (0.5 M NaPi, 7% SDS, 0.001 M EDTA) for 30 minutes at 68°C, and hybridized overnight at 68°C with DIG-dUTP-labeled probes 1:10 diluted in preheated CHURCH

buffer: the membrane containing *HindIII*-digested samples was incubated with the *cMYC* probe, whereas the membrane with *PstI*-digested samples was incubated with the *KLF4* probe. These probes were previously generated through PCR using the PCR DIG probe synthesis kit, the reprogramming plasmids as template and primers specified in table 7.

The following day, membranes were washed twice in preheated 0.04 M NaPi/0.01% SDS buffer for 8 minutes at room temperature, followed by two more 8 minute washes in 0.1 M maleic acid/0.15 M NaCl/0.3% tween at room temperature. Subsequently, membranes were blocked using the blocking reagent for 1 hour at room temperature, incubated with the AP-conjugated anti-DIG antibody (1:25 000 diluted in blocking reagent) for 1 hour at room temperature, washed again for 30 minutes in 0.1 M maleic acid/0.15 M NaCl/0.3% tween followed by a final 5 minute wash in 0.1 M NaCl/0.1 M Tris, and developed with CDP-Star chemilluminiscent substrate. Next, membranes were stripped by incubating them for 10 minutes in 0.5 M NaOH/1.5 M NaCl, followed by a 1 minute wash in milliQ water and a 2 minute incubation in 50 mM NaPi. Finally, membranes were hybridized with the probes generated against *OCT4* (membrane containing *HindIII*-digested samples) and *SOX2* (membrane containing *PstI*-digested samples).The southern blot was completed similarly for *cMYC* and *KLF4* detection. Primary fibroblasts of each sample were used as a negative control.

	Forward primer	**Reverse primer**
SOX2	5'-AGTACAACTCCATGACCAGC-3'	5'-TCACATGTGTGAGAGGGGC-3'
OCT4	5'-TAAGCTTCCAAGGCCCTCC-3'	5'-CTCCTCCGGGTTTTGCTCC-3'
KLF4	5'-AATTACCCATCCTTCCTGCC-3'	5'-TTAAAAATGCCTCTTCATGTGTA-3'
cMYC	5'-TCCACTCGGAAGGACTATCC-3'	5'-TTACGCACAAGAGTTCCGTAG-3'

Table 7. Primers used to generate probes against the indicated targets: *SOX2, OCT4, KLF4* and *cMYC*. (From: Aasen *et al.,* 2008)

Characterization: immunodetection of pluripotency markers. To assess the expression of a panel of pluripotency markers comprising the nuclear transcription factors OCT4, SOX2 and NANOG, the glycolipid antigens SSEA3 and SSEA4, and the keratin sulfate antigens TRA-1-60 and TRA-1-81, immunofluorescence detection was performed on reprogrammed cell colonies cultured on top of feeder cells, following the protocols described by Martí and colleagues (Martí *et al.,* 2013). Cells were fixed in 4% paraformaldehyde for 20 minutes and stored in tris-buffered saline (TBS) at 4°C until immunofluorescence was performed. For immunofluorescence detection, cells were washed three times in TBS/0.1% triton-X100 for 15 minutes, and blocked in TBS/0.5% triton-X100/6% donkey serum for 2 hours at room temperature. Hereafter, samples were incubated with the corresponding primary antibody combinations, diluted in TBS/0.1% triton-X100/6% donkey serum, for 72 hours at 4°C: A) Anti-OCT4 + anti-SSEA3, B) Anti-SOX2 + anti-SSEA4 + anti-TRA-1-60 and C) anti-NANOG + anti-TRA- 1-81 (table 8). Next, samples were washed three times with TBS/0.1% triton-X100, blocked for 1 hour

in TBS/0.1% tritonX-100/6% donkey serum, and incubated with the corresponding secondary antibody combinations diluted in TBS/0.5% triton-X100/6% donkey serum, for two hours at room temperature, protected from light: A) goat-anti-mouseIgG-Cy2 + goat-anti-ratIgM-Cy3, B) donkey-anti-RabbitIgG-Cy2 + goat-anti-mouseIgG-Cy3 + goat-anti-mouseIgG-Cy5, C) donkey-anti-goatIgG-Cy2 + donkey-anti-mouseIgM-Cy3 (table 8). Finally, samples were washed 3 more times, incubated for 10 minutes in 100 ng/ml 4',6-diamino-2-fenilindol (DAPI), washed twice in TBS and mounted in 2.5% DABCO mounting medium. Samples were imaged with a Leica SP5 confocal microscope.

	Primary antibodies		Secondary antibodies	
	Target	**Dilution**	**Antibody**	**Dilution**
A	OCT4	1:60	Goat-anti-mouseIgG-Cy2	1:200
	SSEA3	1:3	Goat-anti-ratIgM-Cy3	1:200
B	SOX2	1:100	Donkey-anti-RabbitIgG-Cy2	1:200
	SSEA4	1:3	Goat-anti-mouseIgG-Cy3	1:200
	TRA-1-60	1:200	Goat-anti-mouseIgM-Cy5	1:200
C	NANOG	1:50	Donkey-anti-goatIgG-Cy2	1:200
	TRA-1-81	1:200	Donkey-anti-mouseIgM-Cy3	1:200

Table 8. Antibody combinations and dilutions for multiple detection of pluripotency markers in reprogrammed cells. (From: Martí *et al.,* 2013).

Characterization: in vitro differentiation of reprogrammed cells. Differentiation of reprogrammed cells into cell types derived from each of the three primordial germ layers of the embryo was achieved by culturing matrigel-adapted cells in specific culture media. Differentiation was initiated by culturing reprogrammed cells in suspension in conditioned medium until cell aggregates known as embryoid bodies (EBs) were visible after 5-7 days. Mesoderm differentiation was induced by seeding the EBs in 0.1% gelatin-coated plates and culturing them with KO-DMEM medium supplemented with 10% FBS, 1x NEAA, 2 mM GlutaMAX, 50 µM 2-mercaptoethanol and 100 µM ascorbic acid for 3-4 weeks. For endodermal differentiation, EBs were cultured in KO- DMEM medium supplemented with 10% FBS, 1x NEAA, 2mM GlutaMAX and 50 µM 2-mercaptoethanol for 3-4 weeks. Ectodermal differentiation was induced by culturing the EBs in suspension for 10 more days in N2B27 medium, which consisted of a 1:1 combination of DMEM/F12 medium and neurobasal medium, supplemented with 0.5x B-27 supplement, 0.5x N-2 supplement, 2 mM GlutaMAX, 100 U/ml penicillin, 100 µg/ml streptomycin and 10 ng/ml FGF_2, followed by their culture in matrigel-coated plates in N2B27 medium without FGF_2 for 3-4 weeks. All media were replaced every 2-3 days.

The differentiation rate was assessed by immunofluorescence analysis of lineage-specific markers. Cells were fixed in 4% paraformaldehyde for 20 minutes, washed 3 times in TBS/0.1% triton X-100 for 15 minutes and blocked in TBS/0.5% triton X-100/6%

donkey serum for 2 hours at room temperature. Next, samples were incubated with the corresponding primary antibody combinations, diluted in TBS/0.1% triton X- 100/6% donkey serum, for 48 hours at 4°C: A) for endoderm differentiation: anti-AFP + anti-FOXA2, B) for ectoderm differentiation: anti- TUJ1 + anti-GFAP, and C) for mesoderm differentiation: anti-α-SMA + anti-GATA4 (table 9). Then, samples were washed 3 times in TBS/0.1% triton X-100 for 15 minutes, blocked in TBS/0.5% triton X- 100/6% donkey serum for 1 hour at room temperature and incubated with the corresponding secondary antibody combinations diluted in TBS/0.5% triton X-100/6% donkey serum, for 2 hours at room temperature, protected from light: A) anti-rabbit-IgG-Cy2 + anti-goat-IgG-Cy3, B) anti-mouse-IgG-Cy2 + anti-rabbit-IgG-Cy3, and C) anti-mouse-IgG-Cy2 + anti-rabbit-IgG-Cy3 (table 9). Finally, samples were washed 3 more times, incubated for 10 minutes with 100 ng/ml DAPI, washed twice in TBS and mounted in 2.5% DABCO mounting medium. Samples were imaged using a Leica SP5 confocal microscope.

	Primary antibodies		**Secondary antibodies**	
	Target	**Dilution**	**Antibody**	**Dilution**
Endoderm	AFP FOXA2	1:400 1:50	anti-rabbit-IgG-Cy2 anti-goat-IgG-Cy3	1:200 1:200
Mesoderm	α-SMA GATA4	1:400 1:50	anti-mouse-IgG-Cy2 anti-rabbit-IgG-Cy3	1:200 1:200
Ectoderm	TUJ1 GFAP	1:500 1:1000	anti-mouse-IgG-Cy2 anti-rabbit-IgG-Cy3	1:200 1:200

Table 9. Antibody combinations for multiple detection of lineage-specific markers in reprogrammed cells. (From: Martí *et al.,* 2013)

***Characterization: study of the methylation profile of OCT4 and NANOG promoters*.** The methylation profile of CpG islands located in the promoter region of two pluripotency genes, *OCT4* and *NANOG*, was studied to verify that cell reprogramming was also effective at the epigenetic level. To establish this pattern, genomic DNA was extracted from reprogrammed cells and mutagenized using the Methylamp DNA modification kit, which converts unmethylated cytosine bases into uracil bases. The two promoter sequences were amplified by double PCR (Freberg *et al.,* 2007) (table 10), electrophoresed in a 1% agarose gel, purified using the QIAquick gel extraction kit and cloned into the pCRII vector. Cloning products were transformed into competent TOP10 bacteria and seeded onto LB agar plus ampicillin plates, where IPTG was previously added in order to activate the expression of LacZ. Plates were incubated overnight at 37°C and the following day, 10 white colonies (presumably containing the plasmid with a cloned PCR product insert) were picked and grown in 3 ml of LB medium. Correct cloning of the PCR product was verified through PCR. Plasmids were purified using a QIAprep spin miniprep kit and sequencing reactions were set using the BigDye 3.1 kit.

The sequencing results were aligned with the wild type sequence of the amplified region and CpG islands were studied to detect C>T conversions, indicative of demethylation.

	Forward primer	Reverse primer
OCT4	5'-TTAGGAAAATGGGTAGTAGGGATTT-3'	5'-TACCCAAAAAACAAATAAATTATAAAACCT-3'
NANOG	5'-AGAGATAGGAGGGTAAGTTTTTTTT-3'	5'-ACTCCCACACAAACTAACTTTTATTC-3'

Table 10. Primers used to amplify the promoter region of *OCT4* and *NANOG* genes. (From: Freberg *et al.,* 2007).

Characterization: karyotype analysis. Karyotype analysis was performed on highly proliferating reprogrammed cell cultures to maximize the number of cells arrested in the metaphase stage. This is important because it is when chromosomes are condensed and chromosomal abnormalities can be detected under the microscope. Cells were incubated in conditioned medium supplemented with 20 ng/ml colcemid for 45 minutes, washed twice in PBS, detached using 0.25% trypsin to ensure maximal cell separation, neutralized and washed with PBS again. The cell pellet was detached from the bottom of the tube, and 10 ml of previously warmed hypotonic solution (0.075 M KCl) was added to the cells drop wise, while the cells were being vortexed. Samples were incubated at 37°C for 10 minutes, and then 1 ml of chilled Carnoy's fixative solution (methanol:acetic acid, 3:1) was also added to the cells drop wise, while vortexing. Finally, cells were pelleted by centrifugation and resuspended in 10 ml of chilled Carnoy's fixative solution, and stored at -20°C until karyotype analysis was performed through the G-banding method by a cytogeneticist at the Donostia University Hospital. Karyotypes of 20 metaphases were analyzed per each cell line. If chromosomal abnormalities, such as trisomies or loss of chromosomes, were detected, cells were subcloned three times and karyotype analysis was repeated to select a subclone that was free of karyotype abnormalities.

Myogenic differentiation: production of lentiviruses harboring the two components of the PAX7-inducible system. rtTA-FUGW and hPAX7-pSAM2 vectors that comprise the doxycycline-inducible PAX7 system (figure 21) were packaged in 293T cells using VSV-G and Delta-8.9 plasmids as coating and packaging plasmids, respectively (plasmids were kindly provided by Dr. Perlingeiro, University of Minnesota). Each vector was packaged in separated plates and the supernatants of both virus-producing plates were combined prior to iPSC (induced Pluripotent Stem Cell) infection. Viral production was initiated by seeding 10^6 293T cells in two 60mm-tissue culture plates in DMEM medium supplemented with 10% FBS, 100 U/ml penicillin and 100 µg/ml streptomycin. The following day, each plate was simultaneously transfected with a combination of 3 plasmids (5 µg of rtTA-FUGW or hPAX7-pSAM2 + 2 µg of VSV- G + 3 µg of Delta 8.9) using Lipofectamine LTX with Plus reagent as transfection reagent, as described by Darabi and Perlingeiro (Darabi and Perlingeiro, 2014). Twenty-four hours following transfection, culture media was replaced with 5 ml of mTeSR1. Forty-eight hours following transfection, the supernatants of the virus-producing plates were harvested and used for iPSC infection, and an additional 5 ml of mTeSR1 were added to the virus-

producing plates for the second viral production. Seventy-two hours following transfection, culture supernatants were harvested and used to infect iPSCs for a second time, and virus-producing plates were discarded.

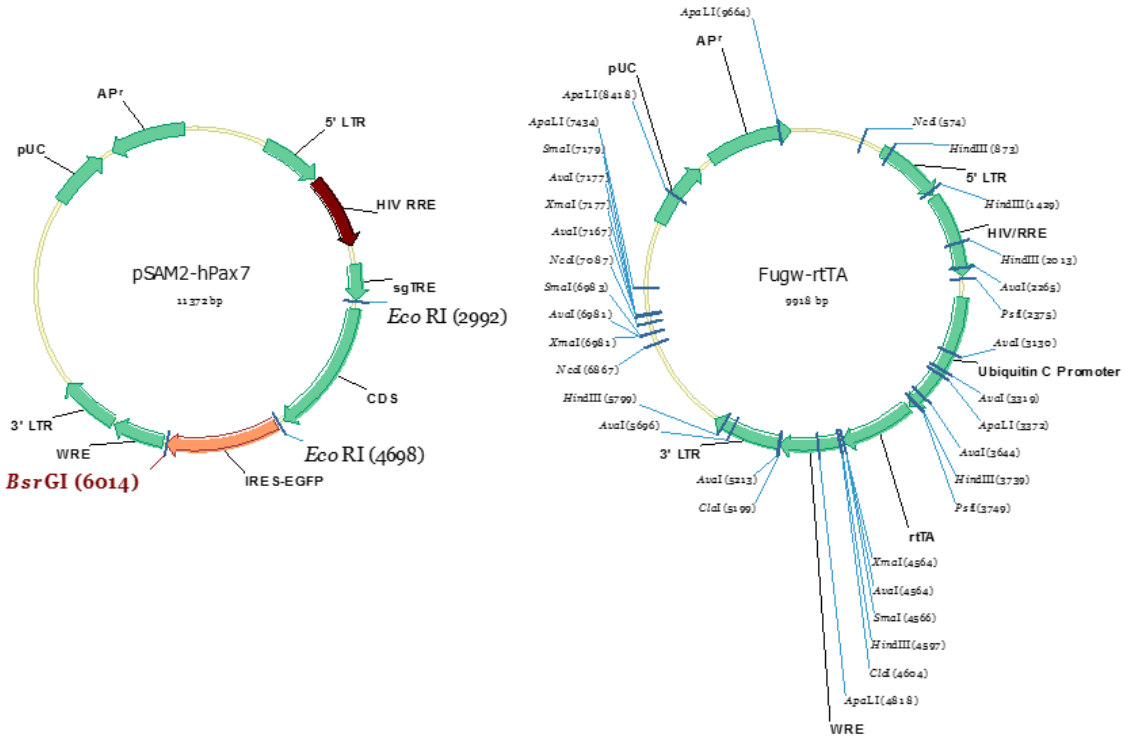

Figure 21. Maps of the plasmids comprising the doxycycline-inducible *PAX7* expression system.

Myogenic differentiation: infection of iPSCs with rtTA-FUGW- and hPAX7-pSAM2-carrying lentiviruses. Matrigel-adapted iPSCs were harvested using accumax to maximize cell disaggregation prior to infection. Between $5x10^5$ and $7x10^5$ cells were seeded in a well of a matrigel-coated 6 well-plate in mTeSR1 medium supplemented with 100 U/ml penicillin, 100 µg/ml streptomycin and 10 µM of Y-27632 ROCK inhibitor. The following day, iPSCs, which were at 40-50% confluence, were infected using the virus-containing supernatants. To this effect, hPAX7-pSAM2 and rtTA-FUGW lentivirus-containing supernatants were combined by mixing equal volumes of each supernatant, filtered through a low protein-binding filter and supplemented with polybrene to a final concentration of 1 µg/ml. The medium of iPSCs to be infected was aspirated and 5 ml of this viral supernatant were added to the well. Cells were spin-infected at 2 500 rpm for 90 minutes at 33°C. Following infection, the medium was replaced with mTeSR1. The following day, the same iPSCs were infected again with the second viral supernatant, following the protocol described as for the first infection. From that point on, mTeSR1 was replaced daily.

Myogenic differentiation: analysis of infection efficiency. Once the infected cells reached 70-80% confluence, they were expanded in two T25 matrigel-coated flasks, and a small aliquot was plated in two 24-well matrigel-coated wells. Cells seeded in the T25 flasks were cultured until they reached 70% confluence, and frozen to generate a stock

of infected iPSC vials. Infection efficiency was determined by estimating the percentage of GFP-positive cells by flow cytometry, after incubating the cells seeded in one of the P24 wells with 1 μg/ml doxycycline for 24 hours. Only the cells infected with the two viral vectors and incubated with doxycycline are able to induce the expression of *PAX7* and its *GFP* reporter. Cells seeded in the other well were used as a negative control. Infection rates over 15% were considered sufficient to proceed with the myogenic induction of the iPSCs.

Myogenic differentiation: induction of iPSCs into muscle progenitor cells. iPSCs infected with the *rtTA-hPAX7* system and cultured in a T25 flask at 70% confluence were harvested using accumax and plated in 6 P60mm plates, non-treated for tissue culture to avoid their attachment, in 5 ml mTeSR1 medium supplemented with 10 μM ROCK inhibitor. These plates were incubated in a 5% CO_2 incubator and 100% humidity for 2 days, on top of an orbital shaker at 20 rpm. After 2 days, homogeneous EBs formed in the culture dishes. At that point, culture medium was switched to EB medium (IMDM medium supplemented with 15% FBS, 10% horse serum, 1% chick embryo extract, 2 mM GlutaMAX, 50 μg/ml ascorbic acid, 4.5 mM monothioglycerol, 100 U/ml penicillin and 100 μg/ml streptomycin) supplemented with 5 μM ROCK inhibitor, and plates were incubated shaking for another 3 days. At day 5 of the induction protocol, the medium of the plates was replaced with 5 ml of EB medium supplemented with 5 μM ROCK inhibitor, and EBs were incubated shaking for two more days. At day 7 of the induction protocol, EBs formed in each P60mm dish were transferred to a gelatinized T75 flask containing 12 ml of EB medium supplemented with 5 ng/ml FGF_2. Flasks were incubated for 3 days in the incubator, with special care to avoid their movement to maximize EB attachment to the surface. Following those three days (day 10 of the protocol), when cell outgrowths were visible, expression of *PAX7* was induced by switching the culture medium to EB medium supplemented with 1 μg/ml doxycycline and 5 ng/ml FGF_2. Cells were cultured in these conditions for 4 more days, replacing their medium on day 12 of the protocol. At day 14, cultures were harvested using 0.25% trypsin, and taken to the cell sorting facility in sorting buffer (PBS supplemented with 0.5% BSA, 25 mM HEPES and 5 mM EDTA, pH 7.2). Figure 22 represents the induction protocol. Cells were sorted in a BD FACSAria III sorting cytometer, and GFP-positive cells were plated in gelatin-coated dishes in EB medium supplemented with 1 μg/ml doxycycline and 10 ng/ml FGF_2 (and 5 μM ROCK inhibitor during the first 24 hours) at a density of 50 000 cells/cm^2. Cells were cultured for 2-3 days, until they reached 90% confluence. At that point, they were split 1:5 in order to get the maximum number of cells. At passage 1 and 2 following sorting, GFP-positive cells were considered myogenic precursors and they were frozen for future experiments.

Due to recent publications claiming that GSK3β inhibition activates the canonical Wnt signaling pathway, promoting the mesodermal differentiation of stem cells (van der Velden *et al.,* 2007; Xu *et al.,* 2013), transient inhibition of GSK3β was assessed as a

potential optimization of the induction protocol. To do so, the previously described EB medium was supplemented with 5 µM GSK3β inhibitor CHIR99021 between day 2 and day 3 (24-hour inhibition) or between day 2 and day 4 (48-hour inhibition), as indicated in figure 22. The effect of transient GSK3β inhibition was assessed by checking the morphology of EBs and the percentage of GFP-positive cells at day 14 of the induction protocol. Moreover, these progenitors were differentiated for 5 days in *15% KOSR medium* (detailed below) and differentiation efficiencies were assessed by comparing the frequency of sarcomeric myosin-positive cells in culture.

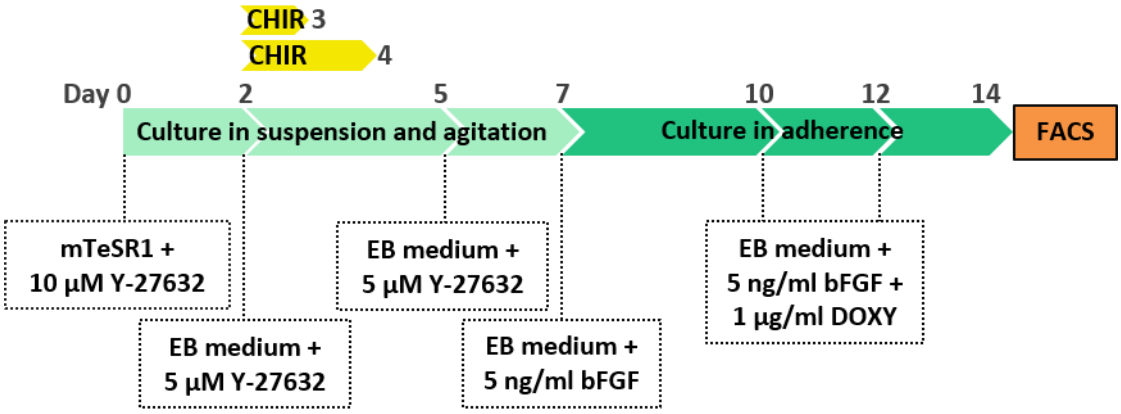

Figure 22. Schematic representation of the myogenic induction protocol. EBs were formed in agitation in mTeSR1 medium supplemented with 10 µM ROCK inhibitor (Y-27632). At day 2 of the protocol, cells were switched to EB medium supplemented with 5 µM ROCK inhibitor, and at this point, the GSK3β inhibitor CHIR99021 (CHIR) was added at a final concentration of 5 µM and kept for 24 or 48 hours (represented in yellow). At day 7, EBs were seeded in 0.1% gelatin-coated flasks in EB medium, and *PAX7* expression was induced at day 10 of the protocol by adding doxycycline (DOXY) to the culture medium. At day 14, PAX7-expressing muscle progenitors were sorted according to their GFP expression. (Adapted from Darabi and Perlingeiro, 2014).

Myogenic differentiation: terminal differentiation of PAX7-expressing iPSC-derived myogenic progenitors into myotubes. iPSC-derived myogenic precursors at passage 3 or 4 post-sorting were cultured on 0.1% gelatin-coated wells or chambers in EB medium supplemented with 10 ng/ml FGF_2 and 1 µg/ml doxycycline until they reached 80-100% confluence. At that point, cells were washed once with DPBS and terminal differentiation medium was added to the cultures. Several terminal differentiation media were tested: A) *2% HS medium* (low glucose DMEM supplemented with 2% HS, 100 U/ml penicillin and 100 µg/ml streptomycin) (Darabi and Perlingeiro, 2014), B) *20% KOSR medium* (KO- DMEM supplemented with 20% KOSR, 1x NEAA, 2mM GlutaMAX, 100 U/ml penicillin and 100 µg/ml streptomycin) , C) *conditioned medium* (2% HS medium or 20% KOSR medium exposed to differentiating C2C12 cultures for 24 hours and filtered) and D) *15% KOSR medium* (high glucose DMEM supplemented with 15% KOSR, 2 ng/ml IGF1 and 10 ng/ml HGF) (Chal *et al.,* 2016). Differentiations were performed in 24- well plates for RNA and Western blot analysis, and in 4-well chamber slides for immunofluorescence detection, using 700 µl of differentiation medium per well/chamber. In the *sandwich coating*, an additional layer of 1:3-diluted matrigel was

added on top of the cells to be differentiated (200 µl per well), and incubated for 30 minutes in the incubator at 37°C (Toral-Ojeda *et al.,* unpublished data). Next, 700 µl of the corresponding differentiation medium were added to each well. Comparative differentiations were performed, where two differentiation media were tested in each differentiation test, as detailed below:

Test 1: *2% HS medium* versus *conditioned 2% HS medium.* Control 1 and patient 1-derived progenitors at passage 4 post sorting were cultured up to 80% confluence. Next, cells were washed once with DPBS and cultured in *HS medium* or *conditioned 2% HS medium* for 12 days. Culture media were replaced every two days. Myogenic differentiation was assessed through immunofluorescence at day 12 of differentiation, based on the density of sarcomeric myosin-positive cells found in the cultures.

Test 2: *2% HS medium* versus *20% KOSR medium.* Control 1 and patient 4-derived muscle progenitor cells at passage 4 were cultured up to 100% confluence and then switched to 1:1 induction-differentiation medium without doxycycline for 24 hours. Thereafter, cells were washed once with DPBS, switched to differentiation medium and cultured for 4 more days. Myogenic differentiation was assessed through immunofluorescence based on the density of sarcomeric myosin-positive cells found in the differentiated cultures, as well as on the expression rates of a set of myogenic genes (*PAX7*, desmin, myogenin and dystrophin) assessed through qPCR.

Test 3: *20% KOSR medium* versus *15% KOSR medium,* with *regular coating* versus *the sandwich coating.* Control 1-derived myogenic progenitors were cultured up to 100% confluence, washed with DPBS, switched to the corresponding differentiation medium and incubated for 5 days (regular coating). In parallel, for the sandwich coating, myogenic progenitors were cultured up to 100% confluence, washed once with DPBS and coated with a layer of 1:3-diluted matrigel (approximately 200 µl per well). Finally, cultures were incubated at 37°C for 30 minutes and 700 µl of the corresponding differentiation media were added to each well and cultured in differentiation media for 5 days. Myogenic differentiation was assessed through immunofluorescence detection of sarcomeric myosin-positive cells.

Once terminal differentiation conditions were optimized, differentiated cultures were used for gene expression analysis through qPCR, protein expression through Western blot or immunofluorescence analyses.

Myogenic differentiation: gene expression analysis through qPCR. Cells at day 0 and day 5 of differentiation were washed once with DPBS and harvested on ice using cell scrapers and 700 µl of QIAzol lysis reagent. Samples were stored at -80°C until RNA extraction was performed. Total RNA was extracted using the RNeasy Mini kit and the QIAcube extraction system, following manufacturer's instructions. 1 µg of RNA from each sample was retrotrascribed using the High Capacity cDNA Reverse Transcription Kit, following manufacturer's instructions. Finally, gene expression was assessed

through qPCR in a CFX384 Touch Real-Time PCR Detection System (Biorad), using TaqMan probes and TaqMan gene expression master mix. TATA-binding protein (*TBP*) or glyceraldehyde 3-phosphate dehydrogenase (*GAPDH*) were used as endogenous controls, and gene expression levels were represented relative to *TBP* or *GAPDH* expression, which were considered as 100%. Gene expression differences between healthy control-derived cultures and patient-derived cultures were analyzed using GraphPad Prism 5 (Mann-Whitney test with a 0.05 significance level).

Analysis of *CAPN3* maturation along the differentiation process of healthy control samples was performed at day 0, 2 and 5 of differentiation. Expression results were normalized to 100%, which was calculated by summing the expression rate of the immature isoform (lacking exon 6, delta exon 6) and the mature isoform (probe for exons 5-6) at each timepoint. Evolution of expression rates of each isoform along the myogenic differentiation were analyzed using GraphPad Prism 5 (Friedman test with a 0.05 significance level).

Myogenic differentiation: Western blot analysis. Cells at day 0 and day 5 of differentiation were washed once with DPBS and harvested on ice using cell scrapers and 150 µl of protein extraction buffer per cm^2 of tissue culture area. The buffer consisted on 20 mM Tris HCl, pH 8, 0.1 mM EDTA, 1 mM DTT, 28 µM E-64, 20 µg/ml soybean trypsin inhibitor and 2 mM PMSF supplemented with 5% 2-mercaptoethanol and 1x loading buffer. Samples were transferred to eppendorf tubes, incubated at 95°C for 5 minutes and stored at -80°C. For Western blot analysis, protein extracts were heated at 95°C for 3 minutes, and 20-40 µl of each protein extract were loaded into 6% or 8% acrylamide gels. Human muscle protein extracts were used as a positive control, and the Precision Plus Kaleidoscope Prestained Protein ladder was used as a protein size marker. Gels were run at 50V-80V and proteins were transferred to Hibond Nitrocellulose membranes using the Mini Trans-Blot Electrophoretic Transfer system for 1 hour at 400 mA. Membranes were stained with Ponceau S solution to ensure adequate protein transfer, washed out shaking with tap water, and blocked with 5% skimmed milk diluted in TBST solution (0.05 M Tris, 0.2 M NaCl, 1% triton X-100 in distilled water, pH8) shaking for 1 hour at room temperature. Subsequently, membranes were incubated overnight in rollers in presence of primary antibodies diluted in 5% BSA in TBST (table 11). The following day, membranes were washed three times in TBST (5 minutes per wash) and incubated in secondary antibody (table 11) diluted in 5% skimmed milk in TBST. Finally, membranes were washed three times in TBST (5 minutes per wash) and proteins were detected by chemilluminescence using the SuperSignal West Dura kit as substrate. Protein levels were assessed using Image Studio Lite 5.2, and standardized to GAPDH protein levels.

Primary antibodies			Secondary antibodies	
Target	**Reference**	**Dilution**	**Reference**	**Dilution**
Calpain 3	COP-080049 (IS2), Cosmobio	1:1 000	P0449, Dako	1:2 000
Calpain 3	NCL-CALP-12A2, Novocastra	1:15	P0447, Dako	1:2 000
GAPDH	2118, Cell Signaling Technology	1:10 000	P0448, Dako	1:10 000
PAX7	NBP1-69130, Novusbio	1:50	P0448, Dako	1:5 000
SERCA2	sc-376235, Santa Cruz Biotech	1:500	P0447, Dako	1:1 000

Table 11. Primary and secondary antibodies used for protein detection through Western blot.

Myogenic differentiation: immunofluorescence analysis. Cells were fixed in 4% PFA for 10 minutes at room temperature and permeabilized with PBS/0.3% triton X-100 for 20 minutes at room temperature. Next, samples were blocked in PBS/10% donkey serum/0.01% triton X-100 diluted in PBS, for 1 hour at room temperature, and then incubated with the primary antibody (table 12) diluted in PBS/0,3% triton X-100 overnight at 4°C. The following day, cells were washed twice with DPBS and incubated with the secondary antibody (table 12) diluted 1:500 in DPBS for 1 hour at room temperature, protected from light. Finally, samples were washed twice with DPBS, incubated for 3 minutes in 1 µg/ml Hoechst diluted in PBS, and washed again twice with DPBS, once with distilled water and once with deionized water. Finally, samples were mounted using the fluorogel mounting medium.

Primary antibodies			Secondary antibodies		
Target	**Reference**	**Dilution**	**Antibody**	**Reference**	**Dilution**
Myogenin	DSHB, F5D	1:50	DαM-af555	Invitrogen, A-31570	1:500
PAX7	DSHB, PAX7	1:50	DαM-af555	Invitrogen, A-31570	1:500
Sarcomeric myosin	DSHB, MF20	1:50	DαM-af488 DαM-af555	Invitrogen, A-21202 Invitrogen, A-31570	1:500 1:500

Table 12. Primary and secondary antibodies used for immunofluorescence analysis. Abbreviations: Alexa fluor (af), anti (α), donkey (D), mouse (M).

Transplantation of iPSC-derived muscle progenitor cells. Ten 7 week-old NSG (NOD.Cg-Prkdcscid Il2rgtm1Wjl/SzJ) mice were purchased from Charles River and housed in the animal facility. All procedures were performed following the guidelines and approval provided by Biodonostia Animal Care Committee and the Regional Government of Gipuzkoa (Donostia, Spain), in accordance with the Spanish Royal Decree (53/2013), the European Directive 2010/63/EU and the guidelines established by the National Council on Animal Care. At 8 weeks of age, *tibialis anterior* (TA) muscles were injured one day prior to cell transplantation. To do so, mice were anesthetized by inhaled isoflurane (Forane), administered at 5% concentration for induction and at 3% concentration for maintenance during surgery. Muscles were injured by injecting 7.5 µl of cardiotoxin from *Naja mossambica mossambica* at 100 µM in both TA muscles of each mouse, using a

beveled 26G needle. The following day, control 2- and patient 1-derived 10^6 progenitor cells at passage 4 post-sorting were transplanted into the right TA of each animal (cells from each sample were transplanted into 5 mice) in 15 µl of final volume. 15 µl of DPBS were injected into the left TA of each mouse and these were used as negative controls. Mice were housed in the animal facility for 30 days, to allow muscle regeneration. Thirty days following transplantation, mice were sacrificed by inhalation of 5% isoflurane followed by inhalation of CO_2.

Detection of transplanted cells in TA muscle sections. Immediately following sacrifice, TA muscles were extracted and frozen in nitrogen-chilled isopentane, embedded in O.C.T. Serial 7 µm-thick sections were cut using the cryostat and slides were stored at - 80°C until immunofluorescence analysis was performed. 49 µm-spaced sections (one every 7 sections) were used to assess the engraftment and regenerative potential of transplanted cells. To do so, double immunofluorescence detections were performed, which allowed for the detection of human cell nuclei (detection of human lamin A/C- positive nuclei) and fibers generated by the transplanted human cells (detection of human Dystrophin-positive fibers). To proceed with immunofluorescence analysis, slides were incubated at room temperature for 30 minutes to allow samples to thaw. Next, sections were rehydrated in DPBS for 5 minutes, permeabilized in DPBS/0.3% triton X-100 for 20 minutes, washed in DPBS for 5 minutes, and blocked in 3% BSA in DPBS for 1 hour at room temperature. Then, samples were incubated overnight at 4°C with the primary antibody against human dystrophin diluted in blocking solution. The following day, samples were incubated for 1 hour at room temperature with the second primary antibody, anti-human-lamin A/C, diluted in blocking solution. Thereafter, samples were washed 3 times in DPBS (5 minutes per wash), and then incubated for 45 minutes at room temperature with secondary antibodies (table 13) diluted in blocking solution and protected from light. Finally, samples were washed twice in DPBS (5 minutes per wash), incubated with 1 µg/ml Hoechst for 3 minutes to stain cell nuclei, and washed again twice in DPBS, once in distilled water and once in deionized water (2 minutes per wash). Samples were covered with a coverslip using fluorogel as mounting medium, and stored at 4°C until they were visualized in the fluorescence microscope.

Primary antibodies			**Secondary antibodies**		
Target	Reference	Dilution	Antibody	Reference	Dilution
h-Dystrophin	Leica, NCL-DYS3	1:20	DαM-af555	Invitrogen, A-31570	1:500
h-Lamin A/C	Abcam, ab108595	1:500	DαR-af488	Invitrogen, A-21206	1:500

Table 13. Primary and secondary antibodies used for immunofluorescence analysis. Abbreviations: human (h), alexa fluor (af), anti (α), donkey (D), mouse (M), rabbit (R).

Differences in the number of human lamin A/C-positive cells (indicative of cell engraftment) and human dystrophin-positive fibers (indicative of muscle regeneration) detected in TAs transplanted with healthy control- and patient-derived samples were analyzed using GraphPad Prism 5 (Mann-Whitney test with a 95% confidence interval).

RESULTS

Selection of samples to be reprogrammed. Five LGMD2A patients were chosen as representative samples of the wide genetic and phenotypic variability found among LGMD2A patients examined at the Donostia University Hospital. Patients 2, 3 and 5 carried the most commonly found mutation among the Basque population of LGMD2A patients, which is located in exon 22. Importantly, patient 5 harbored this mutation in homozygosis, whereas the other two patients carried this mutation in combination with a mutation in exon 11 leading to a single amino acid substitution (patient 2) or an intronic mutation in intron 14 that generates a neoexon (patient 3). Patient 1 had an entire deletion of one of the *CAPN3* alleles whereas the other allele harbored a mutation in exon 24. Patient 4 carried a mutation in exon 5 in one of the *CAPN3* alleles, leading to a single amino acid substitution, and a mutation in exon 16 in the other allele, leading to a shift in the codon reading frame that theoretically produced a truncated calpain 3 protein (table 14, figure 23). Next, two age- and sex-matched fibroblasts from healthy donors were selected as controls of the study. One of these primary fibroblast cultures was derived from a female in her late forties, thus being a sex-matched control for patients 1, 3 and 5, and an age-matched control for patients 3 and 5. The second control was derived from a male in his twenties, and was a control sample for patients 2 and 4 accordinng to their sex, and patient 1, 2 and 4 regarding their age.

Patients disability was assessed at the moment of the biopsy according to the modified MVA scale (table 4), and disease phenotype was determined based on the MVA grade and age, according to table 5. Patient 3 and 5 were wheelchair-bound, being classified as grade 8 and thus, with a severe phenotype. Patient 1 and 2 had difficulties to rise from the floor and thus were classified as grade 4. Therefore, according to their age, they were classified as severe and advanced phenotypes, respectively. Patient 4 displayed a grade 3 disability and was classified as an intermediate phenotype.

Table 14 summarizes the data available about the sample donors. Figure 23 represents the location of the mutations found in *CAPN3* gene (blue scheme) and the predicted effect on the synthesized calpain 3 protein (green scheme). Single amino acid substitutions appear to produce a 94 kDa calpain 3 protein that could be detected through Western blot, whereas mutations leading to frame-shifts or loss of the stop codon lead to truncated calpain 3 proteins, which might be more prone to further degradation.

Sample	Age	Sex	Origin of biopsy	MVA grade	Phenotype	Mutated site	DNA mutation	Protein mutation
Control 1	49	Female	Breast	-	Healthy	-	-	-
Control 2	27	Male	Foreskin	-	Healthy	-	-	-
Patient 1	22	Female	Lower back	4	Severe	Entire gene EX24	Complete deletion c.2465G>T	Absent X822Leuext62*
Patient 2	33	Male	Buttock	4	Advanced	EX11 EX22	c.1468C>T 2362_2363delinsTCATCT	Arg490Trp Arg788Serfs*14
Patient 3	47	Female	Abdomen	8	Severe	In14 EX22	1782+1072G>C 2362_2363delinsTCATCT	Lys595Valfs*70 Arg788Serfs*14
Patient 4	27	Male	Proximal arm	3	Intermediate	EX5 EX16	c.760A>G c.1910delC	Lys254Glu Pro637Hisfs*25
Patient 5	48	Female	Upper back	8	Severe	EX22 EX22	2362_2363delinsTCATCT 2362_2363delinsTCATCT	Arg788Serfs*14 Arg788Serfs*14

Table 14. Summary of clinical and molecular data available from sample donors. A 'Sample' name was given to each donor-derived fibroblasts used in the study. 'Age' indicates the age of the donors when the biopsies were performed. 'Origin of the biopsy' indicates the body region where the skin biopsy was performed. 'MVA grade' indicates the degree of disability of the patients at the moment of the biopsy, according to the MVA scale.'Phenotype' refers to the disease severity, considering the MVA grade and age of each patient. 'Mutated site' refers to the gene region where the mutation is located. 'DNA mutation' indicates the mutations found in *CAPN3* gene in these patients. 'Protein mutation' indicates the predicted variation in the calpain 3 protein outcome caused by the mutations.

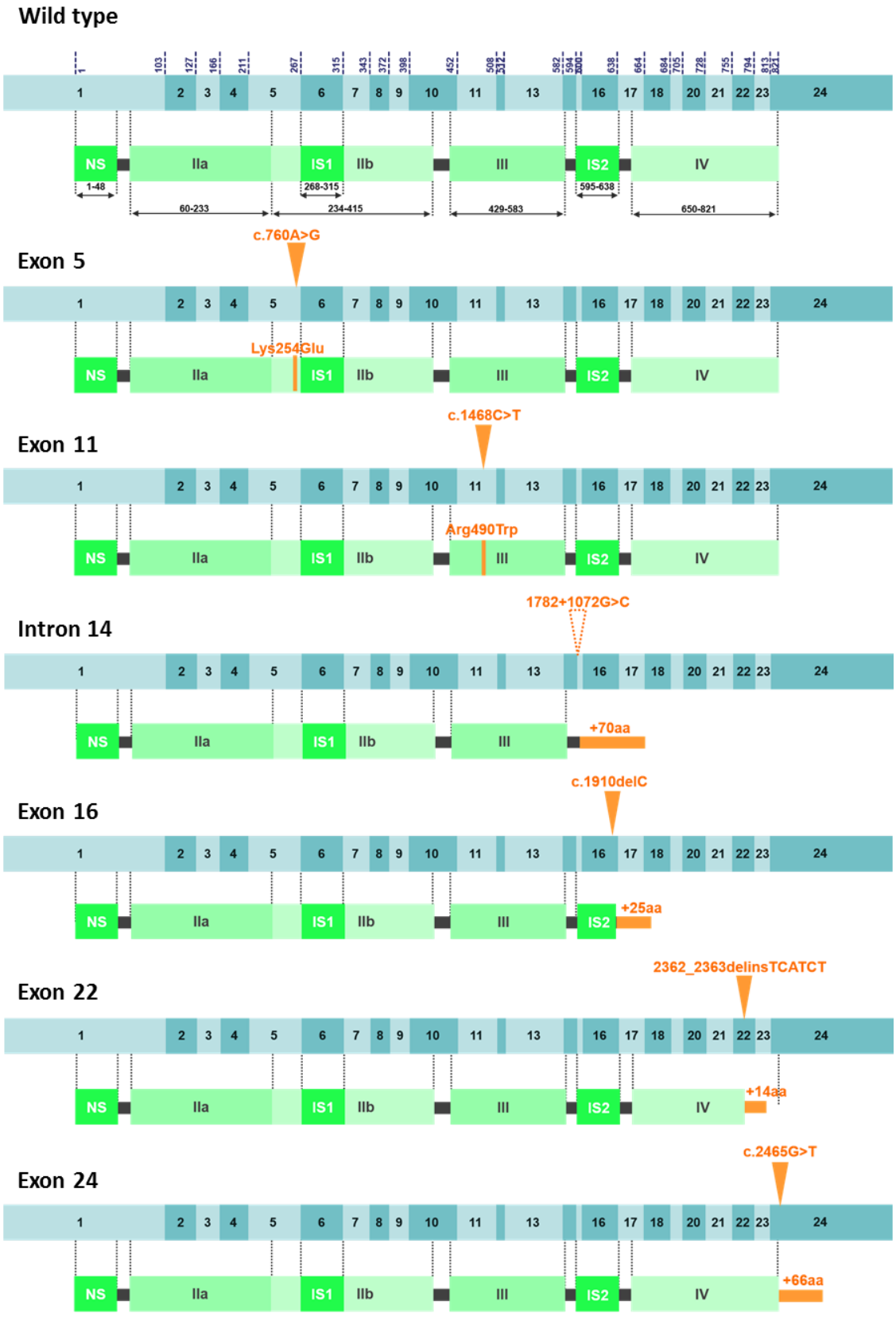

Figure 23. Schematic representation of *CAPN3* exons (in blue, from 1 to 24) and calpain 3 protein (in green). The different domains and calpain 3-specific regions are indicated in green. Mutations found in patients are indicated in orange over the blue scheme, whereas the predicted protein modifications caused by the mutations are also indicated in orange over the green scheme. Numbers on top of the blue scheme of the wild type allele indicate the amino acids encoded by each exon.

Establishment of patient-specific fibroblast cultures. Patient-specific primary fibroblast cultures were established as previously described, and frozen at early passages (passage 5 or lower). Healthy donor-derived fibroblasts were obtained from the Basque Biobank and expanded in the same way as patient-derived fibroblasts. Cultures were highly proliferative and displayed no evident morphologic differences among patient- and control-derived cells.

Induction of cell reprogramming. Fibroblasts at early passages (passages 3-5) were infected with retroviral vectors expressing the four Yamanaka factors: *OCT4, SOX2, KLF4* and *cMYC*. Three to six weeks after seeding the infected fibroblasts over feeder cells and culturing them in hES medium, colonies of cells resembling the morphology of embryonic stem cells (i.e., homogeneous surface of the colonies with smooth and well defined edges) were visible. Six colonies from each plate were selected and independently seeded over feeder cells to establish clonally independent cell lines. However, only 3 colonies were observed in the patient 5-specific reprogramming plate, and therefore, only three colonies could be picked. Most of the selected colonies led to stable cultures that could be passaged over time for more than 20 passages. Five clones were established for each of the control-derived samples, 6 clones were obtained from patients 2, 3 and 4 and only three clones were established for patient 1 and 5.

These cell lines were mechanically expanded over feeder cells, and they were also adapted to feeder-free culture conditions by culturing them on matrigel-coated dishes, as previously described. Reprogrammed cells cultured in both conditions were used to test their pluripotency following a set of characterization tests. These tests enabled the selection of one specific clone per reprogrammed sample that met all the characterization requirements to be considered as a pluripotent cell line, and thus as an iPSC line.

Characterization of reprogrammed cells

- ***AP staining.*** AP-positive colony formation has been reported as a sensitive indicator of embryonic stem cells (O'Connor *et al.,* 2008). Thus, detection of AP activity in reprogrammed samples is considered as an indicator of pluripotency (Martí *et al.,* 2013). AP staining was assessed in each of the clones established from each sample, and consistent AP activity was detected in all the clones tested (figure 24), as shown by the blue staining of the colonies.

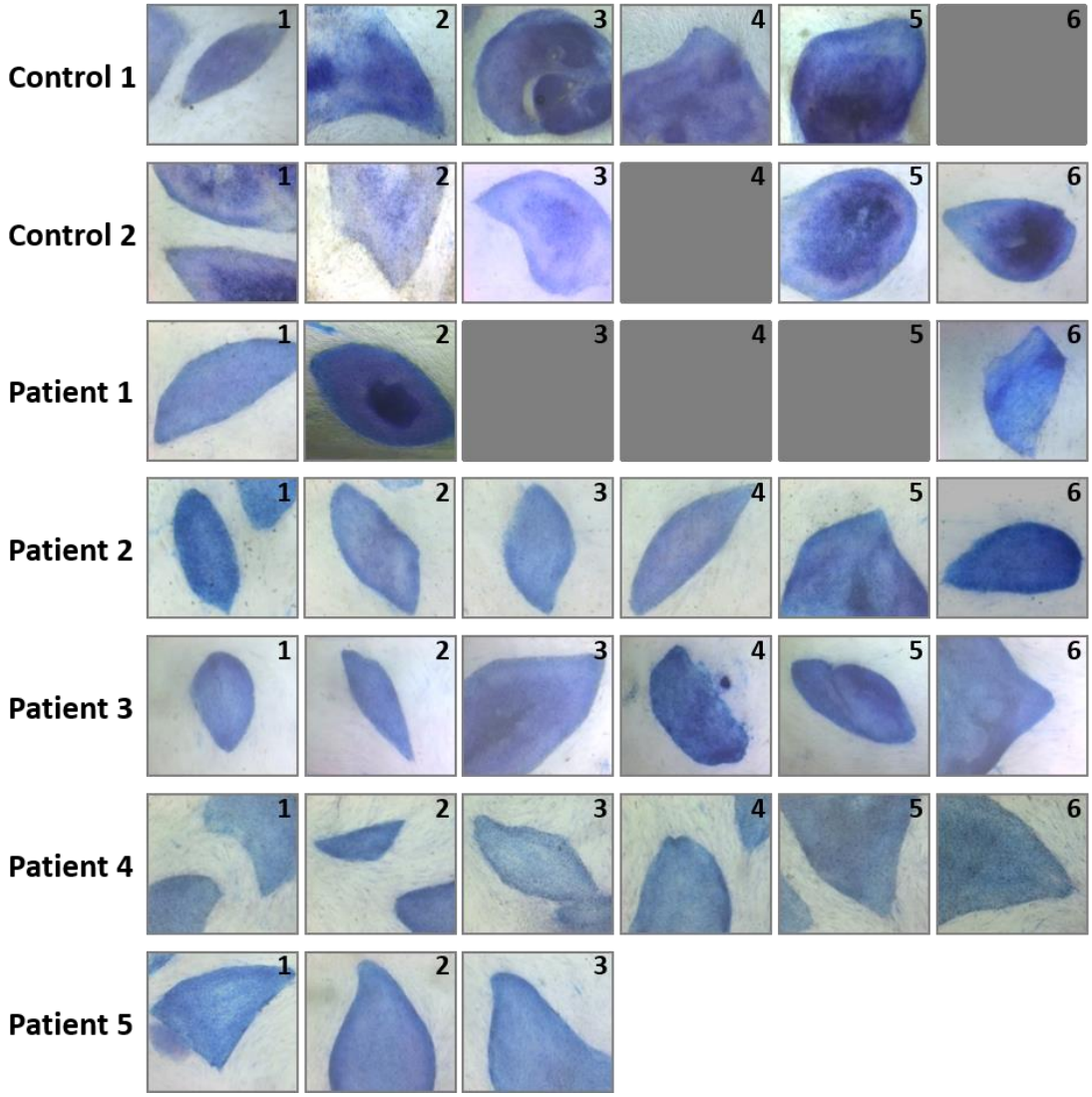

Figure 24. Representative picture of an AP-stained colony from each cell line, captured with an optical microscope. The blue color indicates AP activity, as a result of the colorimetric reaction occurred when colonies were incubated with the AP Blue Membrane Substrate Solution. Numbers in the pictures indicate the clones (clonal cell line) established for each reprogrammed sample. Grey squares represent colonies that were picked to establish a clone but failed to lead to a stable cell line.

- ***Silencing of transgenes and induction of pluripotency genes.*** The second characterization test assessed the expression of pluripotency genes. Currently, it is widely accepted that the correct reprogramming of cells implies the silencing of reprogramming transgenes (Brambrink *et al.,* 2008; Aasen *et al.,* 2008), as well as the induction of endogenous pluripotency genes. Therefore, expression of a set of pluripotency genes and the transgenes used for cell reprogramming were assessed by qPCR (figure 25.a, 25.b and 25.c). Transgene silencing was considered successful if only the expression level of each of the four transgenes was clearly downregulated. In this study, expression levels lower than 0.5% of that of *GAPDH* were considered

optimal. Induction of endogenous pluripotency genes was considered successful if their expression was detectable and not higher than *GAPDH* expression.

Based on these results, two clones per sample were selected for further characterization. Control 1-derived cell lines successfully induced the expression of endogenous pluripotency genes.However, clones 1, 2 and 3 failed to clearly silence transgene expression. Therefore, clones 4 and 5 were selected for further characterization. As for control 2, induction of pluripotency genes and transgene silencing were achieved by all the cell lines, and thus, clones 2 and 5 were selected for further characterization because these two clones showed the most consistent transgene silencing. Among the three cell lines derived from patient 1, endogenous pluripotency genes were induced in the three clones established, but transgenic *KLF4* expression was not silenced in clone 2 and thus, clones 1 and 6 were selected for further characterization. Similarly, based on transgene silencing data, clones 1 and 6 were selected for patient 2. As for patient 3, endogenous pluripotency genes were not induced in clone 1, and transgenic *OCT4* was not silenced for clones 2 and 3. Therefore, clones 5 and 6 were selected for further characterization. Transgenes were not silenced in clones 3, 4, 5 and 6 of patient 4, and moreover, endogenous *OCT4* expression level was abnormally high in clones 5 and 6. Hence, clones 1 and 2 were selected for further characterization. Finally, clones 2 and 3 of patient 5 were analyzed and only clone 2 met the transgene silencing criteria. However, clone 3 was also included in the following characterization tests due to the lack of alternative clones for this specific patient.

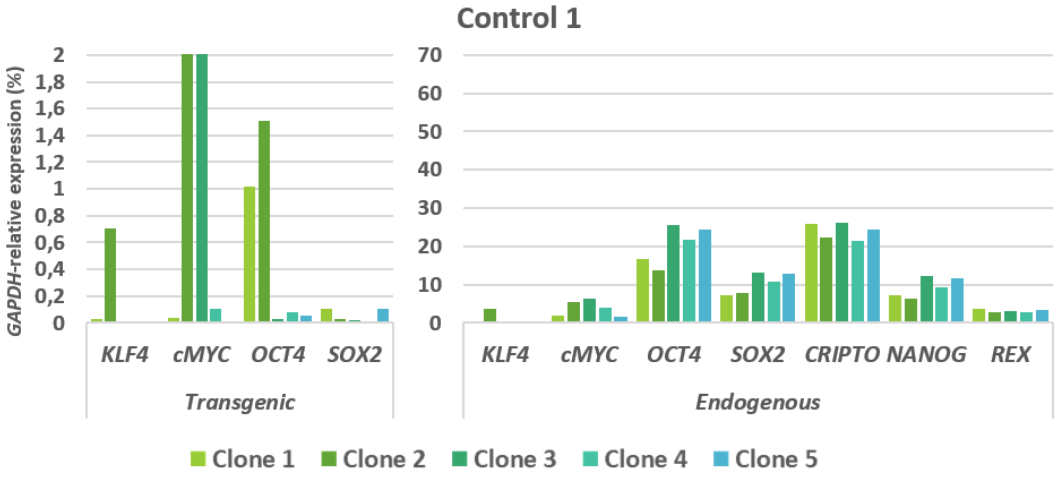

Figure 25.a. Expression rates of transgenic and endogenous pluripotency genes quantified by qPCR and represented relative to *GAPDH* expression (100%) in C1-derived reprogrammed cells.

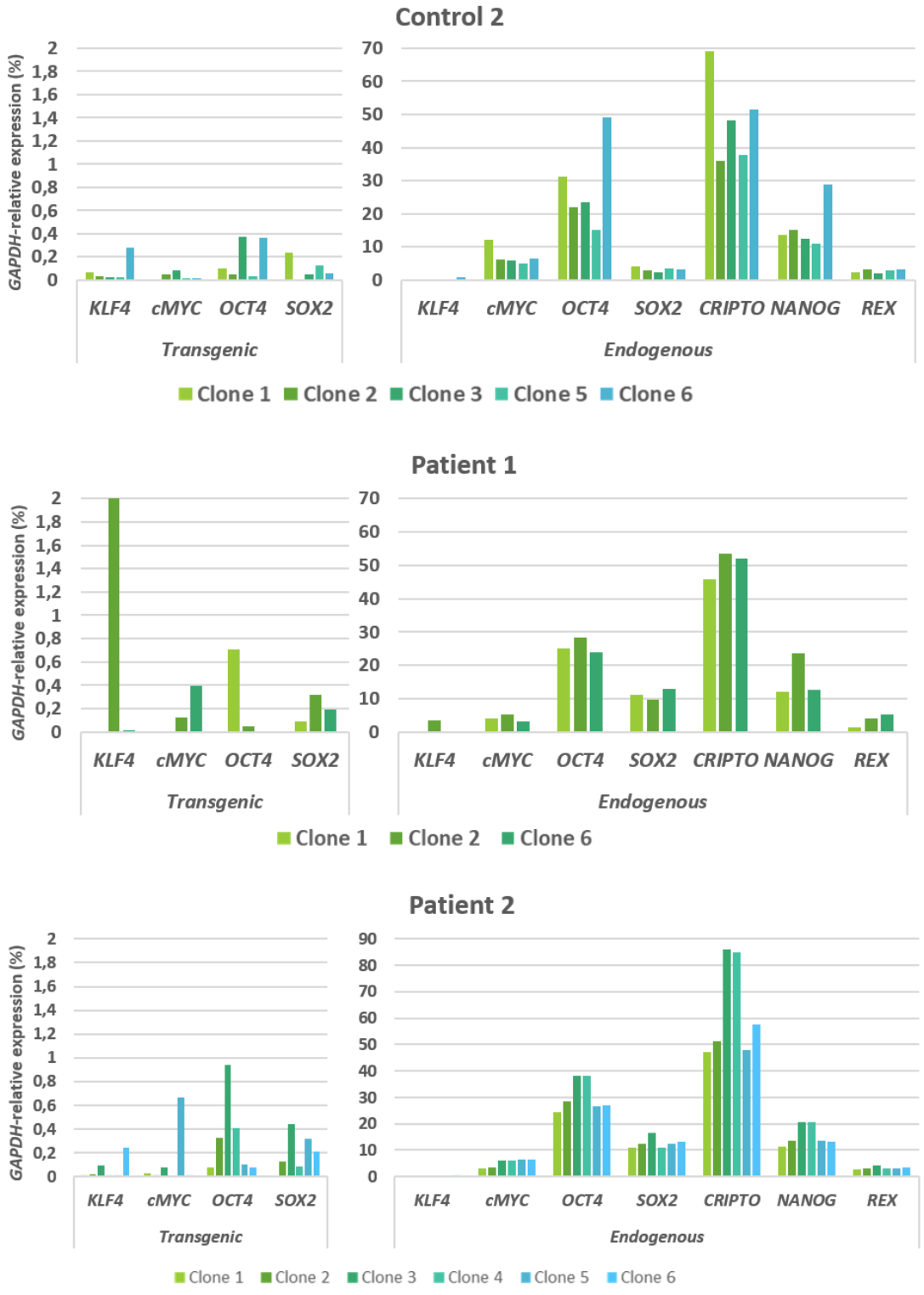

Figure 25.b. Expression rates of transgenic and endogenous pluripotency genes quantified by qPCR and represented relative to *GAPDH* expression (100%) in C2, P1 and P2-derived reprogrammed cells.

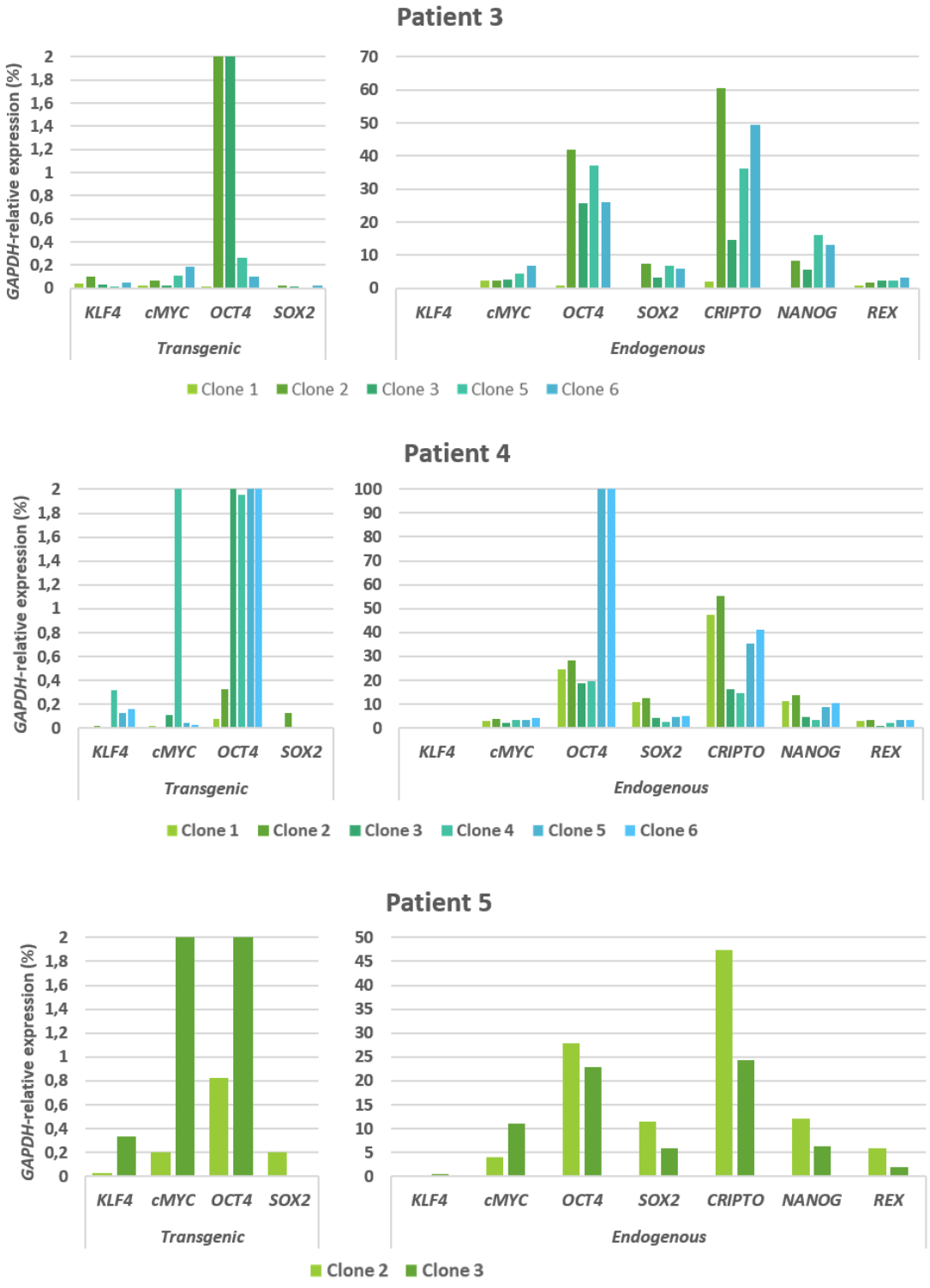

Figure 25.c. Expression rates of transgenic and endogenous pluripotency genes quantified by qPCR and represented relative to *GAPDH* expression (100%) in P3, P4 and P5-derived reprogrammed cells.

- ***Determination of clonal independence.*** Southern blot analysis was performed to detect the number of transgene insertions in the two clones selected for each sample based on gene expression results. Fibroblast-derived DNA from each sample was

used as a negative control. The number of transgene inserts was determined by comparing the number and size of the bands detected in reprogrammed samples versus their corresponding fibroblasts. The different number and/or size of bands (corresponding to transgenes) found between the two clones selected for each sample confirmed their independent origin. Detection of *cMYC* (figure 26) and *OCT4* (figure 27) through Southern blot analysis provided adequate information to confirm that the two reprogrammed cell lines selected for each donor had an independent origin. The data was inconclusive with regards to the Southern blot results for *KLF4* and *SOX2* transgene insertions.

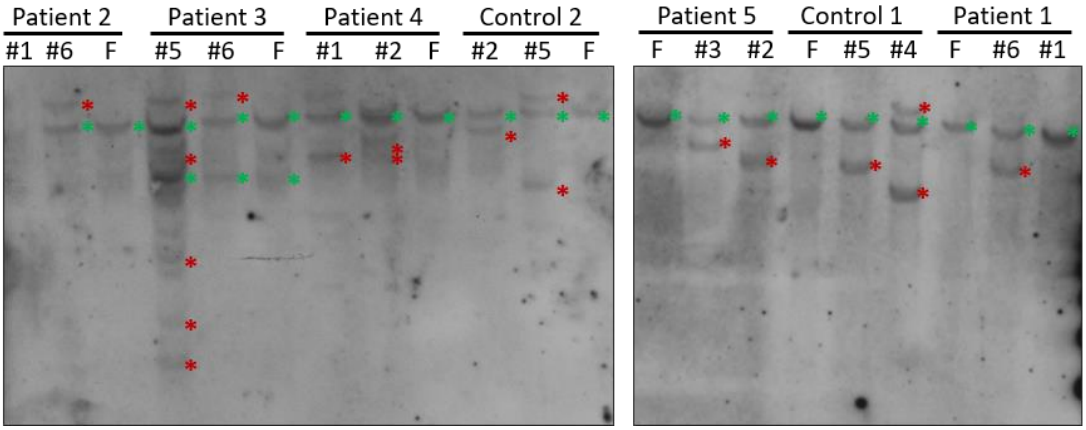

Figure 26. Southern blot images show bands corresponding to endogenous *cMYC* (Green asterisks), and transgenic *cMYC* (red asterisks). Samples are indicated as F (fibroblasts) and reprogrammed cell clones (#).

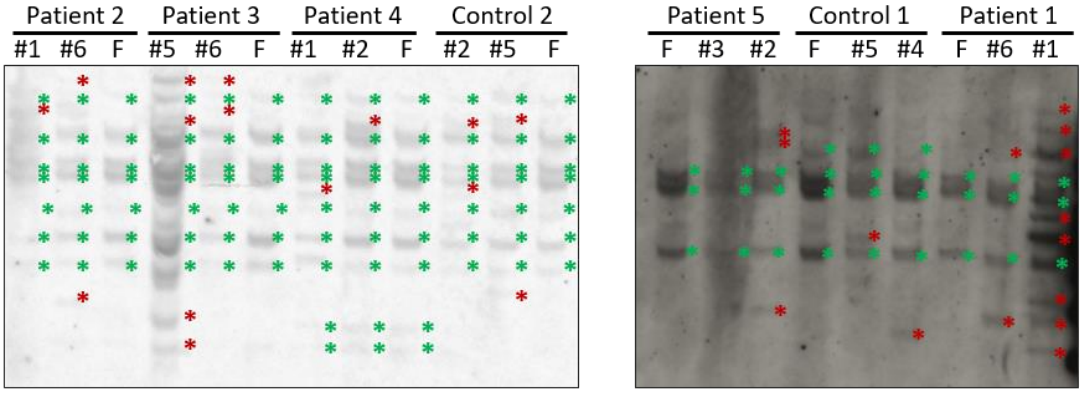

Figure 27. Southern blot images show bands corresponding to endogenous *OCT4* (Green asterisks), and transgenic *OCT4* (red asterisks). Samples are indicated as F (fibroblasts) and reprogrammed cell clones (#).

Following verification of clonal independence, one clone per sample was selected for further characterization. These clones were the following: Clone 4 for control 1, clone 5 for control 2, clone 6 for patient 1, clone 1 for patient 2, clone 6 for patient 3, clone 1 for patient 4 and clone 2 for patient 5. The selection performed was based on previous gene expression data, as well as discarding the cell lines that displayed an elevated number of transgene insertions, such as clone 1 of patient 1 and clone 5 of patient 3.

- ***Detection of pluripotency markers in reprogrammed samples.*** Expression of a set of seven pluripotency markers was studied by immunofluorescence: OCT4, NANOG, SOX2, SSEA-3, SSEA-4, TRA1-60 and TRA1-81.

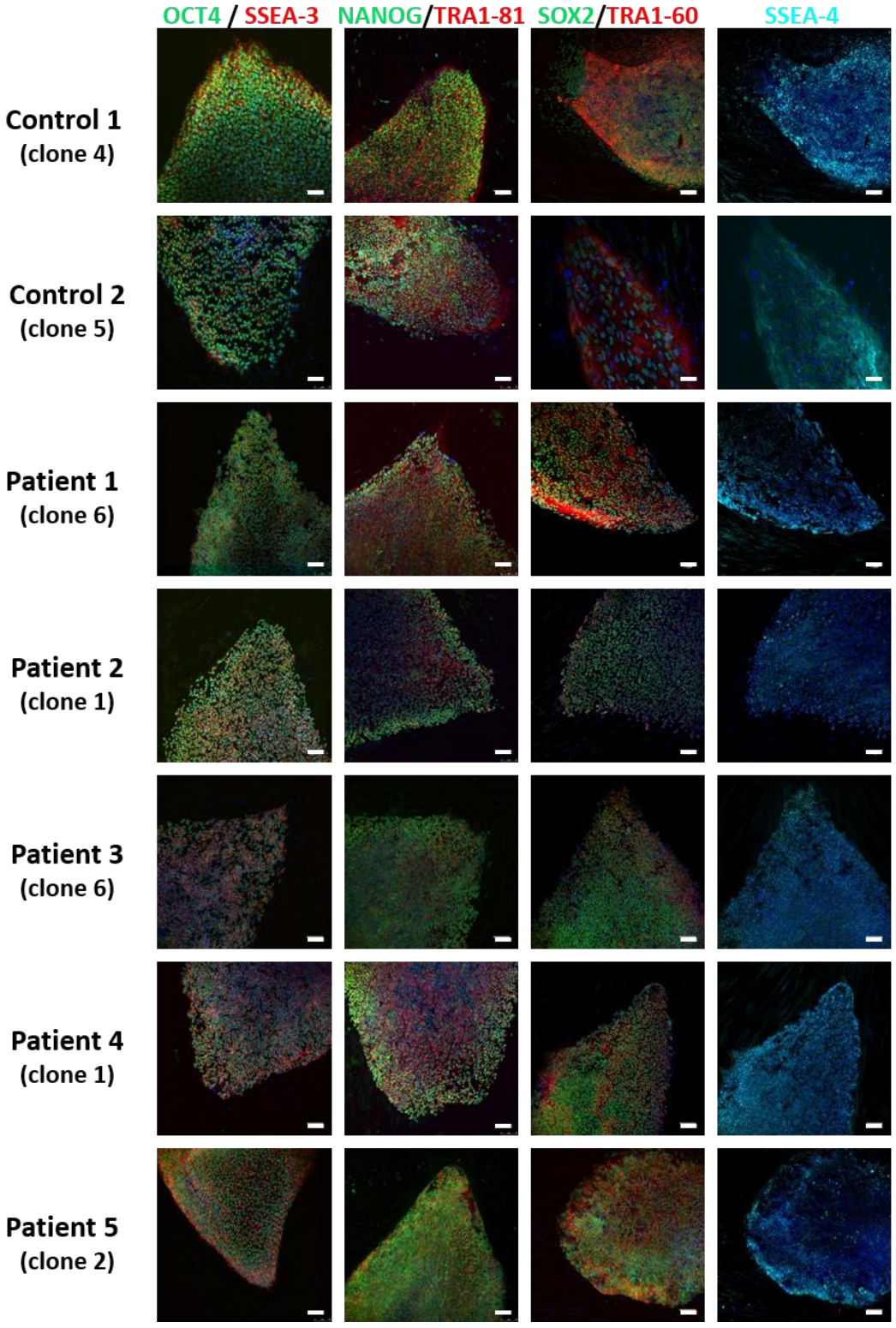

Figure28. Multiple immunofluorescence images of pluripotency markers. Images in column 1 prove the expression of OCT4 (green) and SSEA-3 (red). Images in column 2 show the expression of NANOG (green) and TRA1-81 (red). Images in column 3 and 4 correspond to a triple immunodetection of SOX2 (green), TRA1-60 (red) and SSEA-4 (cyan). Cell nuclei are shown in blue in all the images. Scale bars: 75 μm.

Fully reprogrammed cell lines are expected to express the entire set of markers (Martí *et al.,* 2013). As shown in figure 28, all the selected cell lines stained intensely for each of the seven markers detected by multiple immunofluorescence.

- ***In vitro differentiation potential of reprogrammed cell lines.*** Once the expression of pluripotency markers was proven, the next characterization test intended to demonstrate that these cells had the potential to differentiate into cell types derived from the three primordial germ layers found in the embryo. Therefore, reprogrammed cells were cultured in specific culture conditions to induce their differentiation into these cell types. Immunofluorescence detection of lineage-specific markers was used to verify their successful differentiation. Expression of at least one of the lineage-specific markers was sufficient to validate that cells had differentiated into each of the three lineages.

  As for the directed differentiation towards ectoderm, expression of the neuron-specific class III beta-tubulin (TUJ1) was detected in each of the cell lines, whereas glial fibrillary acidic protein (GFAP) was only detected in some samples (figure 29).

  As for the differentiation into mesoderm lineage, α-smooth muscle actin (α-SMA) was broadly expressed in each of the differentiated samples, whereas the transcription factor GATA4, known to be essential during cardiac development, was detected in most, but not all the samples (figure 29).

  As for endoderm differentiation, the transcriptional activator of liver-specific genes FOXA2 was detected in all the samples, whereas expression of α-fetoprotein (AFP), considered as the fetal form of serum albumin, was only detected in some samples (figure 29).

  Therefore, these results indicate that the reprogrammed cell lines possessed the potential to differentiate into cell types derived from the three primordial cell layers, providing strong evidence of their pluripotency.

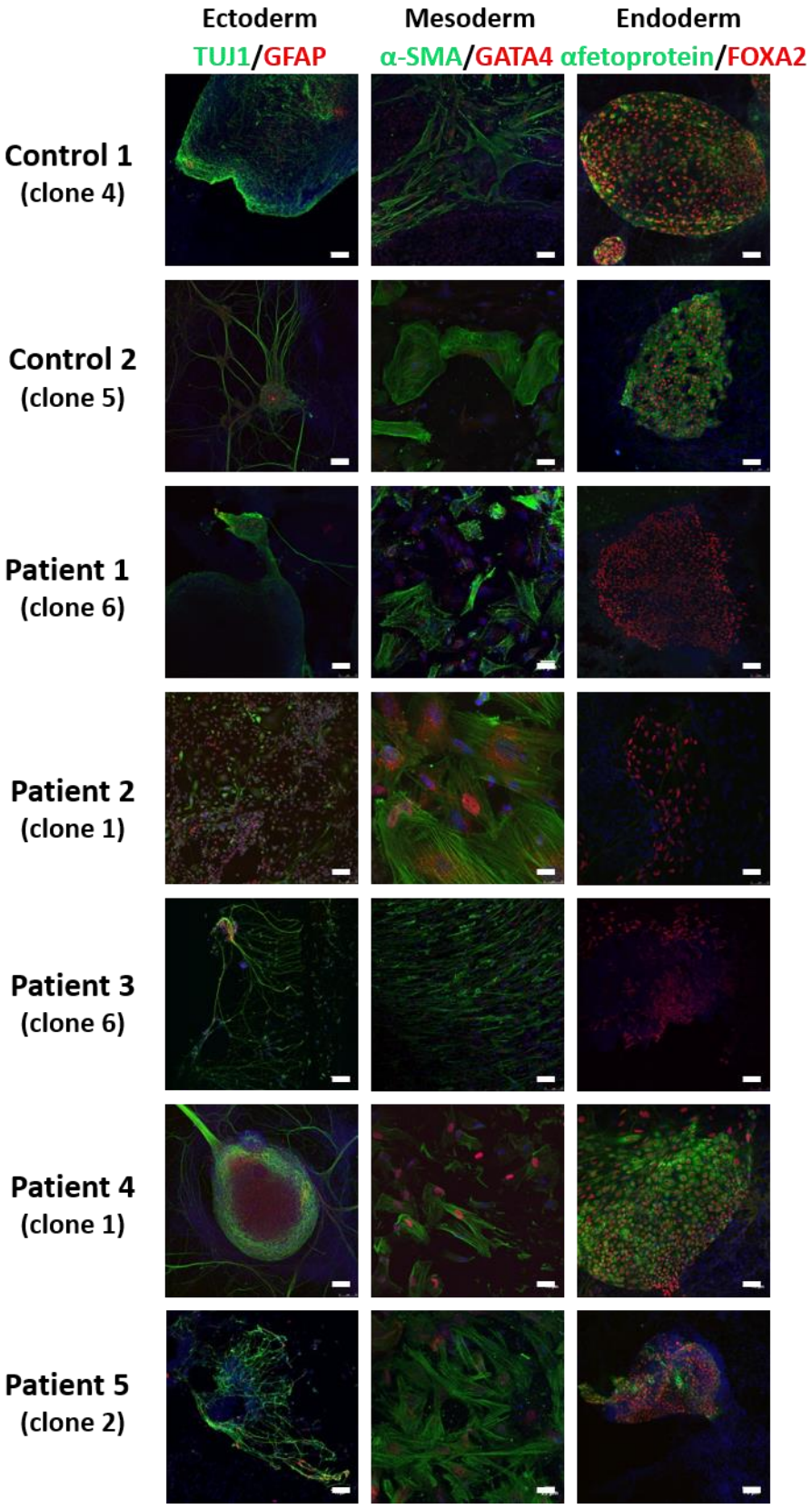

Figure 26. Multiple immunofluorescence images of lineage-specific markers. Images in column 1 show the detection of TUJ1 (green) and GFAP (red), used as ectoderm markers. Images in column 2 show the expression of α-SMA (green) and GATA4 (red), used as mesoderm markers. Images in column 3 correspond to a double immunodetection of the endoderm markers AFP (green) and FOXA2 (red). Cell nuclei are shown in blue in all the images. Scale bars: 75 µm.

- ***Epigenetic reprogramming.*** Methylation of CpG islands located in the promoter regions is considered to be a strong epigenetic modification that represses gene transcription. Consistent with this, promoters of the pluripotency genes *OCT4* and *NANOG* have been found to be highly methylated in differentiated cell types, such as fibroblasts (Freberg *et al.,* 2007), preventing their expression. Since reprogramming induces the expression of these and other pluripotency genes, their promoters are expected to be considerably demethylated in fully reprogrammed iPSC lines.

  Therefore, we studied their methylation status through bisulfite sequencing and found that CpG islands located in the promoter regions of these genes were highly demethylated. Overall, 98.3% of the CpG islands analyzed in the promoter region of *OCT4* were found unmethylated (figure 30), whereas 86.9% of the CpG islands found in the *NANOG* promoter region were unmethylated (figure 31). These unmethylation percentages are substantially higher compared to the percentage of non-methylated CpG islands found in some of our fibroblast cell lines analyzed (data not shown) and those percentages found in differentiated cells that have been reported in the literature (Freberg *et al.,* 2007).

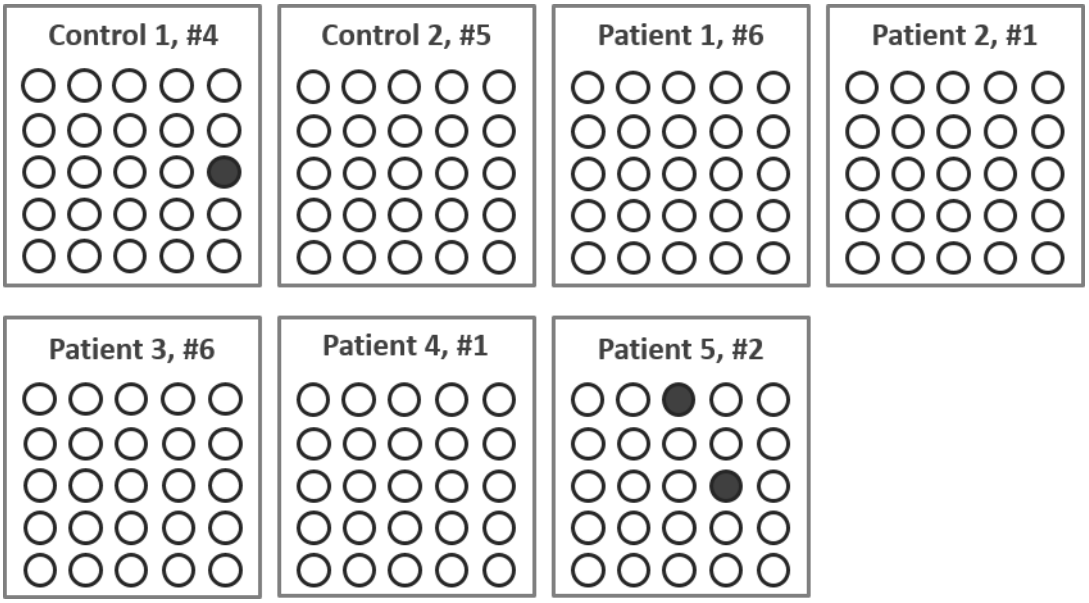

Figure 30. Schemes representing the methylation pattern of CpG islands in the *OCT4* promoter region. Five bacterial clones, each one representing the promoter region of one reprogrammed cell, were sequenced for each reprogrammed cell line. Circles in each line correspond to the methylation status of five CpG islands located in this promoter region in each of the bacterial clones studied. White circles represent a demethylated CpG island whereas black circles represent a methylated CpG island. #: clone (reprogrammed cell line).

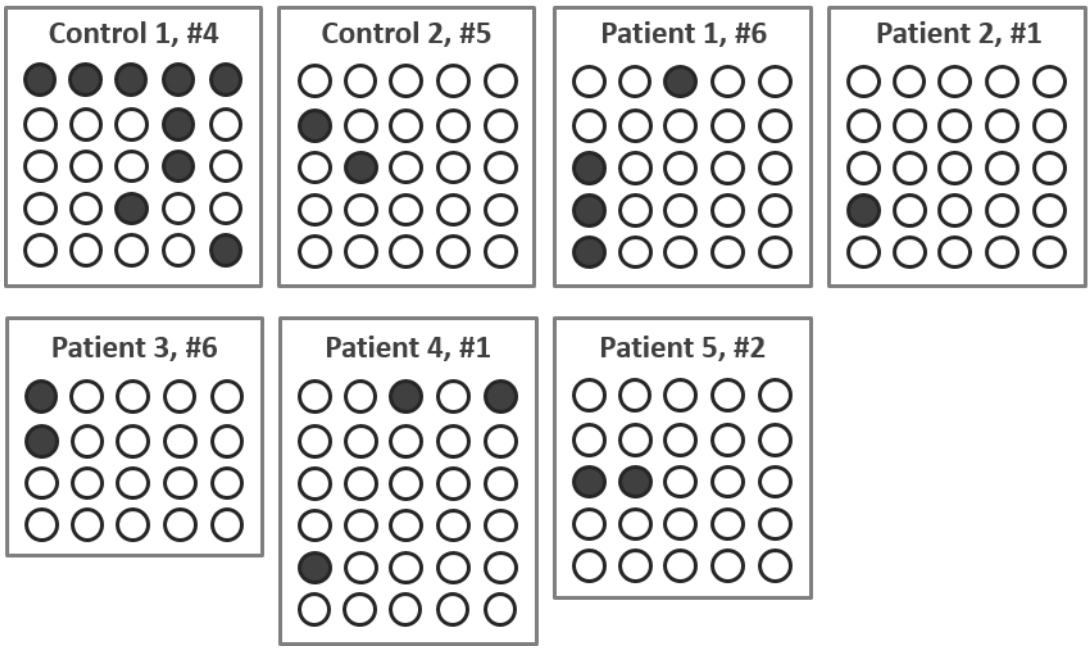

Figure 31. Schemes representing the methylation pattern of CpG islands in the *NANOG* promoter region. Between 4 and 6 bacterial clones, each one representing the promoter region of one reprogrammed cell, were sequenced for each reprogrammed cell line. Circles in each line correspond to the methylation status of five CpG islands located in this promoter region in each of the bacterial clones studied. White circles represent a demethylated CpG island whereas black circles represent a methylated CpG island. #: clone (reprogrammed cell line).

- ***Karyotype stability.*** Cell reprogramming using integrative vectors, as well as the extensive culture of the cells, facilitates the emergence of chromosomal abnormalities. To circumvent chromosomal abnormalities in our newly generated cell lines, karyotype analysis through G-banding was performed in each of the cell lines. This analysis detected chromosomal abnormalities in control 1 clone 4, patient 2 clone 1 and patient 5 clone 2 cell lines, such as loss of a chromosome or appearance of trisomies. Importantly, these abnormalities affected less than 20% of the metaphases analyzed (data not shown). Therefore, these cell lines were subcloned for three passages over feeder cells, establishing 6 subclones for each clone (e.g., Control 1 clone 4 a-f), and these subclones were karyotyped again to ensure the absence of chromosomal abnormalities in each of the cell lines (figure 32). Newly established subclones displayed no chromosomal abnormalities and were named as control 1 subclone 4a, patient 2 subclone 1d and patient 5 subclone 2f. These cell lines were used in following myogenic differentiation experiments, together with control 2 clone 5, patient 1 clone 6 and patient 4 clone 1 cell lines.

The patient 3-derived cell line (patient 3 clone 6) met each of the characterization requirements to be considered as a fully reprogrammed cell line. However, it showed a strong tendency to spontaneously differentiate after 4-5 passages growing in pure (matrigel-adapted) culture conditions. This fact raised doubts regarding the degree of pluripotency acquired by this cell line and consequently, it was excluded from the following myogenic differentiation tests.

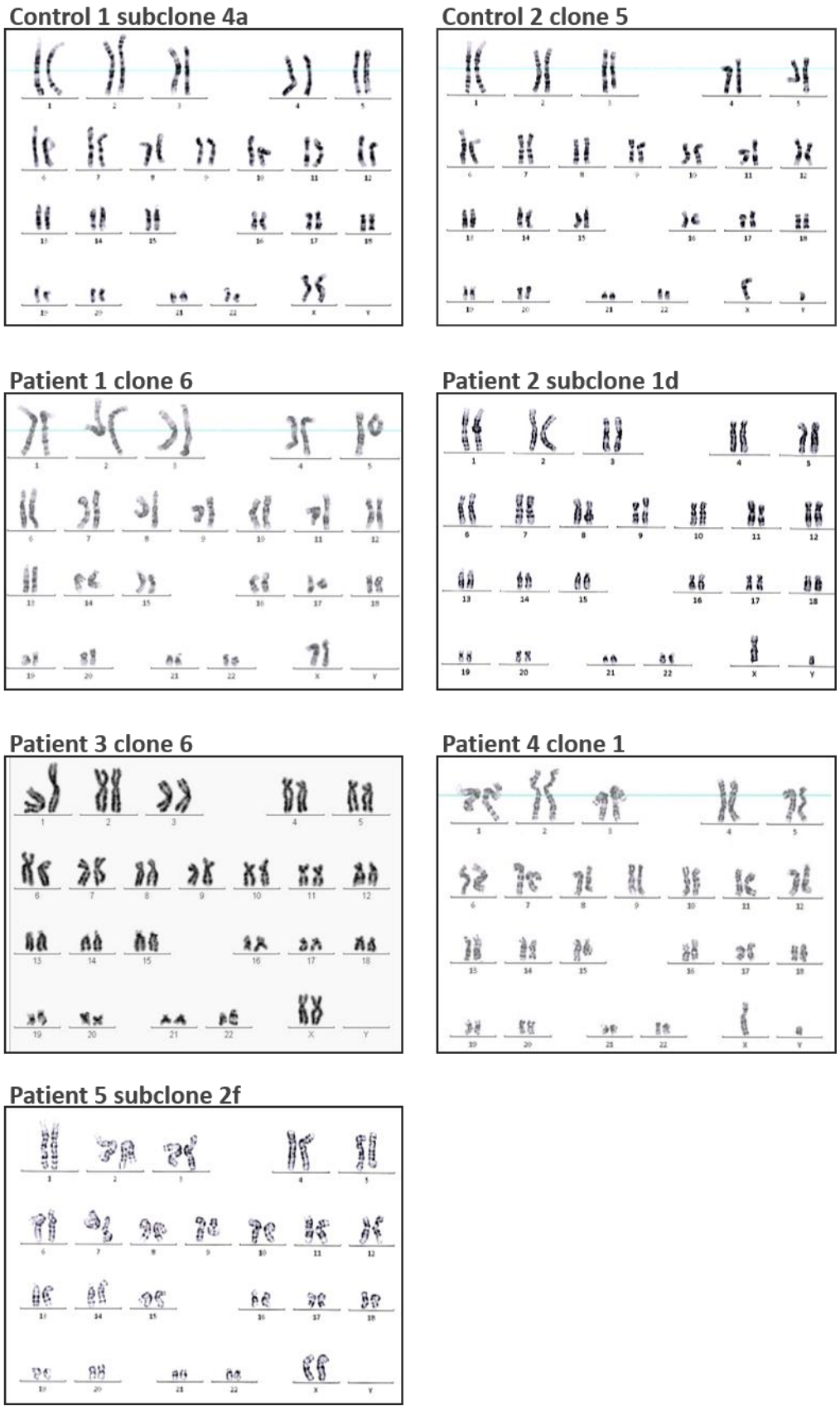

Figure 32. Representative karyotype images for each of the reprogrammed cell lines analyzed, once further subcloning was performed in the cell lines in which karyotype abnormalities were previously detected.

Infection of iPSCs with lentiviruses comprising the doxycycline-inducible PAX7 expression system. Matrigel-adapted iPSCs were infected with the *PAX7-rtTA* vector system and infection efficiencies were determined by assessing the percentage of GFP- expressing cells by flow cytometry.

Overall, the infection efficiencies were high (over 25% of cells infected) for some of the cell lines, such as control 1 and patient 1, whereas other cell lines appeared to be especially resistant to infection, such as control 2 and patient 5. However, several infection attempts performed with some of the cell lines indicated that infection efficiency was greatly influenced by other technical factors, such as cell confluence at the time of infection, quality of the viral production and cell disaggregation reagent used when seeding the iPSCs to be infected (data not shown). Figure 33 shows histograms representing the analysis of the infection efficiency performed on the six iPSC lines of the study.

Myogenic induction of PAX7-rtTA-infected iPSC lines and selection of GFP-positive progenitors. Myogenic induction of the six iPSC lines was performed as previously described. Each of the iPSC lines grown on matrigel displayed a very similar morphology both before and after being infected with the *PAX7-rtTA* system. During the myogenic induction process, minor differences were visible among the different cell lines with regards to EB size and morphology (figure 34). However, since these differences were also observed in different inductions performed for each cell line, they could be attributed to small variations in the number of cells plated at the beginning of the induction, rather than to cell line-specific features.

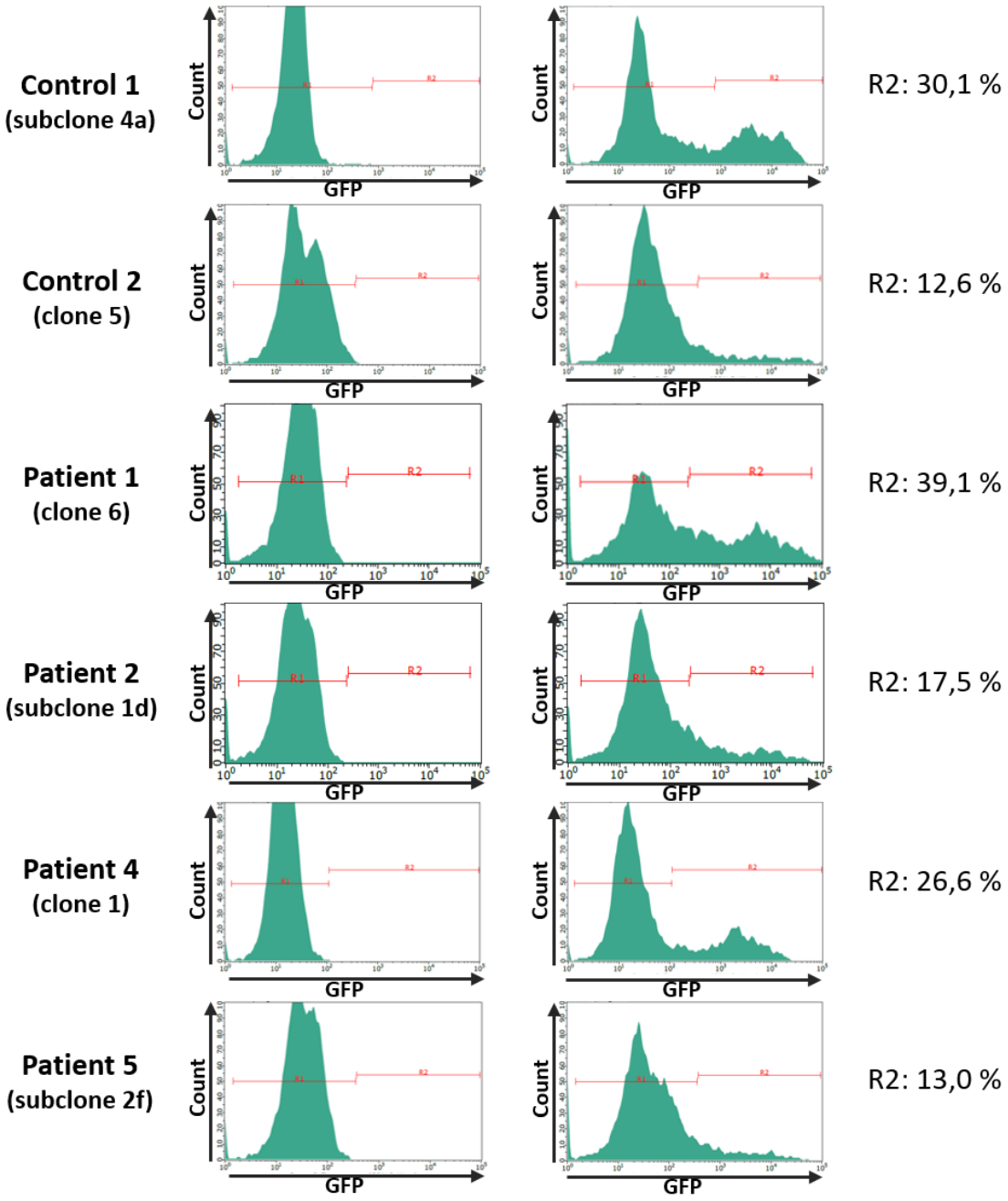

Figure 33. Representative histograms showing the infection efficiencies achieved for each of the iPSC lines infected with the *PAX7-rtTA* vector system. Histograms in the left column represent the fluorescence detected in iPSCs that had not been incubated with doxycycline, and were used to determine the GFP-negative region (R1). Histograms in the right column correspond to infected cell lines incubated with doxycycline to induce the expression of *PAX7-GFP*. GFP-positive events are detected in the R2 region. Percentages of events located in the R2 region determine the infection efficiency.

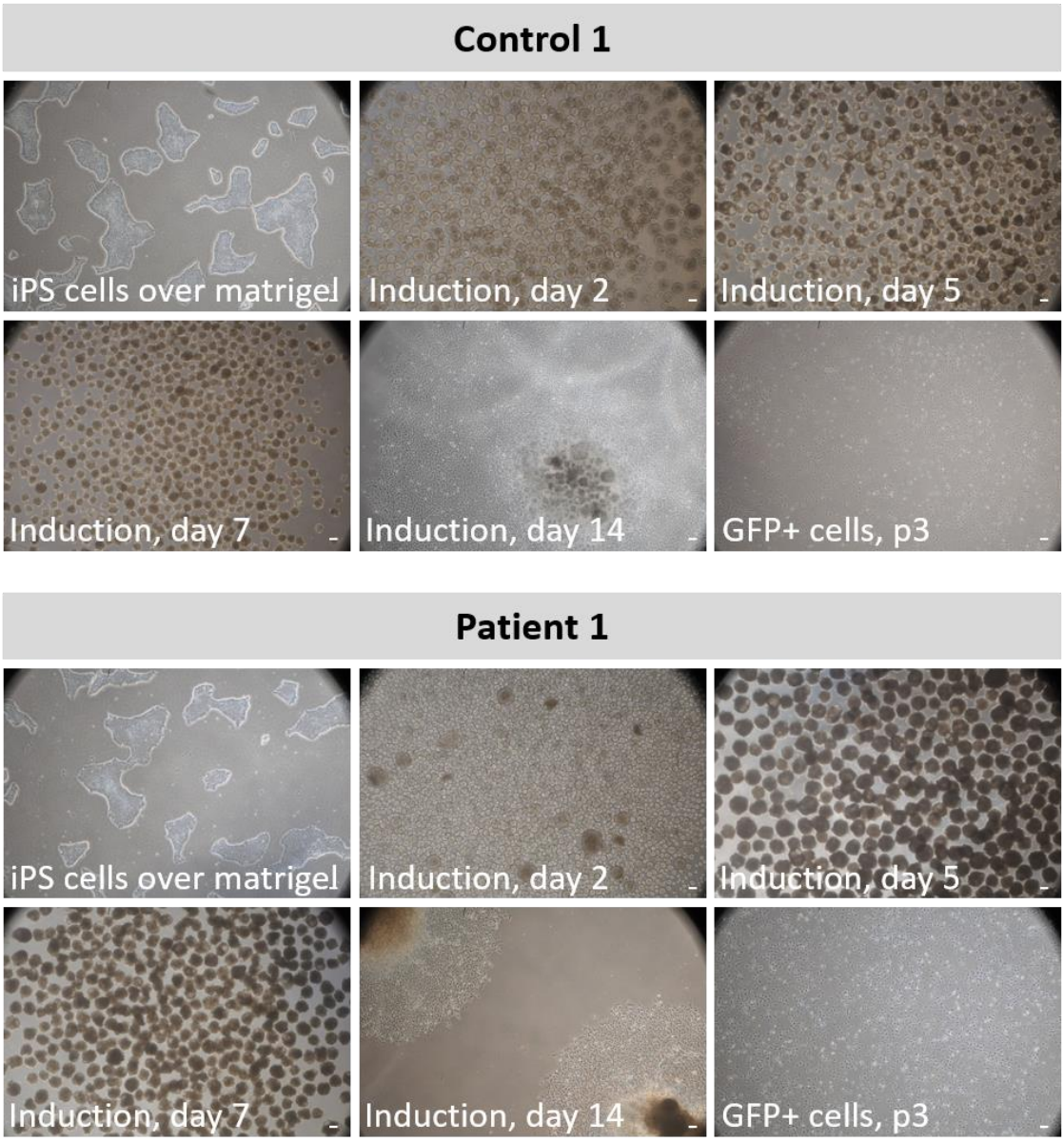

Figure 34: Representative light microscopy images of the two cell lines (control 1 and patient 1) before, during and after the induction process. Pictures illustrate iPSCs cultured on matrigel before the induction protocol was initiated, EB cultures at day 2, 5 and 7 of the induction process, adherent cultures at day 14 of the induction protocol, and sorted GFP-positive cells at passage 3 post-sorting. Scale bars: 100 µm.

FACS plots of cell separations performed on day 14 of the myogenic induction protocol also indicate that there was considerable variability among the six cell lines regarding cell size and granularity (figure 35, SSC-A vs. FSC-A plots). Importantly, sorted GFP+ cells (green events) were fairly homogeneous regarding their size, granularity and shape of the population (figure 35, green events).

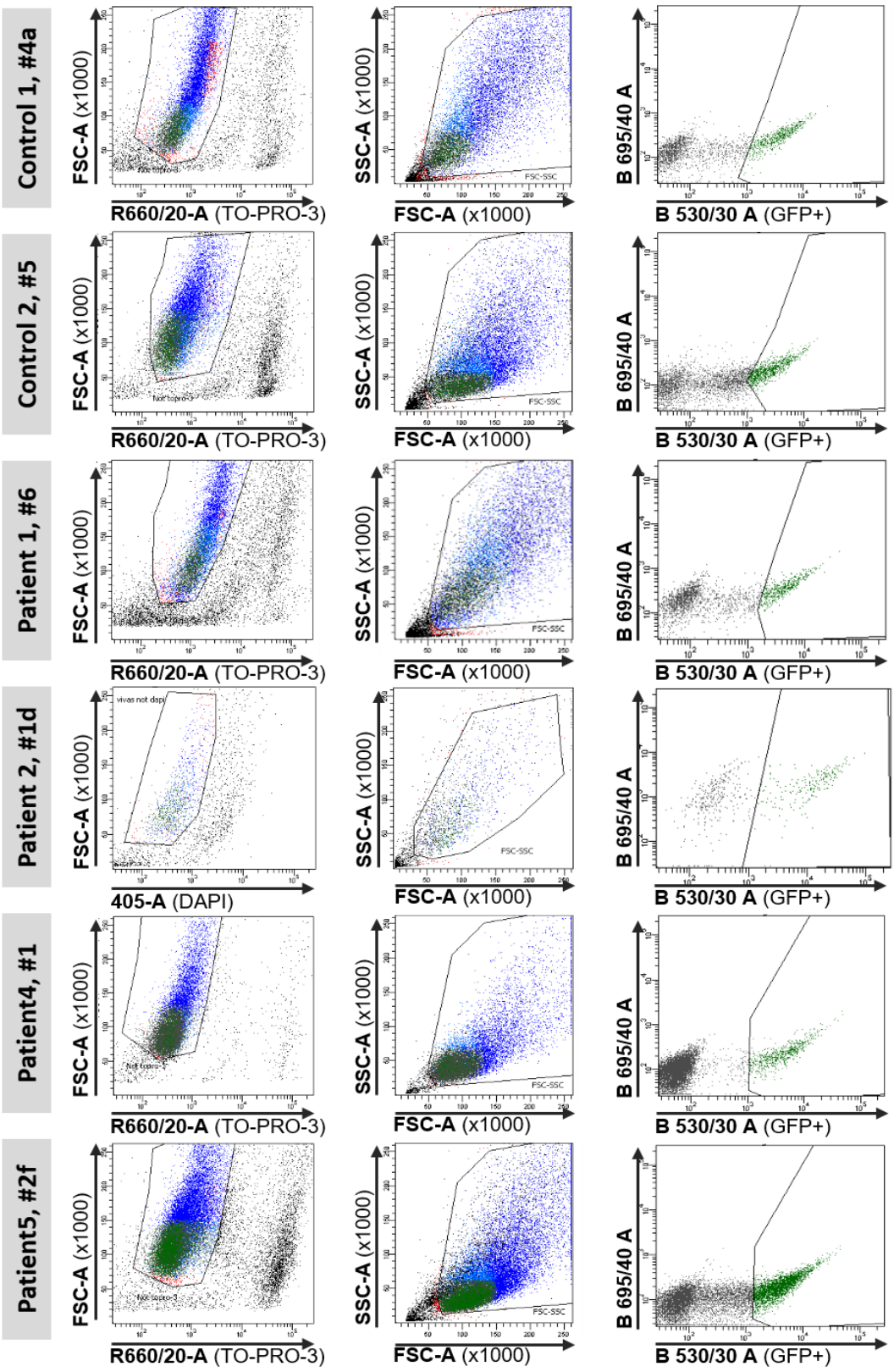

Figure 35. FACS plots corresponding to the isolation of GFP-positive cells at day 14 of the myogenic induction protocol. Plots in the first column represent the staining of the cells with the viability marker TO-PRO-3. TO-PRO-3-negative events (live cells) were gated and represented according to their size and granularity (second column). The second gate selected events corresponding to cells, and small events, likely corresponding to cell debris, were not selected. Finally, events were plotted according to their GFP signal and GFP-positive events (in green in all the plots) were gated and sorted. #: clone (reprogrammed cell line).

Optimization of the myogenic induction protocol of iPSCs. Based on publications that report that GSK3β inhibition promotes the differentiation of pluripotent cells into mesodermal progenitors (Bakre *et al.,* 2007; Borchin *et al.,* 2013), we aimed to test the effect of transiently inhibiting GSK3β during the previously described induction protocol. Addition of 5 μM of the GSK3β inhibitor CHIR99021 during the myogenic induction of patient 2-derived iPSCs slightly modified the size and morphology of the EBs (figure 36.a), these looking somewhat smaller and rougher following a 24 hour-inhibition. However, no evident morphologic differences were detected following a 48 hour-inhibition. Importantly, the addition of CHIR99021 increased the percentage of GFP-positive cells at day 14 of the induction process, suggesting that inhibition of GSK3β promotes the proliferation of myogenic progenitor cells. However, this increase was evident when GSK3β was inhibited for 24 hours (from 38% to 52.4%) but it was diminished when GSK3β inhibition was sustained for 48 hours (from 38% to 42.1%) (figure 36.b). This result indicates that long lasting GSK3β inhibition might negatively impact cell proliferation.

Despite transient inhibition of GSK3β clearly performed over our regular myogenic induction process, terminal differentiation of GFP-positive progenitor cells did not improve, as evidenced by the frequency of sarcomeric myosin-positive cells observed in these cultures (figure 36.c). Moreover, progenitor cells derived from cells treated with CHIR99021 for 48 hours during the induction process showed a reduced differentiation potential compared to the myogenic cultures differentiated following the regular protocol. Therefore, transient GSK3β inhibition in our protocol was not found to improve myogenic differentiation of iPSCs. Thus, this additional step was not included in the myogenic induction protocol.

Optimization of the terminal differentiation protocol of iPSC-derived PAX7-positive muscle progenitor cells. Several differentiation protocols were evaluated to establish the optimal conditions to terminally differentiate iPSC-derived PAX7-positive progenitor cells into myotubes. First, we pursued the terminal differentiation of progenitor cells from control 1 and patient 1 by following the protocol described by Darabi and colleagues (Darabi *et al.,* 2012), with minor modifications. Briefly, progenitors were cultured on gelatin-coated wells until they reached 80% confluence. Next, cells were switched to *2% HS differentiation medium* or *conditioned 2% HS differentiation medium*. Differentiation media were replaced every two days through day 12. At that time point, no myotubes were visible under a light microscope. Immunofluorescence detection of sarcomeric myosin displayed a few sporadic myosin-positive cells that were not multinucleated in most cases (figure 37). However, overall, no myogenic differentiation of cultures was achieved with either type of differentiation media tested. Nevertheless, it should be noted that *conditioned 2% HS medium* appeared to induce a higher maturation rate of the myogenic cells, since striations were frequently visible in myosin-positive cells differentiated with this medium, compared to differentiations performed

with *2% HS medium*. Visually, no major differences were detected among healthy control- and patient-derived myogenic cultures.

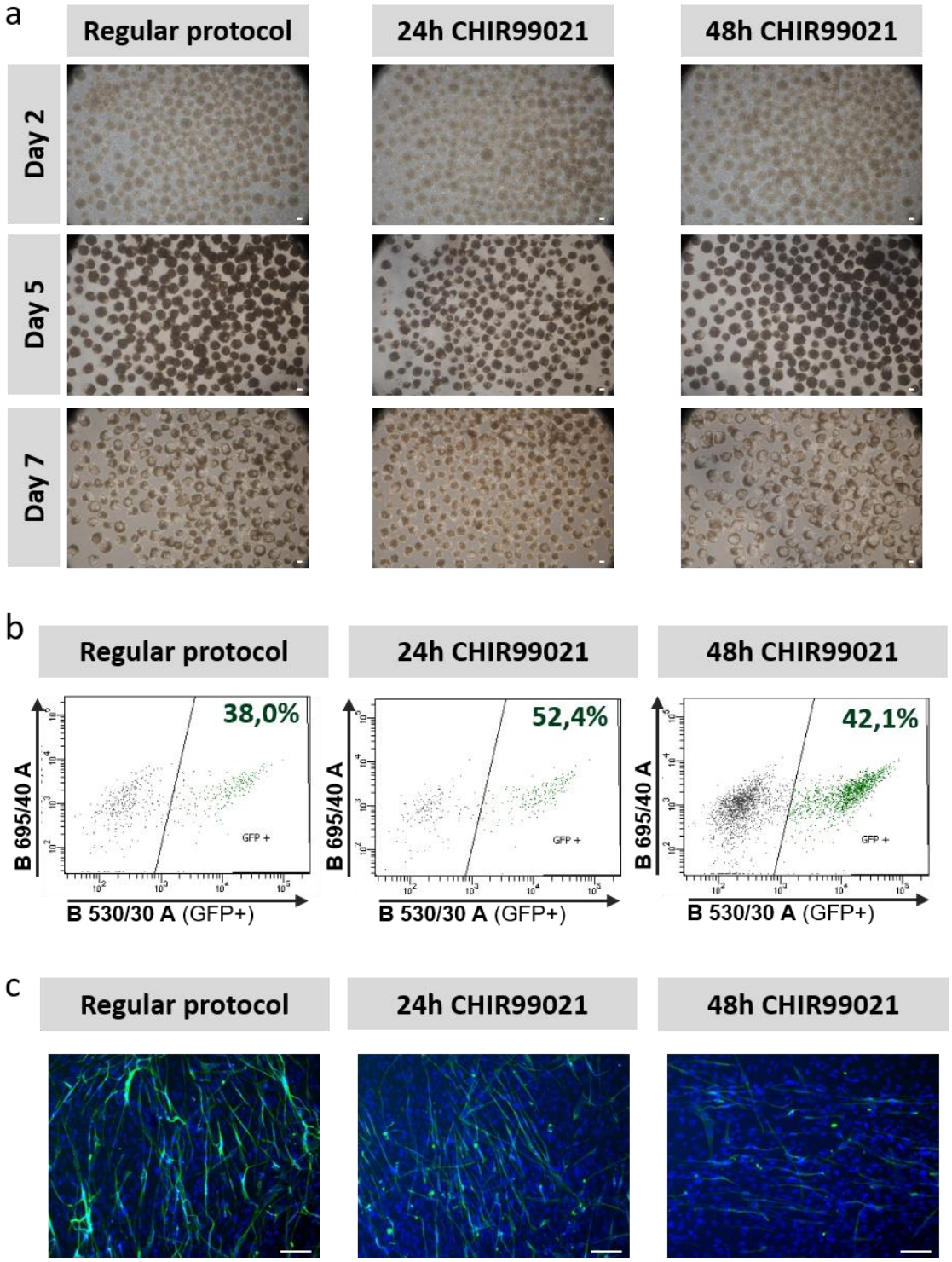

Figure 36. Effect of transient GSK3β inhibition during the induction of iPSCs towards GFP-positive myogenic progenitor cells. a) Light microscopy images of EBs during the myogenic induction following the regular protocol (left column), CHIR99021-supplemented for 24 hours (second column) and CHIR99021-supplemented for 48 hours (third column). b) Plots corresponding to the isolation of GFP-positive events by FACS at the end of each induction protocol. c) Immunofluorescence images of sarcomeric myosin detection (in green) and cell nuclei (in blue) at day 5 of differentiation. Scale bars: 100 µm.

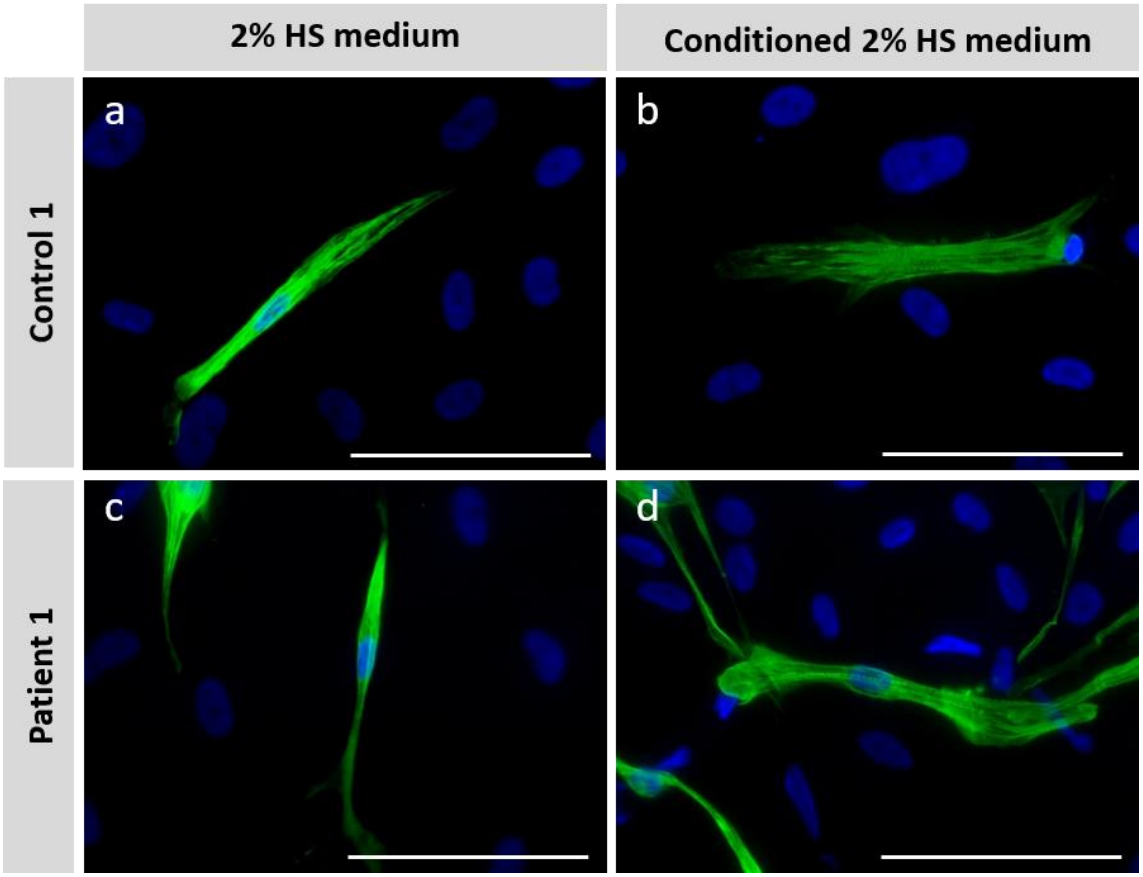

Figure 37. Immunofluorescence detection of sarcomeric myosin (green) in PAX7-positive progenitor-derived cultures on day 12 of differentiation. Control 1-derived cells (a,b) and patient 1-derived cells (c,d) were differentiated with *2% HS medium* (a, c) or *conditioned 2% HS medium* (b,d). Cell nuclei are stained in blue. Scale bars: 100 µm.

Since these two differentiation protocols were not successful on driving PAX7-positive progenitors into myotubes, we evaluated alternative myogenic differentiation protocols. In the second test, cells were cultured for 5 days in differentiation conditions. This was established because the authors of the original myogenic differentiation protocol (Darabi *et al.,* 2012; Darabi and Perlingeiro, 2014) claimed that the highest differentiation rate of PAX7-positive muscle progenitor cells was achieved at day 5-6 of differentiation. Therefore, we cultured PAX7-positive progenitor cells from control 1 and patient 4 up to 100% confluence and then switched to 1:1 induction-differentiation medium for 24 hours. Finally, cells were differentiated in *2% HS medium* for an additional 4 days. Alternatively, cells were also differentiated in *20% KOSR medium*, as suggested by the authors of the original differentiation protocol. Gene expression analysis of the myogenic genes myogenin, desmin, dystrophin and *PAX7* on day 5 of differentiation indicated that in the majority of the cases, *20% KOSR medium* induced higher myogenic gene expression rates when compared to *2% HS medium*, both in control 1- and patient 4-derived cultures (figure 38). However, these gene expression differences were modest. Similarly, there were no substantial differences between cultures differentiated with *2% HS medium* and *20% KOSR medium* regarding myosin expression detected by immunofluorescence, as displayed in figure 38. Overall, the

differentiation rate achieved for both control- and patient-derived cultures was not considered successful.

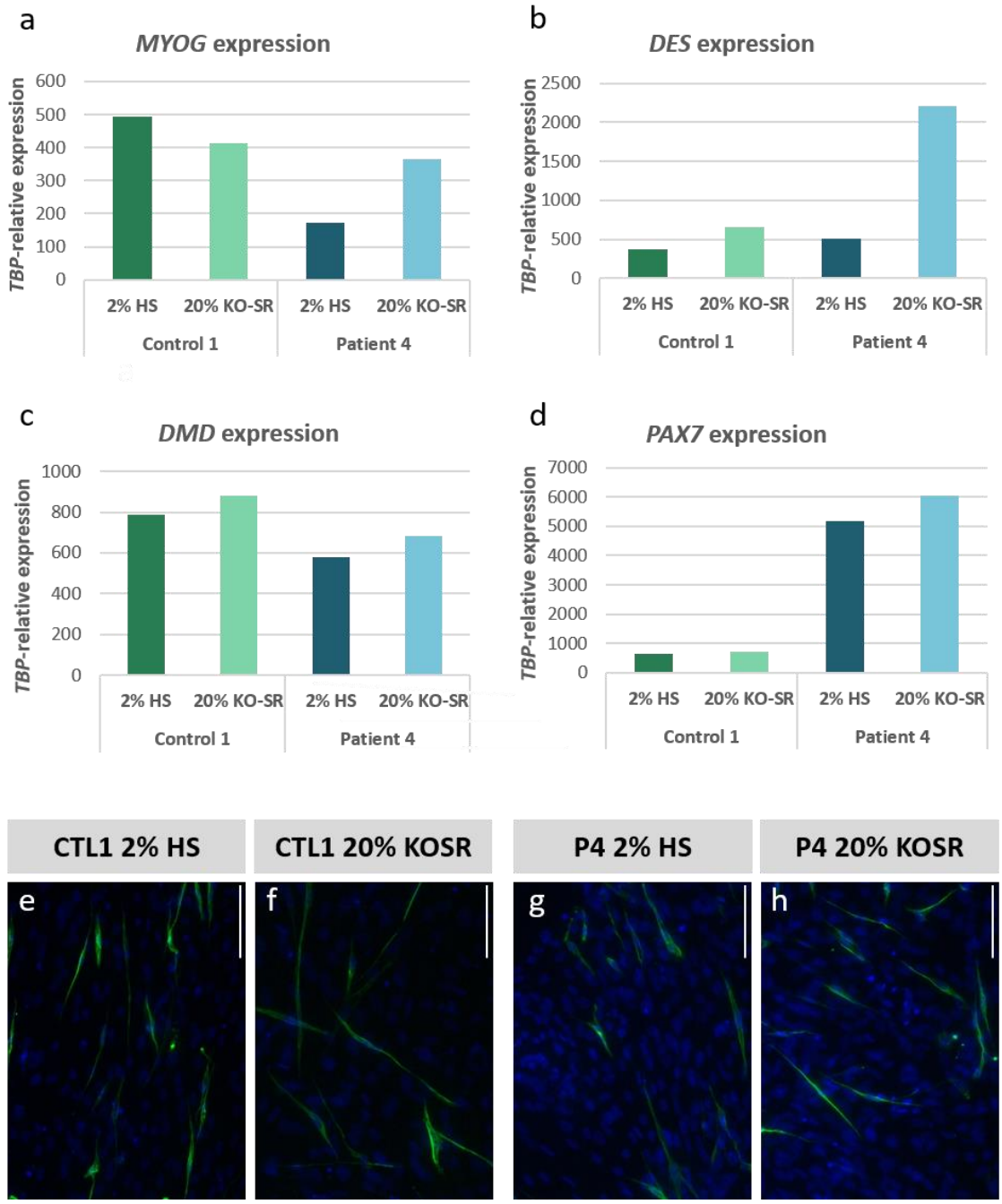

Figure 38. Assessment of myogenic terminal differentiation by gene expression analysis and immunofluorescence detection of sarcomeric myosin. (a-d) Gene expression rates at day 5 of differentiation relative to *TBP* expression (100%), in control 1-derived cultures (green bars) and patient 4-derived cultures (blue bars) differentiated with *2% HS medium* (dark bars) or *20% KOSR medium* (light bars). (e-h) immunofluorescence detection of sarcomeric myosin (green) in control 1-derived and patient 4-derived cultures after 5 days of differentiation in *2% HS medium* (e,g) or *20% KOSR medium* (f,h). Cell nuclei are stained in blue. Scale bars: 100 µm.

Finally, the last optimization attempt consisted of inducing the terminal myogenic differentiation of PAX7-positive progenitors using the *15% KOSR medium* (Chal *et al.,*

2015). Moreover, an alternative coating system was also tested, referred to as *sandwich coating*, due to the two layers of coating used during the differentiation process: 0.1% gelatin underneath the cells and a 1-mm thick matrigel layer on top of the cells. This double coating has been reported to improve myogenic differentiation and maturation since it provides a tridimensional scaffold to the differentiating myogenic cells (Toral-Ojeda *et al.,* unpublished data). Control 1-derived cells were differentiated in these four conditions. As shown in the following image, the frequency of myosin-positive cells in culture was considerably increased when differentiations were performed with *15% KOSR medium* (figure 39.b and d), compared to *20% KOSR* medium (figure 39.a and c). As for the *sandwich coating*, this system led to more heterogeneous cultures, where the frequency of myosin-positive cells was high in some areas but low in other areas (figure 39.d). Therefore, *15% KOSR medium* and 0.1% gelatin coating were considered to be optimal conditions to drive the terminal myogenic differentiation of iPSC-derived PAX7-expressing progenitor cells.

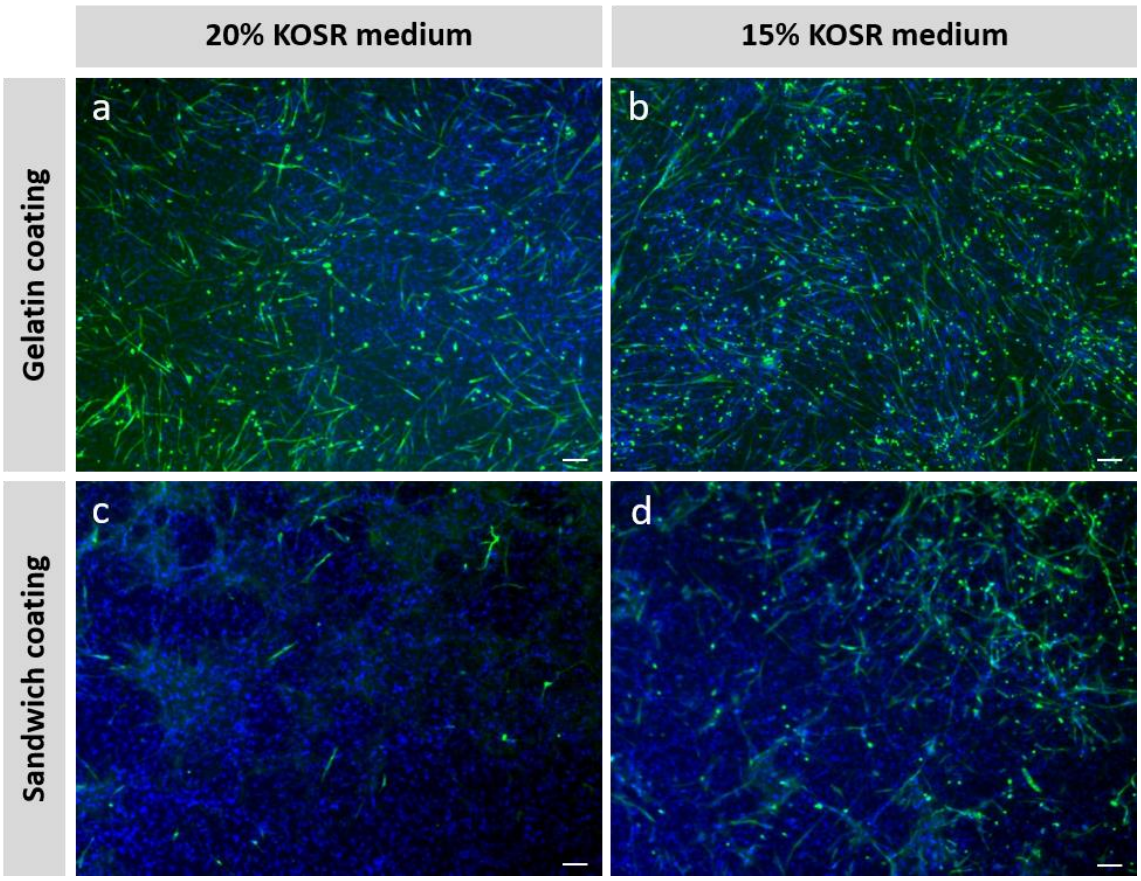

Figure 39. Immunofluorescence images of control 1-derived myogenic progenitor cells at day 5 of differentiation. Sarcomeric myosin (in green) is detected in the four differentiation conditions. Cell nuclei are stained in blue. Scale bars: 100 µm.

Characterization of iPSC-derived myogenic cultures. To determine the myogenic differentiation potential of iPSC-derived cells, myogenic progenitors at passage 3-4 were

cultured up to 100% confluence and then differentiated for 5 days using *15% KOSR medium*.

Immunofluorescence analyses showed that frequency of myotubes, detected through sarcomeric myosin-expression, was highest in patient 1 (P1)-derived cells, followed by control 1 (C1)-derived cells. Differentiation rates were lower in control 2 (C2) and patient 4 (P4)-derived cultures, and minimal or even abset in patient 2 (P2) and patient 5 (P5)-derived cultures (figure 40.a). Myogenin-positive nuclei displayed a concomitant frequency in these differentiated cultures (figure 40.b).

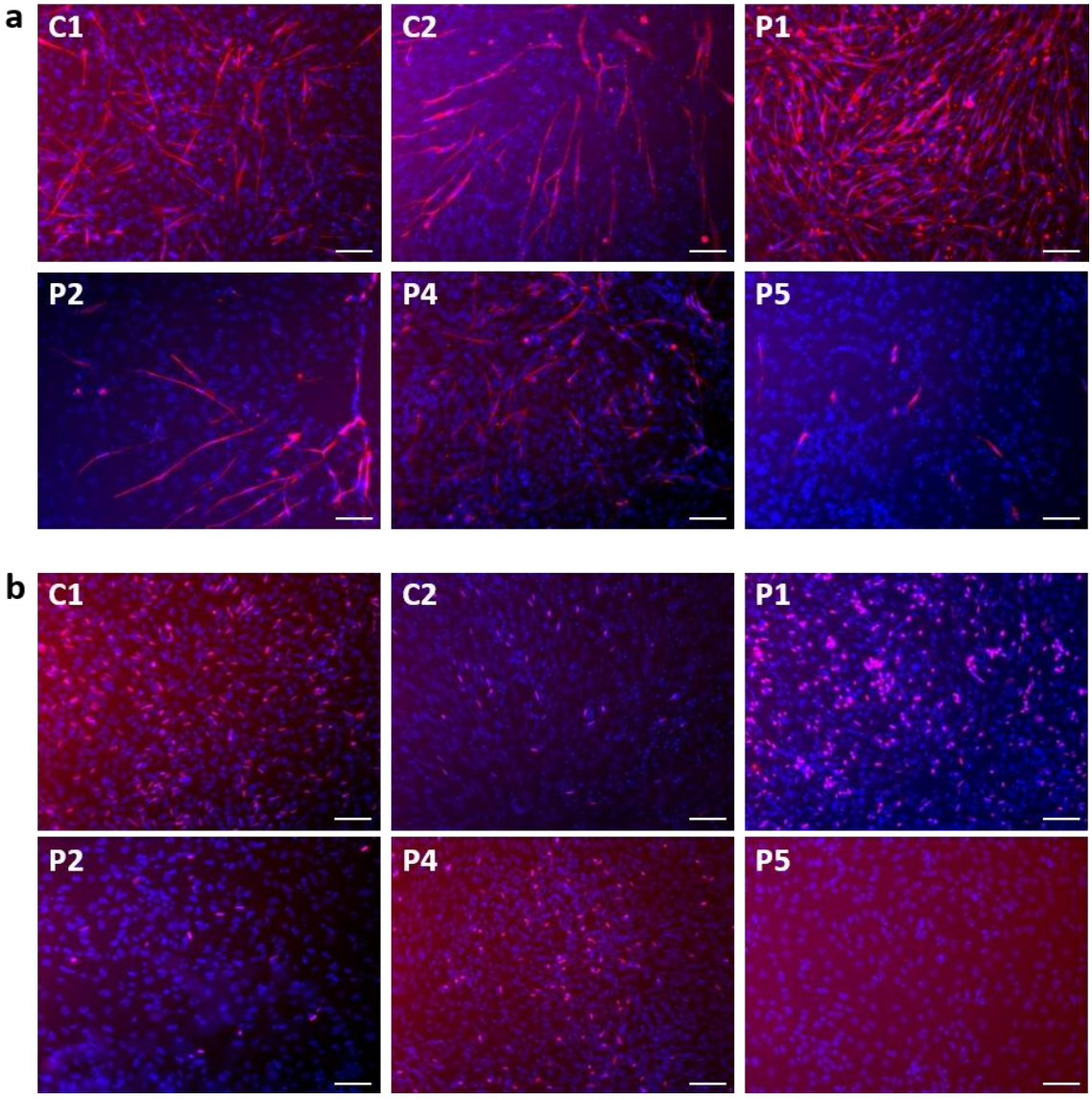

Figure 40. Immunofluorescence detection of a) sarcomeric myosin (red) and b) myogenin (red) in cell cultures at day 5 of differentiation. Cell nuclei are stained in blue. Scale bars: 100 µm.

Consistent with the immunofluorescence results, myogenic gene expression in cultures before (day 0, progenitors) and after terminal differentiation (day 5, differentiated) showed that certain cell lines, such as C1 and P1, were able to induce myogenic gene

expression upon differentiation. Other cell lines had a limited (C2 and P4), or even very reduced (P2 and P5), differentiation potential (figure 41). Embryonic myosin heavy chain (*MYH3*) and adult myosin heavy chain (*MYH2*) displayed a similar induction pattern, being considerably induced in C1 and P1 cell lines after 5 days of differentiation, and to a lower extent in C2 and P4. Only basal expression was detectable in P2 and P5 cells. It is noteworthy that adult myosin heavy chain levels were considerably lower than embryonic myosin heavy chain rates for each of the cell lines, suggesting that these differentiated cultures could potentially further differentiate and mature. Expression of *MYOD1* and *MYOG* were consistent with myosin expression, demonstrating the highest expression rates in C1 and P1 differentiated cultures, moderate expression rates in C2 and P4-derived cultures and basal rates in P2 and P5-derived cultures (figure 41).

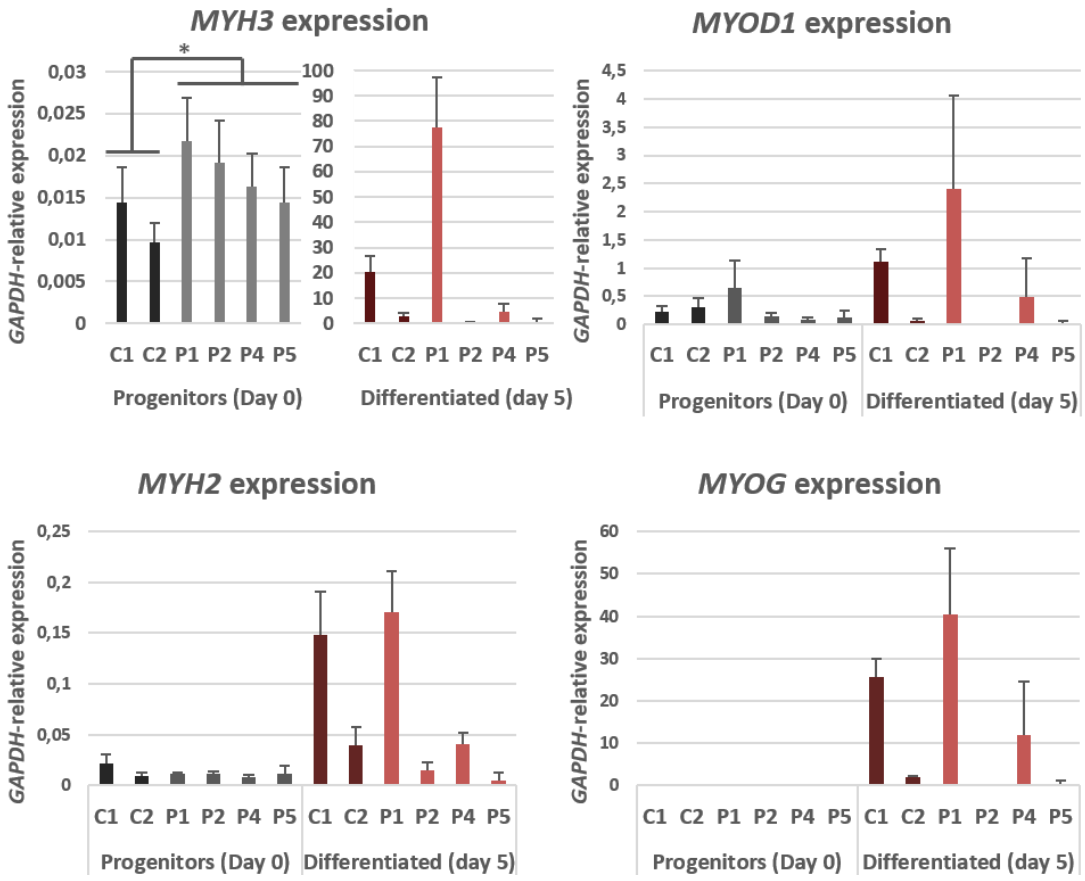

Figure 41. Gene expression of myogenic markers in differentiated cultures. Bar graphs indicate *GAPDH*-relative expression rates of myogenic genes (*MYH3, MYH2, MYOD1* and *MYOG*) in undifferentiated (progenitors, day 0) and differentiated (day 5) cultures. Bars represent mean values and standard deviations of 3 experimental replicates.* ($p<0.05$).

There were no statistically significant differences found on differential gene expression rates between patient- and control-derived cell lines for any of the genes evaluated

except for embryonic myosin in muscle progenitor cells, whose expression was increased in patient-derived progenitor cells compared to control-derived cells.

Overall, the variable differentiation potential of the established cellular models did not correlate with mutations in *CAPN3*. In other words, the variable differentiation potential of the cultures did not depend on whether the cell line was derived from a healthy control or a patient.

Expression of *PAX7* was also assessed in these myogenic cultures. As expected, total *PAX7* levels (endogenous and exogenous *PAX7*) were the highest at day 0 of differentiation, which is consistent with the presence of doxycycline in the culture medium that activated the expression of exogenous PAX7 (figure 42.a). These *PAX7* mRNA levels decreased significantly at day 5 due to doxycycline withdrawal. No statistically significant differences were observed between healthy control- and patient-derived progenitors or differentiated cultures.

PAX7 protein levels followed a similar trend. Therefore, PAX7 protein detected at day 5 of differentiation may primarily correspond to endogenous *PAX7* expression (figure 42.b and c). Importantly, the frequency of PAX7-positive cells at day 5 of differentiation was still considerably high, except for P5-derived cultures, where practically no PAX7-positive cells were detected (figure 42.d).

CAPN3 and calpain 3 expression in iPSC-derived myogenic cultures. qPCR analysis results demonstrated that *CAPN3* expression was induced following differentiation. Interestingly, *CAPN3* rates for each cell line varied greatly and they did not correlate strictly with the differentiation efficiency of each cell line (figure 43.a). Notably, *CAPN3* expression in P5-derived cells was higher than in C2, P2 and P4-derived cultures, despite its poor myogenic differentiation. *CAPN3* levels were considerably high in P1-derived cultures, which only has one *CAPN3* allele. No statistically significant differences were detected between control- and patient-derived cultures regarding *CAPN3* expression rates.

Calpain 3 protein levels were assessed by Western blot (figure 43.b and c) using two antibodies that recognize different epitopes. As previously mentioned, commercial antibodies against calpain 3 are not fully specific and unexpected bands are detected by these antibodies. Some of these bands potentially correspond to calpain 3 proteolytic products, whereas other bands are considered nonspecific. Therefore, we assessed calpain 3 levels in differentiated cultures using antibodies against different epitopes of calpain 3 and we focused our attention on the 94 kDa band corresponding to full-size calpain 3.

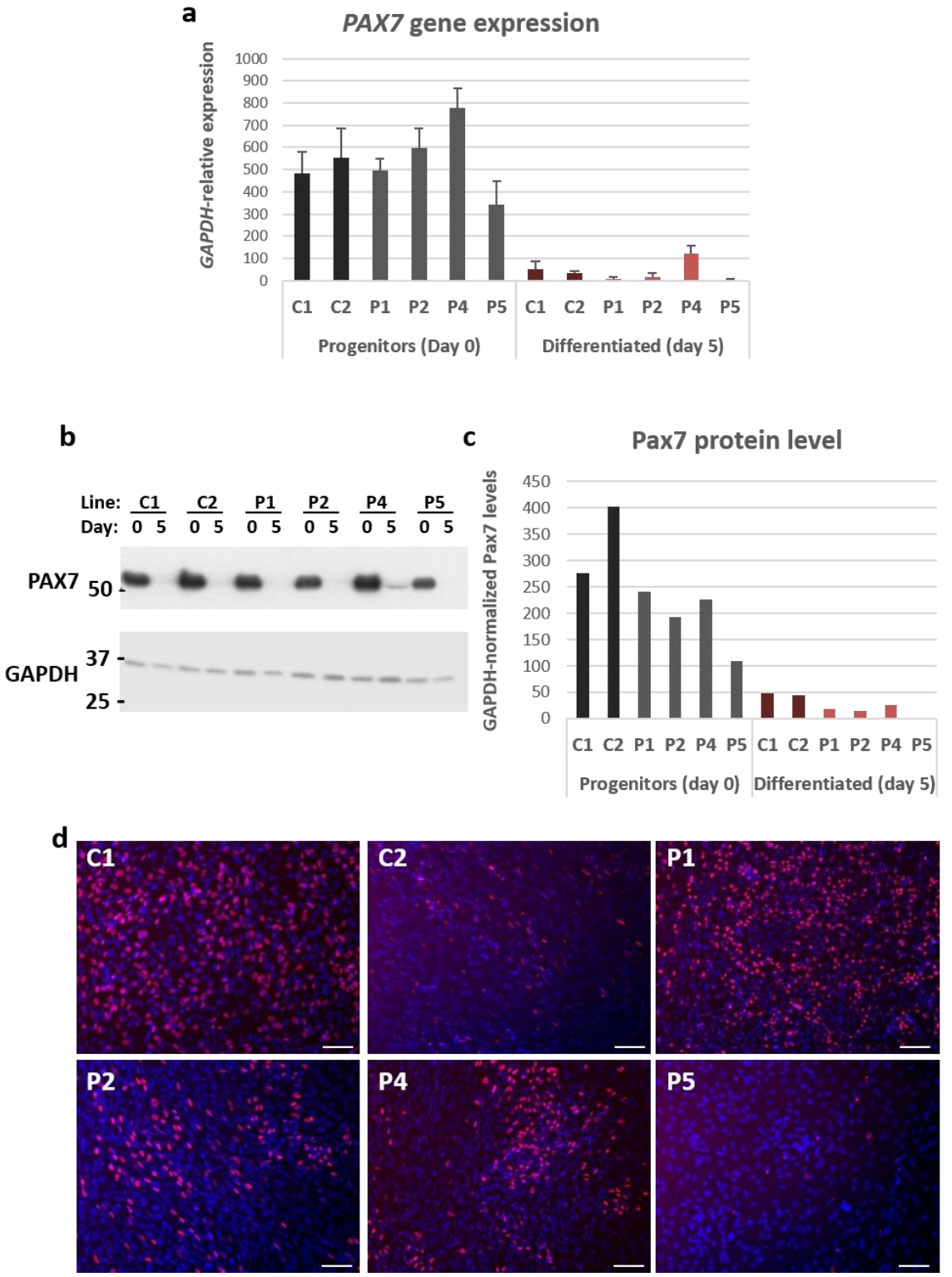

Figure 42. Analysis of *PAX7* mRNA and PAX7 protein expression. a) Bar graph showing *GAPDH*-relative expression rates of total *PAX7* (endogenous and exogenous) in undifferentiated (progenitors, day 0) and differentiated (day 5) cultures. Bars represent mean values and standard deviations of 3 experimental replicates. b) Western blot detection of PAX7 (upper blot) and GAPDH (lower blot) in undifferentiated (day 0) and differentiated (day 5) cultures. c) Quantification of PAX7 protein levels detected in (b) through densitometry and normalized to GAPDH protein levels. d) Immunofluorescence detection of PAX7 protein (in red) and cell nuclei (in blue) in differentiated cultures. Scale bars: 100 µm.

Both antibodies proved the presence of full-size calpain 3 in each of the terminally differentiated cultures, except for P5-derived cultures (figure 43.b and c). Calpain 3 protein levels were greatly variable among the different cell lines. The calpain 3 protein levels detected with two different antibodies did not exactly correlate. Considering both Western blots, the 94 kDa band found in C1- and C2-derived cultures was attributed to wild type calpain 3. The low intensity of these bands could be due to its autocatalytic activity. P1, P2 and P4 also expressed full-size calpain 3. Importantly, P2 and P4 harbor one missense mutation in one of the *CAPN3* alleles, which likely led to these 94 kDa bands. Moreover, these amino acid substitutions may confer resistance to degradation to calpain 3, resulting in intense 94 kDa bands upon Western blot analysis with both antibodies. P1 has only one *CAPN3* allele and the mutation located in this allele would synthesize a 101 kDa calpain 3 protein, which might not be distinguishable from the 94 kDa bands observed in these blots. Finally, P5, which contains the Basque mutation in homozygosis, resulted in practically no 94 kDa calpain 3 bands, despite its considerable expression at the mRNA level. This is consistent with the absence of the 94 kDa calpain 3 band in muscle extracts of a patient with the Basque mutation in homozygosis (data not shown). Notably, very low *CAPN3* expression rates appear to be sufficient to synthesize calpain 3 protein.

These data provide evidence that calpain 3 is expressed in myogenic cultures upon differentiation. Interestingly, calpain 3 is also detected in poorly-differentiating cell lines at day 5 of differentiation, such as P2 and P4.

In addition to studying *CAPN3* mRNA and full-size calpain 3 levels in differentiated cultures, expression of different *CAPN3* isoforms along terminal myogenic differentiation was also assessed. As previously described, several splicing variants lacking exon 6 and/or exon 15 and exon 16 are detected during developmental stages, as well as during regenerative processes. This switch from immature to mature isoforms is recapitulated during *in vitro* myogenic differentiation (Herasse *et al.,* 1999). Therefore, we studied the proportion of immature calpain 3 (lacking exon 6) and mature calpain 3 (including exon 6) isoforms at day 0, 2 and 5 of the terminal differentiation process in C1- and C2-derived cells, as well as in the H9 human embryonic stem (ES) cell line, which was included as a positive differentiation control. As shown in figure 44.a, total *CAPN3* expression was significantly induced upon differentiation in C1- and H9-derived cells. However, this induction was very limited, although still significant, in poorly differentiating C2-derived cells.

As for *CAPN3* isoforms, the proportion of the immature isoform (lacking exon 6) was progressively reduced, while the mature form (including exon 6) increased as differentiation proceeded in C1 and H9-derived cells (figure 44.b and d). However, this switch from immature to mature isoforms was only statistically significant ($p<0.05$) in C1-derived cultures. Importantly, this change from the immature to the mature form

was absent in C2-derived cells, which only presented a limited differentiation potential (figure 44.c).

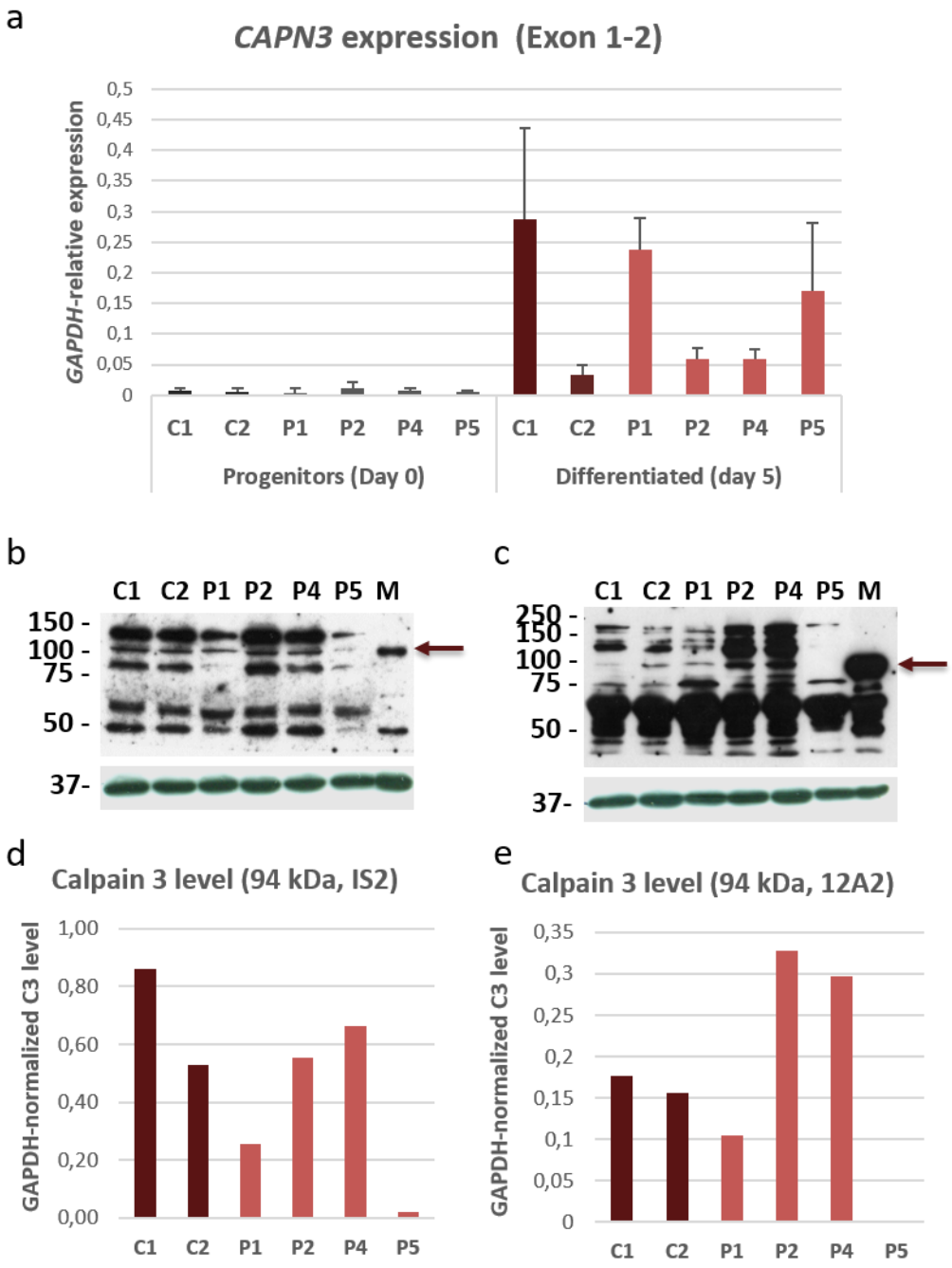

Figure 43. *CAPN3* expression and Calpain 3 levels in iPSC-derived myogenic cultures. a) Bar graph illustrating *GAPDH*-relative *CAPN3* expression rates (probe for exon 1-2) in undifferentiated (progenitors, day 0) and differentiated (day 5) cultures. Bars represent mean values and standard deviations of 3 experimental replicates. b) Western blot of calpain 3 protein detection using the IS2 antibody, and GAPDH as endogenous control (lower blot). c) Western blot of calpain 3 protein detection using the 12A2 antibody, and GAPDH as endogenous control (lower blot). d and e) Quantification of full size (94 kDa, pointed with arrows) calpain 3 levels detected with IS2 and 12A2 antibodies, respectively, and normalized to GAPDH levels. M: human muscle extract.

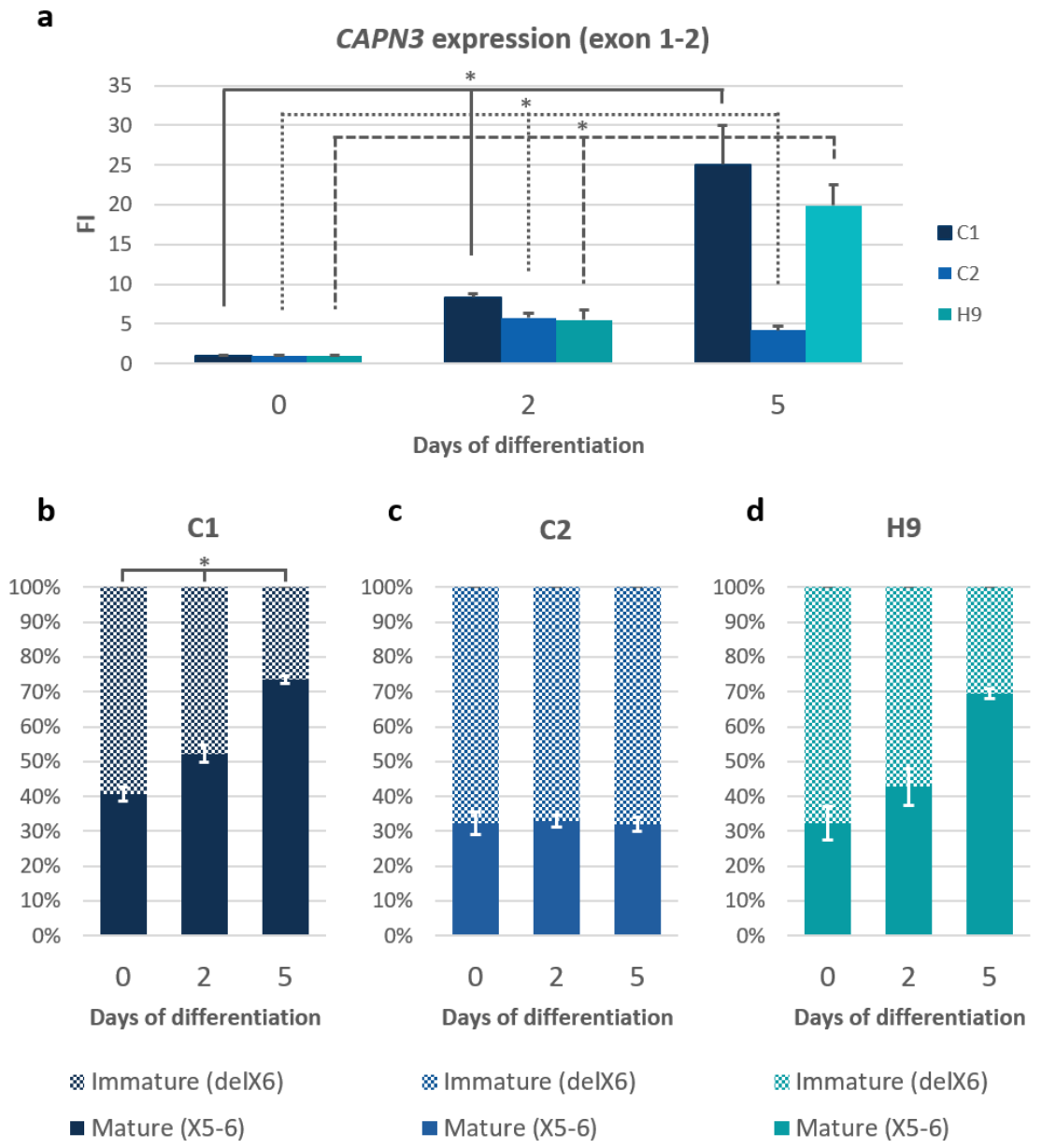

Figure 44. Study of total *CAPN3* expression and its immature and mature isoforms during terminal differentiation of iPSC-derived progenitor cells. a) Bar graph illustrating the quantification of total *CAPN3* expression (probe for exon 1-2) during the differentiation of control 1 and control 2 cell lines, as well as H9 embryonic stem cells. b, c and d) Bar charts indicate the proportion (%) of immature (lacking exon 6) and mature (including exon 6) isoforms of *CAPN3* at day 0, 2 and 5 of differentiation. Bars represent mean values and standard deviations of 3 experimental replicates. * ($p<0.05$).

Expression of dystrophin in iPSC-derived muscle progenitors and terminally differentiated cultures. Dystrophin is one of the most thoroughly studied proteins in skeletal muscle due to its implication in Duchenne Muscular Dystrophy (DMD). Moreover, this protein has been considered as a marker of maturation since its expression is highest in late myogenic differentiation stages (Hildyard and Wells, 2014). However, it is worth noting that DMD expression levels are also significantly upregulated in quiescent satellite cells, whereas its expression decreases significantly upon satellite

cell activation (Dumont *et al.,* 2015b). This suggests that dystrophin potentially has multiple roles, both at the initial and terminal stages of myogenic differentiation. *DMD* expression was reduced in patient-derived cultures compared to healthy control-derived cells, both in progenitor and terminal differentiation stages (figure 45).

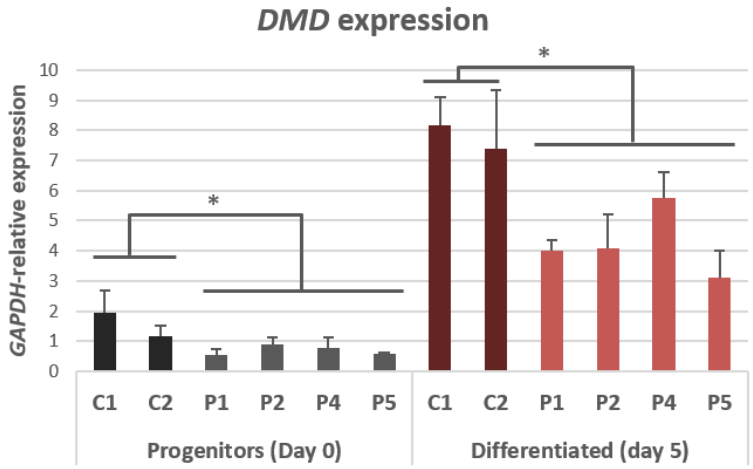

Figure 45. *DMD* expression in iPSC-derived myogenic progenitor cells and terminally differentiated cultures, relative to *GAPDH* expression (100%). Bars represent mean values and standard deviations of 3 experimental replicates. * ($p<0.05$).

Expression of genes encoding extracellular matrix proteins in iPSC-derived muscle progenitors and terminally differentiated cultures. Since progressive increase of fibrotic tissue is a histological feature of LGMD2A and other muscle dystrophies, expression of fibronectin (*FN1*) and alpha-1 type I collagen (*Col1α1*) was assessed in iPSC-derived muscle progenitors and terminally differentiated cultures. Overall, induction of terminal differentiation activated the expression of both genes. Expression rates of both genes were higher in healthy control-derived terminally differentiated cultures compared to patient-derived cultures, although no statistically significant differences were detected (figure 46). Expression trends did not correlate with the myogenic differentiation potential of each cell line.

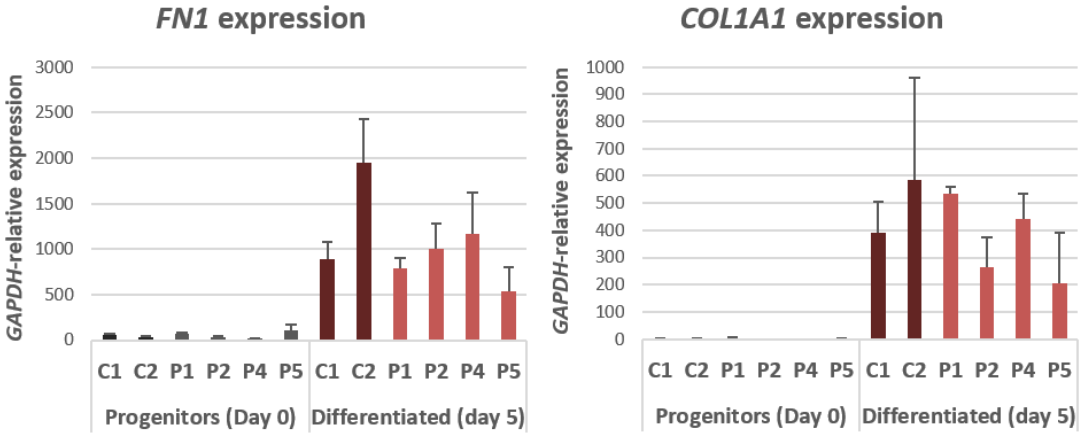

Figure 46. Expression of extracellular protein-coding genes *FN1* and *COL1A1* in iPSC-derived myogenic progenitor cells and terminally differentiated cultures, relative to *GAPDH* expression (100%). Bars represent mean values and standard deviations of 3 experimental replicates.

SERCA2 protein levels in iPSC-derived progenitors and terminally differentiated cultures. It has been recently reported that calpain 3 is potentially involved in stabilizing the SERCA2 protein (Toral-Ojeda *et al.,* 2016). Thus, SERCA2 protein levels were assessed in iPSC-derived cultures. Western blot analysis demonstrated that SERCA2 protein was detected in both muscle progenitors and terminally differentiated cells. However, SERCA2 protein levels did not correlate with calpain 3 protein levels. Interestingly, SERCA2 was absent in terminally differentiated P5-derived cultures, as well as calpain 3. SERCA2 protein was also detected in PAX7-expressing progenitors in all the cell lines, where expression of *CAPN3* was basal (figure 47).

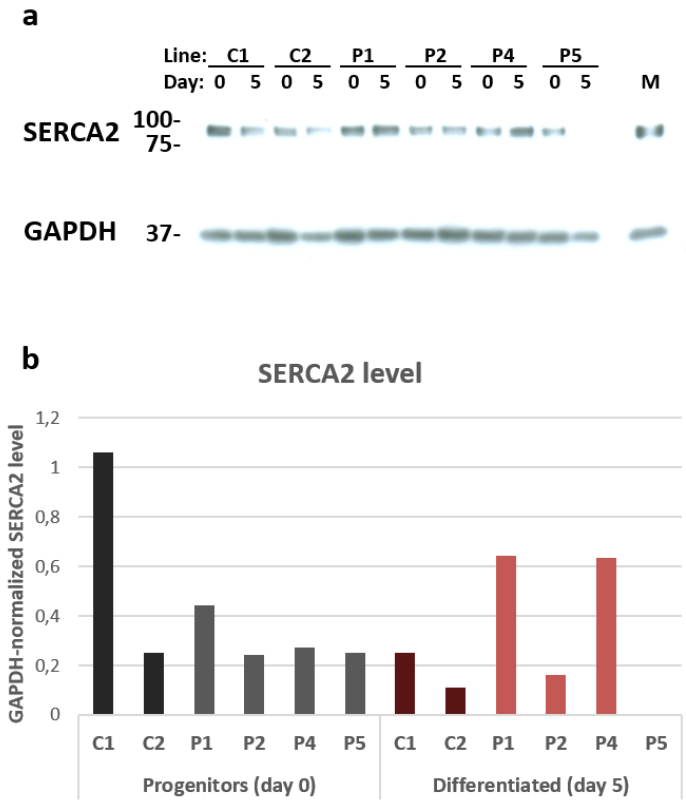

Figure 47. SERCA2 protein levels in iPSC-derived muscle progenitors and terminally differentiated cultures. a) Western blots detecting SERCA2 (upper blot) and GAPDH (lower blot) in cell cultures at day 0 (progenitors) and day 5 of differentiation. b) Quantification of SERCA2 protein levels through densitometry, normalized to endogenous GAPDH levels. M: human muscle extract.

In vivo regenerative potential of iPSC-derived progenitor cells. To determine the regenerative potential of iPSC-derived muscle progenitor cells, 10^6 PAX7-expressing cells at passage 4 post-sorting were transplanted into cardiotoxin-injured TA muscles. Due to the complexity of the experiment, only P1-derived and its age-matched C2-derived cells were transplanted. One month after transplantation, muscles were collected and analyzed to assess the regenerative potential of the transplanted cells. Immunofluorescence detection of human lamin A/C allowed for the visualization of

human cell nuclei, which were derived from transplanted cells. This staining was used to determine the engraftment potential of C2- and P1-derived progenitor cells. As illustrated in figure 48.c, P1-derived cells showed an increased engraftment compared to C2-derived cells. Similarly, patient-derived cells generated more human dystrophin-expressing fibers (figure 48.d), indicative of their greater regenerative potential compared to C2- derived cells. Figure 48 a and b display representative images of immunofluorescence detection of human cells in mouse TA sections.

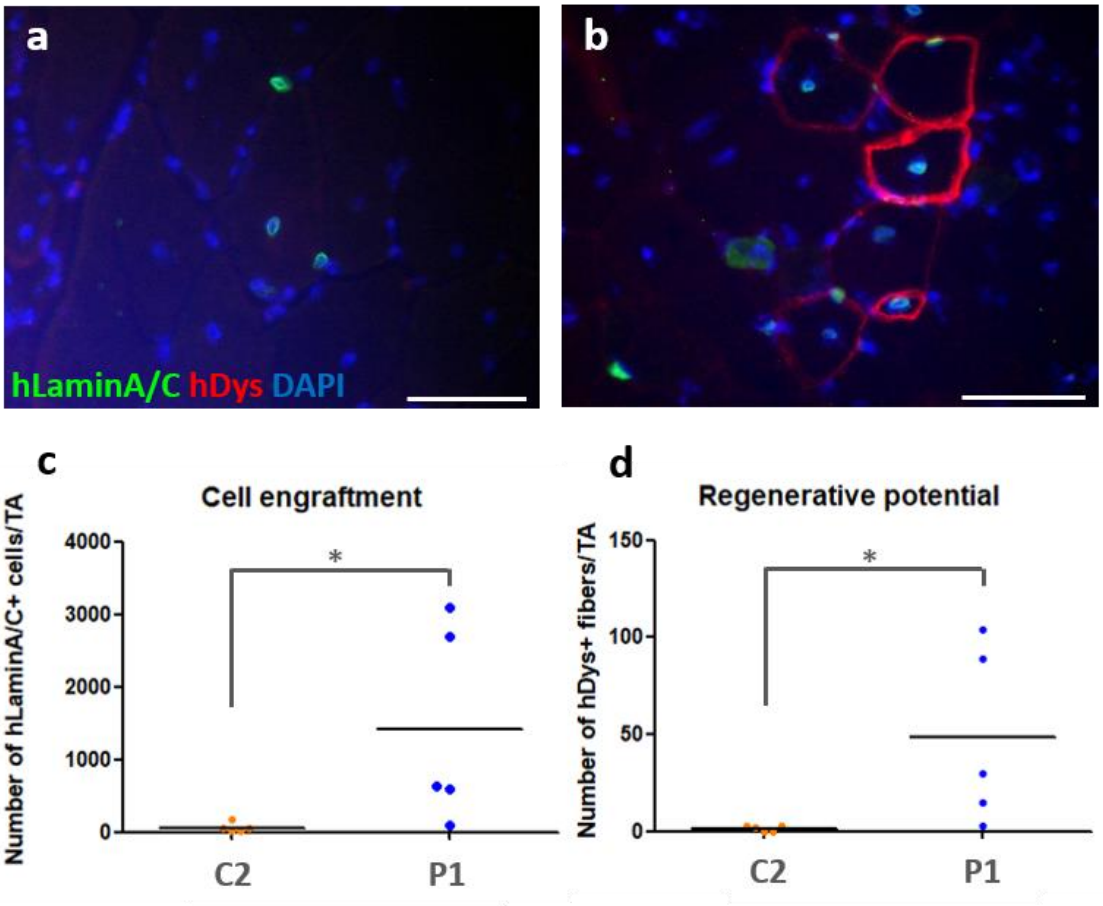

Figure 27. Analysis of the *in vivo* regenerative potential of iPSC-derived muscle progenitor cells. a and b) immunofluorescence images of control 2(a)- and patient 1(b)-transplanted TA sections where human cell nuclei are visualized in green, and human dystrophin-expressing fibers are seen in red. All nuclei are stained in blue. Scale bars: 50 µm c) total number of human lamin A/C-positive nuclei detected in all the sections analyzed for each TA, and d) total number of human dystrophin-positive fibers detected in all the sections analyzed for each TA. * ($p<0.05$).

DISCUSSION

In vitro disease modeling is a valuable and relatively affordable approach to study the physiopathology of diseases, as well as to test the efficacy of potential therapies. Research on skeletal muscle and the diseases directly affecting this tissue has been performed using animal models, patient-derived muscle biopsies, and *in vitro* myogenic cell cultures. Importantly, patient muscle-derived primary cultures have been

predominantly used for research purposes since the early 90s and, *in vitro* culture systems have been constantly evolving to optimize their use, as well as to generate cultures that closely represent their tissue of origin. In this regard, several disease-specific myoblasts have been immortalized to extend their utility, and more complex extracellular matrixes and three-dimensional setups, as well as specific culture media, have been developed to achieve highly mature and long-lasting cultures.

In recent years, myogenic cell culture systems have developed in parallel with cell transplantation approaches to treat muscular dystrophies, which require methods to generate large amounts of transplantable myogenic cells in an *ex vivo* setup.

Currently, myogenic cultures derived from non-muscle tissues are offering alternative patient-specific sources of cells for both therapeutic approaches and *in vitro* disease modeling. Among them, reprogramming of somatic cells to pluripotency offers an unlimited source of patient-specific cells that later on can be differentiated into myogenic cells. Therefore, we aimed to establish LGMD2A patient-specific iPSC-derived myogenic cultures to address the role of calpain 3 in the myogenic differentiation process. As a result, this project has demonstrated the feasibility of this approach, while highlighting the challenges that are required to be addressed to further optimize the system and leverage this newly generated research tool, as discussed below.

Establishment of LGMD2A patient- and healthy control-derived iPSC lines. Selection of samples to be reprogrammed was performed based on the mutations and disease severity. Next, two age- and sex-matched healthy samples were selected as controls for the study.

Due to the broad spectrum of mutations observed in LGMD2A patients and their variable severity, it was not possible to select samples that directly represented each of the patients examined in the Neurology Service of the Donostia University Hospital, nor the worldwide population of LGMD2A patients. Among the five patients selected for this study, two of them, P3 and P5, had a severe phenotype, being wheelchair-bound in their forties. P1 and P2 were in an advanced grade, although still ambulant. Patient 4 displayed the most benign phenotype among the five patients selected, with an intermediate phenotype. As for the mutations, we selected samples with the most commonly found mutation in this population (the *Basque mutation* in exon 22) both in homozygosis (P5) and in heterozygosis, combined with a missense mutation (P2) or another null mutation (P3). We also selected one sample with a complete deletion of one of the *CAPN3* alleles (P1), and another sample with two mutations located in exon 5 and 16 (P4), and thus fulfilling the requirements for a potential intermolecular complementation (Ono *et al.,* 2014). In general, as described in the literature, patients with at least one missense mutation (P2 and P4) displayed a milder phenotype compared to patients with two null mutations (P3 and P5). Importantly, patient 1, which has only one *CAPN3* allele that generates a mutant calpain 3 protein with a 62 amino

acid extension, was not classified as a severe case, suggesting that this *CAPN3* allele is potentially able to synthesize a partially functional protein. Variable origin of the biopsies was not considered a hurdle since fibroblast cultures were obtained following the same protocol and cultures were morphologically similar.

Upon induction of cell reprogramming, each of the cell lines generated a considerable number of potentially reprogrammed colonies, except for P5, which only led to three colonies (data not shown). Several factors can affect cell reprogramming efficiency, such as the age of the biopsy (Trokovic *et al.,* 2015; Lo Sardo *et al.,* 2016), the proliferative potential of the fibroblasts (Trokovic *et al.,* 2015) or the infection efficiency achieved with the set of reprogramming vectors. In this study, P5 was one of the oldest donors. However, its age matched C1 and P3-derived fibroblasts led to a large number of colonies. Therefore, this reduced reprogramming rate cannot be directly attributed to the age of the donor. Except for P5, the remainder of fibroblasts generated a comparable number of colonies in the reprogramming plates. Hence, we conclude that mutations in *CAPN3* do not alter the reprogramming potential and survival of the generated cell lines, as is the case for other disease-specific cell lines, such as Fanconi anemia (Raya *et al.,* 2009). Henceforth, variations in the reprogramming rates achieved with different fibroblast cultures could be attributed to the stochastic nature of the reprogramming process. This is in line with theories that claim that cultured cells are heterogeneous, and only a small subpopulation of these cells appear to be in energetically favorable positions that facilitate their efficient reprogramming (reviewed by Del Sol and Buckley, 2014). Thus, different reprogramming efficiencies could be related to the amount of these specific cells that are randomly infected with the retroviral vectors. Once ES cell-like colonies emerged in the reprogramming plates, six colonies were individually picked and cultured, to establish several clonally-independent reprogrammed cell lines derived from each sample. As P5 only generated three colonies, only these three colonies were picked. These cell lines were mechanically expanded over feeder cells, and then adapted to feeder-free culture conditions and enzymatically expanded. Cells grown over feeder cells, as well as matrigel-adapted cells, were used to examine their pluripotency. During this process, cell lines that progressively lost the ES cell-like morphology (uniform surface and smooth edges) were discarded for subsequent characterization tests as it was considered an indicator of lack of pluripotency.

Subsequently, cells were evaluated using a battery of characterization tests that have been widely used in the literature (Freberg *et al.,* 2007; Raya *et al.,* 2009; Martí *et al.,* 2013). The first test focused on the detection of AP activity in the reprogrammed cells, which is a feature of ES cells (O'Connor *et al.,* 2008). This was assessed using a specific kit that reports AP activity through a colorimetric reaction. Each of the established cell lines (clones) from each sample displayed an intense AP staining. Moreover, this staining allowed for easier visualization of the morphology of the colonies. In this regard, patient-

and control-derived colonies showed a uniform appearance with smooth edges, being indistinguishable from ES cell lines cultured in the lab and also from examples reported in the literature. Therefore, each of the cell lines were deemed suitable for further characterization tests.

Next, expression of pluripotency genes was evaluated by qPCR. Several studies have reported that fully reprogrammed cell lines tend to silence the expression of the transgenes used to induce pluripotency, whereas expression of endogenous pluripotency genes is simultaneously induced (Brambrink *et al.,* 2008). Therefore, by using specific primer pairs, we assessed the expression of transgenic and endogenous Yamanaka factors, as well as the expression of *CRIPTO*, a membrane glycoprotein that acts as a growth factor receptor (Fiorenzano *et al.,* 2016), and the pluripotency-related transcription factors *REX1* and *NANOG*. Based on the *GAPDH*-relative expression rates, cell lines that demonstrated the lowest expression of the four transgenes, as well as induction of pluripotency genes, were selected for further experiments. Cell lines that showed high transgene expression rates (above 0.5% relative to *GAPDH* expression) were discarded, since this lack of silencing may potentially be a sign of incomplete reprogramming. In the case of patient 4, endo-*OCT4* levels above *GAPDH* expression rates were detected in clones 5 and 6. These expression rates were considered abnormally high, and consequently, these clones were also discarded from further characterization tests. An exception was made for the P5 clone 3 cell line, since only two clones were established for this sample. In other words, although clone 3 did not strictly meet the transgene silencing criteria, it was included in the following characterization step. Regarding the induction of endogenous pluripotency genes, variable induction rates were similar to those reported in the literature (Sánchez-Danés *et al.,* 2012). Endogenous *OCT4* and *CRIPTO* rates were the highest for each of the reprogrammed samples, whereas *REX1* and *KLF4* levels were very low, or barely detectable.

The number of clones that efficiently silenced transgene expression and induced endogenous pluripotency gene expression did not differ among the patient- and healthy control-derived cell lines. These gene expression results indicate that, despite each of the established cell lines displaying the typical ES cell morphology and AP staining, a more restrictive test based on the quantification of pluripotency gene expression allowed the identification of cell lines that did not strictly meet the criteria to be considered fully reprogrammed cell lines.

Once two reprogrammed cell lines (clones) per sample were selected for further characterization, the number of transgene insertions in each cell line were analyzed through Southern blot. This technique identified bands corresponding to Yamanaka factors contained in the genome. By comparing the bands detected in reprogrammed samples and non-infected fibroblasts, bands corresponding to transgene insertions were identified. Based on these results, variable number or sizes of the bands allowed us to confirm the independent clonal origin of each pair of cell lines selected per sample.

Generally, between 1 and 3 insertions of each analyzed transgene were detected in the reprogrammed samples. When a large number of insertions were detected for a specific transgene, such as the 8 bands detected for transgenic *OCT4* in P1 clone 1, or the 5 bands detected for transgenic *cMYC* in P3 clone 5, these cell lines were discarded from future experiments, since this fact could potentially lead to increased random mutagenesis, abnormal reprogramming and/or abnormal differentiation traits. However, due to technical challenges, we were not able to determine the number of insertions for transgenic *SOX2* and *KLF4* in each cell line, and therefore, we were unable to test if any of the cell lines had a high number of these transgene insertions. Nevertheless, the Southern blots obtained for *OCT4* and *cMYC* provided sufficient information to confirm the independent clonal origin of the established cell lines. Based on these results, one cell line per sample was selected and further characterized.

Immunofluorescence-based detection of a panel of extensively characterized, and widely accepted pluripotency markers, is one of the main characterization tests that proves the pluripotency of reprogrammed cell lines. Pluripotency-associated transcription factors OCT4, NANOG and SOX2, the stage-specific embryonic antigens SSEA-3 and SSEA-4, and podocalyxin-epitopes TRA1-60 and TRA1-81 were detected in each of the samples analyzed. Moreover, their expression was detected throughout the colonies, although the intensity of the staining varied slightly in some colonies. Therefore, it was assumed that the selected clones expressed the entire set of pluripotency markers studied, which was indicative of the pluripotency achieved.

The term 'pluripotency' refers to the ability of a cell to differentiate into a wide range of cell types. Accordingly, an essential characterization test consists on proving the ability of the reprogrammed cell lines to differentiate into several cell types. By culturing reprogrammed cells in previously defined conditions, they differentiated into cell types derived from the three embryonic germ layers. Finally, immunofluorescence detection of lineage-specific markers proved the pursued differentiation. Ectoderm-derived cell types include neurons, glial cells and melanocytes. In this differentiation test, TUJ1 and GFAP were evaluated as markers of neurons and astrocytes, respectively. Mesoderm derivatives include muscle and blood cells, connective tissue and kidneys, among others. α-SMA and GATA4, which are expressed in the contractile apparatus and during myocardial differentiation, respectively, were detected to prove mesoderm differentiation. Finally, endoderm derivatives include the epithelium of lungs, liver, pancreas, prostate, vagina and several glands. Therefore, expression of AFP, a developmental plasma protein, and FOXA2, a transcriptional activator of liver-specific genes, were studied as indicators of endoderm differentiation. Moreover, formation of round-shaped structures resembling glands was also considered indicative of endoderm differentiation. Each of the differentiated samples expressed at least one out of the two lineage-specific markers studied, proving the differentiation of the reprogrammed samples into cell types belonging to the three cell lineages. Negative detection of the

second lineage-specific marker could be due to different issues. For example, TUJ1 expression was detected in each of the cultures differentiated into ectoderm lineages, but GFAP was only detected on some samples. This suggests that the ectoderm induction medium used appears to induce neuronal differentiation better than astrocyte differentiation, or that our cell lines potentially had an intrinsic tendency to better differentiate into neurons compared to astrocytes. As for endoderm differentiation, FOXA2 is expressed in each of the samples, but AFP is absent in some of them. This is potentially due to the fact that these markers are expressed at specific differentiation stages. FOXA2 is a broadly expressed marker along the endoderm differentiation, whereas AFP is only expressed at later stages (Si-Tayeb *et al.,* 2010). Thus, detection of one or both endoderm markers depends on the differentiation rate achieved by each sample. Therefore, detection of at least one of the two markers tested was considered sufficient to prove the differentiation of the reprogrammed samples into cell types derived from the three germ lines.

Epigenetic regulation of gene expression is tightly controlled during cell reprogramming and differentiation processes (Guo *et al.,* 2017). Methylation of the CpG islands located in promoter sequences is one of the most important modifications that strongly inhibits gene expression. In this regard, it has been shown that during differentiation of human ES cells, promoters of pluripotency genes such as *NANOG* and *OCT4* are quickly methylated upon induction of differentiation, thereby silencing their expression, whereas induction of reprogramming of differentiated cells into pluripotency reduces their methylation (Freberg *et al.*, 2007; Yeo *et al.,* 2007). Therefore, we evaluated the methylation status of the promoter regions of *OCT4* and *NANOG* as part of the characterization of the reprogrammed cell lines, and observed that both promoters were considerably demethylated (methylation rates below 18%) in each of the established cell lines. Thus, we concluded that cell reprogramming led to epigenetic modifications required to acquire pluripotency.

Cell reprogramming using integrative vectors, as well as prolonged *in vitro* culture of reprogrammed cells, often lead to chromosomal abnormalities, which might confer selective advantages to the modified cells. To circumvent this, regular karyotype analyses are recommended to ensure the genomic stability of the established cell lines. Karyotype analyses of the reprogrammed cell lines through G-banding identified chromosomal abnormalities in a small percentage of cells in three of the cell lines. Subsequent subcloning of these cell lines allowed for derivation of cell lines without chromosomal abnormalities.

In conclusion, this set of characterization tests allowed us to select one pluripotent cell line per sample, which were referred to as induced pluripotent stem cells (iPSCs). However, further culture of these iPSCs led to consistent spontaneous differentiation of patient 3-derived iPSCs after 4 passages in feeder-free conditions. Consequently, this cell line was excluded from further experiments, since this spontaneous differentiation

raised questions about the incomplete pluripotency that this specific cell line might have achieved.

The fact that one of the cell lines that had passed each of the characterization tests displayed signs of incomplete pluripotency, raised doubts about the stringency of the set of pluripotency tests selected for the characterization process. Questions that require further evaluation include: Is this set of characterization experiments strict enough to prove the pluripotency of a cell line? Can we discuss different pluripotency degrees in the field of cell reprogramming? Are these characterization tests able to detect and differentiate among variable pluripotency status?

The set of characterization tests performed in this project agreed with the tests required by the Spanish National Bank of Cell Lines (Banco Nacional de Líneas Celulares, Instituto de Salud Carlos III) to deposit the generated cell lines in this cell bank, which is mandatory for any iPSC line generated in any of the Spanish research centers. However, our results strongly suggest that these tests are potentially not enough to prove that the generated cell lines had acquired full pluripotency. Indeed, many authors perform additional characterization tests, such as the *in vivo* teratoma assay and the reactivation of the X chromosome, to further confirm pluripotency of their reprogrammed cells.

Teratomas are encapsulated tumors that generally contain tissues and organ-like structures derived from the three germ layers. In stem cell research, teratoma formation is considered to be one of the most demanding tests to prove cell pluripotency. The test relies on the transplantation of reprogrammed cells, together with extracellular matrix (usually matrigel) into immunosuppressed mice, subcutaneously or into the gonads, to allow for teratoma formation. Irradiated feeder cells may be transplanted as well to improve teratoma formation (Gropp *et al.,* 2012). Moreover, teratoma formation efficiency and the duration of the process appear to depend on the cell number transplanted and the site of injection. Once teratomas are formed, these are extracted and analyzed through histological characterization and immunodetection to prove the presence of cell types and tissues derived from the three germ layers. This test has been considered a gold standard to characterize human iPSCs (Zhang *et al.,* 2012), although some researchers claim that partially reprogrammed cells may also lead to positive results (Chan *et al.,* 2009). In our case, we did not perform this test with our cell lines since it is not considered as an indispensable characterization test by the Spanish National Bank of Cell Lines, despite the prolonged duration of the experiment that raises the cost of the characterization considerably. Importantly, this test may be useful to detect anomalies in P3-derived iPSCs, as well as in other cell lines.

X chromosome reactivation has additionally been studied as a feature of cells reprogrammed to pluripotency (reviewed by Pasque and Plath, 2015). During the development of mammalian female embryos, one of the X chromosomes is epigenetically repressed upon differentiation. Therefore, reactivation of the inactivated

X chromosome has been used as a characterization test in cell reprogramming experiments. However, this is not always the case in human iPSCs, since they tend to acquire a primed pluripotent state (similar to the pluripotency grade found in the inner cell mass of post-implantation embryos) and may still keep one X chromosome inactivated. This is contrary to mouse iPSCs that usually achieve a naïve pluripotency (ground state pluripotency, corresponding to the pluripotency grade found in the inner cell mass of pre-implantation embryos) (Hackett and Surani, 2014). Therefore, study of X chromosome reactivation in the characterization of human iPSCs has been deemed controversial and it was not considered as part of our characterization tests. Further, this test can only be used for female-derived samples and this was an additional reason to exclude it from our set of characterization tests.

Some additional *in vivo* tests have been used to characterize mouse pluripotent cells, such as the study of chimera generation and germline transmission through tetraploid complementation assays (Zhao *et al.,* 2009). However, these tests are not suitable to characterize human iPSCs due to technical and ethical issues.

Despite each of these standard characterization tests being necessary to prove the pluripotency of reprogrammed cells, alternative high throughput tests with broader coverage are currently available. Among them, D'Antonio and colleagues have published a method to accelerate this process by characterizing iPSCs based on cytometry-mediated detection of pluripotency markers, gene expression analysis through qPCR and digital karyotyping using SNP arrays (D'Antonio *et al.,* 2017).

Another test consists of analyzing the transcriptomic profile of the reprogrammed cell lines, comparing them with the profile of the original somatic cells and ES cell lines that are used as positive controls of pluripotency (Guenther *et al.,* 2010; Bock *et al.,* 2011; Araúzo-Bravo, 2016). Comparison of methylation profiles is also useful for characterization purposes (Bock *et al.,* 2011; Ruiz *et al.,* 2012).

A more thorough characterization of our iPSC lines, for example through transcriptomic analysis, would likely detect differences on the degree of pluripotency achieved by our reprogrammed cell lines. Moreover, these expression results will potentially contribute to aid in determining whether P3-derived iPSCs have only been partially reprogrammed.

In this regard, different research teams have aimed to investigate the degree of pluripotency achieved by reprogrammed cell lines. Although these studies have demonstrated a wide variety of experimental outcomes, it is generally agreed that mouse iPSCs tend to acquire a higher pluripotency degree, comparable to that of pre-implantation epiblast cells, and are thus termed naïve pluripotent cells. On the contrary, human cell reprogramming leads to pluripotent cells corresponding to more advanced post-implantation embryonic stages, and are thus classified as primed pluripotent cells (De Los Angeles, *et al.,* 2012; reviewed by Hackett & Surani, 2014). This may be attributed to divergences in signaling pathways controlling cell pluripotency in mice and

humans. As an example of these differences, mouse iPSCs depend on leukemia inhibitory factor (LIF) to maintain their pluripotency, whereas human iPSCs do not respond to LIF and depend on FGF_2. In parallel, the use of 2i (a combination of the FGF/ERK pathway inhibitor PD03 and the GSK3β inhibitor CHIR99021) promotes the self-renewal of mouse iPSCs, whereas it induces neural and mesodermal differentiation in human iPSCs (reviewed by Hackett and Surani, 2014). Importantly, epigenetic regulation appears to play a key role in the transition from the primed state to naïve pluripotency and vice versa (Leitch *et al.,* 2013; Guo *et al.,* 2017). This has led to the development of protocols that are able to reset primed human pluripotent stem cells back to a naïve state (Takashima *et al.,* 2014; Theunissen *et al.,* 2014, 2016; Guo *et al.,* 2017).

In parallel, partial or incomplete reprogramming is also concerning when the established cell lines are intended to be used for disease modeling or for future therapeutic purposes. Epigenetic memory is likely the main cause of this problem. Proper cell reprogramming implies robust genome wide demethylation (Shipony *et al.,* 2014; Lee *et al.,* 2014). Lack of complete reprogramming has been correlated with incomplete erasure of specific methylation sites (Lister *et al.,* 2011; Ohi *et al.,* 2011). This abnormality often causes a biased differentiation, leading to an increased ability of reprogrammed cells to differentiate into the cell type of origin (Bar-Nur *et al.,* 2011; Kim *et al.,* 2011; Hiler *et al.,* 2015).

Considering all of the characterization tests available and the hurdles of cell reprogramming, a wider characterization of our iPSC lines may had made it possible to determine the degree of pluripotency achieved, allowing us to classify them as *partially reprogrammed*, *primed* or *naïve pluripotent stem cells*. Moreover, this information would be useful to interpret the phenotype of the cell lines upon their subsequent myogenic differentiation.

Optimizing the myogenic differentiation of iPSCs. Efficient and reproducible differentiation of iPSCs into specific cell types is crucial to generate *in vitro* disease models, as well as for future therapeutic applications. Despite innumerable differentiation protocols have been reported to induce differentiation of pluripotent cells into specific cell types, *in vitro* myogenic differentiation remains being a challenge, generally showing low efficiency and reproducibility (reviewed by Świerczek *et al.,* 2015). Therefore, to optimize the differentiation rate of the cultures, the majority of protocols include transient expression of specific transgenes and/or FACS-mediated selection of cells with myogenic potential (reviewed by Kodaka *et al.,* 2017).

Myogenic differentiation of pluripotent cells is generally achieved through a biphasic protocol, consisting of the initial mesodermal induction followed by myogenic differentiation (reviewed by Kodaka *et al.,* 2017) A limited number of protocols have achieved myogenic differentiation by culturing the pluripotent cells in specific culture conditions, avoiding the overexpression of exogenous genes. Some of these protocols

induce an initial differentiation and perform a FACS-mediated selection of muscle progenitor cells, followed by their terminal differentiation (Borchin *et al.,* 2013; Barberi *et al.,* 2007). Recently, a few research teams have additionally established protocols to generate myogenic cultures from human iPSCs using neither transgene overexpression nor FACS-mediated purification of myogenic cells (Swartz *et al.,* 2016; Chal *et al.,* 2016). However, these protocols lead to heterogeneous cultures that contain myogenic cells, but also a large amount of undefined cell (Kim *et al.,* 2017). Therefore, this heterogeneity, together with the limited expansion ability of these myogenic cells, casts doubts on their suitability for therapeutic purposes (Kim *et al.,* 2017).

Overexpression of myogenic transcription factors has achieved the greatest myogenic induction rates. Among them, *MYOD1* (Goudenege *et al.,* 2012; Tedesco *et al.,* 2012; Tanaka *et al.,* 2013; Yasuno *et al.,* 2014; Abujarour *et al.,* 2014; Li *et al.,* 2015; Maffioletti *et al.,* 2015) and *PAX7* (Darabi *et al.,* 2012) have been the most widely utilized transgenes for myogenic induction of human iPSCs. As previously mentioned, *PAX7* is a crucial transcription factor in the generation and maintenance of satellite cells, which actively regenerate skeletal muscle tissue (reviewed by Dumont *et al.,* 2015a). Darabi and colleagues demonstrated that transient overexpression of exogenous *PAX7* in human ES and iPSCs*,* followed by their FACS-mediated selection, leads to a population of muscle progenitor cells that express surface markers described in mouse satellite cells, muscle progenitors cells and mesenchymal stem cells (Darabi *et al.,* 2012). These myogenic progenitors can be terminally differentiated into myogenin- and MyHC-expressing myotubes. Compared to *PAX7*-mediated myogenic induction, overexpression of *MYOD1* leads to myogenic cells in more advanced stages of the differentiation process and thus, these cells can be quickly differentiated into myotubes.

Considering this variety of approaches to induce myogenic differentiation of our iPSC lines, transgene expression was selected due to its high efficiency and shortened duration of the protocols. In particular, we decided to reproduce the protocol described by Darabi and colleagues (2012), which uses transient *PAX7* overexpression to generate a pool of muscle progenitor cells, in order to study the role of calpain 3 in early as well as late myogenic differentiation stages. Overexpression of *MYOD1* was not considered due to the potential interaction of this protein with calpain 3 (Stuelsatz *et al.,* 2010), which could interfere with the phenotypes observed upon terminal differentiation.

As an initial step, iPSC lines were infected with the doxycycline-inducible *PAX7*-expression system. Various conditions were evaluated to optimize the infection efficiency, such as variable iPSC confluence, different cell dissociation reagents and increasing polybrene concentrations (data not shown). However, despite using optimized conditions, some cell lines were difficult to infect, whereas cell lines, such as C1, P1 and P4-derived iPSCs, were more prone to be infected. It has to be taken into consideration that iPSCs are one of the most difficult cell types to infect, likely due to

their compact shape and the fact that they grow in colonies, which hinders access of the viruses to the surface of the cells.

The *PAX7*-inducible system consists of two vectors, and thus, a further difficulty derives from the fact that only the cells that are infected with both lentiviral vectors are capable of expressing exogenous *PAX7* when cultured with doxycycline (Darabi and Perlingeiro, 2014). Therefore, efficiencies of 20-25% were considered acceptable. Importantly, the percentage of GFP-positive cells increased throughout the induction process, and muscle progenitors purified at day 14 of the myogenic induction protocol were highly proliferative. Hence, 20-25% infection efficiencies allowed for the generation of a large pool of progenitor cells for subsequent experiments.

It was not possible to achieve satisfactory infection rates for C2, P2 and P5-derived iPSC lines, as these cell lines were especially difficult to infect for unknown reasons. However, we proceeded with their myogenic induction since 12-17% infection rates were sufficient to generate a considerable pool of muscle progenitor cells following their myogenic induction.

Once a stock of *PAX7*-infected iPSC lines was generated, we proceeded to induce differentiation into muscle progenitor cells, following the protocol described by Darabi and colleagues (Darabi *et al.,* 2012, 2014). Throughout the induction protocol, cell morphology was comparable among the various cell lines. At the beginning of the process, each of the iPSC lines displayed a similar morphology. At day 2, EBs were already formed and looked visually similar regarding their smooth and transparent shape. However, considerable differences were detected regarding their size, likely due to differences in the amount of cells plated in each induction protocol, and/or the proliferative potential of these cells in suspension. These differences did not depend on the origin of the iPSC lines, as no differences were detected among healthy control and patient-derived cells. Notably, cell outgrowths had a similar morphology at day 10 and 14 of the differentiation process, and also after selection and culture of GFP-positive cells.

FACS-based analysis of the cell cultures at day 14 of the induction protocol allowed for the evaluation of cell distribution with regards to size and granularity. Of note, although slight variations were detected among the analyzed cell lines, distribution of the GFP-positive cell population was very similar for each of the six cell lines, with relatively small size and granularity compared to the entire cell population. Sorted GFP-positive cells were also similar regarding their green fluorescence intensity, and only highly fluorescent cells were sorted and expanded through passage 3, generating a stock of frozen vials for subsequent experiments.

Inhibition of GSK3β has been shown to activate the canonical Wnt signaling pathway, leading to enhanced myogenic differentiation (van der Velden *et al.,* 2007; Xu *et al.,* 2013). Therefore, CHIR99021, one of the most selective GSK3β inhibitors described to

date, has been included in several myogenic differentiation protocols for human ES and iPSCs (Borchin *et al.,* 2013; Shelton *et al.,* 2014; Chal *et al.,* 2016). Transient treatment of our cell lines with CHIR99021 during the induction process slightly altered the morphology of the EBs, which displayed a rougher surface. In addition, the percentage of GFP-positive cells was significantly increased following a 24 hour treatment with CHIR99021, although this increase was modest when the treatment was extended up to 48 hours. It was interesting to notice that GSK3β inhibition at days 2-3 had a strong effect on the percentage of *PAX7*-expressing GFP-positive cells obtained at day 14 of the protocol. This is potentially due to the fact that an improved mesoderm induction at early stages of the induction protocol may positively act on the proliferative capacity of muscle progenitor cells, both before and after induction of PAX7 expression at day 10 of the protocol, thereby increasing the percentage of GFP-positive cells at day 14 of the induction protocol. However, contrary to our expectations, the use of CHIR99021 in the myogenic induction process did not improve the terminal differentiation efficiency, which was reduced in the cells treated for 48 hours. Previously published studies have clearly proven the beneficial effect of transient GSK3β inhibition in the myogenic induction process. Therefore, it may be necessary to further optimize GSK3β inhibition during the induction protocol described by Darabi and Perlingeiro (2014) to benefit from its positive effect on myogenesis. For example, GSK3β inhibition could be tested in later stages of the myogenic induction process, using various concentrations of the inhibitor and fluctuating the duration of the treatment. Since addition of CHIR99021 did not improve the terminal differentiation of our iPSC lines, we did not include it in our optimized differentiation protocol.

iPSC-derived myotube cultures were generated by culturing GFP-positive cells to confluence, followed by their culture in terminal differentiation medium. Terminal differentiation media contained low serum levels or serum replacement, with neither FGF_2 nor doxycycline. These conditions were expected to induce cell cycle withdrawal and cell fusion, leading to the expression of late myogenic markers such as *MyHC*, myogenin and dystrophin. Several differentiation protocols were evaluated to optimize myotube formation, which was assessed through immunofluorescence based on the detection of sarcomeric myosin-positive cells.

The first differentiation medium evaluated contained only 2% of horse serum in DMEM medium. Horse serum is widely used to induce myogenic differentiation, due to its lower growth factor content and higher insulin levels. We additionally tested C2C12-conditioned medium, as it has been shown to support and improve myogenic differentiation of several cell lineages (Dezawa *et al.,* 2005; Patruno *et al.,* 2017;). Lack of robust myogenic differentiation after 12 days of differentiation highlighted the need to examine alternative differentiation conditions that would lead to higher differentiation rates. Although conditioned medium appeared to improve cell maturation based on the presence of striations, overall myogenic differentiation was

inefficient. Moreover, conditioned medium is an undefined and highly variable medium and therefore, its use would be challenging to reproduce myogenic differentiations. Thus, alternative differentiation protocols were subsequently tested to achieve the desired terminally differentiated myogenic cultures.

In the next optimization attempt, the protocol was shortened to 5 days based on the recommendations of the authors of the original differentiation protocol, since longer incubations may favor cell detachment. The use of a defined differentiation medium containing 20% knockout serum replacement was also compared with the previously tested 2% horse serum medium. Overall, these protocols did not improve considerably the myogenic differentiation rates, and differentiation outcomes were similar with both terminal differentiation media evaluated. Gene expression analysis of a set of myogenic differentiation markers did not contribute to determine the best differentiation medium. *20% KOSR medium* was chosen for the following optimization experiments because myogenic gene expression rates were overall slightly higher compared to *2% HS*-differentiated samples.

As previously mentioned, Chal and colleagues (2016) described a transgene-free and purification-free myogenic differentiation protocol. In the final optimization attempt we tested the terminal differentiation medium used in this protocol to differentiate *PAX7*-expressing muscle progenitor cells. This medium, compared to the previously tested *20% KOSR* medium, led to a higher density of MyHC-positive cells in culture. Importantly, this differentiation medium contained IGF-I, which is known to promote proliferation and myogenic differentiation (Engert *et al.,* 1996), and HGF, a crucial molecule for myogenic cell migration during development, as well as for epithelial to mesenchymal transition that occurs in early myogenesis during embryonic development (Brand-Saberi *et al.,* 1996). Therefore, these two factors may play a crucial role in the myogenic differentiation of our *PAX7*-expressing muscle progenitor cells. In parallel, we evaluated the effect of providing a more complex extracellular matrix to the cells by covering them with a layer of extracellular matrix (matrigel), compared to the regular gelatin coating. This system was expected to improve cell differentiation and maturation (Toral-Ojeda *et al.,* unpublished data). However, in our hands, the sandwich method did not improve the previous differentiation system, and it led to non-uniform cultures with similar, or even reduced, density of MyHC-positive myotubes in cultures. Henceforth, all differentiations were performed in *15% KOSR* medium and in gelatin-coated wells.

To date, it is not fully understood why iPSC lines display variable differentiation potentials, and to what extent these differentiation efficiencies can be improved by optimizing culture conditions. Our data demonstrate that myogenic differentiation of some cell lines can be considerably altered by using specific culture media. Serum types and concentrations, as well as growth factors included in these media may directly influence differentiation potential. However, although some cell lines are highly influenced by these culture conditions, other cell lines are highly resistant to

differentiate. In these cases, the pluripotency grade acquired during cell reprogramming may importantly impact the myogenic differentiation potential.

Comparative myogenic differentiation of iPSCs. Simultaneous terminal differentiation of iPSC-derived muscle progenitor cells led to highly variable cultures. Immunofluorescence detection of terminal myogenic markers, such as sarcomeric myosin and myogenin, revealed inconsistent differentiation potential of the cell lines. These differences in the myogenic differentiation potential among the different cell lines, were not attributed to the mutations in *CAPN3,* since there were no expression patterns distinguishable between healthy control- and patient-derived cultures. Moreover, variability between the two healthy control-derived cells was as large as the variability observed among some patient-derived cells and among patient- and healthy control-derived cells.

Gene expression results were consistent with immunofluorescence results. Cell lines with a greater differentiation potential displayed a higher expression of embryonic myosin (*MYH3*), adult myosin (*MYH2*), *MYOD1* and myogenin (*MYOG*). As for myosin expression, embryonic myosin levels in differentiated cultures were much higher than adult myosin expression levels, which suggests that these cultures had room for further differentiation and/or maturation. *MYOD1* was detected in progenitor cells, and its expression was augmented in differentiating cultures, whereas it was reduced in mildly or poorly differentiating cultures. Myogenin expression, together with myosin expression is considered a terminal myogenic differentiation marker. Results showed a similar expression trend in differentiated cultures, although expression rates were considerably higher compared to *MYOD1* levels.

Poorly differentiating cell lines appeared to have differentiated into non myogenic cell lineages based on their morphology. According to the previously discussed role of epigenetic memory, we suggest that our reprogrammed iPSC lines may have achieved a variable degree of pluripotency and thus, this would directly affect their differentiation potential into myogenic cells. It has been shown that pluripotent cells that retain strong epigenetic marks have a greater tendency to differentiate into the original cell type (Bar-Nur *et al.,* 2011; Hiler *et al.,* 2015; Kim *et al.,* 2011). In our case, poor epigenetic erasure in some of the reprogrammed cell lines may have led to limited myogenic differentiation potential, together with an intrinsic tendency to differentiate into the cell type of origin, fibroblasts. However, presence of fibroblasts in the differentiated cultures has not been assessed in our experiments.

Despite the tremendous variability in the differentiation potential observed among the iPSC-derived myogenic cultures, two genes showed a differential expression among healthy control- and patient-derived cultures. On the one hand, embryonic myosin (*MYH3*) expression was upregulated in patient-derived muscle progenitor cells, which may be indicative of the increased differentiation tendency of patient-derived

progenitors. Conversely, dystrophin (*DMD*), traditionally considered as a terminal differentiation and maturation marker and recently described as a regulator of satellite cell activity (Dumont *et al.,* 2015b), was downregulated in patient-derived cultures both in progenitors and differentiated cells. This may be indicative of a potential role of calpain 3 in the biology of muscle progenitor cells and differentiated cultures. In agreement with this, studies performed with C3KO mice demonstrated that calpain 3 participates in the maturation of skeletal muscle (Kramerova *et al.,* 2004). However, despite these differences being statistically significant, the low *CAPN3* expression observed in muscle progenitor cells suggests that the phenotypes observed in progenitors may probably be calpain 3-independent. Moreover, the large variability observed among the cell lines highlights the need to perform gene rescue experiments to determine if these phenotypes are capain 3-specific. For example, correction of mutations in *CAPN3* in patient-derived cell lines, or the generation of *CAPN3*-knockout cell lines from healthy control-derived cells through gene editing technologies would lead to isogenic cell lines that would clarify if these phenotypes are calpain 3-dependent or independent.

Expression of *PAX7* was also assessed in these differentiated cultures as well as in myogenic precursors. Both gene expression analysis through qPCR and protein detection through Western blot revealed that PAX7 was highly expressed in muscle progenitor cells. Both techniques detected total PAX7 levels, regardless of the exogenous or endogenous origin of the protein. However, at day 0 of differentiation (muscle progenitors), most of these gene expression and protein rates were potentially attributed to exogenous PAX7 since these cells were cultured with doxycycline, which activates the expression of transgenic *PAX7*. As expected, both gene expression and protein levels decreased dramatically following 5 days of terminal differentiation in the absence of doxycycline. Therefore, gene expression and protein levels at day 5 of differentiation were considered to derive primarily from endogenous *PAX7.* Importantly, a considerable proportion of cells stained positively for PAX7 in differentiated cultures, which suggests that these cultures still retain a strong myogenic identity, despite their variable myogenic terminal differentiation potential. However, this large proportion of PAX7-positive cells in differentiated cultures is inconsistent with the residual PAX7 expression reported by Darabi and colleagues (Darabi *et al.*, 2012).

PAX7-positive cells were nearly absent in P5-derived differentiated cultures. This fact, together with the null myogenic differentiation potential of this cell line, suggests that this specific cell line has not achieved the desired myogenic identity, despite the fact that it went through the previously described myogenic induction protocol, including transient exogenous *PAX7* expression. Again, this may potentially be attributed to the epigenetic memory retained by the reprogrammed cells that may override its myogenic differentiation ability.

Since LGMD2A and other dystrophies cause a progressively increasing fibrosis, we questioned whether patient-derived muscle progenitor cells would have an increased tendency to express fibrosis-related genes upon differentiation. In this regard, fibronectin 1 and collagen type 1 α1 were both highly induced upon differentiation, although no statistically significant differences were detected between control- and patient-derived cultures, as it is the case for other dystrophies (Mehuron *et al.,* 2014).

Study of CAPN3 and calpain 3 expression in iPSC-derived cellular models. The study of calpain 3 encounters numerous challenges caused by its quick autocatalytic activity. Consequently, protein extraction from muscle biopsies require the use of specific protocols and buffers that prevent its degradation. Detection of calpain 3 in cell culture extracts is even more challenging than in skeletal muscle extracts, since the amount of calpain 3 protein is reduced when compared to muscle extracts. Moreover, calpain 3 protein levels may be related to the myogenic maturity of the cultures, and thus, lack of proper maturation may lead to low calpain 3 protein levels. Finally, the presence of non-specific bands and degradation bands hinders the study of calpain 3 via Western blot, and prevents its study through immunofluorescence. Considering each of these difficulties, the lack of calpain 3 in our differentiated cultures was one of our main concerns.

Total *CAPN3* expression was analyzed through qPCR using a Taqman probe against exon 1 and 2. This probe was capable of detecting all the transcripts expressed by our cell lines, regardless of the mutations. Results demonstrated that *CAPN3* expression was induced upon differentiation. Although overall gene expression levels were relatively low, the largest induction rates were observed in C1 and P1-derived cell lines. Notably, P1 had only one *CAPN3* allele. Therefore, high myogenic differentiation capacity may promote *CAPN3* expression. However, P5-derived cells also expressed *CAPN3* upon induction of differentiation, despite this cell line not differentiating into myotubes. *CAPN3* expression in the remainder of the cell lines did not strictly correlate with their differentiation potential either. This lack of correlation can be explained by two facts. First, *CAPN3* is additionally expressed in non-myogenic cells (e.g. fibroblast and blood cells) at the mRNA level (Blázquez *et al.,* 2008, 2013). Therefore, differentiated cultures at day 5 that do not display a strong myogenic differentiation may also activate *CAPN3* expression, which could vary according to the differentiated cell type. Alternatively, nonsense-mediated RNA decay has been described in LGMD2A-derived patients (Krahn *et al.,* 2007). This phenomenon appears to be specific to certain mutations, which could likely alter the total amount of *CAPN3* transcripts measured in the cultures.

Due to the previously discussed difficulties when studying calpain 3 protein levels through Western blot, detection of calpain 3 was performed using two antibodies that recognize different epitopes of calpain 3. One of them, IS2, is a polyclonal antibody generated against the calpain 3-specific sequence IS2, whereas the second one, 12A2, is a monoclonal antibody generated against the protein region encoded by exon 8 of

CAPN3 and it recognizes ubiquitous calpains in addition to calpain 3 (Anderson *et al.,* 1998). Multiple bands were observed in Western blots, some of them potentially corresponding to calpain 3 proteolitic products and others to non-specific protein detection. Thus, we only focused on the full-size calpain 3 (94 kDa).

Full-size calpain 3 was detected in each of the cell lines after 5 days of differentiation, with the exception of P5. This was consistent with the mutations found in the patients. P2 and P4 contained at least one missense mutation that potentially led to full size calpain 3, whereas P1 had only one *CAPN3* allele that theoretically produces a 101 kDa band, which was hardly distinguishable from the 94 kDa band observed in the muscle extract used as a positive control. As expected, the 94 kDa calpain 3 was practically undetectable with both antibodies in patient 5-derived differentiated cultures, since the *Basque mutation* is expected to synthesize a truncated 91.5 kDa calpain 3 form that is quickly degraded. Moreover, previously, researchers in our lab reported a lack of 94 kDa band in Western blot analysis of a patient's muscle extract with the *Basque mutation* in homozygosis (unpublished data). However, although unlikely, lack of myogenic differentiation could also cause the immediate degradation of the mutated calpain 3 in this cell line, due to the absence of myogenic structural proteins, such as titin, that protect calpain 3 from degradation.

Densitometry-based quantification of full-size calpain 3 detected with these two antibodies did not strictly correlate, but showed somewhat similar patterns, where calpain 3 expression was residual or absent in P5-derived extracts. Calpain 3 levels in P2 and P4-derived cultures were comparable to healthy controls. This may be attributed to the idea that some missense mutations may prevent calpain 3 autolysis, leading to partially functional, but structurally similar, calpain 3 variants. Overall, calpain 3 protein levels did not correlate with *CAPN3* expression rates, not even in control-derived cell lines. This lack of correlation may be due to several factors that affect calpain 3 stability and autolysis, such as the presence of additional proteins that act over calpain 3.

The results from this study indicate that patient- and control-specific iPSC-derived myogenic cultures express calpain 3 and therefore, could be used to study several aspects of the physiopathology of LGMD2A. However, improvements in the reprogramming process are required to achieve similar pluripotency levels that allow high myogenic differentiation rates, comparable among different iPSC lines. Alternatively, the development and comparison of isogenic cell lines through gene editing technologies would provide valuable information to elucidate the role of calpain 3 in myogenesis.

Differential splicing of *CAPN3* transcripts occurs during development, and this maturation is also recapitulated during *in vitro* myogenic differentiation (Herasse *et al.,* 1999; Spencer *et al.,* 2002). Study of different *CAPN3* transcripts revealed that *CAPN3* maturation occurred in C1 and H9 derived cultures, which showed a consistent

differentiation, whereas this switch from immature to mature *CAPN3* transcripts was absent in mildly differentiating C2-derived cells. This correlates with total *CAPN3* transcript rates, which increase progressively along the myogenic differentiation process in C1- and H9-derived cells, whereas only a modest, although statistically significant, induction is detected in C2-derived cells. Therefore, these iPSC-derived *in vitro* models of myogenesis were able to recapitulate *CAPN3* maturation as long as they possessed a robust myogenic differentiation potential, mimicking the maturation observed in muscle-derived *in vitro* models, as well as *in vivo* during development and muscle regeneration processes.

In summary, we have generated iPSC-derived myogenic cultures from healthy donors and LGMD2A patients that can be used as tools to study the role of calpain 3 in myogenesis, as well as the physiopathology of LGMD2A. However, further improvements are necessary to achieve a higher and similar degree of pluripotency of iPSC lines. The transition of our set of iPSC lines to a naïve pluripotent state would likely allow comparative studies among our different cell lines, which could contribute to elucidate the role of calpain 3 in myogenesis.

In discussion of differential expression of dystrophin in our differentiated cultures, it is notable that calpain 3 levels do not correlate with dystrophin levels. Therefore, if downregulation of dystrophin levels in patient-derived cultures are indeed related to calpain 3, functional calpain 3 would be required to induce proper dystrophin expression in the differentiated cultures.

Finally, based on recent findings describing a direct correlation between calpain 3 and SERCA2 protein levels in skeletal muscle extracts, and their role in the control of calcium homeostasis, we studied SERCA2 in our cellular models. Contrary to our expectations, SERCA2 was detected in each of the cell lines in progenitor stage, where *CAPN3* expression rates were minimal. Upon induction of myogenic differentiation, SERCA2 was observed in each of the cell lines except for P5, where calpain 3 was also absent. Thus, in differentiated cultures, calpain 3 may interact with SERCA2 to promote its stability, whereas in muscle progenitors, SERCA2 is potentially stabilized through a calpain 3-independent mechanism.

Role of calpain 3 in the in vivo regenerative potential of iPSC-derived muscle progenitor cells. Intramuscular transplantation studies with control- and patient-derived muscle progenitor cells proved the muscle regenerative potential of these cells. Human lamin A/C detection labeled human cell nuclei and was used to study cell engraftment, whereas detection of human dystrophin represented the *in vivo* myogenic potential of the transplanted human cells, and was therefore indicative of their regenerative potential. Both healthy control-derived and patient-derived cells were clearly detected in transplanted mouse TAs, and these cells occasionally led to human dystrophin-positive fibers. However, human cells were often incorporated to mouse fibers, but did

not express human dystrophin. Comparison of the regenerative capacity of P1- derived muscle progenitors and its age-matched C2-derived progenitors revealed large differences. Contrary to what was expected, patient-derived cells demonstrated a higher engraftment rate and a greater regenerative potential. Nevertheless, these differences are likely attributed to calpain 3-independent processes, since these two cell lines have previously shown a dissimilar myogenic differentiation potential *in vitro*. Of note, patient-derived cells did engraft and generate muscle fibers, which suggests that calpain 3 is not essential for *in vivo* regeneration of skeletal muscle. However, lack of functional calpain 3 may lead to regenerative defects that are not detectable with this experimental approach.

Overall, considering the significant variability observed among the iPSC lines, which might probably be caused by variable pluripotency rates achieved by each cell line, it is not possible to perform comparative studies among the different cell lines to elucidate the role of calpain 3 in myogenesis. However, since iPSC-derived myogenic cultures do indeed express calpain 3, these cell lines could be used to study the role of calpain 3 by knocking out the *CAPN3* gene in healthy donor-derived cell lines, or correcting the genetic mutations in patient-derived cell lines. Recently developed gene editing systems, such as the CRISPR/Cas9 technology, allow the generation of isogenic cell lines in a relatively quick and easy manner. Using this technology, we could generate isogenic cell lines that would only differ in their *CAPN3* gene, and thus, any phenotype described in transplantation studies, as well as in *in vitro* differentiation experiments, would be attributable to calpain 3.

CHAPTER 2

Study of the potential role of calpain 3 in the regulation of muscle satellite cells.

BACKGROUND AND HYPOTHESIS

Since the discovery of mutations in *CAPN3* as the origin of LGMD2A in 1995, numerous studies have aimed to elucidate the etiology of this disease. Calpain 3 is potentially implicated in numerous cellular processes, playing a structural as well as an enzymatic role (Baghdiguian *et al.,* 1999; Kramerova *et al.,* 2004, 2008; Ojima *et al.,* 2010; Toral-Ojeda *et al.,* 2016). This is supported by the fact that calpain 3 has been described in several subcellular locations, interacting with a wide range of proteins. Moreover, *in vitro* studies have identified many substrates of calpain 3, although it is still unknown whether calpain 3 proteolyzes these molecules *in vivo* (Guyon *et al.,* 2003; Taveau *et al.,* 2003; Ono *et al.,* 2007). Despite the intense efforts to elucidate the role of calpain 3 in skeletal muscle, the mechanism still remains unknown. Current questions include why does a lack of functional calpain 3 lead to LGMD2A and, why does a calpain 3 deficiency affect a specific subset of muscles? Further, it is unknown why the muscle weakness is absent in newborns, but develops later in life.

This late onset of muscle weakness leads us to consider that calpain 3 may be implicated in muscle regeneration processes, with minor activity during muscle generation. This fact would contribute to understand the late onset of the symptoms, which would become increasingly evident when muscle development or growth is diminished and muscle maintenance relies on regenerative mechanisms. Similar to the gradual age-associated switch from muscle growth to regeneration, LGMD2A symptoms appear progressively. This implies that the development of biochemical and histological changes, such as hypeCKemia and eosinophilia in LGMD2A patients, usually occur silently before muscle weakness becomes evident.

While investigating the potential role of calpain 3 in muscle regeneration, we questioned whether calpain 3 could directly participate in satellite cell biology, playing a role in their activation, proliferation, differentiation and/or return to quiescence. Each skeletal muscle has specific regenerative requirements and therefore, activity of satellite cells varies among different muscles (Ippolito *et al.,* 2012). Thus, the implication of calpain 3 in the regulation of satellite cells could partially explain why some specific muscles are predominantly affected in LGMD2A patients. Interestingly, a recent study has reported a novel type of autosomal recessive form of limb girdle muscular dystrophy mainly affecting proximal muscles with a late onset, caused by mutations in the *POGLUT1* gene, which directly impairs satellite cell activity (Servián-Morilla *et al.,* 2016). Therefore, the fact that satellite cell impairment leads to an LGMD phenotype supports the fact that calpain 3 may be implicated in satellite cell biology. However, mutations in *POGLUT1* cause loss of satellite cells, whereas the number of PAX7-positive cells increases in LGMD2A patients as the disease progresses (Rosales *et al.,* 2013).

How could calpain 3 participate in satellite cell biology? Differential expression of calpain 3 observed in cancer cells supports the hypothesis that calpain 3 is potentially able to contribute to the control of cell cycle progression in some specific cell types (Moretti *et al.,* 2009; Roperto *et al.,* 2010). Moreover, the fact that calpain 3 has a nuclear localization sequence in its IS2 region (Sorimachi *et al.,* 1989) suggests that it might localize in cell nuclei in one or more stages along the myogenic differentiation process. Since skeletal muscle is primarily constituted by post-mitotic multinucleated cells, this hypothetic role could be mainly conducted in muscle satellite cells, which tend to be quiescent in homeostasis, but proliferate upon injury. Satellite cell activation, proliferation, differentiation and return to quiescence need to be strictly controlled to maintain the regenerative potential of skeletal muscles throughout life. In this regard, Stuelsatz and colleagues (Stuelsatz *et al.,* 2010) suggested a role for calpain 3 in the maintenance of *reserve cells***,** which are quiescent muscle progenitors found in *in vitro* myogenic cultures. Overexpression of calpain 3 in C2C12 cells (a murine myoblast cell line) increased the population of reserve cells in culture, whereas its downregulation promoted their myogenic differentiation. These authors provided strong evidence that calpain 3 participates in the early stages of the myogenic differentiation process by reducing the transcriptional activity of MYOD1. These results suggest that calpain 3 could potentially play a role in the maintenance of satellite cells *in vivo* and thus, lack of functional calpain 3 in LGMD2A patients would increase MYOD1 activity, leading to satellite cell depletion. However, similar to DMD biopsies, LGMD2A biopsies demonstrate that the number of PAX7-positive cells increases throughout the progression of the disease (Rosales *et al.,* 2013). Therefore, it is unclear how calpain 3 deficiency impacts on satellite cells of LGMD2A patients.

In an attempt to evaluate whether calpain 3 is implicated in satellite cell biology, we aimed to study *Capn3* expression in mouse satellite cells, as well as its potential role in the proliferative and differentiation potential of these cells. To do so, initially, we performed a *Capn3* gene expression study in wild type satellite cells, both in quiescence and following *in vivo* activation, to prove its expression in these cells and its possible activation-dependent expression. Conversely, we analyzed if lack of calpain 3 had a functional effect in these cells by performing a colony assay with wild type and C3KO mouse-derived satellite cells. This test assesses the *in vitro* proliferative and differentiation potential of satellite cells.

MATERIALS AND METHODS

The following figures represent the experimental outline of both approaches, which are detailed below. Briefly, in order to investigate *Capn3* expression in satellite cells in quiescence and following activation, mice were injured in one of their legs via intramuscular cardiotoxin injection. Muscle injury induced satellite cell activation,

whereas the other leg was not injected, and satellite cells were expected to remain quiescent. At days 3, 5 and 7 post injury, satellite cells were FACS-purified from injected and non injected TA (slightly affected in calpain 3-deficient mice) and *soleus* (notably affected in calpain 3-deficient mice), isolating activated and quiescent satellite cells, respectively. Finally, gene expression analysis was performed in these cells and *Capn3* expression was assessed in TA and *soleus*-derived satellite cells extracted from injured and non-injured muscles, at different timepoints (figure 49). Due to the low amount of satellite cells found in skeletal muscle, it was necessary to pool the samples extracted from 6 mice to achieve the minimum amount of RNA required for qPCR analysis.

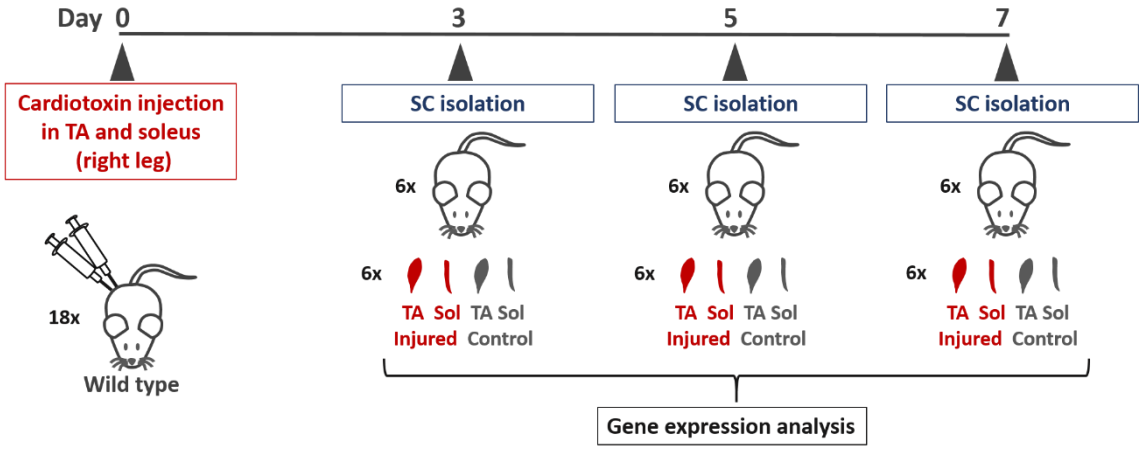

Figure 28. Experimental outline of the gene expression study. TA and *soleus* of the right leg of 18 mice were injured by intramuscular cardiotoxin injection at day 0. Satellite cells were isolated at days 3, 5 and 7 after injury. Muscles of 6 mice were combined in 4 tubes at each experimental timepoint: TA non-injured (control), TA injured, *soleus* non-injured (control), and *soleus* injured. SC: satellite cells; Sol: *soleus.* Finally, gene expression was assessed in these samples.

Alternatively, a colony assay was performed to determine if the lack of calpain 3 alters the proliferative and/or differentiation potential of satellite cells *in vitro.* To do so, satellite cells were extracted from TA and *soleus* muscles of WT and C3KO mice, and plated in 96 well-plates at a density of 1 satellite cell per well. After 8 days in culture in hypoxia, which is expected to favor satellite cell proliferation and differentiation, colonies were fixed and stained to detect cell nuclei and sarcomeric myosin expression. Using the G-tool software, the number of cell nuclei in each well were assessed as indicative of the proliferative potential of satellite cells. In parallel, myosin expression and cell fusion were assessed to estimate the differentiation potential of these satellite cells. Finally, WT and C3KO-derived colonies were compared to determine whether calpain 3 plays a role in satellite cell activity (figure 50).

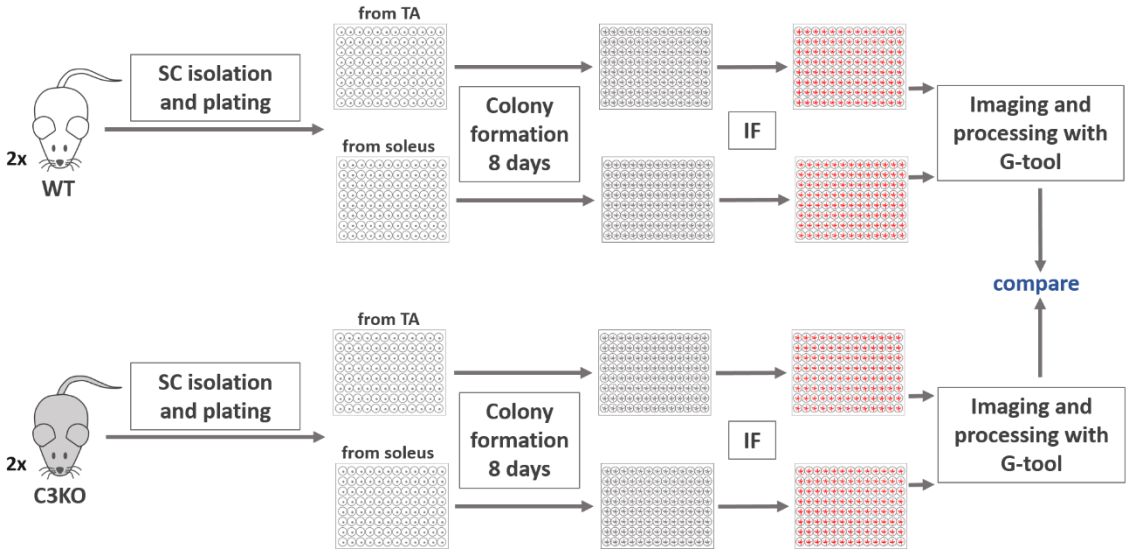

Figure 50. Experimental outline of colony assay. Two WT and two C3KO mice were used to isolate satellite cells from their TA and *soleus* muscles. These cells were plated in 96 well-plates at a density of 1 cell per well, and cultured for 8 days to allow colony formation. Proliferation potential of WT and C3KO satellite cells, as well as their differentiation potential and fusion index were determined using the G-tool software and compared in order to find calpain 3-specific *in vitro* phenotypes.

Experimental animals. For the gene expression experiment, eighteen adult wild type C57BL/6 mice were purchased from Charles River Laboratories and housed in the animal facility. Mice were 8-weeks-old at the time of satellite cell isolation. All procedures were performed following the guidelines and approval provided by Biodonostia Animal Care Committee and the Regional Government of Gipuzkoa (Donostia, Spain), in accordance with the Spanish Royal Decree (53/2013), the European Directive 2010/63/EU and the guidelines established by the National Council on Animal Care.

The colony assay was performed at the Lillehei Heart Institute (University of Minnesota, USA). Two C3KO mice and two wild type controls were born and housed at the Lillehei Heart Institute's animal facility until the experiment was performed at 6 weeks of age. All procedures were performed following the guidelines and approval of the Institutional Animal Care and Use Committee (IACUC).

Cardiotoxin injury. Mice were anesthetized by inhaled isoflurane (Forane), administered at 5% concentration for induction and 3% concentration for maintenance during surgery. A lateral incision was made in the right leg of the mice to facilitate cardiotoxin administration. 3 µl of 50 µM cardiotoxin from *Naja mossambica mossambica* were injected in the TA, whereas the same volume of cardiotoxin at 16.7 µM was injected in the *soleus* of each animal, using a beveled 26G needle. Finally, the incision was sutured using a 6/0 suture thread, and mice were kept in a warm atmosphere until they recovered from anesthesia.

Satellite cell isolation. For gene expression analysis, 6 wild type mice were sacrificed by inhalation of 5% isoflurane followed by inhalation of CO_2 at 3, 5 and 7 days following cardiotoxin administration. For the colony assay, two 6-week-old C3KO mice and two

age-matched wild type controls were sacrificed by dislocation. Satellite cell isolation was performed following the same protocol in both experiments, as specified below. The skin of the hind limbs was removed and the TA and *soleus* muscles were harvested, chopped longitudinally using a razor blade and kept in 15 ml-tubes containing 5 ml of DS1 solution (DMEM High Glucose Media containing 0.2% collagenase II, 100 U/ml penicillin and 100 µg/ml streptomycin) on ice until all muscles were harvested. Muscles were collected in four tubes: *TA from non-injured (control) legs, soleus from non-injured (control) legs, TA from injured legs* and *soleus from injured legs*. Once all the muscles were harvested, chopped and placed in DS1-containing tubes, samples were incubated at 37°C, shaking at 220 rpm for 75 minutes. Next, tubes were inverted 5 times and centrifuged at 1500 rpm for 5 minutes at 4°C. The pellet was resuspended in 5 ml of F10+ solution (Ham's/F-10 medium containing 10% horse serum, 0.01 M HEPES Buffer Solution, 100 U/ml penicillin and 100 µg/ml streptomycin), pipetted up and down with a P1000 micropipette and centrifuged again at 1500 rpm for 5 minutes at 4°C. This step was repeated 4 times, but in the third repetition, cells were pipetted using a pasteur pipette with the edge jagged, which favors the removal of adipose tissue and other contaminants. After the fourth repetition, each pellet was resuspended in 5 ml of freshly prepared DS2 solution (F10+ solution containing 0.06% dispase and 5.7% of DS1 solution), vortexed for 30 seconds, incubated at 37°C shaking at 220 rpm for 30 minutes and vortexed again for 30 seconds. Hereafter, fibers were further disaggregated by drawing and releasing the mixtures into syringes with a 16-gauge needle 5 times and another 5 times into an 18-gauge needle. Then, samples were filtered using 40 µm cell strainers, and digestions were stopped by adding 5 ml of F10+ solution to each tube. Samples were centrifuged again at 1500 rpm for 5 minutes at 4°C and pellets were resuspended in 500 µl of staining media (Dulbecco's Phosphate-buffered saline (DBPS) supplemented with 2% Fetal Bovine Serum (FBS)).

Cells were stained by adding the corresponding amounts of each antibody (as indicated in table 15) and incubated on ice for 30 minutes, protected from light.

Antibody	**Complete staining**	**FMO controls**		
		FM alexa-647	**FM PE**	**FM PE-Cy7**
Anti -integrin-α7-647	2.0 µg	-----	2.0 µg	2.0 µg
Anti-CD106/VCAM-Biotin	0.5 µg	0.5 µg	-----	0.5 µg
Anti-Streptavidin-PE	0.2 µg	0.2 µg	-----	0.2 µg
Anti-CD45-PE-Cy7	0.2 µg	0.2 µg	0.2 µg	-----
Anti-CD31-PE-Cy7	0.2 µg	0.2 µg	0.2 µg	-----

Table 15. Antibodies for SC isolation. Antibody amounts indicated in the table refer to the amount of antibody added per muscle. Therefore, in order to calculate the amount of antibody added to each tube, these values were multiplied by the number of muscles processed in each tube.

Following the staining, cells were washed by adding 5 ml of staining medium to each tube followed by a centrifugation at 1500 rpm for 5 minutes at 4°C. Finally, cells were resuspended in 500 µl of staining medium containing 10 U/ml of DNAse II to prevent cell aggregation. Fifteen minutes prior to the sorting, SYTOX Green Nucleic Acid Stain was added to the cells at a final concentration of 30 nM.

FACS gating approach. Cell sortings were performed on a BD FACsaria III (BD Biosciences) cell sorter equipped with 3 laser lines (488,635 and 561 nm). SYTOX-signal was collected from 488 nm blue laser line, PE and PE-Cy7 signals from the yellow-green 561 nm laser line and alexa 647 fluorescence from 635 nm red laser line. FSC parameter was adquired in linear mode and SSC and fluorescence parameters were acquired in log amplification mode. Prior to each cell sorting, cell separation performance was verified using CS&T quality control beads. Cell sorting was performed using purity masks and a 100 µm nozzle.

Due to the large amount of blood cells found in the samples, a "dump channel" on PE- Cy7 was used to exclude blood and endothelial cells (CD31+ and CD45+). Next, PE- Cy7-negative cells were plotted for FSC- A (Forward scatter, representing cell size) versus green (BP530/30) SYTOX-derived fluorescence. SYTOX-negative cells were considered live cells and gated and plotted in a SSC- A versus FSC- A dot plot, where cells were distributed according to their granularity and size, respectively. The gate was set excluding the events corresponding to the smallest events, which were considered to be cell debris. Thereafter, gated cells were plotted according to FSC-H versus FSC-W, and only single events (singlets) were selected for the final gating, discarding the events that would potentially correspond to doublets or even larger cell aggregates. The final plot represented cells according to PE and Alexa fluor- 647 fluorescence corresponding to CD106/VCAM and integrin-α7 detection, respectively. This allowed the selection of CD106/VCAM and integrin-α7 double positive events, which corresponded to muscle satellite cells. Analysis of cell sorting was performed using the BD FACSDiva (BD Biosciences) software.

Gating strategy based on FMO controls. Fluorescence Minus One (FMO) controls are commonly used to properly set the gates in a multicolor cytometry or FACS procedure. These controls use cells stained with the entire set of antibodies that will be used in the FACS procedure, except for the antibodies that are conjugated with one specific fluorochrome (minus one). One by one, all the *minus one* controls were tested, one for each fluorochrome: fluorescence minus PE, fluorescence minus PE-Cy7 and fluorescence minus Alexa fluor- 647. Each of them was used to set the gate for that specific fluorochrome, since the signal detected for that fluorochrome was considered to be unspecific or basal signal, and thus negative.

Cell sorting and gene expression analysis. Sorted CD31-/CD45-/integrin-α7+/CD106+ cells from injured TA, injured *soleus*, uninjured TA and uninjured *soleus* of wild type mice

were collected in RNAprotect Cell Reagent, which promotes quick RNA stabilization following cell sorting. Samples were stored at -80°C until RNA was extracted using the NucleoSpin RNA XS extraction kit, as indicated by the manufacturer's instructions. 18 ng of RNA were retrotranscribed using the High Capacity cDNA Reverse Transcription Kit, following manufacturer's instructions. Due to the low amount of RNA extracted from the sorted cells, cDNA of target genes was preamplified using the TaqMan PreAmp Master Mix, following manufacturer's instructions. Finally, gene expression was assessed through qPCR in a CFX384 Touch Real-Time PCR Detection System, using Taqman probes. TATA-Binding Protein (*Tbp*) was used as an internal control and gene expression rates were represented in relation to *Tbp* expression, which was considered as 100%.

Cell sorting and colony assay. Sorted CD31-/CD45-/integrin-α7+/CD106+ cells from TA and *soleus* muscles of wild type and C3KO mice were individually plated in gelatinized 96-well plates in DMEM/F12 medium containing 20% FBS, 10% horse serum, 50 ng/ml human FGF_2, 100 U/ml penicillin, 100 µg/ml streptomycin and 0.5% chick embryo extract. Ninety-six wells were plated for each condition: *C3KO TA-derived satellite cells, C3KO soleus-derived satellite cells, wild type TA-derived satellite cells and wild type soleus-derived satellite cells*. In this experiment, previous muscle injury was not required since the *in vitro* culture of satellite cells itself induces their activation, proliferation and differentiation. Cells were incubated for 8 days in hypoxia (3% O_2) to allow for colony formation. Following the incubation, cells were fixed in 4% paraformaldehyde for 20 minutes at room temperature, permeabilized with 0.3% triton X-100 in PBS for 20 minutes and blocked with 3% bovine serum albumin (BSA) in PBS for 1 hour at room temperature. Cells were stained overnight at 4°C with MF20 antibody diluted 1:25 in 3% BSA to detect sarcomeric myosin. The following day, plates were washed with PBS and incubated with goat-anti-mouse Alexa fluor- 555 (1:500) diluted in 3% BSA, as well as with 100 ng/ml 4',6-diamidino-2-phenylindole (DAPI) to stain cell nuclei. Finally, cells were washed once with PBS and colonies were imaged using an inverted fluorescence microscope. Cell proliferation and differentiation were assessed in at least 30 colonies per each condition, using the G-tool GUI algorithm developed by Ippolito and colleagues (Ippolito *et al.,* 2012). This algorithm processed the images to increase the color contrast and was used to assess the following features of the colonies: *proliferative potential*, measured as the number of nuclei per colony, *differentiation potential*, measured as the proportion of nuclei within a myosin-positive cytoplasm, and *fusion index*, measured as the proportion of nuclei within myotubes containing three or more nuclei. Statistical significance of index values observed among wild type and C3KO mice-derived colony assays were analyzed though independent t-tests at a 95% confidence interval.

RESULTS

FACS gating approach for SC isolation. The following gating approach was designed to optimize satellite cell isolation by FACS (figure 51). First, blood cells and endothelial cells were discarded by selecting PE-Cy7-negative cells (negative for CD45, a marker of leukocytes, and CD31, which labels endothelial cells, platelets, macrophages, and other blood cells)(not P1 region) (figure 51.a). Secondly, live cells were gated (P2) by negative selection of cells stained with the viability marker SYTOX Green (figure 51.b). Thirdly, cells were plotted according to their size and granularity and gated (P3) to exclude cell debris, corresponding to the smallest events represented in the FSC-A axis (figure 51.c). Next, cells were plotted according to FSC-H versus FSC-W, which makes it possible to exclude cell doublets and aggregates by gating the events with the size and shape corresponding to single cells (P4) (figure 51.d). Finally, cells were plotted according to Alexa fluor- 647 fluorescence versus PE fluorescence, corresponding to integrin-α7 and CD106/VCAM staining, respectively. Events positive for both markers were sorted and considered to be satellite cells (P5). Blue events in figure 51.a, figure 51.b and figure 51.e correspond to sorted CD31-/CD45-/integrin-α7+/CD106+ live cells.

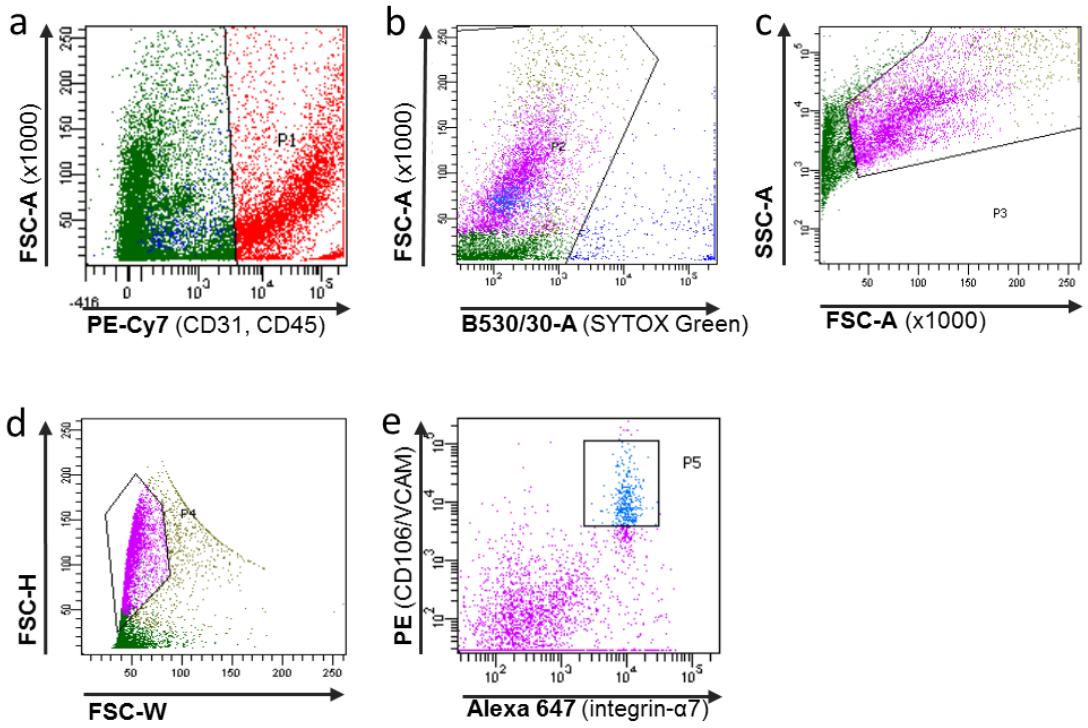

Figure 51. SC isolation strategy. a) Cells plotted according to their size (FSC-A) and PE-Cy7 fluorescence. b) PE-Cy7-negative cells plotted according to their size (FSC-A) and green fluorescence. c) Cells negative for SYTOX green (live cells) plotted according to their cell size (FSC-A) and cell granularity (SSC-A). Cells are gated in P3. Cell debris (green events) is excluded. d) Plot representing FSC-H versus FSC-W. Singlets (purple events) are selected. e) Plot representing Alexa fluor- 647 staining (integrin-α7) versus PE staining (CD106/VCAM). Events positive for both markers (blue events) are sorted and considered as satellite cells (P5).

Gating strategy based on FMO controls. To accurately set the gates for this isolation setup, FMO controls were used as negative control samples for each of the fluorophores. Figure 52 illustrates plots for each of the three FMO controls tested: Fluorescence Minus PE-Cy7 (figure 52.a, b and c), Fluorescence Minus PE (figure 52.d, e and f) and Fluorescence Minus Alexa fluor- 647 (figure 52.g, h and i).

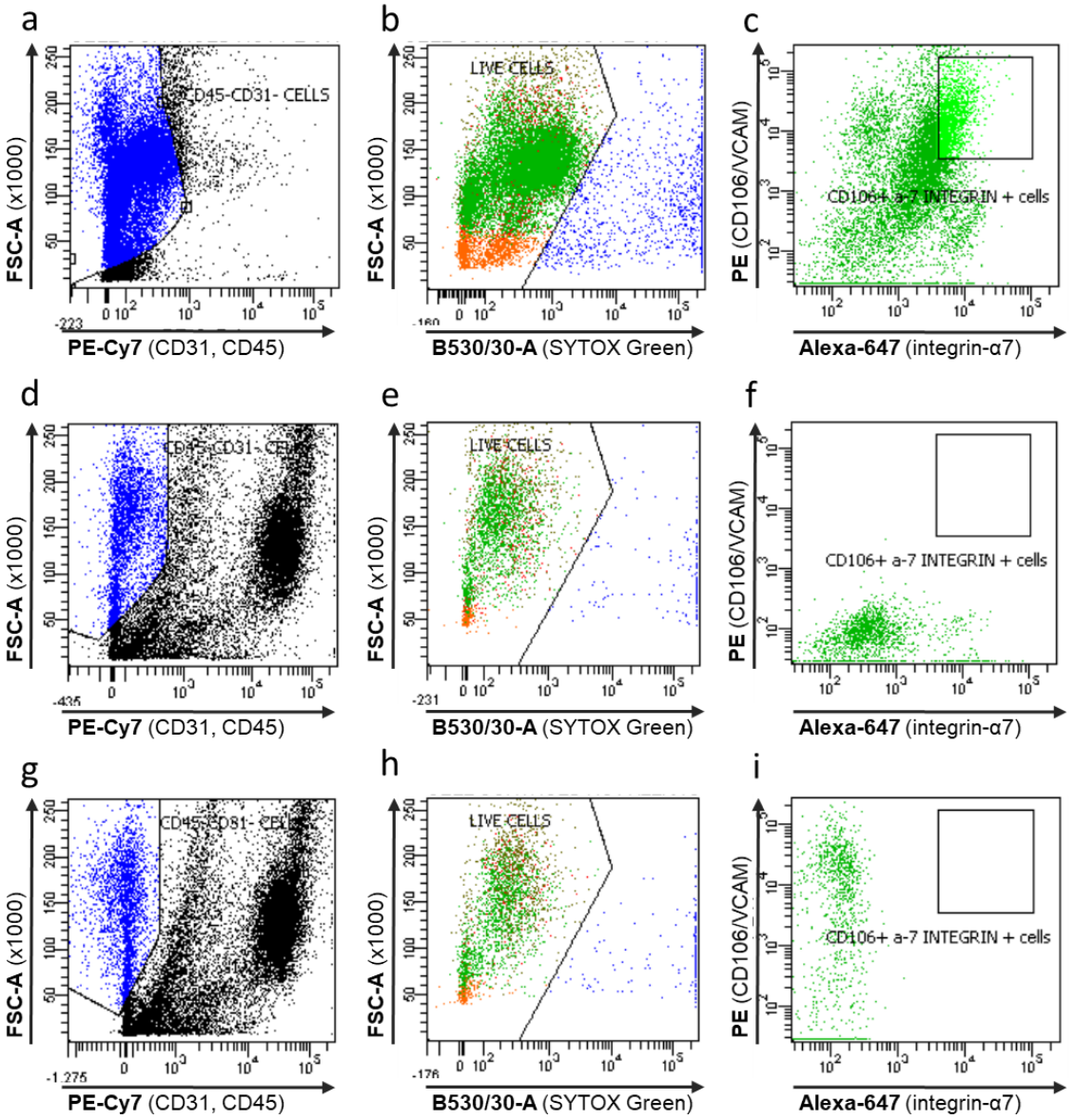

Figure 52. Plots corresponding to FMO controls. a, b and c correspond to Fluorescence Minus PE-Cy7 staining. d, e and f correspond to Fluorescence Minus PE staining. g, h and i correspond to Fluorescence Minus Alexa fluor-647 staining. b, e and h represent events according to their size (FSC-A) and green fluorescence (SYTOX green). a, d and g represent events according to their size (FSC-A) and PE-Cy7 fluorescence. Finally, c, f and i represent events according to their PE (CD106/VCAM) and Alexa fluor- 647 (integrin- α7) fluorescence.

Figure 52.a displays some events highly fluorescent for PE-Cy7 fluorescence, likely corresponding to dead cells. Therefore, these events were excluded when the gate for PE- Cy7 negative cells was set. Figure 52.f shows the staining for Alexa fluor- 647, and

this plot was used to set the gate for PE-positive staining since the PE signal detected in this plot was considered to be nonspecific. Figure 52.i shows cells positive for PE, and this plot was used to set the gate for Alexa fluor-647-positive cells since the events detected were considered to be a nonspecific signal. Therefore, information on figure 52.f and.i was used to set the gate for CD106/integrin-α7 double positive cells.

Cardiotoxin injury and satellite cell isolation. Once the strategy for satellite cell isolation was defined, satellite cell activation was induced by performing a muscle injury in the TA and *soleus* of one of the legs of wild type C57BL/6 mice via intramuscular injection of cardiotoxin, as specified in the materials and methods. Satellite cells were isolated at 3, 5 and 7 days post-injury from the injured and non-injured muscles, to optimize the timing for the isolation of activated satellite cells from the injured muscles following cardiotoxin administration. Figure 53 displays FACS plots corresponding to the sorted cells from both injured and non-injured (control) TA and *soleus* at different timepoints after injury. Sorted events are represented in cyan in both plots corresponding to each sample. Distribution of the sorted events, gated in PE versus Alexa fluor-647 plots, can be visualized in the SSC-A versus FSC-A plots. These results showed that the distribution of quiescent satellite cell populations (isolated from non-injured, control muscles) according to their size and granularity was similar for both TA- and *soleus*-derived satellite cells, being considerably uniform. However, the population of satellite cells extracted from cardiotoxin-injured legs demonstrated a prominent dispersion in the FSC-A axis, which was highest at day 3 post-injury and decreased at day 5 and 7. Importantly, the distribution of cells in the PE versus Alexa fluor-647 plots was greatly affected by cardiotoxin injury, since a population of CD106+/integrin-α7- cells was clearly visible in these samples and absent in non-injured (control) muscle plots. The intensity of this staining progressively decreased as the days following injury increased.

Therefore, these results suggest that cardiotoxin injury likely induced satellite cell activation, since the distribution of the satellite cell population was greatly influenced by muscle injury in both TA and *soleus*. The greatest change in distribution was observed at day 3 post-injury, and therefore, this seemed to be the timepoint at which the most prominent activation of satellite cells was achieved.

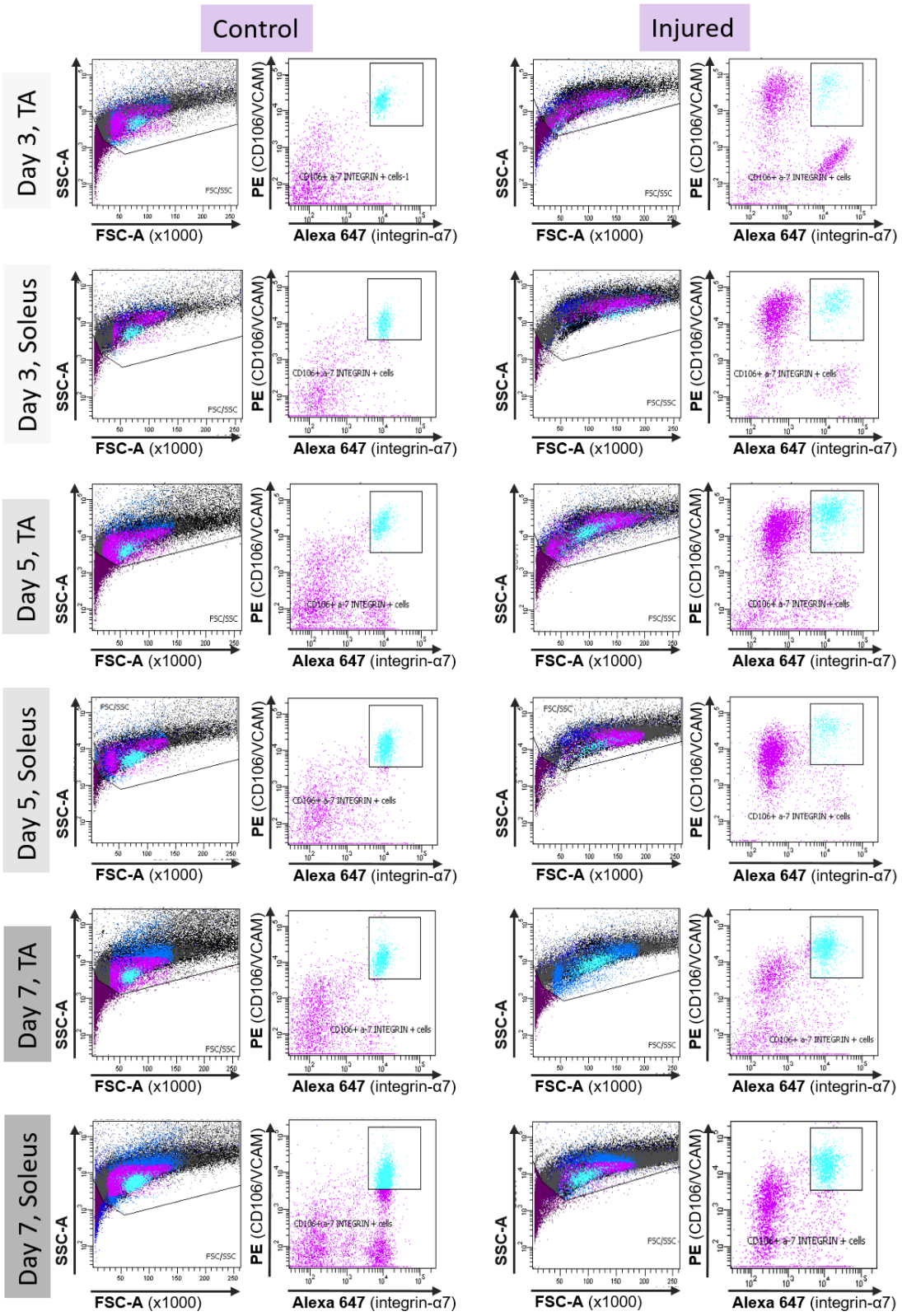

Figure 53. SC isolation. Dot plots corresponding to satellite cell isolation from injured and non-injured TA and *soleus* at days 3, 5 and 7 after intramuscular cardiotoxin administration. Plots in columns 1 and 3 represent the entire cellular population according to their size and granularity. Plots in columns 2 and 4 represent CD45- and CD31- live singlets, according to CD106 and integrin-α7 expression. Events corresponding to sorted cells are represented in cyan.

Gene expression analysis. Gene expression analysis demonstrated that *Pax7* was highly expressed in satellite cells isolated from non-injured (control) muscles whereas its expression in satellite cells from injured legs was down-regulated to expression rates lower than 15% of that observed in control satellite cells at day 3 post-injury. Contrarily, expression of *Myod1* was lower in satellite cells isolated from non-injured muscles, but was considerably induced (around 3-fold in TA-derived satellite cells and 4.5-fold in *soleus*-derived satellite cells) in satellite cells isolated at day 3 post injury (figure 54). Therefore, results confirmed that quiescent satellite cells were obtained from uninjured muscles whereas activated satellite cells were isolated from cardiotoxin-injured muscles. Moreover, the highest satellite cell activation rate was achieved at 3 days post-injury, as indicated by the most pronounced *Pax7* down-regulation and *Myod1* up-regulation, compared to day 5 and 7 after injury. This is consistent with the highest dispersion of the satellite cell population observed at day 3-post injury in figure 53.

Modulation of *Pax7* and *Myod1* expression in quiescent and activated satellite cells followed a similar tendency in both TA- and *soleus*-derived satellite cells. Of note, *Pax7* and *Myod1* expression in quiescent satellite cells was increased in TA-derived satellite cells compared to soleus-derived satellite cells.

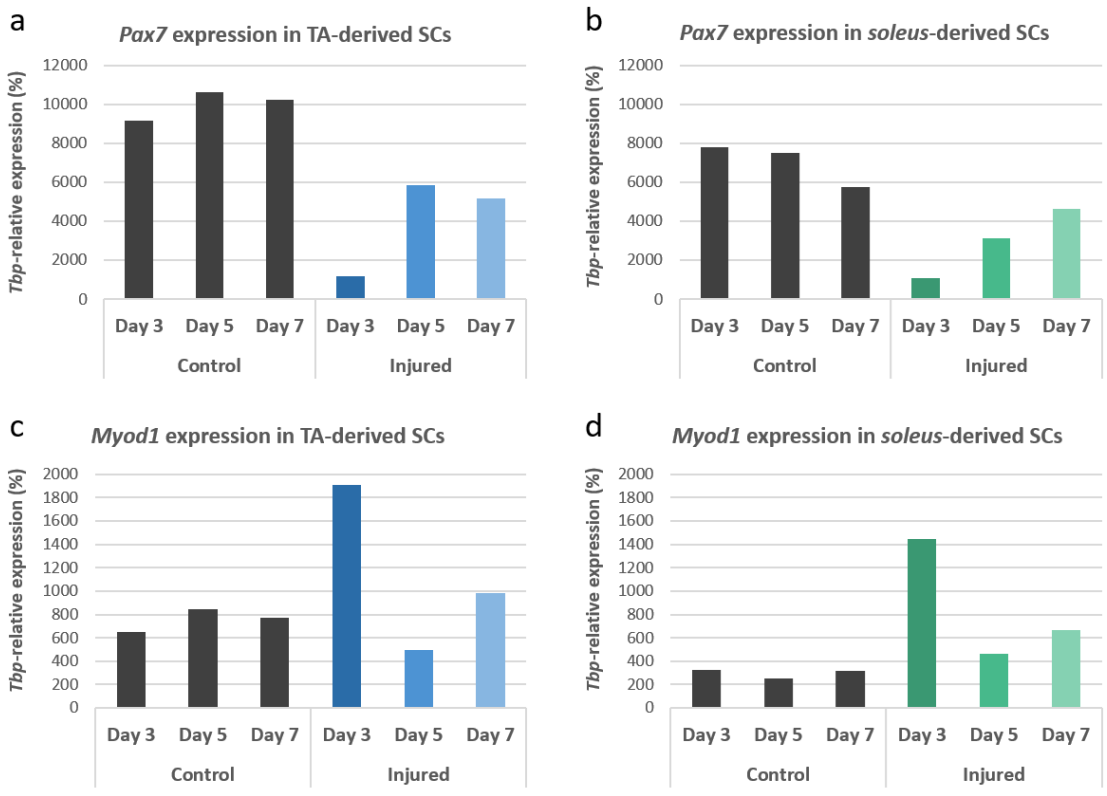

Figure 54. Expression of *Pax7* and *Myod1* in satellite cells. Expression of *Pax7* and *Myod1* relative to the endogenous gene *Tbp* (100%), in %. a) *Pax7* expression in TA-derived satellite cells and b) *soleus*-derived satellite cells. c) *Myod1* expression in TA-derived satellite cells and d) *soleus*-derived satellite cells. Black bars correspond to gene expression rates found in satellite cells extracted from non-injured muscles at day 3, 5 and 7 post-injury. Blue and green bars represent gene expression rates in satellite cells extracted from cardiotoxin-injured TA (blue bars) and *soleus* (green bars) at days 3, 5 and 7 post-injury.

Myogenic markers embryonic myosin (*Myh3*), myogenin (*Myog*) and ryanodine receptor type 1 (*Ryr1*) were also upregulated in activated satellite cells (figure 55). *Myh3* was greatly induced in satellite cells at 3 days post-injury and gradually reduced in satellite cells isolated from injured muscles at day 5 and 7 post-injury. Indeed, *Myh3* expression levels in satellite cells isolated from injured muscles 7 days after injury resembled those of quiescent satellite cells, suggesting that satellite cells from injured muscles at day 7 post-injury are gradually acquiring quiescence (figure 55.a and b). However, expression of *Myog* and *Ryr1* was still considerably up-regulated in satellite cells isolated from injured muscles at day 5 and 7 after injury, compared to quiescent satellite cells (figure 55.c-f).

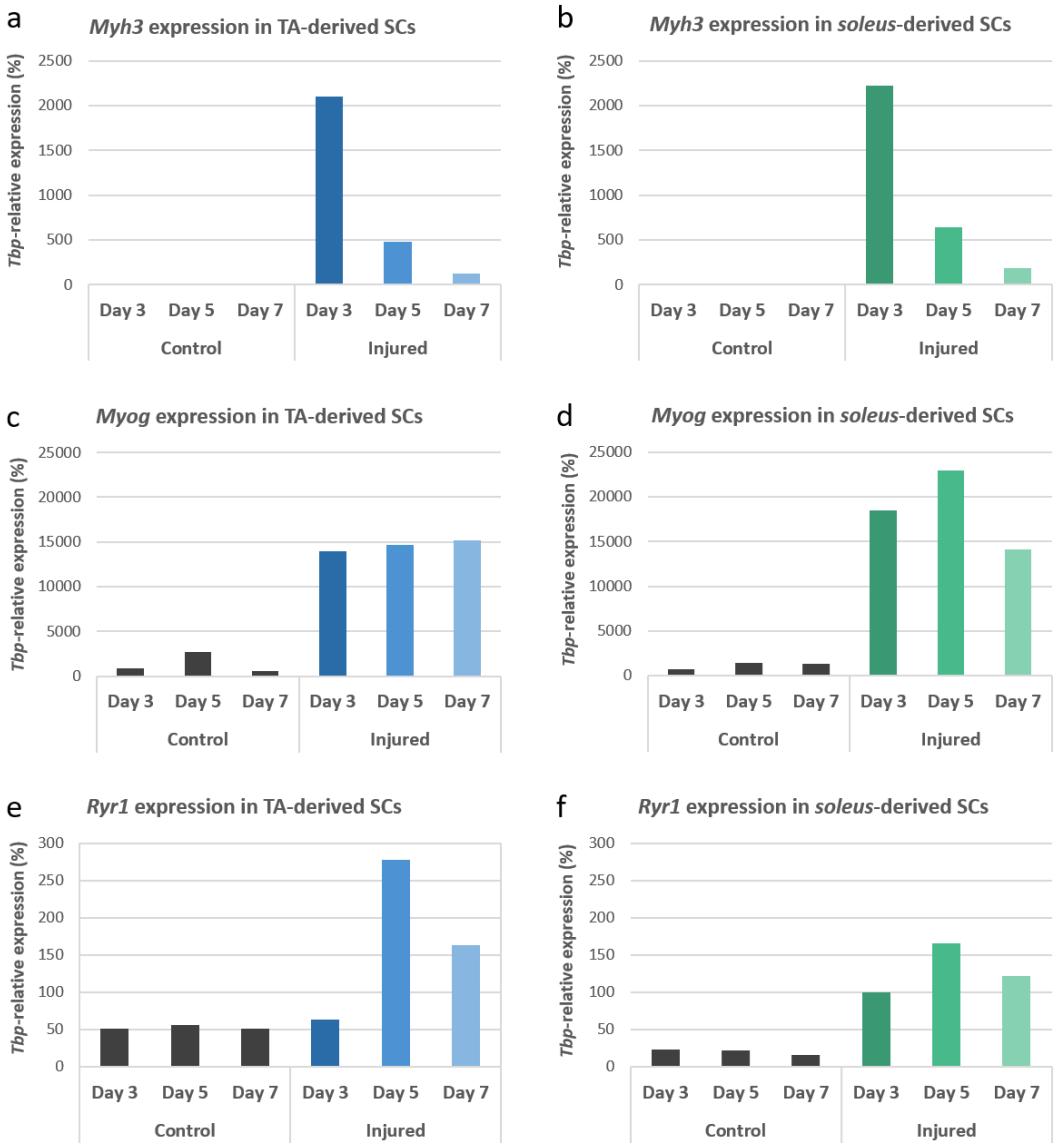

Figure 55. Expression of *Myh3*, *Myog* and *Ryr1* in satellite cells. Expression of *Myh3* (a, b) *Myog* (c, d) and *Ryr1* (e, f) relative to the endogenous gene *Tbp* (100%), in TA-derived satellite cells (a, c, e) and *soleus*-derived satellite cells (b, d, f). Black bars correspond to gene expression rates found in satellite cells isolated from non-injured muscles at day 3, 5 and 7 post injury. Color bars represent gene expression rates in satellite cells isolated from cardiotoxin-injured TA (blue bars) and *soleus* (green bars) at days 3, 5 and 7 post-injury.

These gene expression data provided evidence that intramuscular cardiotoxin administration induced changes in the expression of a set of myogenic genes in satellite cells, which were consistent with their activation. Once isolation of quiescent and activated satellite cells was achieved from uninjured and injured muscles, respectively, expression of *Capn3* was assessed in these cells. qPCR results demonstrated that expression of *Capn3* was induced in activated satellite cells isolated at 3 days post-injury, and subsequently, it was progressively reduced (figure 56). Thus, these results confirmed that calpain 3 was expressed in satellite cells at mRNA level, being upregulated upon satellite cell activation. Notably, *Capn3* expression rates were relatively low compared to expression rates of other genes typically expressed in satellite cells, such as *Pax7* and *MyoD*.

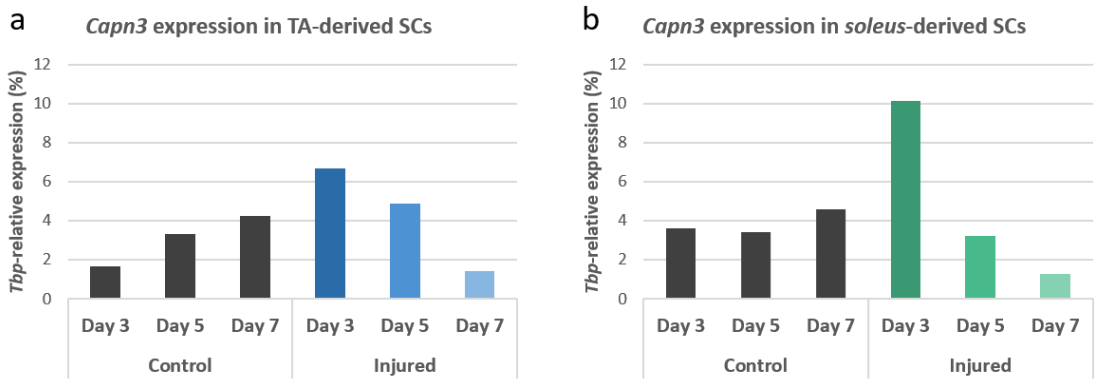

Figure 56. *Capn3* expression in satellite cells. Expression of *Capn3* relative to the endogenous gene *Tbp* (100%), in TA-derived satellite cells (a) and *soleus*-derived satellite cells (b). Black bars correspond to gene expression rates assessed in satellite cells isolated from non-injured muscles (control) at day 3, 5 and 7 post-injury. Blue and green bars represent gene expression rates in satellite cells isolated from cardiotoxin-injured TA (blue bars) and *soleus* (green bars) at days 3, 5 and 7 post-injury.

Expression of dystrophin (*Dmd*) and myosin heavy chain 2 (*Myh2*) in satellite cells were also evaluated. Both genes were found to be up-regulated in quiescent satellite cells, compared to activated satellite cells. Of note, the expression rate of *Dmd* in quiescent satellite cells was considerably high (similar to *Tbp* expression rates) whereas *Myh2* expression was markedly lower (figure 57).

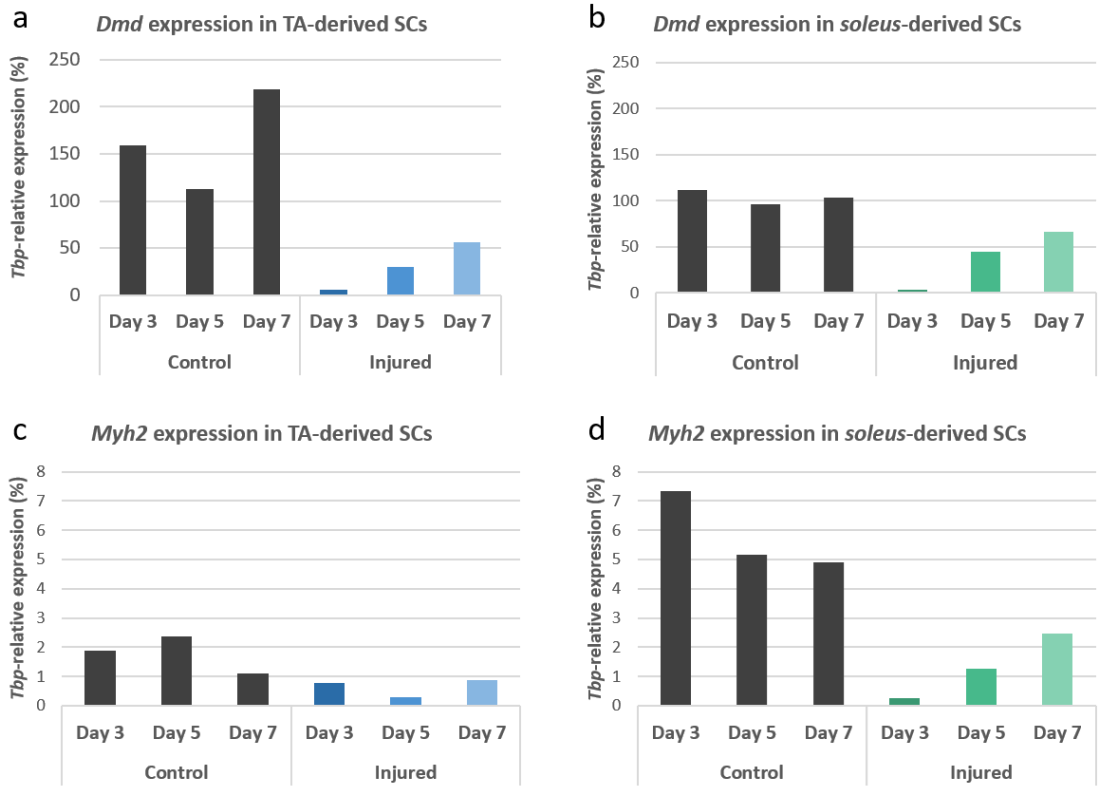

Figure 57. Expression of *Dmd* and *Myh2* in satellite cells. Expression of dystrophin (a,b) and *Myh2* (c,d) relative to the endogenous gene *Tbp* (100%), in TA-derived satellite cells (a,c) and *soleus*-derived satellite cells (b,d). Grey bars correspond to gene expression rates found in satellite cells isolated from non-injured muscles at day 3, 5 and 7 post-injury. Color bars represent gene expression rates in satellite cells isolated from cardiotoxin-injured TA (blue bars) and *soleus* (green bars) at days 3, 5 and 7 post-injury.

Colony assay. Satellite cells were isolated following the previously described protocol and gating approach from the TA and *soleus* of two 6 week-old C3KO mice and two age-matched wild type controls. Cardiotoxin injury was not performed because *in vitro* culture of satellite cells itself leads to their activation and differentiation. The following figure shows FACS plots corresponding to CD106/VCAM and integrin-α7 double positive cells isolated and plated for the colony assay (figure 58).

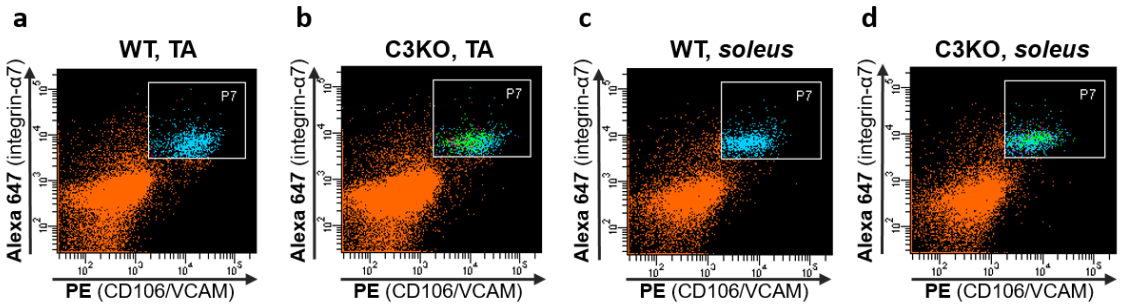

Figure 58. SC isolation for colony assay. Dot plots corresponding to CD106/VCAM and integrin-α7 double positive cells isolated (gated as P7) from the TA (a,b) and *soleus* (c, d) of wild type (a, c) and C3KO (b, d) mice.

Following 8 days of incubation, when colonies containing differentiated and undifferentiated cells were grown, these were processed to detect cell nuclei and sarcomeric myosin through immunofluorescence. Next, colonies were imaged and processed though the G-tool software, which sharpened and increased the contrast of the images (figure 59), and evaluated the number of cell nuclei detected in each colony, as well as the differentiation and fusion index. Overall, there was a high variability among the colonies generated from each muscle type (WT TA, WT *soleus*, C3KO TA and C3KO *soleus*), as represented in figure 60.

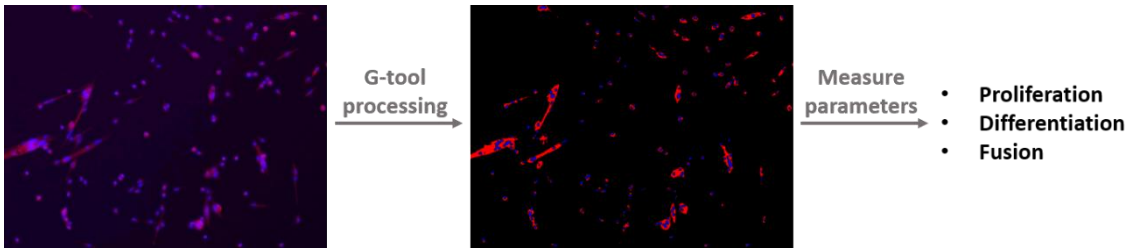

Figure 59. Example of processing colony images with the G-tool software. Immunofluorescence images of colonies where sarcomeric myosin is stained in red and cell nuclei are visualized in blue. These images were processed with the G-tool software, generating colony images with very high contrast. Then, the same software measures the proliferation, differentiation and fusion index of each colony.

No statistical differences ($p<0.05$) were observed between the proliferative capacity, differentiation potential and fusion index of WT and C3KO-derived satellite cells, regardless of their origin (TA or *soleus*).

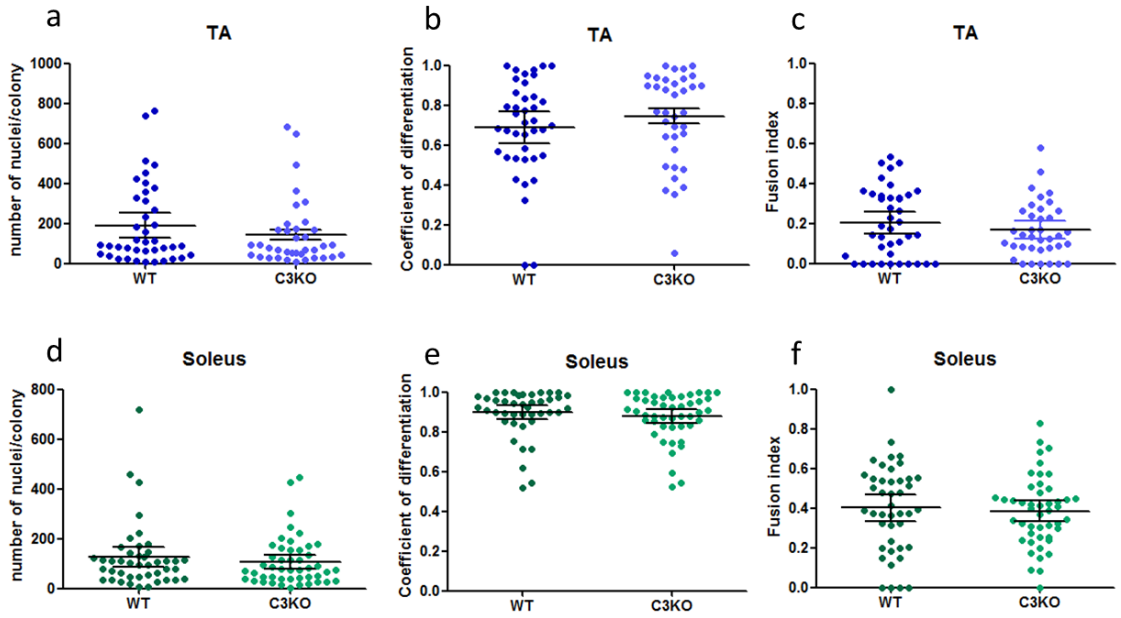

Figure 60. Colony assay results. Number of nuclei per colony (a, d), coefficient of differentiation (b, e) and fusion index (c,f) represented for TA-derived wild type and C3KO satellite cells (a, b, c) and *soleus*-derived wild type and C3KO satellite cells (d, e, f). Black bars represent mean and 95% confidence intervals.

DISCUSSION

This project aimed at studying a potential role of calpain 3 in satellite cell biology. To do so, two experimental approaches were designed. The first approach consisted of gene expression analysis of *Capn3* in quiescent and activated satellite cells, to test whether *Capn3* is expressed in satellite cells, and if so, if it follows an activation-dependent expression pattern. The verification of its expression at the mRNA level in satellite cells would not directly prove that this protein plays a role in satellite cells, but it would establish a foundation for further experiments. Contrarily, lack of *Capn3* expression in satellite cells would have ruled that possibility out.

The designed experimental approach allowed us to successfully isolate both quiescent and *in vivo* activated satellite cells for gene expression analysis, as proven by the modulation *Pax7* and *Myod1* expression. Due to the small amount of satellite cells found in skeletal muscle (approximately only 2% of nuclei found in skeletal muscle correspond to satellite cells), samples of 6 mice were pooled to obtain the minimum amount of RNA required for gene expression analysis.

Results indicated that the highest rate of activation was achieved in satellite cells isolated 3 days following injury, as this is the timepoint at which the most prominent down-regulation of *Pax7* and the highest induction of *Myod1* were observed in injured muscle-derived satellite cells. Later on, their expression rate tended to slowly moderate, resembling those of quiescent satellite cells. This is consistent with the distribution of sorted events in FACS plots, which showed the highest dispersion regarding cell size and granularity at day 3 after injury and receded at day 5 and 7 post injury. Muscle injury also led to the emergence of a CD106+/integrin-α7- population of cells, which was highest at 3 days after injury. The emergence of a population of CD106+/integrin- α7- cells could be a result of myogenic cells that induced CD106 expression following injury to recruit leukocytes to the site of injury (Jesse *et al.,* 1998).

Downregulation of *Pax7* in activated cells attracted our attention since this transcription factor has also been described as a marker of activated satellite cells, despite of quiescent cells. This might be due to the fact that the panel of surface markers used for satellite cell isolation may also potentially select cells entering myogenesis in injured muscles, and these cells might have already downregulated Pax7 expression at mRNA level. However, further experiments are required to verify this fact.

Besides *Myod1*, expression of other myogenic genes such as embryonic myosin, myogenin and ryanodine receptor type 1, was induced upon injury. *Myh3* expression was rapidly and progressively down-regulated in satellite cells at day 5 and 7 post-injury, whereas *Myog* and *Ryr1* kept being considerably expressed in satellite cells at day 5 and 7 post-injury. Relevance of these different expression trends cannot be determined since we did not verify whether the expressed genes eventually led to protein synthesis in these cells. However, upregulation of myogenic genes in activated satellite cells is not

unexpected since the majority of these cells will activate their myogenic differentiation as to repair muscle damage.

As for *Capn3*, its expression was highest in activated satellite cells at 3 days post injury, both in TA and *soleus*, and it was progressively down-regulated at day 5 and 7 post-injury. Therefore, *Capn3* displayed an expression pattern that resembled the expression of *Myh3*, although its *Tbp*-relative expression rate was much lower than that of *Myh3*. These results proved that calpain 3 is expressed in satellite cells at the mRNA level, showing an activation-dependent expression pattern. Contrary to expected, expression rates were similar in TA- and *soleus*-derived satellite cells, despite *soleus* is more affected in calpain 3-deficient mice compared to TA. This could be related to the age of the mice used in the experiment. Due to the progressive feature of LGMD2A, greater *Capn3* expression rates and more evident differences between TA and *soleus*-derived satellite cells may potentially be observed as mice age. Despite *Capn3* expression levels were modest, this might be significant since low expression rates may lead to calpain 3 protein, as seen in the *in vitro* model of LGMD2A generated in chapter 1.

Capn3 expression data have been contrasted with alternative gene expression studies performed in satellite cells by different research groups. When comparing these data to our results, it has to be kept in mind that each of the published studies were performed using a different mouse strain and a specific satellite cell isolation setup (i.e. combination of markers and FACS protocol, age of the mice and muscles), as well as various approaches to induce satellite cell activation. For example, Fukada and colleagues (Fukada *et al.,* 2007) performed gene expression studies in quiescent and activated satellite cells isolated from hindlimb muscles based on the expression of the surface marker SM/C-2.6. Satellite cell activation was achieved by culturing the isolated cells *ex vivo* for 3-4 days. Expression of *Capn3* in these cells was similar in quiescent and activated satellite cells.

Additional transcriptome analysis performed by Pallafacchina and colleagues (Pallafacchina *et al.,* 2010) compared satellite cells isolated from adult wild type, young wild type and adult *mdx* mice, as well as adult *ex vivo*-activated satellite cells, which were isolated based on *Pax3* expression. This study reported that calpain 3 expression in adult quiescent satellite cells was 1.54 times higher compared to *mdx* satellite cells, and 2.23 times higher compared to *ex vivo*-activated satellite cells.

However, despite these data showing *Capn3* expression in satellite cells, it would be necessary to prove the presence of calpain 3 protein in satellite cells to elucidate whether satellite cells are directly implicated in the pathophysiology of LGMD2A. Due to the high instability of calpain 3, it is assumed that in the hypothetical case that calpain 3 was expressed in satellite cells, it would probably be autolyzed during the satellite cell isolation process, which can take up to 12 hours. Therefore, we considered that a functional test to look for phenotype differences between C3KO-derived and wild

type-derived satellite cells would be more informative to unravel a potential role of calpain 3 in satellite cells.

Hence, a colony assay was performed with C3KO and wild type satellite cells isolated from the TA and *soleus* of 6 weeks-old mice. This assay measured the *in vitro* proliferative potential of satellite cells isolated from each mice and muscle, as well as their differentiation and fusion potential. Although no statistically significant differences were found among their phenotypes, this could be attributed to the fact that the animals used in the experiment were too young to display a phenotype. As previously indicated, animal models of calpainopathy show a very mild phenotype that is more evident as the mice age. Therefore, calpain 3-dependent phenotypes in satellite cells may be evident if the colony assay is performed with satellite cells isolated from older animals.

Dmd was found to be highly expressed in quiescent satellite cells, whereas its expression decreased dramatically in activated satellite cells. This result confirms the findings reported by Dumont and colleagues (Dumont *et al.,* 2015b), who also reported that dystrophin protein is synthetized in activated satellite cells and participates in the asymmetric division of these cells upon activation. Lack of dystrophin in the *mdx* mouse model of DMD leads to increased numbers of Pax7-positive cells at the beginning of the symptoms, as well as a reduced number of asymmetric divisions. Moreover, these Pax7- positive cells display reduced myogenin rates when myogenic differentiation is induced (Kottlors and Kirschner, 2010). Therefore, although dystrophin expression in satellite cells has only been reported once, such a strict regulation of *Dmd* in satellite cells might hide specific roles of this protein in satellite cells that are unknown to date.

Myh2 is also up-regulated in quiescent satellite cells compared to activated satellite cells, although expression rates are considerably lower. To our knowledge, myosin protein expression in satellite cells has never been reported. Similar to *Dmd* expression, future studies may clarify the significance of these activation-dependent gene expression patterns in satellite cells.

Overall, in an attempt to compare gene expression in TA- and *soleus*-derived satellite cells, only minor differences were found regarding gene expression rates. Importantly, none of the genes studied behaved contrarily in TA- and *soleus*-derived satellite cells upon activation.

Variable gene expression rates in non-injured muscle-derived satellite cells at days 3, 5 and 7 also attracted our attention. Satellite cells derived from these muscles were quiescent and expression of each specific gene was expected to be kept constant at the different experimental timepoints. However, these expression rates sometimes varied more than expected, as it is the case for *Dmd* in TA-derived satellite cells. This could be attributed to systemic factors released by immune cells concentrated at the site of the injury performed in the contralateral leg, which could activate an adaptive response in the quiescent satellite cells found in non-injured muscles, inducing minor modifications

in quiescent satellite cells that pushed them to a pre-activation state (Rodgers *et al.,* 2014).

In summary, we were able to isolate quiescent and *in vivo*-activated satellite cells from TA and *soleus* to perform gene expression studies. The largest satellite cell activation rate was achieved at day 3 post-injury. Myogenic gene expression followed a comparable trend in TA and *soleus*-derived satellite cells in quiescence and following activation, although *Tbp*-relative gene expression rates varied in many of the genes studied. *Capn3* was expressed in satellite cells and satellite cell activation seemed to increase its expression, which was progressively down-regulated as satellite cells returned to quiescence.

Therefore, these experiments require repeating to statistically verify the results obtained in this study. However, gene expression results provide a basis to speculate that calpain 3 may potentially play a role in the regulation of satellite cells. Further gene expression, proteomics and functional studies on satellite cells will provide data to determine this potential role of calpain 3 in muscle regeneration.

FINAL DISCUSSION

Research on satellite cells has significantly increased in recent years as a result of studies that have elucidated their relevance in muscle regeneration. In line with this, satellite cells have been pointed as key players in muscle aging processes, and thus, as targets for therapeutic approaches to confront age-related muscle wasting. Lastly, the role of satellite cells in several muscular dystrophies is currently being evaluated. Satellite cells may potentially be implicated in many pathological conditions in two different ways: directly, due to the fact that the disease-causing gene and protein are expressed in these cells, playing a specific role in their biology, or indirectly, due to the continuous regenerative requirements of the affected muscles that exceed the regenerative potential of these cells, leading to their exhaustion.

Studies of satellite cells in any of the previously mentioned conditions face numerous challenges. On the one hand, the proportion of satellite cells in skeletal muscle tissue is very low. Moreover, isolation protocols are tedious and time-consuming. On the other hand, satellite cells are defined based in their anatomic location; isolation and *in vitro* culture of these cells alters their properties and leads to their differentiation, which makers it unfeasible to expand the cells *in vitro* for future studies.

In our attempt to explore the potential role of calpain 3 in satellite cells to contribute to the understanding of the physiopathology of LGMD2A, we developed two different approaches to address the issue. First, we established patient-specific iPSC-derived cellular models of the disease that allowed the generation of patient-specific muscle progenitor cells, as well as terminally differentiated cultures. Secondly, we studied *Capn3* expression in mouse satellite cells and explored its potential role in the biology of these cells. This way, we hoped to address the hypothesis in two different set ups, minimizing the effect of the differences found among patients and murine mouse models of the disease.

Overall, iPSCs allowed LGMD2A modeling in a dish, since these cultures were able to terminally differentiate, leading to calpain 3 expression. Moreover, these cell lines were also able to reproduce the maturation of *CAPN3* isoforms *in vitro.* However, the generated set of muscle progenitor cells differed considerably from *bona fide* satellite cells, since these cells were constantly cycling in an *in vitro* set up and were expected to express markers of mesenchymal cells, despite satellite cell-specific markers. Moreover, the high variability observed among the different cells lines, which seems to be calpain 3-independent, prevented comparative studies among the different cell lines. This fact leaves room for the generation of improved cellular models.

Recent publications suggest protocols to induce a greater pluripotency degree in reprogrammed cell lines. This could improve the pluripotency of our cell lines, allowing a better myogenic differentiation. An alternative approach to better study the role of calpain 3 in myogenesis would consist on generating isogenic cell lines that only differentiate in their *CAPN3* gene. To do so, we could correct the mutations found in

patient-derived cell lines, as well as generating *CAPN3* knockout cell lines in healthy control-derived cell lines through gene editing technologies such as CRISPR/Cas9. Comparison of isogenic cell lines would probably decipher the role of calpain 3 in myogenesis, as well as offering a platform to screen the effect of a wide range of molecules with therapeutic potential.

After considering the limitations of the iPSC-derived cellular model generated in the first chapter, we decided to address the study of satellite cells in mice, despite the differences observed among the patients and the murine models of LGMD2A. This experimental approach allowed confirmation of the expression of *Capn3* in satellite cells, which showed an activation-dependent gene expression pattern. This suggests that calpain 3 may play a role in satellite cells and muscle regeneration, since as shown in chapter 1, modest *CAPN3* levels were sufficient to synthetize calpain 3 protein.

Due to the anticipated difficulties to directly detect calpain 3 in satellite cells as a result of its high autolytic activity, we aimed at analyzing calpain 3-dependent phenotypes in an *in vitro* set up. Isolation of satellite cells from the TA and *soleus* of WT and C3KO mice did not report any calpain 3-specific differences upon colony assay. The early age of the mice used in these studies might have prevented the detection of calpain 3-specific phenotypes in these cells. Thus, studies performed with older mice will confirm or refute this potential role of calpain 3 in satellite cells.

In parallel, transcriptomic and proteomic analyses of murine quiescent and active satellite cells isolated from predominantly and mildly affected muscles will also provide data to clarify the potential implication of calpain 3 in satellite cells and muscle regeneration, as well as in the development of LGMD2A. This final goal will likely require further experiments in patient and healthy donor-derived cells.

CONCLUSIONS

CHAPTER 1. *In vitro* modeling of LGMD2A through patient-specific iPSC-derived cells.

I. Mutations in *CAPN3* do not alter the reprogramming potential of skin-derived fibroblasts. Therefore, calpain 3 is not required for cell reprogramming.

II. The set of characterization tests performed in this project do not provide enough information to thoroughly study the degree of pluripotency achieved by the reprogrammed cells.

III. Human iPSC-derived myogenic cultures can achieve calpain 3 expression and thus, they can be used to model LGMD2A.

IV. Variable myogenic differentiation potential observed among the established cell lines is calpain 3-independent. Consequently, this fact prevents the comparison of control- and patient-derived cellular phenotypes.

V. Patient-derived muscle progenitor cells and terminally differentiated cultures express lower dystrophin levels compared to healthy control-derived cultures. This might be indicative of the role of calpain 3 in myogenic differentiation and/or maturation, although it could also be an artifact of the variable differentiation potential of the cell lines.

VI. Patient-derived muscle progenitor cells express higher embryonic myosin levels compared to healthy control-derived cultures. This might be indicative of the role of calpain 3 in the maintenance of the population of muscle progenitor cells, although it could also be an artifact of the variability of the established cell lines.

VII. Both control- and patient-specific iPSC-derived muscle progenitor cells possess *in vivo* regenerative potential. Thus, calpain 3 may not be essential in iPSC-derived progenitor-mediated muscle regeneration.

CHAPTER 2. Study of the potential role of calpain 3 in the regulation of muscle satellite cells.

VIII. Intramuscular cartiotoxin administration leads to a robust activation of satellite cells in TA and *soleus*. This activation is highest at three days post-injury (among the studied timepoints) and decreases progressively over time.

IX. Satellite cell activation induces changes in gene expression rates of early, middle and late myogenic markers.

X. *Capn3* is expressed in satellite cells, and it is upregulated upon satellite cell activation, suggesting that calpain 3 may play a role in satellite cells.

However, its expression rate is moderate compared to the expression rates of classical satellite cell markers.

XI. Lack of calpain 3 in young mice-derived satellite cells does not alter their *in vitro* proliferative potential or their differentiation and fusion capacity.

APPENDIX I: Product references chapter 1.

Product	Brand	Reference
Alkaline Phosphatase Blue Membrane Substrate Solution	Sigma-Aldrich	AB0300
Ampicillin (Gobemicin) 250mg	Laboratorios Normon	624619.1
AP-conjugated anti-DIG antibody	Roche	000000011093274910
Ascorbic acid (L)	Sigma-Aldrich	A4544
Beta-mercaptoethanol	Sigma-Aldrich	M3148
BigDye terminator v3.1 cycle sequencing kit	Thermofisher	4337455
Blocking Reagent	Roche Diagnostics	11096176001
Bovine serum albumin	Linus	P6154
B-27 supplement (50x)	Gibco	17504044
Cardiotoxin from *Naja mossambica mossambica*	Sigma	C9759
CDP-Star Chemiluminiscent Substrate	Sigma-Aldrich	C0712
Chick embryo extract	Seralab	CE-650-J
CRL-2429 cell line, feeder cells	ATCC	CRL-2429
DMEM/F-12 medium	Gibco	11330057
DMEM high glucose	Gibco	11965-092
DMEM low glucose	Gibco	21885-025
Donkey-anti-goat-IgG-Cy2	Jackson	705-225-147
Donkey-anti-goat-IgG-Cy3	Jackson	705-165-147
Donkey-anti-mouse-IgG-Cy2	Jackson	715-225-151
Donkey-anti-mouse-IgG-488	Invitrogen	A-21202
Donkey-anti-mouse-IgG-555	Invitrogen	A-31570
Donkey-anti-mouse-IgM-Cy3	Jackson	715-165-140
Donkey-anti-rabbit-IgG-Cy2	Jackson	711-225-152
Donkey-anti-rabbit-IgG-Cy3	Jackson	711-165-152
Donkey-anti-rabbit-IgG-488	Invitrogen	A-21206
Donkey Serum	Jackson-Vitro	JAC-017-000
Doxycycline	Sigma-Aldrich	D9891
DTT	Sigma-Aldrich	000000010197777001
Dulbecco's Phosphate-Buffered Saline (DPBS)	Gibco	14190144
EDTA 0,5M	Ambion	AM9260G
Embryomax 0,1% gelatin solution	Merck-Millipore	ES-006-B
EDTA Titriplex III, powder	Merck-Millipore	108418
E-64	Sigma-Aldrich	E3132
Fetal Bovine Serum	Gibco	10099141/16000044
Fluoro-Gel	EMS	17985-10
Formaldehyde solution about 37%	Merck-Millipore	104002
GlutaMAX™ Supplement	Gibco	35050061
Goat-anti-calpain 3 (IS2)	Cosmobio	COP-080049
Goat-anti-hHNF-3β/FoxA2	R&D Systems	AF2400
Goat-anti-mouse-HRP	Dako	P0447
Goat-anti-mouse-IgG-Cy2	Jackson	115-225-071
Goat-anti-mouse-IgG-Cy3	Jackson	115-165-071
Goat-anti-mouse-IgM-Cy5	Jackson	115-175-075
Goat-anti-Nanog	R&D	AF1997
Goat-anti-rabbit-HRP	Dako	P0448
Goat-anti-rat-IgM-Cy3	Jackson	112-165-020
GSK3-inhibitor CHIR99021	StemCell Technologies	72052
HEPES Buffer Solution, 1M	Gibco	15630-106
HGF, human recombinant	Merck-Millipore	GF116
High Capacity cDNA Reverse Transcription Kit	Applied Biosystems	4368814

HindIII restriction enzyme	NEB	R0104S
Hoeschst (bisBenzimide H 33258)	Sigma	B2883
Horse serum, heat inactivated	Gibco	26050-088
Hybond nylon membrane 0,45 µm	Amersham	10600002
Hydrochloric acid, fuming, 37%	EMD Millipore	100317
IGF1, human	Sigma-Aldrich	I3769
IMDM medium	Gibco	12440053
Isopentane, 2-methylbutane	Millipore	106065
Isopropyl β-D-1-thiogalactopyranoside (IPTG)	Sigma-Aldrich	I6758
KaryoMAX® Colcemid™ solution in PBS	Gibco	15212012
KaryoMAX® Potassium Chloride Solution	Gibco	10575090
KnockOut™ DMEM	Gibco	10829018
KnockOut™ Serum Replacement	Gibco	10828028
LB broth	Lennox – Sigma	L3022
LB-Agar	Lennox	A41083
L-glutamine 200mM	Gibco	25030081
Lipofectamine LTX with plus reagent	Invitrogen	15338100
Matrigel Basement Membrane Matrix	BD-Corning	354234
MEM medium	Gibco	11090-081
Methylamp DNA modification kit	Epigentek	P-1001
Monothioglycerol	Sigma-Aldrich	M6145
Mouse-anti-calpain 3	Novocastra	NCL-CALP-12A2
Mouse-anti-humanDystrophin	Leica	NCL-DYS3
Mouse-anti-Myogenin	DSHB	F5D
Mouse-anti-Oct4	Santa Cruz	Sc-5279
Mouse-anti-Pax7	DSHB	Pax7, concentrated
Mouse-anti-sarcomeric myosin	DSHB	MF20
Mouse-anti-Serca2	Santa Cruz Biotech	Sc-376235
Mouse-anti-SSEA4	Hybridoma Bank	MC-813-70
Mouse-anti-Tra-1-60	Chemicon	MAB4360
Mouse-anti-Tra-1-81	Chemicon	MAB4381
Mouse-anti-α-smooth muscle actin	Sigma-Aldrich	A5228
Mouse-anti-β-III-Tubulin Tuj1	Covance	MMS-435P
mTeSR™1	StemCell Technologies	85850
Neurobasal medium	Gibco	21103049
Newborn calf serum	Gibco	16010159
Non Essential Amino acids Solution (100X)	Gibco	11140050
N-2 supplement (100x)	Gibco	17502001
O.C.T. compound	Tissue-Tek, Sakura	4583
One shot TOP10 Chemically competent *E. coli*	Invitrogen	C404010
Optimem	Gibco	31985-047
Paraformaldehyde 4%	Electron Micro. Sci.	175-4-100
PCR DIG Probe Synthesis Kit	Roche Diagnostics	11636090910
pCRII-TOPO vector	Addgene	pCRII-TOPO
Penicillin/Streptomycin	Gibco	15140-122
Phoenix Amphotropic cells	ATCC	SD 3443
Phosphate-buffered saline PBS	Biosystems	44592
pMSCV-Flag-hOct4	Addgene	20072
pMSCV-Flag-hSox2	Addgene	20073
pMSCV-Flag-hKlf4	Addgene	20074
pMSCV-Flag-cMyc T58A	Addgene	20075
PMSF	Sigma-Aldrich	78830
Polybrene 10 mg ml^{-1}	Merck-Millipore	TR-1003-G

Polyvinyl alcohol mounting medium with DABCO®	Sigma-Aldrich	10981
Ponceau S solution	Sigma-Aldrich	P7170
Precision Plus Kaleidoscope Prestained Protein Standards	Biorad	1610375
PstI restriction enzyme	NEB	R0140S
Rabbit-anti-α -1-fetoprotein	Dako	A0008
Rabbit-anti-GATA4	Santa Cruz	sc-9053
Rabbit-anti-GFAP	Dako	Z0334
Rabbit-anti-goat-HRP	Dako	P0449
Rabbit-anti-humanLaminA/C	Abcam	ab108595
Rabbit anti-Pax7	Novusbio	NBP1-69130
Rabbit-anti-Sox2	Thermofisher	AI-16968
Rat-anti-SSEA3	Hybridoma Bank	MC-631
Recombinant Human Basic Fibroblast Growth Factor	Peprotech	100-18B
ReLeSR™	StemCell Technologies	05872
RNeasy mini kit	Qiagen	74104
ROCK inhibitor	StemCell Technologies	Y-27632
RPMI 1640 medium	Gibco	31870-082
Skimmed milk powder	Sigma-Aldrich	70166
Sodium chloride for analysis	Panreac Applichem	131659
Soybean trypsin inhibitor	Sigma-Aldrich	T6522
StemPro Accutase Cell Dissociation Reagent	Gibco	A1110501
Stripper micropipetter	Origio	MXL3-STR
Stripper tips 100 µm	Origio	MXL3-100
SuperScript® III First-Strand Synthesis SuperMix for qRT-PCR	Invitrogen	11752050
SuperSignal™ West Dura Extended Duration Substrate	ThermoFisher scientific	34075
SYBR green Real-Time Master Mix	AB - Thermofisher	4309155
Taqman gene expression master mix	Applied biosystems	4369016
Taqman probe for *CAPN3* exon 1-2	Applied biosystems	Hs00181057_m1
Taqman probe for *CAPN3* exon 5-6	Applied biosystems	Hs01115988_m1
Taqman probe for *CAPN3* delta6	Applied biosystems	*Custom*
Taqman probe for *COL1A1*	Applied biosystems	Hs00164004
Taqman probe for *DES*	Applied biosystems	Hs00157258_m1
Taqman probe for *DMD*	Applied biosystems	Hs00758098_m1
Taqman probe for *FN1*	Applied biosystems	Hs00365052_m1
Taqman probe for *GAPDH*	Applied biosystems	Hs99999905_m1
Taqman probe for *MYH2*	Applied biosystems	Hs00430042_m1
Taqman probe for *MYH3*	Applied biosystems	Hs01074230_m1
Taqman probe for *MYOD1*	Applied biosystems	Hs00159528_m1
Taqman probe for *MYOG*	Applied biosystems	Hs01072232_m1
Taqman probe for *PAX7*	Applied biosystems	Hs00242962_m1
Taqman probe for *TBP*	Applied biosystems	Hs00427620_m1
Tris pure, pharma grade	Panreac Applichem	141940
Triton X-100	Sigma-Aldrich	T8787
TRIzol Reagent	Invitrogen	15596026
Trypsin-EDTA 0,05%, phenol red	Gibco	25300054
Trypsin-EDTA 0,25%, phenol red	Gibco	25200056
QIAamp DNA mini kit	Qiagen	51304
QIAprep Spin Miniprep Kit	Qiagen	27104
QIAquick Gel Extraction Kit	Qiagen	28704
QIAzol Lysis Regent	Qiagen	79306
X-tremeGene9 DNA Transfection reagent	Roche	XTG9-RO
0,45 µm pore filter, PVDF, low protein binding, Durapore	Merck-Millipore	SLHV033RS
2-mercaptoethanol	Gibco	31350010

4',6-diamidino-2-phenylindole (DAPI)	Sigma-aldrich	D9542

APPENDIX II: Product references chapter 2.

Product	Manufacturer	Reference
Anti-CD106/VCAM-Biotin Clone 429	eBioscience	13-1061-85
Anti-CD31-PE-Cy7 Clone 390	eBioscience	25-0311-82
Anti-CD45-PE-Cy7 Clone 30-F11	eBioscience	25-0451-82
Anti-integrin-α7-647 Clone R2F2	Ablab	67-0010-05
Anti-sarcomeric-myosin	DSHB	MF20
Bovine serum albumin	Linus	P6154
Cardiotoxin from *Naja mossambica mossambica*	Sigma	C9759
Cell strainers 40 µm	BD	352340
Chick embryo extract	Seralab	CE-650-J
Collagenase II	Gibco	17101-015
CS&T quality control beads	BD	656504
Dispase	Gibco	17105-041
DMEM/F12 medium	Gibco	31331-028
DMEM/High Glucose Media	Hyclone	SH30243.01
DNAse II from bovine	Sigma	D8764-30KU
Dulbecco's Phosphate-Buffered Saline (DPBS)	Gibco	14190144
Fetal Bovine Serum (FBS)	Gibco	10270-106
Forane (Isoflurane)	Abbott	SPPL030
Goat-anti-mouse alexa fluor 555	Invitrogen	A28180
Ham's/F-10 media	Hyclone	SH30025.01
HEPES Buffer Solution, 1M	Gibco	15630-106
High Capacity cDNA Reverse Transcription Kit	Applied Biosystems	4368814
Horse serum	Gibco	26050-088
Human basic fibroblast growth factor	Peprotech	100-18B
NucleoSpin® RNA XS extraction kit	Macherey-Nagel	740902
Paraformaldehyde 4%	Electron Micros. Sci.	175-4-100
Penicillin/Streptomycin	Gibco	15140-122
RNAprotect Cell Reagent	Qiagen	76526
Streptavidin-PE	eBioscience	12-4317-87
SYTOX Green Nucleic Acid Stain	Molecular Probes	S7020
Taqman gene expression master mix	Applied Biosystems	4369016
TaqMan PreAmp Master Mix	Applied Biosystems	4391128
Taqman probe for Capn3	Applied Biosystems	Mm00482985_m1
Taqman probe for Dmd	Applied Biosystems	Mm01216951_m1
Taqman probe for Gapdh	Applied Biosystems	Mm99999915_g1
Taqman probe for a Myh2	Applied Biosystems	Mm01332564_m1
Taqman probe for Myh3	Applied Biosystems	Mm01332463_m1
Taqman probe for Myod1	Applied Biosystems	Mm00440387_m1
Taqman probe for Myog	Applied Biosystems	Mm00446194_m1
Taqman probe for Pax7	Applied Biosystems	Mm01354484_m1
Taqman probe for Ryr1	Applied Biosystems	Mm01175211_m1
Taqman probe for Tbp	Applied Biosystems	Mm00446973_m1
Triton X-100	Sigma-aldrich	T8787
4',6-diamidino-2-phenylindole (DAPI)	Sigma-aldrich	D9542

APPENDIX III: Publications.

Mateos-Aierdi AJ, Aiastui A, Goicoechea M, López de Munain A. "Advances in gene therapies for limb-girdle muscular dystrophies" *Advances in Regenerative Biology* Vol1 (1) 2014.

Mateos-Aierdi AJ, Goicoechea M, Aiastui A, Fernández-Torrón R,García-Puga M, Matheu A, López de Munain A. "Muscle wasting in myotonic dystrophies: a model of premature aging". Front Aging Neurosci. Vol 7(125) 2015.

BIBLIOGRAPHY

Aasen, T., A. Raya, MJ. Barrero, E. Garreta, A. Consiglio, F. Gonzalez, R. Vassena, et al. 2008. "Efficient and Rapid Generation of Induced Pluripotent Stem Cells from Human Keratinocytes." *Nature Biotechnology* 26 (11): 1276–84. doi:10.1038/nbt.1503.

Abujarour, R., M. Bennett, B. Valamehr, TT. Lee, M. Robinson, D. Robbins, T. Le, K. Lai, and P. Flynn. 2014. "Myogenic Differentiation of Muscular Dystrophy- Specific Induced Pluripotent Stem Cells for Use in Drug Discovery" 1: 149–60.

Allamand, V., O. Broux, N. Bourg, I. Richard, JA. Tischfield, ME. Hodes, PM. Conneally, M. Fardeau, CE. Jackson, and JS. Beckmann. 1995. "Genetic Heterogeneity of Autosomal Recessive Limbgirdle Muscular Dystrophy in a Genetic Isolate (Amish) and Evidence for a New Locus." *Human Molecular Genetics* 4 (3): 459–63. doi:10.1093/hmg/4.3.459.

Amato, AA. 2008. "Adults with Eosinophilic Myositis and Calpain-3 Mutations." *Neurology*, 730–32.

Amici, DR., I. Pinal-Fernandez, DG. Mázala, TE. Lloyd, AM. Corse, L. Christopher-Stine, AL. Mammen, and ER. Chin. 2017. "Calcium Dysregulation, Functional Calpainopathy, and Endoplasmic Reticulum Stress in Sporadic Inclusion Body Myositis." *Acta Neuropathologica Communications* 5 (1). Acta Neuropathologica Communications: 24. doi:10.1186/s40478-017-0427-7.

Anderson, LV., K. Davison, JA. Moss, I. Richard, M. Fardeau, FM. Tomé, C. Hübner, A. Lasa, J. Colomer, and JS. Beckmann. 1998. "Characterization of Monoclonal Antibodies to Calpain 3 and Protein Expression in Muscle from Patients with Limb-Girdle Muscular Dystrophy Type 2A." *The American Journal of Pathology* 153 (4): 1169–79. doi:10.1016/S0002-9440(10)65661-1.

Anderson, LVB., RM. Harrison, R. Pogue, E. Vafiadaki, C. Pollitt, K. Davison, JA. Moss, et al. 2000. "Secondary Reduction in Calpain 3 Expression in Patients with Limb Girdle Muscular Dystrophy Type 2B and Miyoshi Myopathy (Primary Dysferlinopathies)." *Neuromuscular Disorders* 10 (8): 553–59. doi:10.1016/S0960-8966(00)00143-7.

Angelini, C., E. Tasca, AC. Nascimbeni, and M. Fanin. 2014. "Muscle Fatigue, nNOS and Muscle Fiber Atrophy in Limb Girdle Muscular Dystrophy." *Acta Myologica : Myopathies and Cardiomyopathies : Official Journal of the Mediterranean Society of Myology / Edited by the Gaetano Conte Academy for the Study of Striated Muscle Diseases* 33 (3): 119–26.

Araúzo-Bravo, MJ. 2016. "Computational Biology Methods for Characterization of Pluripotent Cells." *Methods in Molecular Biology*, no. 1357: 195–220. doi:10.1007/7651.

Awaya, T., T. Kato, Y. Mizuno, H. Chang, A. Niwa, K. Umeda, T. Nakahata, and T. Heike. 2012. "Selective Development of Myogenic Mesenchymal Cells from Human Embryonic and Induced Pluripotent Stem Cells." *PLoS ONE* 7 (12): 1–9. doi:10.1371/journal.pone.0051638.

Azuma, M., C. Fukiage, M. Higashine, T. Nakajima, H. Ma, and TR. Shearer. 2000. "Identification and Characterization of a Retina-Specific Calpain (Rt88) from Rat." *Current Eye Reserch* 21 (3): 710–20.

Baghdiguian, S., M. Martin, I. Richard, F. Pons, C. Astier, N. Bourg, RT. Hay, et al. 1999. "Calpain 3 Deficiency Is Associated with Myonuclear Apoptosis and Profound Perturbation of the IkappaB alpha/NF-kappaB Pathway in Limb-Girdle Muscular Dystrophy Type 2A." *Nature Medicine* 5 (5): 503–11. doi:10.1038/8385.

Baghdiguian, S., I. Richard, M. Martin, P. Coopman, JS. Beckmann, P. Mangeat, and G. Lefranc.

2001. “Pathophysiology of Limb Girdle Muscular Dystrophy Type 2A: Hypothesis and New Insights into the I??B??/NF-??B Survival Pathway in Skeletal Muscle.” *Journal of Molecular Medicine* 79 (5–6): 254–61. doi:10.1007/s001090100225.

Bakre, MM., A. Hoi, J. Chen, Y. Mong, YY. Koh, KY. Wong, and LW. Stanton. 2007. “Generation of Multipotential Mesendodermal Progenitors from Mouse Embryonic Stem Cells via Sustained Wnt Pathway Activation * □” 282 (43): 31703–12. doi:10.1074/jbc.M704287200.

Baldwin, AS. 1996. “The NF-Kappa B and I Kappa B Proteins: New Discoveries and Insights.” *Annual Review of Immunology* 14: 649–83. doi:10.1146/annurev.immunol.14.1.649.

Bar-Nur, O., HA. Russ, S. Efrat, and N. Benvenisty. 2011. “Epigenetic Memory and Preferential Lineage-Specific Differentiation in Induced Pluripotent Stem Cells Derived from Human Pancreatic Islet Beta Cells.” *Cell Stem Cell* 9 (1). Elsevier Inc.: 17–23. doi:10.1016/j.stem.2011.06.007.

Barberi, T., M. Bradbury, Z. Dincer, G. Panagiotakos, ND. Socci, and L. Studer. 2007. “Derivation of Engraftable Skeletal Myoblasts from Human Embryonic Stem Cells.” *Nature Medicine* 13 (5): 642–48. doi:10.1038/nm1533.

Bartoli, M., J. Poupiot, A. Vulin, F. Fougerousse, L. Arandel, N. Daniele, C. Roudaut, et al. 2007. “AAV-Mediated Delivery of a Mutated Myostatin Propeptide Ameliorates Calpain 3 but Not Alpha-Sarcoglycan Deficiency.” *Gene Therapy* 14 (9): 733–40. doi:10.1038/sj.gt.3302928.

Bartoli, M., C. Roudaut, S. Martin, F. Fougerousse, L. Suel, J. Poupiot, E. Gicquel, F. Noulet, O. Danos, and I. Richard. 2006. “Safety and Efficacy of AAV-Mediated Calpain 3 Gene Transfer in a Mouse Model of Limb-Girdle Muscular Dystrophy Type 2A.” *Molecular Therapy : The Journal of the American Society of Gene Therapy* 13 (2): 250–59. doi:10.1016/j.ymthe.2005.09.017.

Bartus, RT., NJ. Hayward, PJ. Elliott, SD. Sawyer, KL. Baker, RL. Dean, A. Akiyama, et al. 1994. “Calpain Inhibitor AK295 Protects Neurons from Focal Brain Ischemia: Effects of Postocdusion Intra-Arterial Administration.” *Stroke* 25 (11): 2265–70. doi:10.1161/01.STR.25.11.2265.

Beedle, AM. 2016. “Distribution of Myosin Heavy Chain Isoforms in Muscular Dystrophy: Insights into Disease Pathology.” *Musculoskeletal Regeneration* 2. http://www.ncbi.nlm.nih.gov/pubmed/27430020%5Cnhttp://www.pubmedcentral.nih.gov/articlerender.fcgi?artid=PMC4943764.

Benayoun, B., S. Baghdiguian, A. Lajmanovich, M. Bartoli, N. Daniele, E. Gicquel, N. Bourg, et al. 2008. “NF-kappaB-Dependent Expression of the Antiapoptotic Factor c-FLIP Is Regulated by Calpain 3, the Protein Involved in Limb-Girdle Muscular Dystrophy Type 2A.” *The FASEB Journal : Official Publication of the Federation of American Societies for Experimental Biology* 22 (5): 1521–29. doi:10.1096/fj.07-8701com.

Benchaouir, R., M. Meregalli, A. Farini, G. D’Antona, M. Belicchi, A. Goyenvalle, M. Battistelli, et al. 2007. “Restoration of Human Dystrophin Following Transplantation of Exon-Skipping-Engineered DMD Patient Stem Cells into Dystrophic Mice.” *Cell Stem Cell* 1 (6): 646–57. doi:10.1016/j.stem.2007.09.016.

Bernet, JD., JD. Doles, JK. Hall, K. Kelly Tanaka, TA. Carter, and BB. Olwin. 2014. “p38 MAPK Signaling Underlies a Cell-Autonomous Loss of Stem Cell Self-Renewal in Skeletal Muscle of Aged Mice.” *Nature Medicine* 20 (3). Nature Publishing Group: 265–71. doi:10.1038/nm.3465.

Biancheri, R., A. Falace, A. Tessa, M. Pedemonte, S. Scapolan, D. Cassandrini, C. Aiello, et al. 2007. "POMT2 Gene Mutation in Limb-Girdle Muscular Dystrophy with Inflammatory Changes." *Biochemical and Biophysical Research Communications* 363 (4): 1033–37. doi:10.1016/j.bbrc.2007.09.066.

Bione, S., E. Maestrini, S. Rivella, M. Mancini, S. Regis, G. Romeo, and D. Toniolo. 1994. "Identification of a Novel X-Linked Gene Responsible for Emery-Dreifuss Muscular Dystrophy." *Nature Genetics* 8 (4): 323–27. doi:10.1038/ng1294-323.

Biressi, S., M. Molinaro, and G. Cossu. 2007. "Cellular Heterogeneity during Vertebrate Skeletal Muscle Development." *Developmental Biology* 308 (2): 281–93. doi:10.1016/j.ydbio.2007.06.006.

Biswas, S., F. Harris, S. Dennison, J. Singh, and DA. Phoenix. 2004. "Calpains: Targets of Cataract Prevention?" *Trends in Molecular Medicine* 10 (2): 78–84. doi:10.1016/j.molmed.2003.12.007.

Bjornson, CRR., TH. Cheung, L. Liu, PV. Tripathi, KM. Steeper, and TA. Rando. 2012. "Notch Signaling Is Necessary to Maintain Quiescence in Adult Muscle Stem Cells." *Stem Cells* 30 (2): 232–42. doi:10.1002/stem.773.

Blázquez, L., A. Aiastui, M. Goicoechea, M. Martins de Araujo, A. Avril, C. Beley, L. García, J. Valcárcel, P. Fortes, and A. López de Munain. 2013. "In Vitro Correction of a Pseudoexon-Generating Deep Intronic Mutation in LGMD2A by Antisense Oligonucleotides and Modified Small Nuclear RNAs." *Human Mutation* 34 (10): 1387–95. doi:10.1002/humu.22379.

Blázquez, L., M. Azpitarte, A. Sáenz, M. Goicoechea, D. Otaegui, X. Ferrer, I. Illa, E. Gutierrez-Rivas, J. J. Vilchez, and A. López De Munain. 2008. "Characterization of Novel CAPN3 Isoforms in White Blood Cells: An Alternative Approach for Limb-Girdle Muscular Dystrophy 2A Diagnosis." *Neurogenetics* 9 (3): 173–82. doi:10.1007/s10048-008-0129-1.

Bock, C., E. Kiskinis, G. Verstappen, H. Gu, G. Boulting, ZD. Smith, M. Ziller, et al. 2011. "Reference Maps of Human Es and Ips Cell Variation Enable High-Throughput Characterization of Pluripotent Cell Lines." *Cell* 144 (3). Elsevier Inc.: 439–52. doi:10.1016/j.cell.2010.12.032.

Bonne, G., MR. Di Barletta, S. Varnous, HM. Bécane, EH. Hammouda, L. Merlini, F. Muntoni, et al. 1999. "Mutations in the Gene Encoding Lamin A/C Cause Autosomal Dominant Emery-Dreifuss Muscular Dystrophy." *Nature Genetics* 21 (march): 285–88. doi:10.1038/6799.

Borchin, B., J. Chen, and T. Barberi. 2013. "Derivation and FACS-Mediated Purification of PAX3+/PAX7+ Skeletal Muscle Precursors from Human Pluripotent Stem Cells." *Stem Cell Reports* 1 (6). The Authors: 620–31. doi:10.1016/j.stemcr.2013.10.007.

Bou Saada, Y., C. Dib, P. Dmitriev, A. Hamade, G. Carnac, D. Laoudj-Chenivesse, M. Lipinski, and YS. Vassetzky. 2016. "Facioscapulohumeral Dystrophy Myoblasts Efficiently Repair Moderate Levels of Oxidative DNA Damage." *Histochemistry and Cell Biology* 145 (4). Springer Berlin Heidelberg: 475–83. doi:10.1007/s00418-016-1410-2.

Brack, AS., IM. Conboy, MJ. Conboy, J. Shen, and TA. Rando. 2008. "A Temporal Switch from Notch to Wnt Signaling in Muscle Stem Cells Is Necessary for Normal Adult Myogenesis." *Cell Stem Cell* 2 (1): 50–59. doi:10.1016/j.stem.2007.10.006.

Brack, AS., MJ. Conboy, S. Roy, M. Lee, CJ. Kuo, C. Keller, and TA. Rando. 2007. "Increased Wnt Signaling during Aging Alters Muscle Stem Cell Fate and Increases Fibrosis." *Science (New York, N.Y.)* 317 (5839): 807–10. doi:10.1126/science.1144090.

Brais, B., JP. Bouchard, YG. Xie, DL. Rochefort, N. Chrétien, FM. Tomé, RG. Lafrenière, et al. 1998. "Short GCG Expansions in the PABP2 Gene Cause Oculopharyngeal Muscular Dystrophy." *Nature Genetics* 18 (2): 164–67. doi:10.1038/ng0298-164.

Brambrink, T., R. Foreman, GG. Welstead, CJ. Lengner, M. Wernig, H. Suh, and R. Jaenisch. 2008. "Sequential Expression of Pluripotency Markers during Direct Reprogramming of Mouse Somatic Cells." *Cell Stem Cell* 2 (2): 151–59. doi:10.1016/j.stem.2008.01.004.

Brand-Saberi, B., TS. Müller, J. Wilting, B. Christ, and C. Birchmeier. 1996. "Scatter Factor/hepatocyte Growth Factor (SF/HGF) Induces Emigration of Myogenic Cells at Interlimb Level in Vivo." *Developmental Biology* 179 (1): 303–8. doi:10.1006/dbio.1996.0260.

Brooks, NE., MD. Schuenke, and RS. Hikida. 2009. "No Change in Skeletal Muscle Satellite Cells in Young and Aging Rat Soleus Muscle." *The Journal of Physiological Sciences: JPS* 59 (6): 465–71. doi:10.1007/s12576-009-0058-2.

Buckingham, M., and PWJ. Rigby. 2014. "Gene Regulatory Networks and Transcriptional Mechanisms That Control Myogenesis." *Developmental Cell* 28 (3). Elsevier Inc.: 225–38. doi:10.1016/j.devcel.2013.12.020.

Cai, D., JD. Frantz, NE. Tawa, PA. Melendez, BC. Oh, HGW. Lidov, PO. Hasselgren, et al. 2004. "IKKb/NF-kB Activation Causes Severe Muscle Wasting in Mice." *Cell* 119 (2): 285–98. doi:10.1016/j.cell.2004.09.027.

Campbell, KA., A. Terzic, and TJ. Nelson. 2015. "Induced Pluripotent Stem Cells for Cardiovascular Disease: From Product-Focused Disease Modeling to Process-Focused Disease Discovery." *Regenerative Medicine* 10 (6): 773–83. doi:10.2217/rme.15.41.

Campbell, RL., and PL. Davies. 2012. "Structure–function Relationships in Calpains 1." *Biochem. J* 447: 335–51. doi:10.1042/BJ20120921.

Carlson, ME., M. Hsu, and IM. Conboy. 2008. "Imbalance between pSmad3 and Notch Induces CDK Inhibitors in Old Muscle Stem Cells." *Nature* 454 (7203): 528–32. doi:10.1038/nature07034.

Carter, Gregory T., Nanette C. Joyce, Allison L. Abresch, Amanda E. Smith, and Gregg K. VandeKeift. 2012. "Using Palliative Care in Progressive Neuromuscular Disease to Maximize Quality of Life." *Physical Medicine and Rehabilitation Clinics of North America* 23 (4). Elsevier Inc: 903–9. doi:10.1016/j.pmr.2012.08.002.

Chae, J., N. Minami, Y. Jin, M. Nakagawa, K. Murayama, F. Igarashi, and I. Nonaka. 2001. "Calpain 3 Gene Mutations: Genetic and Clinico-Pathologic Findings in Limb-Girdle Muscular Dystrophy." *Neuromuscular Disorders* 11 (6–7): 547–55. doi:10.1016/S0960-8966(01)00197-3.

Chakkalakal, JV., KM. Jones, MA. Basson, and AS. Brack. 2012. "The Aged Niche Disrupts Muscle Stem Cell Quiescence." *Nature* 490 (7420). Nature Publishing Group: 355–60. doi:10.1038/nature11438.

Chal, J., M. Oginuma, ZA. Tanoury, B. Gobert, O. Sumara, A. Hick, F. Bousson, et al. 2015. "Differentiation of Pluripotent Stem Cells to Muscle Fiber to Model Duchenne Muscular Dystrophy." *Nature Biotechnology* 33 (August): 962–69. doi:10.1038/nbt.3297.

Chal, J., ZA. Tanoury, M. Hestin, B. Gobert, S. Aivio, A. Hick, T. Cherrier, AP. Nesmith, KK. Parker, and O. Pourquié. 2016. "Generation of Human Muscle Fibers and Satellite-like Cells from Human Pluripotent Stem Cells in Vitro." *Nature Protocols* 11 (10). doi:10.1038/nprot.2016-

110.

Chan, EM., S. Ratanasirintrawoot, IH. Park, PD. Manos, YH. Loh, H. Huo, JD. Miller, et al. 2009. "Live Cell Imaging Distinguishes Bona Fide Human iPS Cells from Partially Reprogrammed Cells." *Nature Biotechnology* 27 (11): 1033–37. doi:10.1038/nbt.1580.

Choi, J., ML. Costa, CS. Mermelstein, C. Chagas, S. Holtzer, and H. Holtzer. 1990. "MyoD Converts Primary Dermal Fibroblasts, Chondroblasts, Smooth Muscle, and Retinal Pigmented Epithelial Cells into Striated Mononucleated Myoblasts and Multinucleated Myotubes." *Proceedings of the National Academy of Sciences of the United States of America* 87 (20): 7988–92. doi:10.1073/pnas.87.20.7988.

Chrobáková, T., M. Hermanová, I. Kroupová, P. Vondráček, T. Maříková, R. Mazanec, J. Zámečník, J. Staněk, M. Havlová, and L. Fajkusová. 2004. "Mutations in Czech LGMD2A Patients Revealed by Analysis of calpain3 mRNA and Their Phenotypic Outcome." *Neuromuscular Disorders* 14 (10): 659–65. doi:10.1016/j.nmd.2004.05.005.

Comai, G., and S. Tajbakhsh. 2014. *Molecular and Cellular Regulation of Skeletal Myogenesis*. *Current Topics in Developmental Biology*. 1sted. Vol. 110. Elsevier Inc. doi:10.1016/B978-0-12-405943-6.00001-4.

Conboy, IM., MJ. Conboy, AJ. Wagers, ER. Girma, IL. Weissman, and TA. Rando. 2005. "Rejuvenation of Aged Progenitor Cells by Exposure to a Young Systemic Environment." *Nature* 433 (7027): 760–64. doi:10.1038/nature03260.

Cooper, ST., E. Kizana, JD. Yates, HP. Lo, N. Yang, ZH. Wu, IE. Alexander, and KN. North. 2007. "Dystrophinopathy Carrier Determination and Detection of Protein Deficiencies in Muscular Dystrophy Using Lentiviral MyoD-Forced Myogenesis." *Neuromuscular Disorders* 17 (4): 276–84. doi:10.1016/j.nmd.2006.12.010.

Cosgrove, BD., PM. Gilbert, E. Porpiglia, F. Mourkioti, SP. Lee, SY. Corbel, ME. Llewellyn, SL. Delp, and HM. Blau. 2014. "Rejuvenation of the Muscle Stem Cell Population Restores Strength to Injured Aged Muscles." *Nature Medicine* 20 (3). Nature Publishing Group: 255–64. doi:10.1038/nm.3464.

D'Amico, A., A. Tessa, C. Bruno, S. Petrini, R. Biancheri, M. Pane, M. Pedemonte, et al. 2006. "Expanding the Clinical Spectrum of POMT1 Phenotype." *Neurology* 66 (10): 1564–67. doi:10.1212/01.wnl.0000216145.66476.36.

D'Antonio, M., G. Woodruff, JL. Nathanson, A. D'Antonio-Chronowska, A. Arias, H. Matsui, R. Williams, et al. 2017. "High-Throughput and Cost-Effective Characterization of Induced Pluripotent Stem Cells." *Stem Cell Reports* 8 (4). ElsevierCompany.: 1101–11. doi:10.1016/j.stemcr.2017.03.011.

Darabi, R., RW. Arpke, S. Irion, JT. Dimos, M. Grskovic, M. Kyba, and RC. Perlingeiro. 2012. "Human ES- and iPS-Derived Myogenic Progenitors Restore DYSTROPHIN and Improve Contractility upon Transplantation in Dystrophic Mice." *Cell Stem Cell* 10 (5). Elsevier Inc.: 610–19. doi:10.1016/j.stem.2012.02.015.

Darabi, R, and RC. Perlingeiro. 2014. "Derivation of Skeletal Myogenic Precursors from Human Pluripotent Stem Cells Using Conditional Expression of PAX7." *Methods in Molecular Biology* 1357 (1341): 423–39. doi:10.1007/7651_2014_134.

Dayanithi, G., I. Richard, C. Viero, E. Mazuc, S. Mallie, J. Valmier, N. Bourg, et al. 2009. "Alteration of Sarcoplasmic Reticulum ca Release in Skeletal Muscle from Calpain 3-Deficient Mice." *International Journal of Cell Biology* 2009: 340346. doi:10.1155/2009/340346.

Delaporte, C., B. Dautreaux, A. Rouche, and M. Fardeau. 1990. “Changes in Surface Morphology and Basal Lamina of Cultured Muscle Cells from Duchenne Muscular Dystrophy Patients.” *J.Neurol.Sci.* 95 (1): 77–88. doi:10.1016/0022-510X(90)90118-7.

Dellavalle, A., M. Sampaolesi, R. Tonlorenzi, E. Tagliafico, B. Sacchetti, L. Perani, A. Innocenzi, et al. 2007. “Pericytes of Human Skeletal Muscle Are Myogenic Precursors Distinct from Satellite Cells.” *Nature Cell Biology* 9 (3): 255–67. doi:10.1038/ncb1542.

Dezawa, M., H. Ishikawa, Y. Itokazu, T. Yoshihara, M. Hoshino, S. Takeda, C. Ide, and Y. Nabeshima. 2005. “Bone Marrow Stromal Cells Generate Muscle Cells and Repair Muscle Degeneration.” *Science* 309 (5732): 314–17. doi:10.1126/science.1110364.

Difranco, M., I. Kramerova, JL. Vergara, and MJ. Spencer. 2016. “Attenuated Ca 2 + Release in a Mouse Model of Limb Girdle Muscular Dystrophy 2A.” *Skeletal Muscle* 6 (11). Skeletal Muscle: 1–15. doi:10.1186/s13395-016-0081-y.

Dinçer, P., F. Leturcq, I. Richard, F. Piccolo, D. Yalnizoglu, C. De Toma, Z. Akçoren, et al. 1997. “A Biochemical, Genetic, and Clinical Survey of Autosomal Recessive Limb Girdle Muscular Dystrophies in Turkey.” *Annals of Neurology* 42 (2): 222–29. doi:10.1002/ana.410420214.

Dubowitz, V., and CA. Sewry. 2007. *Muscle Biopsy, a Practical Approach*. Edited by Saunders Elsevier. 3rd ed.

Dumont, NA., CF. Bentzinger, MC. Sincennes, and MA. Rudnicki. 2015a. “Satellite Cells and Skeletal Muscle Regeneration.” *Compr Physiol* 5 (3): 1027–59. doi:10.1002/cphy.c140068.

Dumont, NA., YX. Wang, J. von Maltzahn, A. Pasut, CF. Bentzinger, CE. Brun, and MA. Rudnicki. 2015b. “Dystrophin Expression in Muscle Stem Cells Regulates Their Polarity and Asymmetric Division.” *Nature Medicine* 21 (12). Nature Publishing Group: 1455–63. doi:10.1038/nm.3990.

Emery, AE. 2002. “The Muscular Dystrophies.” *The Lancet* 359 (9307): 687–95. doi:10.1016/S0140-6736(02)07815-7.

Engert, JC., EB. Berglund, and N. Rosenthal. 1996. “Proliferation Precedes Differentiation in IGF-I Stimulated Myogenesis.” *The Journal of Cell Biology* 135 (2): 431–40. doi:10.1083/jcb.135.2.431.

Ermolova, N., E. Kudryashova, M. Difranco, J. Vergara, I. Kramerova, and MJ. Spencer. 2011. “Pathogenity of Some Limb Girdle Muscular Dystrophy Mutations Can Result from Reduced Anchorage to Myofibrils and Altered Stability of Calpain 3.” *Human Molecular Genetics* 20 (17): 3331–45. doi:10.1093/hmg/ddr239.

Fanin, M., and C. Angelini. 2015. “Protein and Genetic Diagnosis of Limb Girdle Muscular Dystrophy Type 2A: The Yield and the Pitfalls.” *Muscle and Nerve* 52 (2): 163–73. doi:10.1002/mus.24682.

Fanin, M., L. Nardetto, AC. Nascimbeni, E. Tasca, M. Spinazzi, R. Padoan, and C. Angelini. 2007a. “Correlations between Clinical Severity, Genotype and Muscle Pathology in Limb Girdle Muscular Dystrophy Type 2A.” *Journal of Medical Genetics* 44 (10): 609–14. doi:10.1136/jmg.2007.050328.

Fanin, M., AC. Nascimbeni, and C. Angelini. 2007b. “Screening of Calpain-3 Autolytic Activity in LGMD Muscle: A Functional Map of CAPN3 Gene Mutations.” *Journal of Medical Genetics* 44 (1): 38–43. doi:10.1136/jmg.2006.044859.

Fanin, M., AC. Nascimbeni, L. Fulizio, CP. Trevisan, M. Meznaric-Petrusa, and C. Angelini. 2003.

"Loss of Calpain-3 Autocatalytic Activity in LGMD2A Patients with Normal Protein Expression." *The American Journal of Pathology* 163 (5). American Society for Investigative Pathology: 1929–36. doi:10.1016/S0002-9440(10)63551-1.

Fardeau, M., B. Eymard, C. Mignard, FM. Tomé, I. Richard, and JS. Beckmann. 1996a. "Chromosome 15-Linked Limb-Girdle Muscular Dystrophy: Clinical Phenotypes in Reunion Island and French Metropolitan Communities." *Neuromuscular Disorders* 6 (6): 447–53. doi:10.1016/S0960-8966(96)00387-2.

Fardeau, M., D. Hillaire, C. Mignard, N. Feingold, J. Feingold, D. Mignard, B. De Ubeda, et al. 1996b. "Juvenile Limb-Girdle Muscular Dystrophy Clinical, Histopathological and Genetic Data from a Small Community Living in the Reunion Island." *Brain* 119: 295–308.

Federici, C., Y. Eshdat, I. Richard, B. Bertin, JL. Guillaume, M. Hattab, JS. Beckmann, AD. Strosberg, and L. Camoin. 1999. "Purification and Identification of Two Putative Autolytic Sites in Human Calpain 3 (p94) Expressed in Heterologous Systems." *Archives of Biochemistry and Biophysics* 363 (2): 237–45. doi:10.1006/abbi.1998.1091.

Ferrari, G., G. Cusella, De Angelis, M. Coletta, E. Paolucci, A. Stornaiuolo, G. Cossu, and F. Mavilio. 1998. "Muscle Regeneration by Bone Marrow – Derived Myogenic Progenitors." *Science* 279 (6): 1–4. doi:10.1126/science.279.5356.1528.

Ferrari, G., A. Stornaiuolo, and F. Mavilio. 2001. "Failure to Correct Murine Muscular Dystrophy." *Nature* 411 (6841): 1014–15. doi:10.1038/35082631.

Figarella-Branger, D., M. El-Dassouki, A. Saenz, AM. Cobo, P. Malzac, S. Tong, E. Cassotte, JP. Azulay, J. Pouget, and JF. Pellissier. 2002. "Myopathy with Lobulated Muscle Fibers: Evidence for Heterogeneous Etiology and Clinical Presentation." *Neuromuscular Disorders* 12 (1): 4–12. doi:10.1016/S0960-8966(01)00245-0.

Fiorenzano, A., E. Pascale, C. D'Aniello, D. Acampora, C. Bassalert, F. Russo, G. Andolfi, et al. 2016. "Cripto Is Essential to Capture Mouse Epiblast Stem Cell and Human Embryonic Stem Cell Pluripotency." *Nature Communications* 7: 12589. doi:10.1038/ncomms12589.

Fougerousse, F., M. Durand, L. Suel, O. Pourquié, AL. Delezoide, NB. Romero, M. Abitbol, and JS. Beckmann. 1998. "Expression of Genes (CAPN3, SGCA, SGCB, and TTN) Involved in Progressive Muscular Dystrophies during Early Human Development." *Genomics* 48 (2): 145–56. doi:10.1006/geno.1997.5160.

Freberg, CT., JA. Dahl, S. Timoskainen, and P. Collas. 2007. "Epigenetic Reprogramming of OCT4 and NANOG Regulatory Regions by Embryonal Carcinoma Cell Extract." *Molecular Biology of the Cell* 18 (1): 1543–53. doi:10.1091/mbc.E07.

Frontera, WR., and J. Ochala. 2015. "Skeletal Muscle: A Brief Review of Structure and Function." *Calcified Tissue International* 96 (3): 183–95. doi:10.1007/s00223-014-9915-y.

Fu, X., H. Wang, and P. Hu. 2015. "Stem Cell Activation in Skeletal Muscle Regeneration." *Cellular and Molecular Life Sciences* 72 (9): 1663–77. doi:10.1007/s00018-014-1819-5.

Fukada, S., A. Uezumi, M. Ikemoto, S. Masuda, M. Segawa, N. Tanimura, H. Yamamoto, Y. Miyagoe-Suzuki, and S. Takeda. 2007. "Molecular Signature of Quiescent Satellite Cells in Adult Skeletal Muscle." *Stem Cells* 25 (10): 2448–59. doi:10.1634/stemcells.2007-0019.

Fürst, DO. 1989. "Myogenesis in the Mouse Embryo: Differential Onset of Expression of Myogenic Proteins and the Involvement of Titin in Myofibril Assembly." *The Journal of Cell Biology* 109 (August): 517–27.

Gallardo, E., A. Saenz, and I. Illa. 2011. *Limb-Girdle Muscular Dystrophy 2A*. *Handbook of Clinical Neurology*. 1sted. Vol. 101. Elsevier B.V. doi:10.1016/B978-0-08-045031-5.00006-2.

Galli, R., U. Borello, A. Gritti, MG. Minasi, C. Bjornson, M. Coletta, M. Mora, et al. 2000. "Skeletal Myogenic Potential of Human and Mouse Neural Stem Cells." *Nat Neurosci* 3 (10): 986–91. doi:10.1038/79924.

García-Diaz, B., T. Moldoveanu, MJ. Kuiper, RL. Campbell, and PL. Davies. 2004. "Insertion Sequence 1 of Muscle-Specific Calpain, p94, Acts as an Internal Propeptide." *Journal of Biological Chemistry* 279 (26): 27656–66. doi:10.1074/jbc.M313290200.

García-Díaz, BE., S. Gauthier, and PL. Davies. 2006. "Ca2+ Dependency of Calpain 3 (p94) Activation." *Biochemistry* 45 (11): 3714–22. doi:10.1021/bi051917j.

Garvey, SM., C. Rajan, AP. Lerner, WN. Frankel, and GA. Cox. 2002. "The Muscular Dystrophy with Myositis (Mdm) Mouse Mutation Disrupts a Skeletal Muscle-Specific Domain of Titin." *Genomics* 79 (2): 146–49. doi:10.1006/geno.2002.6685.

Gibson, MC., and E. Schultz. 1983. "Age-Related Differences in Absolute Numbers of Skeletal Muscle Satellite Cells." *Muscle & Nerve*, no. October: 574–80. http://onlinelibrary.wiley.com/doi/10.1002/mus.880060807/abstract.

Gnocchi, VF., RB. White, Y. Ono, JA. Ellis, and PS. Zammit. 2009. "Further Characterisation of the Molecular Signature of Quiescent and Activated Mouse Muscle Satellite Cells." *PLoS ONE* 4 (4). doi:10.1371/journal.pone.0005205.

Goll, DE., VF. Thompson, H. Li, W. Wei, and J. Cong. 2003. "The Calpain System." *Physiological Reviews* 83 (3): 731–801. doi:10.1152/physrev.00029.2002.

Goudenege, S., C. Lebel, NB. Huot, C. Dufour, I. Fujii, J. Gekas, J. Rousseau, and JP. Tremblay. 2012. "Myoblasts Derived From Normal hESCs and Dystrophic hiPSCs Efficiently Fuse With Existing Muscle Fibers Following Transplantation." *Molecular Therapy* 20 (11): 2153–67. doi:10.1038/mt.2012.188.

Goudenege, S., DF. Pisani, B. Wdziekonski, JP. Di Santo, C. Bagnis, C. Dani, and CA Dechesne. 2009. "Enhancement of Myogenic and Muscle Repair Capacities of Human Adipose-Derived Stem Cells with Forced Expression of MyoD." *Molecular Therapy: The Journal of the American Society of Gene Therapy* 17 (6). The American Society of Gene Therapy: 1064–72. doi:10.1038/mt.2009.67.

Granzier, HL., and S. Labeit. 2004. "The Giant Protein Titin: A Major Player in Myocardial Mechanics, Signaling, and Disease." *Circulation Research* 94 (3): 284–95. doi:10.1161/01.RES.0000117769.88862.F8.

Gropp, M., V. Shilo, G. Vainer, M. Gov, Y. Gil, H. Khaner, L. Matzrafi, et al. 2012. "Standardization of the Teratoma Assay for Analysis of Pluripotency of Human ES Cells and Biosafety of Their Differentiated Progeny." *PLoS ONE* 7 (9): 1–10. doi:10.1371/journal.pone.0045532.

Guan, Y., D. Huang, F. Chen, C. Gao, T. Tao, H. Shi, S. Zhao, et al. 2016. "Phosphorylation of Def Regulates Nucleolar p53 Turnover and Cell Cycle Progression through Def Recruitment of Calpain3." *PLoS Biology* 14 (9): 1–31. doi:10.1371/journal.pbio.1002555.

Guenther, MG., GM. Frampton, F. Soldner, D. Hockemeyer, M. Mitalipova, R. Jaenisch, and RA. Young. 2010. "Chromatin Structure and Gene Expression Programs of Human Embryonic and Induced Pluripotent Stem Cells." *Cell Stem Cell* 7 (2). Elsevier Ltd: 249–57. doi:10.1016/j.stem.2010.06.015.

Guerard, MJ., CA. Sewry, and V. Dubowitz. 1985. "Lobulated Fibers in Neuromuscular Diseases." *Journal of the Neurological Sciences* 69 (3): 345–56. doi:10.1016/0022-510X(85)90145-5.

Guo, T., RX. Yin, L. Pan, S. Yang, L. Miao, and F. Huang. 2017. "Integrative Variants, Haplotypes and Diplotypes of the CAPN3 and FRMD5 Genes and Several Environmental Exposures Associate with Serum Lipid Variables." *Scientific Reports* 7 (March). Nature Publishing Group: 45119. doi:10.1038/srep45119.

Guroff, G. 1964. "A Neutral, Calcium-Activated Proteinase Fraction from the Soluble of Rat Brain." *Journal of Biological Chemistry* 239 (1): 149–55.

Gussoni, E., RR. Bennett, KR. Muskiewicz, T. Meyerrose, JA. Nolta, I. Gilgoff, J. Stein, et al. 2002. "Long-Term Persistence of Donor Nuclei in a Duchenne Muscular Dystrophy Patient Receiving Bone Marrow Transplantation." *Journal of Clinical Investigation* 110 (6): 807–14. doi:10.1172/JCI200216098.Introduction.

Gussoni, E., Y. Soneoka, CD. Strickland, EA. Buzney, MK. Khan, AF. Flint, LM. Kunkel, and RC. Mulligan. 1999. "Dystrophin Expression in the Mdx Mouse Restored by Stem Cell Transplantation." *Nature* 401 (6751): 390–94. doi:10.1038/43919.

Guyon, JR., E. Kudryashova, A. Potts, I. Dalkilic, MA. Brosius, TG. Thompson, JS. Beckmann, LM. Kunkel, and MJ. Spencer. 2003. "Calpain 3 Cleaves Filamin C and Regulates Its Ability to Interact with γ- and δ-Sarcoglycans." *Muscle and Nerve* 28 (4): 472–83. doi:10.1002/mus.10465.

Hackett, JA., and AM. Surani. 2014. "Regulatory Principles of Pluripotency: From the Ground State up." *Cell Stem Cell* 15 (4). Elsevier Inc.: 416–30. doi:10.1016/j.stem.2014.09.015.

Haravuori, H., A. Vihola, V. Straub, M. Auranen, I. Richard, S. Marchand, T. Voit, et al. 2001. "Secondary calpain3 Deficiency in 2q-Linked Muscular Dystrophy: Titin Is the Candidate Gene." *Neurology* 56 (7): 869–77. doi:10.1212/WNL.56.7.869.

Hashimoto, A., AT. Naito, JK. Lee, R. Kitazume-Taneike, M. Ito, T. Yamaguchi, R. Nakata, et al. 2015. "Generation of Induced Pluripotent Stem Cells From Patients With Duchenne Muscular Dystrophy and Their Induction to Cardiomyocytes." *International Heart Journal*, 112–17. doi:10.1536/ihj.15-376.

Hasty, P., A. Bradley, JH. Morris, DG. Edmondson, JM. Venuti, EN. Olson, and WH. Klein. 1993. "Muscle Deficiency and Neonatal Death in Mice with a Targeted Mutation in the Myogenin Gene." *Nature* 364 (6437): 501–6. doi:10.1038/364501a0.

Hayashi, C., Y. Ono, N. Doi, F. Kitamura, M. Tagami, R. Mineki, T. Arai, et al. 2008. "Multiple Molecular Interactions Implicate the Connectin/titin N2A Region as a Modulating Scaffold for p94/calpain 3 Activity in Skeletal Muscle." *Journal of Biological Chemistry* 283 (21): 14801–14. doi:10.1074/jbc.M708262200.

Herasse, M., Y. Ono, F. Fougerousse, E. Kimura, D. Stockholm, C. Beley, D. Montarras, et al. 1999. "Expression and Functional Characteristics of Calpain 3 Isoforms Generated through Tissue-Specific Transcriptional and Posttranscriptional Events." *Molecular and Cellular Biology* 19 (6): 4047–55. http://www.pubmedcentral.nih.gov/articlerender.fcgi?artid=104364&tool=pmcentrez&rendertype=abstract.

Hermanová, M., E. Zapletalová, J. Sedláčková, T. Chrobáková, O. Letocha, I. Kroupová, J. Zámečník, et al. 2006. "Analysis of Histopathologic and Molecular Pathologic Findings in Czech LGMD2A Patients." *Muscle and Nerve* 33 (3): 424–32. doi:10.1002/mus.20480.

Herzog, W. 2014. "The Role of Titin in Eccentric Muscle Contraction." *Journal of Experimental*

Biology 217 (16): 2825–33. doi:10.1242/jeb.099127.

Hildyard, JCW., and DJ. Wells. 2014. “Identification and Validation of Quantitative PCR Reference Genes Suitable for Normalizing Expression in Normal and Dystrophic Cell Culture Models of Myogenesis.” *PLoS Currents* 6: 1–32. doi:10.1371/currents.md.faafdde4bea8df4aa7d06cd5553119a6.Authors.

Hiler, D., X. Chen, J. Hazen, S. Kupriyanov, PA. Carroll, C. Qu, B. Xu, et al. 2015. “Quantification of Retinogenesis in 3D Cultures Reveals Epigenetic Memory and Higher Efficiency in iPSCs Derived from Rod Photoreceptors.” *Cell Stem Cell* 17 (1). Elsevier Inc.: 101–15. doi:10.1016/j.stem.2015.05.015.

Hoffman, EP., CM. Knudson, KP. Campbell, and LM. Kunkel. 1987. “Subcellular Fractionation of Dystrophin to the Triads of Skeletal Muscle.” *Nature* 330 (6150): 754–58. doi:10.1038/330754a0.

Hosoyama, T., K. Nishijo, SI. Prajapati, G. Li, and C. Keller. 2011. “Rb1 Gene Inactivation Expands Satellite Cell and Postnatal Myoblast Pools.” *Journal of Biological Chemistry* 286 (22): 19556–64. doi:10.1074/jbc.M111.229542.

Huang, Y., A. de Morrée, A. van Remoortere, K. Bushby, RR. Frants, JT. Dunnen, and SM. van der Maarel. 2008. “Calpain 3 Is a Modulator of the Dysferlin Protein Complex in Skeletal Muscle.” *Human Molecular Genetics* 17 (12): 1855–66. doi:10.1093/hmg/ddn081.

Huang, Y., P. Verheesen, A. Roussis, W. Frankhuizen, I. Ginjaar, F. Haldane, S. Laval, et al. 2005. “Protein Studies in Dysferlinopathy Patients Using Llama-Derived Antibody Fragments Selected by Phage Display.” *European Journal of Human Genetics : EJHG* 13 (6): 721–30. doi:10.1038/sj.ejhg.5201414.

Iovino, S., AM. Burkart, L. Warren, ME. Patti, and CR. Kahn. 2016. “Myotubes Derived from Human-Induced Pluripotent Stem Cells Mirror in Vivo Insulin Resistance.” *Nature Communications* 7 (3): 201525665. doi:10.1073/pnas.1525665113.

Ippolito, J., RW. Arpke, KT. Haider, J. Zhang, and M. Kyba. 2012. “Satellite Cell Heterogeneity Revealed by G-Tool, an Open Algorithm to Quantify Myogenesis through Colony-Forming Assays.” *Skeletal Muscle* 2 (1): 13. doi:10.1186/2044-5040-2-13.

Jaka, O., L. Casas-Fraile, M. Azpitarte, A. Aiastui, A. López de Munain, and A. Sáenz. 2017. “FRZB and Melusin, Overexpressed in LGMD2A, Regulate Integrin β1D Isoform Replacement Altering Myoblast Fusion and the Integrin-Signalling Pathway.” *Expert Reviews in Molecular Medicine* 19: e2. doi:10.1017/erm.2017.3.

Jaka, O., L. Casas-Fraile, A. López de Munain, and A. Sáenz. 2015. “Costamere Proteins and Their Involvement in Myopathic Processes.” *Expert Reviews in Molecular Medicine* 17: e12. doi:10.1017/erm.2015.9.

Jesse TL., R. LaChance, MF. Iademarco, DC. Dean. 1998. "Interferon regulatory factor-2 is a transcriptional activator in muscle where it regulates expression of vascular cell adherion molecule-1". J Cell Biol 140(5):1265-76.

Jiang, C., Y. Wen, K. Kuroda, K. Hannon, MA. Rudnicki, and S. Kuang. 2014. “Notch Signaling Deficiency Underlies Age-Dependent Depletion of Satellite Cells in Muscular Dystrophy.” *Disease Models and Mechanisms* 7 (1): 997–1004. doi:10.1242/dmm.015917.

Joe, AW., L. Yi, A. Natarajan, F. Le Grand, L. So, J. Wang, MA. Rudnicki, and FM. Rossi. 2010. “Muscle Injury Activates Resident Fibro/adipogenic Progenitors That Facilitate Myogenesis.” *Nat Cell Biol* 12 (2). Nature Publishing Group: 153–63. doi:10.1038/ncb2015.

Jones, NC., KJ. Tyner, L. Nibarger, HM. Stanley, DDW. Cornelison, YV. Fedorov, and BB. Olwin. 2005. "The p38a/b MAPK Functions as a Molecular Switch to Activate the Quiescent Satellite Cell." *Journal of Cell Biology* 169 (1): 105–16. doi:10.1083/jcb.200408066.

Jones, SW., T. Parr, PL. Sensky, GP. Scothern, RG. Bardsley, and PJ. Buttery. 1999. "Fibre Type-Specific Expression of p94, a Skeletal Muscle-Specific Calpain." *Journal of Muscle Research and Cell Motility* 20 (4): 417–24. doi:10.1023/A:1005572125827.

Kaplan, JC., and D. Hamroun. 2014. "The 2015 Version of the Gene Table of Monogenic Neuromuscular Disorders (Nuclear Genome)." *Neuromuscular Disorders* 24 (12): 1123–53. doi:10.1016/j.nmd.2014.11.001.

Kassar-Duchossoy, L., B. Gayraud-Morel, D. Gomes, D. Rocancourt, M. Buckingham, V. Shinin, and S. Tajbakhsh. 2004. "Letters To Nature." *Nature* 431 (September): 466–71. doi:10.1038/nature02924.Published.

Kassar-duchossoy, Lina, Ellen Giacone, Barbara Gayraud-morel, Aurélie Jory, Danielle Gomès, and Shahragim Tajbakhsh. 2005. "Pax3/Pax7 Mark a Novel Population of Primitive Myogenic Cells during Development." *Genes and Development* 19: 1426–31. doi:10.1101/gad.345505.

Kastner, S., MC. Elias, AJ. Rivera, Z. Yablonka-Reuveni, S. Kästner, MC. Elias, AJ. Rivera, and Z. Yablonka-Reuveni. 2000. "Gene Expression Patterns of the Fibroblast Growth Factors and Their Receptors during Myogenesis of Rat Satellite Cells." *The Journal of Histochemistry and Cytochemistry : Official Journal of the Histochemistry Society* 48 (8): 1079–96. doi:10.1177/002215540004800805.

Kawabata, Y., S. Hata, Y. Ono, Y. Ito, K. Suzuki, K. Abe, and H. Sorimachi. 2003. "Newly Identified Exons Encoding Novel Variants of p94/calpain 3 Are Expressed Ubiquitously and Overlap the ??-Glucosidase C Gene." *FEBS Letters* 555 (3): 623–30. doi:10.1016/S0014-5793(03)01324-3.

Kawai, H., M. Akaike, M. Kunishige, T. Inui, K. Adachi, C. Kimura, M. Kawajiri, et al. 1998. "Clinical, Pathological, and Genetic Features of Limb-Girdle Muscular Dystrophy Type 2A with New Calpain 3 Gene Mutations in Seven Patients from Three Japanese Families." *Muscle and Nerve* 21 (11): 1493–1501. doi:10.1002/(SICI)1097-4598(199811)21:11<1493::AID-MUS19>3.0.CO;2-1.

Kazior, Z., SJ. Willis, M. Moberg, W. Apro, JAL. Calbet, HC. Holmberg, and E. Blomstrand. 2016. "Endurance Exercise Enhances the Effect of Strength Training on Muscle Fiber Size and Protein Expression of Akt and mTOR." *PLoS ONE* 11 (2): 1–18. doi:10.1371/journal.pone.0149082.

Keira, Y., S. Noguchi, R. Kurokawa, M. Fujita, N. Minami, YK. Hayashi, T. Kato, and I. Nishino. 2007. "Characterization of Lobulated Fibers in Limb Girdle Muscular Dystrophy Type 2A by Gene Expression Profiling." *Neuroscience Research* 57 (4): 513–21. doi:10.1016/j.neures.2006.12.010.

Kelly, RG., LA. Jerome-Majewska, and VE. Papaioannou. 2004. "The del22q11.2 Candidate Gene Tbx1 Regulates Branchiometric Myogenesis." *Human Molecular Genetics* 13 (22): 2829–40. doi:10.1093/hmg/ddh304.

Kim, J., A. Magli, S. Chan, VKP. Oliveira, J. Wu, R. Darabi, M. Kyba, and RC. Perlingeiro. 2017. "Expansion and Purification Are Critical for the Therapeutic Application of Pluripotent Stem Cell-Derived Myogenic Progenitors." *Stem Cell Reports* 9 (1). ElsevierCompany.: 12–22. doi:10.1016/j.stemcr.2017.04.022.

Kim, K., R. Zhao, A. Doi, K. Ng, J. Unternaehrer, P. Cahan, H. Hongguang, et al. 2011. "Donor Cell Type Can Influence the Epigenome and Differentiation Potential of Human Induced Pluripotent Stem Cells." *Nature Biotechnology* 29 (12): 1117–19. doi:10.1038/nbt.2052.

Kinbara, K., S. Ishiura, S. Tomioka, H. Sorimachi, SY. Jeong, S. Amano, H. Kawasaki, et al. 1998. "Purification of Native p94, a Muscle-Specific Calpain, and Characterization of Its Autolysis." *The Biochemical Journal* 335 (Pt 3: 589–96. http://www.pubmedcentral.nih.gov/articlerender.fcgi?artid=1219820&tool=pmcentrez&rendertype=abstract.

Kinbara, K., H. Sorimachi, S. Ishiura, and K. Suzuki. 1997. "Muscle-Specific Calpain, p94, Interacts with the Extreme C-Terminal Region of Connectin, a Unique Region Flanked by Two Immunoglobulin C2 Motifs." *Archives of Biochemistry and Biophysics* 342 (1): 99–107. doi:10.1006/abbi.1997.0108.

Kodaka, Y., G. Rabu, and A. Asakura. 2017. "Skeletal Muscle Cell Induction from Pluripotent Stem Cells." *Stem Cells International* 2017. Hindawi. doi:10.1155/2017/1376151.

Kottlors, M., and J. Kirschner. 2010. "Elevated Satellite Cell Number in Duchenne Muscular Dystrophy." *Cell and Tissue Research* 340 (3): 541–48. doi:10.1007/s00441-010-0976-6.

Krahn, M., M. Goicoechea, F. Hanisch, E. Groen, M. Bartoli, C. Pécheux, F. Garcia-Bragado, et al. 2011. "Eosinophilic Infiltration Related to CAPN3 Mutations: A Pathophysiological Component of Primary Calpainopathy?" *Clinical Genetics* 80 (4): 398–402. doi:10.1111/j.1399-0004.2010.01620.x.

Krahn, M., A. Lopez De Munain, N. Streichenberger, R. Bernard, C. Pécheux, H. Testard, JL. Pena-Segura, et al. 2006. "CAPN3 Mutations in Patients with Idiopathic Eosinophilic Myositis." *Annals of Neurology* 59 (6): 905–11. doi:10.1002/ana.20833.

Krahn, M., C. Pécheux, F. Chapon, C. Béroud, V. Drouin-Garraud, P. Laforet, N. B. Romero, et al. 2007. "Transcriptional Explorations of CAPN3 Identify Novel Splicing Mutations, a Large-Sized Genomic Deletion and Evidence for Messenger RNA Decay." *Clinical Genetics* 72 (6): 582–92. doi:10.1111/j.1399-0004.2007.00906.x.

Kramerova, I., JS. Beckmann, and MJ. Spencer. 2007. "Molecular and Cellular Basis of Calpainopathy (Limb Girdle Muscular Dystrophy Type 2A)." *Biochimica et Biophysica Acta* 1772: 128–44. doi:10.1016/j.bbadis.2006.07.002.

Kramerova, I., N. Ermolova, A. Eskin, A. Hevener, O. Quehenberger, AM. Armando, R. Haller, N. Romain, SF. Nelson, and Melissa J. Spencer. 2016. "Failure to up-Regulate Transcription of Genes Necessary for Muscle Adaptation Underlies Limb Girdle Muscular Dystrophy 2A (Calpainopathy)." *Human Molecular Genetics* 25 (11): 2194–2207. doi:10.1093/hmg/ddw086.

Kramerova, I., E. Kudryashova, N. Ermolova, A. Saenz, O. Jaka, A. López de munain, and M. J. Spencer. 2012. "Impaired Calcium Calmodulin Kinase Signaling and Muscle Adaptation Response in the Absence of Calpain 3." *Human Molecular Genetics* 21 (14): 3193–3204. doi:10.1093/hmg/dds144.

Kramerova, I., E. Kudryashova, JG. Tidball, and MJ. Spencer. 2004. "Null Mutation of Calpain 3 (p94) in Mice Causes Abnormal Sarcomere Formation in Vivo and in Vitro." *Human Molecular Genetics* 13 (13): 1373–88. doi:10.1093/hmg/ddh153.

Kramerova, I., E. Kudryashova, G. Venkatraman, and MJ. Spencer. 2005. "Calpain 3 Participates in Sarcomere Remodeling by Acting Upstream of the Ubiquitin - Proteasome Pathway."

Human Molecular Genetics 14 (15): 2125–34. doi:10.1093/hmg/ddi217.

Kramerova, I., E. Kudryashova, B. Wu, C. Ottenheijm, H. Granzier, and MJ. Spencer. 2008. "Novel Role of Calpain-3 in the Triad-Associated Protein Complex Regulating Calcium Release in Skeletal Muscle." *Human Molecular Genetics* 17 (21): 3271–80. doi:10.1093/hmg/ddn223.

Kramerova, I., E. Kudryashova, Be. Wu, and MJ. Spencer. 2006. "Regulation of the M-Cadherin-Beta-Catenin Complex by Calpain 3 during Terminal Stages of Myogenic Differentiation." *Molecular and Cellular Biology* 26 (22): 8437–47. doi:10.1128/MCB.01296-06.

Kramerova, I., El. Kudryashova, B. Wu, S. Germain, K. Vandenborne, N. Romain, RG. Haller, MA. Verity, and MJ. Spencer. 2009. "Mitochondrial Abnormalities, Energy Deficit and Oxidative Stress Are Features of Calpain 3 Deficiency in Skeletal Muscle." *Human Molecular Genetics* 18 (17): 3194–3205. doi:10.1093/hmg/ddp257.

Kuang, S., SB. Chargé, P. Seale, M. Huh, and MA. Rudnicki. 2006. "Distinct Roles for Pax7 and Pax3 in Adult Regenerative Myogenesis." *Journal of Cell Biology* 172 (1): 103–13. doi:10.1083/jcb.200508001.

Kuang, S., K. Kuroda, F. Le Grand, and MA. Rudnicki. 2007. "Asymmetric Self-Renewal and Commitment of Satellite Stem Cells in Muscle." *Cell* 129 (5): 999–1010. doi:10.1016/j.cell.2007.03.044.

Kudryashova, E., I. Kramerova, and MJ. Spencer. 2012. "Satellite Cell Senescence Underlies Myopathy in a Mouse Model of Limb-Girdle Muscular Dystrophy 2H. - Recherche Google." *The Journal of Clinical Investigation* 122 (5): 1764–1776. doi:10.1172/JCI59581.1764.

Laure, L., L. Suel, C. Roudaut, N. Bourg, A. Ouali, M. Bartoli, I. Richard, and N. Daniele. 2009. "Cardiac Ankyrin Repeat Protein Is a Marker of Skeletal Muscle Pathological Remodelling." *FEBS Journal* 276 (3): 669–84. doi:10.1111/j.1742-4658.2008.06814.x.

Lee, DS., JY. Shin, PD. Tonge, MC. Puri, S. Lee, H. Park, WC. Lee, et al. 2014. "An Epigenomic Roadmap to Induced Pluripotency Reveals DNA Methylation as a Reprogramming Modulator." *Nature Communications* 5. Nature Publishing Group: 5619. doi:10.1038/ncomms6619.

Leitch, HG., J. Nichols, P. Humphreys, C. Mulas, G. Martello, C. Lee, K. Jones, MA. Surani, and A. Smith. 2013. "Rebuilding Pluripotency from Primordial Germ Cells." *Stem Cell Reports* 1 (1). The Authors: 66–78. doi:10.1016/j.stemcr.2013.03.004.

Li, HL., N. Fujimoto, N. Sasakawa, S. Shirai, T. Ohkame, T. Sakuma, M. Tanaka, et al. 2015. "Precise Correction of the Dystrophin Gene in Duchenne Muscular Dystrophy Patient Induced Pluripotent Stem Cells by TALEN and CRISPR-Cas9." *Stem Cell Reports* 4 (1). The Authors: 143–54. doi:10.1016/j.stemcr.2014.10.013.

Li, YP. 2003. "TNF-Alpha Is a Mitogen in Skeletal Muscle." *American Journal of Physiology. Cell Physiology* 285 (2): C370–76. doi:10.1152/ajpcell.00453.2002.

Lister, R., M. Pelizzola, YS. Kida, RD. Hawkins, JR. Nery, G. Hon, J. Antosiewicz-Bourget, et al. 2011. "Hotspots of Aberrant Epigenomic Reprogramming in Human Induced Pluripotent Stem Cells." *Nature* 471 (7336). Nature Publishing Group: 68–73. doi:10.1038/nature09798.

Liu, L., TH. Cheung, GW. Charville, BM. Ceniza-Hurgo, T. Leavitt, J. Shih, A. Brunet, and TA. Rando. 2013. "Chromatin Modifications as Determinants of Muscle Stem Cell Quiescence and Chronological Aging." *Cell Reports* 4 (1). The Authors: 189–204. doi:10.1016/j.celrep.2013.05.043.

Liu, L., TH. Cheung, GW. Charville, and TA. Rando. 2015. "Isolation of Skeletal Muscle Stem Cells by Fluorescence-Activated Cell Sorting." *Nature Protocols* 10 (10). Nature Publishing Group: 1612–24. doi:10.1038/nprot.2015.110.

Los Angeles, A. De, YH. Loh, PJ. Tesar, and GQ. Daley. 2012. "Accessing Naive Human Pluripotency." *Current Opinion in Genetics & Development* 22 (3): 272–82. doi:10.1016/j.gde.2012.03.001.

Ma, H., M. Shih, I. Hata, C. Fukiage, M. Azuma, and TR. Shearer. 2000. "Lp85 Calpain Is an Enzymatically Active Rodent- Specific Isozyme of Lens Lp82." *Curent Eye Research* 3683 (February): 1–8.

Maesner, CC., AE. Almada, and AJ. Wagers. 2016. "Established Cell Surface Markers Efficiently Isolate Highly Overlapping Populations of Skeletal Muscle Satellite Cells by Fluorescence-Activated Cell Sorting." *Skeletal Muscle* 6 (1). Skeletal Muscle: 35. doi:10.1186/s13395-016-0106-6.

Maffioletti, SM, MFM Gerli, M. Ragazzi, S. Dastidar, S. Benedetti, M. Loperfido, T. VandenDriessche, MK. Chuah, and FS. Tedesco. 2015. "Efficient Derivation and Inducible Differentiation of Expandable Skeletal Myogenic Cells from Human ES and Patient-Specific iPS Cells." *Nature Protocols* 10 (7): 941–58. doi:10.1038/nprot.2015.057.

Maltzahn, J. von, AE. Jones, RJ. Parks, and MA. Rudnicki. 2013. "Pax7 Is Critical for the Normal Function of Satellite Cells in Adult Skeletal Muscle." *Proc Natl Acad Sci U S A* 110 (41): 16474–79. doi:10.1073/pnas.1307680110.

Mamchaoui, K., C. Trollet, A. Bigot, E. Negroni, S. Chaouch, A. Wolff, PK. Kandalla, et al. 2011. "Immortalized Pathological Human Myoblasts: Towards a Universal Tool for the Study of Neuromuscular Disorders." *Skeletal Muscle* 1 (1): 34. doi:10.1186/2044-5040-1-34.

Martí, M., L. Mulero, C. Pardo, C. Morera, M. Carrió, L. Laricchia-Robbio, CR. Esteban, and JC Izpisua-Belmonte. 2013. "Characterization of Pluripotent Stem Cells." *Nature Protocols* 8 (2): 223–53. doi:10.1038/nprot.2012.154.

Martinez-Thompson, J., Z. Niu, JA. Tracy, SA. Moore, A. Swenson, ED. Wieben, and M. Milone. 2017. "Autosomal Dominant Calpainopathy due to Heterozygous CAPN3 c.643_663del21." *Muscle & Nerve*, 1–16.

Mateos-Aierdi, AJ., M. Goicoechea, A. Aiastui, R. Fernández-Torrón, M. Garcia-Puga, A. Matheu, and A. López de Munain. 2015. "Muscle Wasting in Myotonic Dystrophies: A Model of Premature Aging." *Frontiers in Aging Neuroscience* 7 (July): 125. doi:10.3389/fnagi.2015.00125.

Mauro, A. 1961. "Satellite Cell of Skeletal Muscle Fibers." *Journal of Biophys Biochem Cytol* 9: 493–98.

Mehuron, T., A. Kumar, L. Duarte, J. Yamauchi, A. Accorsi, and M. Girgenrath. 2014. "Dysregulation of Matricellular Proteins Is an Early Signature of Pathology in Laminin-Deficient Muscular Dystrophy." *Skeletal Muscle* 4 (1): 14. doi:10.1186/2044-5040-4-14.

Mercuri, E., K. Bushby, E. Ricci, D. Birchall, M. Pane, M. Kinali, J. Allsop, et al. 2005. "Muscle MRI Findings in Patients with Limb Girdle Muscular Dystrophy with Calpain 3 Deficiency (LGMD2A) and Early Contractures." *Neuromuscular Disorders* 15 (2): 164–71. doi:10.1016/j.nmd.2004.10.008.

Milic, A., N. Daniele, H. Lochmüller, M. Mora, GP. Comi, M. Moggio, F. Noulet, et al. 2007. "A Third of LGMD2A Biopsies Have Normal Calpain 3 Proteolytic Activity as Determined by an

in Vitro Assay." *Neuromuscular Disorders* 17 (2): 148–56. doi:10.1016/j.nmd.2006.11.001.

Moldoveanu, T., CM. Hosfield, D. Lim, JS. Elce, and Z. Jia. 2002. "Switch Aligns the Active Site of Calpain between Calpain and Its Endogenous Inhibitors like Cal." *Cell* 108: 649–60. doi:10.1016/S0092-8674(02)00659-1.

Moncaut, N., PWJ Rigby, and JJ. Carvajal. 2013. "Dial M(RF) for Myogenesis." *FEBS Journal* 280 (17): 3980–90. doi:10.1111/febs.12379.

Montarras, D., J. Morgan, C. Collins, F. Relaix, S. Zaffran, A. Cumano, T. Partridge, and M. Buckingham. 2005. "Direct Isolation of Satellite Cells for Skeletal Muscle Regeneration." *Science* 309 (5743): 2064–67. doi:10.1126/science.1114758.

Moretti, D., B. Del Bello, E. Cosci, M. Biagioli, C. Miracco, and E. Maellaro. 2009. "Novel Variants of Muscle Calpain 3 Identified in Human Melanoma Cells: Cisplatin-Induced Changes in Vitro and Differential Expression in Melanocytic Lesions." *Carcinogenesis* 30 (6): 960–67.

Moretti, D., B. Del-Bello, G. Allavena, A. Corti, C. Signorini, and E. Maellaro. 2015. "Calpain-3 Impairs Cell Proliferation and Stimulates Oxidative Stress-Mediated Cell Death in Melanoma Cells." *PLoS ONE* 10 (2): 1–22. doi:10.1371/journal.pone.0117258.

Morgan, JE., and PS. Zammit. 2010. "Direct Effects of the Pathogenic Mutation on Satellite Cell Function in Muscular Dystrophy." *Experimental Cell Research* 316 (18). Elsevier Inc.: 3100–3108. doi:10.1016/j.yexcr.2010.05.014.

Mourkioti, F., P. Kratsios, T. Luedde, Y. Song, P. Delafontaine, R. Adami, V. Parente, R. Bottinelli, M. Pasparakis, and N. Rosenthal. 2006. "Targeted Ablation of IKK2 Improves Skeletal Muscle Strength, Maintains Mass, and Promotes Regeneration. [J Clin Invest. 2006] - - PubMed - NCBI" 116 (11). doi:10.1172/JCI28721.Despite.

Mungenast, AE., S. Siegert, and LH. Tsai. 2016. "Modeling Alzheimer's Disease with Human Induced Pluripotent Stem (iPS) Cells." *Molecular and Cellular Neuroscience* 73. Elsevier B.V.: 13–31. doi:10.1016/j.mcn.2015.11.010.

Murphy, RM., and GD. Lamb. 2009. "Endogenous Calpain-3 Activation Is Primarily Governed by Small Increases in Resting Cytoplasmic [Ca2+] and Is Not Dependent on Stretch." *Journal of Biological Chemistry* 284 (12): 7811–19. doi:10.1074/jbc.M808655200.

Nabeshima, Y., K. Hanaoka, M. Hayasaka, E. Esumi, S. Li, I. Nonaka, and Y. Nabeshima. 1993. "Myogenin Gene Disruption Results in Perinatal Lethality because of Severe Muscle Defect." *Nature* 364 (6437): 532–35. doi:10.1038/364532a0.

Nakajima, T., C. Fukiage, M. Azuma, H. Ma, and TR. Shearer. 2001. "Different Expression Patterns for Ubiquitous Calpains and Capn3 Splice Variants in Monkey Ocular Tissues." *Biochimica et Biophysica Acta - Gene Structure and Expression* 1519 (1–2): 55–64. doi:10.1016/S0167-4781(01)00212-3.

Nilsson, MI., LG. Macneil, Y. Kitaoka, F. Alqarni, R. Suri, M. Akhtar, ME. Haikalis, P. Dhaliwal, M. Saeed, and MA. Tarnopolsky. 2014. "Redox State and Mitochondrial Respiratory Chain Function in Skeletal Muscle of LGMD2A Patients." *PLoS ONE* 9 (7). doi:10.1371/journal.pone.0102549.

O'Connor, MD., MD. Kardel, I. Iosfina, D. Youssef, M. Lu, MM. Li, S. Vercauteren, A. Nagy, and CJ. Eaves. 2008. "Alkaline Phosphatase-Positive Colony Formation Is a Sensitive, Specific, and Quantitative Indicator of Undifferentiated Human Embryonic Stem Cells." *Stem Cells* 26 (5): 1109–16. doi:10.1634/stemcells.2007-0801.

Ohi, Y., H. Qin, C. Hong, L. Blouin, JM. Polo, T. Guo, Z. Qi, et al. 2011. "Incomplete DNA Methylation Underlies a Transcriptional Memory of Somatic Cells in Human iPS Cells." *Nature Cell Biology* 13 (5). Nature Publishing Group: 541–49. doi:10.1038/ncb2239.

Ojima, K., Y. Kawabata, H. Nakao, K. Nakao, N. Doi, F. Kitamura, Y. Ono, et al. 2010. "Dynamic Distribution of Muscle-Specific Calpain in Mice Has a Key Role in Physical-Stress Adaptation and Is Impaired in Muscular Dystrophy." *Journal of Clinical Investigation* 120 (8): 2672–83. doi:10.1172/JCI40658.

Ojima, K., Y. Ono, S. Hata, S. Koyama, N. Doi, and H. Sorimachi. 2005. "Possible Functions of p94 in Connectin-Mediated Signaling Pathways in Skeletal Muscle Cells." *Journal of Muscle Research and Cell Motility* 26 (6–8): 409–17. doi:10.1007/s10974-005-9023-8.

Ojima, K., Y. Ono, S. Hata, S. Noguchi, I. Nishino, and H. Sorimachi. 2014. "Muscle-Specific Calpain-3 Is Phosphorylated in Its Unique Insertion Region for Enrichment in a Myofibril Fraction." *Genes to Cells* 19 (11): 830–41. doi:10.1111/gtc.12181.

Ojima, K., Y. Ono, C. Ottenheijm, S. Hata, H. Suzuki, H. Granzier, and H. Sorimachi. 2011. "Non-Proteolytic Functions of Calpain-3 in Sarcoplasmic Reticulum in Skeletal Muscles." *Journal of Molecular Biology* 407 (3). Elsevier Ltd: 439–49. doi:10.1016/j.jmb.2011.01.057.

Olguin, HC., Z. Yang, SJ. Tapscott, and BB. Olwin. 2007. "Reciprocal Inhibition between Pax7 and Muscle Regulatory Factors Modulates Myogenic Cell Fate Determination." *Journal of Cell Biology* 177 (5): 769–79. doi:10.1083/jcb.200608122.

Ono, Y., C. Hayashi, N. Doi, F. Kitamura, M. Shindo, K. Kudo, T. Tsubata, M. Yanagida, and H. Sorimachi. 2007. "Comprehensive Survey of p94/calpain 3 Substrates by Comparative Proteomics--Possible Regulation of Protein Synthesis by p94." *Biotechnology Journal* 2 (5): 565–76. doi:10.1002/biot.200700018.

Ono, Y., SI. Iemura, SM. Novak, N. Doi, F. Kitamura, T. Natsume, CC. Gregorio, and H. Sorimachi. 2013. "PLEIAD/SIMC1/C5orf25, a Novel Autolysis Regulator for a Skeletal-Muscle-Specific Calpain, CAPN3, Scaffolds a CAPN3 Substrate, CTBP1." *Journal of Molecular Biology* 425 (16). The Authors: 2955–72. doi:10.1016/j.jmb.2013.05.009.

Ono, Y., K. Ojima, F. Shinkai-Ouchi, S. Hata, and H. Sorimachi. 2016. "An Eccentric Calpain, CAPN3/p94/calpain-3." *Biochimie* 122. Elsevier B.V: 169–87. doi:10.1016/j.biochi. 2015.09.010.

Ono, Y., K. Ojima, F. Torii, E. Takaya, N. Doi, K. Nakagawa, S. Hata, K. Abe, and H. Sorimachi. 2010. "Skeletal Muscle-Specific Calpain Is an Intracellular Na+- Dependent Protease." *Journal of Biological Chemistry* 285 (30): 22986–98. doi:10.1074/jbc.M110.126946.

Ono, Y., H. Shimada, H. Sorimach, I. Richard, TC. Saido, JS. Beckmann, S. Ishiura, and K. Suzuki. 1998. "Functional Defects of a Muscle-Specific Calpain, p94, Caused by Mutations Associated with Limb-Girdle Muscular Dystrophy Type 2A." *Journal of Biological Chemistry* 273 (27): 17073–78. doi:10.1074/jbc.273.27.17073.

Ono, Y., M. Shindo, N. Doi, F. Kitamura, CC. Gregorio, and H. Sorimachi. 2014. "The N-and C-Terminal Autolytic Fragments of CAPN3/p94/calpain-3 Restore Proteolytic Activity by Intermolecular Complementation." *Proceedings of the National Academy of Sciences of the United States of America* 111 (51): E5527-5536. doi:10.1073/pnas.1411959111.

Ono, Y., and H. Sorimachi. 2012. "Calpains - An Elaborate Proteolytic System." *Biochimica et Biophysica Acta - Proteins and Proteomics* 1824 (1). Elsevier B.V.: 224–36. doi:10.1016/j.bbapap.2011.08.005.

Ono, Y., F. Torii, K. Ojima, N. Doi, K. Yoshioka, Y. Kawabata, D. Labeit, et al. 2006. "Suppressed Disassembly of Autolyzing p94/CAPN3 by N2A Connectin/titin in a Genetic Reporter System." *Journal of Biological Chemistry* 281 (27): 18519–31. doi:10.1074/jbc.M601029200.

Oustanina, S., G. Hause, and T. Braun. 2004. "Pax7 Directs Postnatal Renewal and Propagation of Myogenic Satellite Cells but Not Their Specification." *Embo J* 23 (16): 3430–39. doi:10.1038/sj.emboj.7600346.

Pallafacchina, G., S. François, B. Regnault, B. Czarny, V. Dive, A. Cumano, D. Montarras, and M. Buckingham. 2010. "An Adult Tissue-Specific Stem Cell in Its Niche: A Gene Profiling Analysis of in Vivo Quiescent and Activated Muscle Satellite Cells." *Stem Cell Research* 4 (2). Elsevier B.V.: 77–91. doi:10.1016/j.scr.2009.10.003.

Partha, SK., R. Ravulapalli, JS. Allingham, RL. Campbell, and PL. Davies. 2014. "Crystal Structure of Calpain-3 Penta-EF-Hand (PEF) Domain - A Homodimerized PEF Family Member with Calcium Bound at the Fifth EF-Hand." *FEBS Journal* 281 (14): 3138–49. doi:10.1111/febs.12849.

Pasque, V., and K. Plath. 2015. "X Chromosome Reactivation in Reprogramming and in Development." *Curr Opin Cell Biol.* 37: 75–83. doi:10.1007/128.

Pasut, Al., P. Oleynik, and MA. Rudnicki. 2012. "Isolation of Muscle Stem Cells by Fluorescence Activated Cell Sorting Cytometry." *Myogenesis* 798: 53–64.

Patruno, M., C. Gomiero, R. Sacchetto, O. Topel, A. Negro, and T. Martinello. 2017. "Tat-MyoD Fused Proteins, Together with C2c12 Conditioned Medium, Are Able to Induce Equine Adult Mesenchimal Stem Cells towards the Myogenic Fate." *Veterinary Research Communications* 41 (3). Veterinary Research Communications: 211–17. doi:10.1007/s11259-017-9692-y.

Paula, F. de, M. Vainzof, MR. Passos-Bueno, R. de Cássia M Pavanello, SR. Matioli, L. V B Anderson, V. Nigro, and M. Zatz. 2002. "Clinical Variability in Calpainopathy: What Makes the Difference?" *European Journal of Human Genetics : EJHG* 10 (12): 825–32. doi:10.1038/sj.ejhg.5200888.

Péault, B., M. Rudnicki, Y. Torrente, G. Cossu, JP. Tremblay, T. Partridge, E. Gussoni, LM. Kunkel, and J. Huard. 2007. "Stem and Progenitor Cells in Skeletal Muscle Development, Maintenance, and Therapy." *Mol Ther* 15 (5). The American Society of Gene Therapy: 867–77. doi:10.1038/mt.sj.6300145.

Pénisson-Besnier, I., I. Richard, F. Dubas, JS. Beckmann, and M. Fardeau. 1998. "Pseudometalic Variability of and Phenotypic Variability of Calpain Deficiency in Two Siblings." *Muscle and Nerve* 21 (8): 1078–80. doi:10.1002/(SICI)1097-4598(199808)21:8<1078::AID-MUS15>3.0.CO;2-Q.

Petrov, A., I. Pirozhkova, G. Carnac, D. Laoudj, M. Lipinski, and YS. Vassetzky. 2006. "Chromatin Loop Domain Organization within the 4q35 Locus in Facioscapulohumeral Dystrophy Patients versus Normal Human Myoblasts." *Proc Natl Acad Sci U S A* 103 (18): 6982–87. doi:10.1073/pnas.0511235103.

Pette, D., and RS. Staron. 2000. "Myosin Isoforms, Muscle Fiber Types, and transitions1." *Microsc.Res.Tech.* 50 (6): 500–509. doi:10.1002/1097-0029(20000915)50:6<500::AID-JEMT7>3.0.CO;2-7.

Philippos, M., R. Sambasivan, D. Castel, P. Rocheteau, V. Bizzarro, and S. Tajbakhsh. 2012. "A

Critical Requirement for Notch Signaling in Maintenance of the Quiescent Skeletal Muscle Stem Cell State." *Stem Cells* 30 (2): 243–52. doi:10.1002/stem.775.

Pollitt, C., LVB. Anderson, R. Pogue, K. Davison, A. Pyle, and KMD. Bushby. 2001. "The Phenotype of Calpainopathy: Diagnosis Based on a Multidisciplinary Approach." *Neuromuscular Disorders* 11 (3): 287–96. doi:10.1016/S0960-8966(00)00197-8.

Price, FD., J. von Maltzahn, CF. Bentzinger, NA. Dumont, H. Yin, NC. Chang, DH. Wilson, J. Frenette, and MA Rudnicki. 2014. "Inhibition of JAK-STAT Signaling Stimulates Adult Satellite Cell Function." *Nature Medicine* 20 (10): 1174–81. doi:10.1038/nm.3655.

Rajakumar, D., M. Alexander, and A. Oommen. 2013. "Oxidative Stress, NF-kB and the Ubiquitin Proteasomal Pathway in the Pathology of Calpainopathy." *Neurochemical Research* 38 (10): 2009–18. doi:10.1007/s11064-013-1107-z.

Randolph, ME., and GK. Pavlath. 2015. "A Muscle Stem Cell for Every Muscle: Variability of Satellite Cell Biology among Different Muscle Groups." *Frontiers in Aging Neuroscience* 7 (OCT): 1–14. doi:10.3389/fnagi.2015.00190.

Ravulapalli, R., B. García-Diaz, RL. Campbell, and PL. Davies. 2005. "Homodimerization of Calpain 3 Penta-EF-Hand Domain." *The Biochemical Journal* 388 (Pt 2): 585–91. doi:10.1042/BJ20041821.

Raya, A., I. Rodríguez-pizà, G. Guenechea, R. Vassena, MJ. Barrero, A. Consiglio, M. Castellà, et al. 2009. "Disease-Corrected Haematopoietic Progenitors from Fanconi Anaemia Induced Pluripotent Stem Cells Ángel" 460 (7251): 53–59. doi:10.1038/nature08129.Disease-corrected.

Relaix, F., D. Montarras, S. Zaffran, B. Gayraud-Morel, D. Rocancourt, S. Tajbakhsh, A. Mansouri, A. Cumano, and M. Buckingham. 2006. "Pax3 and Pax7 Have Distinct and Overlapping Functions in Adult Muscle Progenitor Cells." *Journal of Cell Biology* 172 (1): 91–102. doi:10.1083/jcb.200508044.

Relaix, F., D. Rocancourt, A. Mansouri, and M. Buckingham. 2004. "Divergent Functions of Murine Pax3 and Pax7 in Limb Muscle Development." *Genes and Development* 18 (9): 1088–1105. doi:10.1101/gad.301004.

Relaix, F., D. Rocancourt, A. Mansouri, and M. Buckingham. 2005. "A Pax3/Pax7-Dependent Population of Skeletal Muscle Progenitor Cells." *Nature* 435 (7044): 948–53. doi:10.1038/nature03594.

Richard, I., L. Brenguier, P. Dincer, C. Roudaut, B. Bady, JM. Burgunder, R. Chemaly, et al. 1997. "Multiple Independent Molecular Etiology for Limb-Girdle Muscular Dystrophy Type 2A Patients from Various Geographical Origins." *Am J Hum Genet* 60 (5): 1128–38. http://www.ncbi.nlm.nih.gov/entrez/query.fcgi?cmd=Retrieve&db=PubMed&dopt=Citation&list_uids=9150160.

Richard, I., O. Broux, V. Allamand, F. Fougerousse, N. Chiannilkulchai, N. Bourg, L. Brenguier, et al. 1995. "Mutations in the Proteolytic Enzyme Calpain 3 Cause Limb-Girdle Muscular Dystrophy Type 2A." *Cell* 81 (1): 27–40. doi:10.1016/0092-8674(95)90368-2.

Richard, I., JY. Hogrel, D. Stockholm, and CAM. Payan. 2016. "Natural History of LGMD2A for Delineating Outcome Measures in Clinical Trials." *Annals of Clinical and Translational Neurology*, 1–18. doi:10.1002/acn3.287.

Richard, I., C. Roudaut, S. Marchand, S. Baghdiguian, M. Herasse, D. Stockholm, Y. Ono, et al. 2000a. "Loss of Calpain 3 Proteolytic Activity Leads to Muscular Dystrophy and to

Apoptosis-Associated IkBa/nuclear Factor kB Pathway Perturbation in Mice." *Journal of Cell Biology* 151 (7): 1583–90. doi:10.1083/jcb.151.7.1583.

Rodgers, JT., KY. King, JO. Brett, MJ. Cromie, GW. Charville, KK. Maguire, C. Brunson, et al. 2014. "mTORC1 Controls the Adaptive Transition of Quiescent Stem Cells from G0 to G(Alert)." *Nature* 509 (7505). Nature Publishing Group: 393–96. doi:10.1038/nature13255.

Roperto, S., R. De Tullio, C. Raso, R. Stifanese, V. Russo, M. Gaspari, G. Borzacchiello, et al. 2010. "Calpain3 Is Expressed in a Proteolitically Active Form in Papillomavirus-Associated Urothelial Tumors of the Urinary Bladder in Cattle." *PLoS ONE* 5 (4): 1–9. doi:10.1371/journal.pone.0010299.

Rosales, XQ., V. Malik, A. Sneh, L. Chen, S. Lewis, J. Kota, JM. Gastier-Foster, et al. 2013. "Impaired Regeneration in LGMD2A Supported by Increased PAX7-Positive Satellite Cell Content and Muscle-Specific Microrna Dysregulation." *Muscle and Nerve* 47 (5): 731–39. doi:10.1002/mus.23669.

Ross, and Pawlina. 2013. *Histología. Texto Y Atlas En Color Con Biología Celular Y Molecular.* 4th ed. Editorial Médica Panamericana.

Roudaut, C., F. Le Roy, L. Suel, J. Poupiot, K. Charton, M. Bartoli, and I. Richard. 2013. "Restriction of calpain3 Expression to the Skeletal Muscle Prevents Cardiac Toxicity and Corrects Pathology in a Murine Model of Limb-Girdle Muscular Dystrophy." *Circulation* 128 (10): 1094–1104. doi:10.1161/CIRCULATIONAHA.113.001340.

Rudnicki, MA., PNJ. Schnegelsberg, RH. Stead, T. Braun, HH. Arnold, and R. Jaenisch. 1993. "MyoD or Myf-5 Is Required for the Formation of Skeletal Muscle." *Cell* 75 (7): 1351–59. doi:10.1016/0092-8674(93)90621-V.

Ruiz, S., D. Diep, A. Gore, AD. Panopoulos, N. Montserrat, N. Plongthongkum, S. Kumar, et al. 2012. "Identification of a Specific Reprogramming-Associated Epigenetic Signature in Human Induced Pluripotent Stem Cells." *Proc Natl Acad Sci U S A* 109 (40): 16196–201. doi:10.1073/pnas.1202352109/-/DCSupplemental.www.pnas.org/cgi/doi/10.1073/pnas.120 2352109.

Sacco, A., R. Doyonnas, P. Kraft, S. Vitorovic, and HM. Blau. 2008. "Self-Renewal and Expansion of Single Transplanted Muscle Stem Cells." *Nature* 456 (7221): 502–6. doi:10.1038/nature07384.

Sacco, A., F. Mourkioti, R. Tran, J. Choi, M. Llewellyn, P. Kraft, M. Shkreli, et al. 2010. "Short Telomeres and Stem Cell Exhaustion Model Duchenne Muscular Dystrophy in mdx/mTR Mice." *Cell* 143 (7). Elsevier Inc.: 1059–71. doi:10.1016/j.cell.2010.11.039.

Sáenz, A., F. Leturcq, AM. Cobo, JJ. Poza, X. Ferrer, D. Otaegui, P. Camaño, et al. 2005. "LGMD2A: Genotype-Phenotype Correlations Based on a Large Mutational Survey on the Calpain 3 Gene." *Brain* 128 (4): 732–42. doi:10.1093/brain/awh408.

Sáenz, A., Y. Ono, H. Sorimachi, M. Goicoechea, F. Leturcq, L. Blázquez, F. García-Bragado, et al. 2011. "Does the Severity of the LGMD2A Phenotype in Compound Heterozygotes Depend on the Combination of Mutations?" *Muscle and Nerve* 44 (5): 710–14. doi:10.1002/mus.22194.

Sambasivan, R., B. Gayraud-Morel, G. Dumas, C. Cimper, S. Paisant, R. Kelly, and S. Tajbakhsh. 2009. "Distinct Regulatory Cascades Govern Extraocular and Pharyngeal Arch Muscle Progenitor Cell Fates." *Developmental Cell* 16 (6): 810–21. doi:10.1016/j.devcel.2009.05.008.

Sambasivan, R., and S. Tajbakhsh. 2007. “Skeletal Muscle Stem Cell Birth and Properties.” *Seminars in Cell and Developmental Biology* 18 (6): 870–82. doi:10.1016/j.semcdb.2007.09.013.

Sampaolesi, M., Y. Torrente, A. Innocenzi, R. Tonlorenzi, G. D’Antona, MA. Pellegrino, R. Barresi, et al. 2003. “Cell Therapy of -Sarcoglycan Null Dystrophic Mice Through Intra-Arterial Delivery of Mesoangioblasts.” *Science* 301 (5632): 487–92. doi:10.1126/science.1082254.

Sánchez-Danés, A., Y. Richaud-Patin, I. Carballo-Carbajal, S. Jiménez-Delgado, C. Caig, S. Mora, C. Di Guglielmo, et al. 2012. “Disease-Specific Phenotypes in Dopamine Neurons from Human iPS-Based Models of Genetic and Sporadic Parkinson’s Disease.” *EMBO Molecular Medicine* 4 (5): 380–95. doi:10.1002/emmm.201200215.

Sardo, V. Lo, W. Ferguson, GA. Erikson, EJ. Topol, KK. Baldwin, and A. Torkamani. 2016. “Influence of Donor Age on Induced Pluripotent Stem Cells.” *Nature Biotechnology* 35 (1). Nature Publishing Group: 69–74. doi:10.1038/nbt.3749.

Schmalbruch, H., and U. Hellhammer. 1977. “The Number of Nuclei in Adult Rat Muscles with Special Reference to Satellite Cells.” *The Anatomical Record* 189 (2): 169–75. doi:10.1002/ar.1091890204.

Scott, W., J. Stevens, and S. Binder-Macleod. 2001. “Human Skeletal Muscle Fiber Type Classifications.” *Physical Therapy* 81 (11): 1810–16. doi:10.1139/h97-020.

Seale, P., LA. Sabourin, A. Girgis-Gabardo, A. Mansouri, P. Gruss, and MA. Rudnicki. 2000. “Pax7 Is Required for the Specification of Myogenic Satellite Cells Skeletal Muscle Are Mitotically Quiescent and Are Acti- Vated in Response to Diverse Stimuli, Including Stretch- Ing, Exercise, Injury, and Electrical Stimulation (Schultz.” *Cell* 102: 777–86. doi:10.1016/S0092-8674(00)00066-0.

Servián-Morilla, E., H. Takeuchi, TV. Lee, J. Clarimon, F. Mavillard, E. Area-Gómez, E. Rivas, et al. 2016. “A POGLUT1 Mutation Causes a Muscular Dystrophy with Reduced Notch Signaling and Satellite Cell Loss.” *EMBO Molecular Medicine* 8 (11): 1289–1309. doi:10.15252/emmm.201505815.

Shefer, G., DP. Van de Mark, JB. Richardson, and Z. Yablonka-Reuveni. 2006. “Satellite-Cell Pool Size Does Matter: Defining the Myogenic Potency of Aging Skeletal Muscle.” *Developmental Biology* 294 (1): 50–66. doi:10.1016/j.ydbio.2006.02.022.

Shelton, M., J. Metz, J. Liu, R. Carpenedo, SP. Demers, WL. Stanford, and IS. Skerjanc. 2014. “Derivation and Expansion of PAX7-Positive Muscle Progenitors from Human and Mouse Embryonic Stem Cells.” *Stem Cell Reports* 3 (3). The Authors: 516–29. doi:10.1016/j.stemcr.2014.07.001.

Sherwood, RI., JL. Christensen, IM. Conboy, MJ Conboy, TA Rando, IL. Weissman, and AJ Wagers. 2004. “Isolation of Adult Mouse Myogenic Progenitors: Functional Heterogeneity of Cells within and Engrafting Skeletal Muscle.” *Cell* 119 (4): 543–54. doi:10.1016/j.cell.2004.10.021.

Shipony, Z., Z. Mukamel, NM. Cohen, G. Landan, E. Chomsky, SR. Zeliger, YC. Fried, E. Ainbinder, N. Friedman, and A. Tanay. 2014. “Dynamic and Static Maintenance of Epigenetic Memory in Pluripotent and Somatic Cells.” *Nature* 513 (7516). Nature Publishing Group: 115–19. doi:10.1038/nature13458.

Shoji, E., K. Woltjen, and H. Sakurai. 2015. “Directed Myogenic Differentiation of Human Induced Pluripotent Stem Cells.” *Methods in Molecular Biology*. doi:10.1007/7651.

Shoshan-Barmatz, V., S. Weil, H. Meyer, M. Varsanyi, and LMG. Heilmeyer. 1994. "Endogenous, Ca2+-Dependent Cysteine-Protease Cleaves Specifically the Ryanodine receptor/Ca2+ Release Channel in Skeletal Muscle." *The Journal of Membrane Biology* 142 (3): 281–88. doi:10.1007/BF00233435.

Si-Tayeb, K., FK. Noto, M. Nagaoka, J. Li, MA. Battle, C. Duris, PE. North, S. Dalton, and SA. Duncan. 2010. "Highly Efficient Generation of Human Hepatocyte-like Cells from Induced Pluripotent Stem Cells." *Hepatology* 51 (1): 297–305. doi:10.1002/hep.23354.

Siciliano, G., C. Simoncini, S. Giannotti, V. Zampa, C. Angelini, and G. Ricci. 2015. "Muscle Exercise in Limb Girdle Muscular Dystrophies: Pitfall and Advantages." *Acta Myologica* 34 (1): 3–8.

Sol, A. Del, and NJ. Buckley. 2014. "P LURIPOTENT S TEM C ELLS Concise Review : A Population Shift View of Cellular Reprogramming," 1367–72.

Sorimachi, H., S. Imajoh-Ohmi, Y. Emori, H. Kawasaki, S. Ohno, Y. Minamio, and K. Suzuki. 1989. "Molecular Cloning of a Novel Mammalian Calcium-Dependent Protease Distinct from Both M-and U-Types." *The Journal of Biological Chemistry* 264 (33): 20106–11. http://www.jbc.org/content/264/33/20106.long.

Sorimachi, H., K. Kinbara, S. Kimura, M. Takahashi, S. Ishiura, N. Sasagawa, N. Sorimachi, et al. 1995. "Muscle-Specific Calpain, p94, Responsible for Limb Girdle Muscular Dystrophy Type 2A, Associates with Connectin through IS2, a p94-Specific Sequence." *Journal of Biological Chemistry* 270 (52): 31158–62. doi:10.1074/jbc.270.52.31158.

Sorimachi, H., N. Toyama-Sorimachi, TC. Saido, H. Kawasaki, H. Sugita, M. Miyasaka, KI. Arahata, S. Ishiura, and K. Suzuki. 1993. "Muscle-Specific Calpain, p94, Is Degraded by Autolysis Immediately after Translation, Resulting in Disappearance from Muscle." *Journal of Biological Chemistry* 268 (14): 10593–605.

Sousa-Victor, P., S. Gutarra, L. García-Prat, J. Rodriguez-Ubreva, L. Ortet, V. Ruiz-Bonilla, M. Jardí, et al. 2014. "Geriatric Muscle Stem Cells Switch Reversible Quiescence into Senescence." *Nature* 506 (7488): 316–21. doi:10.1038/nature13013.

Spencer, MJ., JR. Guyon, H. Sorimachi, A. Potts, I. Richard, M. Herasse, J. Chamberlain, I. Dalkilic, LM. Kunkel, and JS. Beckmann. 2002. "Stable Expression of Calpain 3 from a Muscle Transgene in Vivo: Immature Muscle in Transgenic Mice Suggests a Role for Calpain 3 in Muscle Maturation." *Proceedings of the National Academy of Sciences of the United States of America* 99 (13): 8874–79. doi:10.1073/pnas.132269299.

Starling, A., F. De Paula, H. Silva, M. Vainzof, and M. Zatz. 2003. "Calpainopathy How Broad Is the Spectrum of Clinical Variability? Alessandra." *Journal of Molecular Neuroscience* 21: 233–36.

Stuelsatz, P., F. Pouzoulet, Y. Lamarre, E. Dargelos, S. Poussard, S. Leibovitch, P. Cottin, and P. Veschambre. 2010. "Down-Regulation of MyoD by Calpain 3 Promotes Generation of Reserve Cells in C2C12 Myoblasts." *Journal of Biological Chemistry* 285 (17): 12670–83. doi:10.1074/jbc.M109.063966.

Swartz, EW., J. Baek, M. Pribadi, KJ. Wojta, S. Almeida, A. Karydas, F. Gao, BL. Miller, and G. Coppola. 2016. "A Novel Protocol for Directed Differentiation of C9orf72-Associated Human Induced Pluripotent Stem Cells Into Contractile Skeletal Myotubes." *STEM CELLS Translational Medicine* 5 (11): 1461–72. doi:10.5966/sctm.2015-0340.

Świerczek, B., M.A. Ciemerych, and K. Archacka. 2015. "From Pluripotency to Myogenesis: A Multistep Process in the Dish." *Journal of Muscle Research and Cell Motility* 36 (6): 363–

75. doi:10.1007/s10974-015-9436-y.

Tagawa, K., C. Taya, Y. Hayashi, M. Nakagawa, Y. Ono, R. Fukuda, H. Karasuyama, et al. 2000. "Myopathy Phenotype of Transgenic Mice Expressing Active Site-Mutated Inactive p94 Skeletal Muscle- Specific Calpain, the Gene Product Responsible for Limb Girdle Muscular Dystrophy Type 2A." *Human Molecular Genetics* 9 (9): 1393–1402.

Tajbakhsh, S. 2009. "Skeletal Muscle Stem Cells in Developmental versus Regenerative Myogenesis." *Journal of Internal Medicine* 266 (4): 372–89. doi:10.1111/j.1365-2796.2009.02158.x.

Takahashi, K., K. Tanabe, M. Ohnuki, M. Narita, T. Ichisaka, K. Tomoda, and S. Yamanaka. 2007. "Induction of Pluripotent Stem Cells from Adult Human Fibroblasts by Defined Factors." *Cell* 131 (5): 861–72. doi:10.1016/j.cell.2007.11.019.

Takahashi, K., and S. Yamanaka. 2006. "Induction of Pluripotent Stem Cells from Mouse Embryonic and Adult Fibroblast Cultures by Defined Factors." *Cell* 126 (4): 663–76. doi:10.1016/j.cell.2006.07.024.

Takashima, Y., G. Guo, R. Loos, J. Nichols, G. Ficz, F. Krueger, D. Oxley, et al. 2014. "Erratum: Resetting Transcription Factor Control Circuitry toward Ground-State Pluripotency in Human *Cell* 2014, 158 (1254-1269)." doi:10.1016/j.cell.2014.08.029.

Tanaka, A., K. Woltjen, K. Miyake, A. Hotta, M. Ikeya, T. Yamamoto, T. Nishino, et al. 2013. "Efficient and Reproducible Myogenic Differentiation from Human iPS Cells: Prospects for Modeling Miyoshi Myopathy In Vitro." *PLoS ONE* 8 (4). doi:10.1371/journal.pone.0061540.

Tao, T., H. Shi, Y. Guan, D. Huang, Y. Chen, DP. Lane, J. Chen, and J. Peng. 2013. "Def Defines a Conserved Nucleolar Pathway That Leads p53 to Proteasome-Independent Degradation." *Cell Research* 23 (5). Nature Publishing Group: 620–34. doi:10.1038/cr.2013.16.

Tatsumi, R., JE. Anderson, CJ. Nevoret, O. Halevy, and RE. Allen. 1998. "HGF/SF Is Present in Normal Adult Skeletal Muscle and Is Capable of Activating Satellite Cells." *Developmental Biology* 194 (1): 114–28. doi:10.1006/dbio.1997.8803.

Taveau, M., N. Bourg, G. Sillon, C. Roudaut, M. Bartoli, and I. Richard. 2003. "Calpain 3 Is Activated through Autolysis within the Active Site and Lyses Sarcomeric and Sarcolemmal Components." *Molecular and Cellular Biology* 23 (24): 9127–35. doi:10.1128/MCB.23.24.9127-9135.2003.

Tedesco, F. S., M. F. M. Gerli, L. Perani, S. Benedetti, F. Ungaro, M. Cassano, S. Antonini, et al. 2012. "Transplantation of Genetically Corrected Human iPSC-Derived Progenitors in Mice with Limb-Girdle Muscular Dystrophy." *Science Translational Medicine* 4 (140): 140ra89-140ra89. doi:10.1126/scitranslmed.3003541.

Tedesco, FS., A. Dellavalle, J. Diaz-manera, G. Messina, and G. Cossu. 2010. "Review Series Repairing Skeletal Muscle : Regenerative Potential of Skeletal Muscle Stem Cells." *Journal of Clinical Investigation* 120 (1): 11–19. doi:10.1172/JCI40373.and.

Theunissen, TW., M. Friedli, Y. He, E. Planet, RC. O'Neil, S. Markoulaki, J. Pontis, et al. 2016. "Molecular Criteria for Defining the Naive Human Pluripotent State." *Cell Stem Cell* 19 (4): 502–15. doi:10.1016/j.stem.2016.06.011.

Theunissen, TW., BE. Powell, H. Wang, M. Mitalipova, DA. Faddah, J. Reddy, ZP. Fan, et al. 2014. "Systematic Identification of Culture Conditions for Induction and Maintenance of Naive Human Pluripotency." *Cell Stem Cell* 15 (4). The Authors: 471–87. doi:10.1016/j.stem.2014.07.002.

Thornell, LE., M. Lindstöm, V. Renault, A. Klein, V. Mouly, T. Ansved, G. Butler-Browne, and D. Furling. 2009. “Satellite Cell Dysfunction Contributes to the Progressive Muscle Atrophy in Myotonic Dystrophy Type 1.” *Neuropathology and Applied Neurobiology* 35 (6): 603–13. doi:10.1111/j.1365-2990.2009.01014.x.

Tierney, MT, T. Aydogdu, D. Sala, B. Malecova, S. Gatto, PL. Puri, L. Latella, and A. Sacco. 2014. “STAT3 Signaling Controls Satellite Cell Expansion and Skeletal Muscle Repair.” *Nature Medicine* 20 (10): 1182–86. doi:10.1038/nm.3656.

Topaloglu, H., P. Dincer, I. Richard, Z. Akcoren, D. Alehan, S. Ozme, M. Caglar, A. Karaduman, JA. Urtizberea, and J S Beckmann. 1997. “Calpain-3 Deficiency Causes a Mild Muscular Dystrophy in Childhood.” *Neuropediatrics* 28 (4): 212–16.

Toral-Ojeda, I., G. Aldanondo, J. Lasa-Elgarresta, H. Lasa-Fernandez, R. Fernandez-Torron, A. Lopez de Munain, and A. Vallejo-Illarramendi. 2016. “Calpain 3 Deficiency Affects SERCA Expression and Function in the Skeletal Muscle.” *Expert Reviews in Molecular Medicine* 18: e7. doi:10.1017/erm.2016.9.

Torrent, R., F. De, A. Rigotti, P. Dell ’era, M. Memo, A. Raya, and A. Consiglio. 2015. “Using iPS Cells toward the Understanding of Parkinson’s Disease.” *J. Clin. Med* 4: 548–66. doi:10.3390/jcm4040548.

Torrente, Y., M. Belicchi, M. Sampaolesi, F. Pisati, M. Meregalli, G. D’Antona, R. Tonlorenzi, et al. 2004. “Human Circulating AC133+ Stem Cells Restore Dystrophin Expression and Ameliorate Function in Dystrophic Skeletal Muscle.” *Journal of Clinical Investigation* 114 (2): 182–95. doi:10.1172/JCI200420325.

Trokovic, R., J. Weltner, P. Noisa, T. Raivio, and T. Otonkoski. 2015. “Combined Negative Effect of Donor Age and Time in Culture on the Reprogramming Efficiency into Induced Pluripotent Stem Cells.” *Stem Cell Research* 15 (1). The Authors: 254–62. doi:10.1016/j.scr.2015.06.001.

Ueki, J., M. Nakamori, M. Nakamura, M. Nishikawa, Y. Yoshida, A. Tanaka, A. Morizane, et al. 2017. “Myotonic Dystrophy Type 1 Patient-Derived iPSCs for the Investigation of CTG Repeat Instability.” *Scientific Reports* 7: 42522. doi:10.1038/srep42522.

Urtasun, M., A. Sáenz, C. Roudaut, JJ. Poza, JA. Urtizberea, AM. Cobo, I. Richard, et al. 1998. “Limb-Girdle Muscular Dystrophy in Guipúzcoa (Basque Country, Spain).” *Brain* 121: 1735–47. http://www.ncbi.nlm.nih.gov/pubmed/9762961.

Vallejo-Illarramendi, A., I. Toral-Ojeda, G. Aldanondo, and A. López de Munain. 2014. “Dysregulation of Calcium Homeostasis in Muscular Dystrophies.” *Expert Reviews in Molecular Medicine* 16 (October): e16. doi:10.1017/erm.2014.17.

Velden, JLJ. van der, RCJ. Langen, MCJM. Kelders, J. Willems, EFM Wouters, YMW Janssen-Heininger, and AM Schols. 2007. “Myogenic Differentiation during Regrowth of Atrophied Skeletal Muscle Is Associated with Inactivation of GSK-3beta.” *American Journal of Physiology. Cell Physiology* 292 (5): C1636-44. doi:10.1152/ajpcell.00504.2006.

Verburg, E., RM. Murphy, I. Richard, and GD. Lamb. 2009. “Involvement of Calpains in Ca 2 ε - Induced Disruption of Excitation-Contraction Coupling in Mammalian Skeletal Muscle Fibers.” *Am J Physiol Cell Physiol 296:*, no. 31: 1115–22. doi:10.1152/ajpcell.00008.2009.

Verdijk, LB., T. Snijders, M. Drost, T. Delhaas, F. Kadi, and LJC. Van Loon. 2014. “Satellite Cells in Human Skeletal Muscle; From Birth to Old Age.” *Age* 36 (2): 545–57. doi:10.1007/s11357-013-9583-2.

Vieira, NM., I. Elvers, MS. Alexander, YB. Moreira, A. Eran, JP. Gomes, JL. Marshall, et al. 2015. "Jagged 1 Rescues the Duchenne Muscular Dystrophy Phenotype." *Cell* 163 (5). Elsevier Ltd: 1204–13. doi:10.1016/j.cell.2015.10.049.

Vissing, J., R. Barresi, N. Witting, M. Van Ghelue, L. Gammelgaard, LA. Bindoff, V. Straub, et al. 2016. "A Heterozygous 21-Bp Deletion in CAPN3 Causes Dominantly Inherited Limb Girdle Muscular Dystrophy." *Brain* 139 (8): 2154–63. doi:10.1093/brain/aww133.

Volonte, D., AJ. Peoples, and F. Galbiati. 2003. "Modulation of Myoblast Fusion by Caveolin-3 in Dystrophic Skeletal Muscle Cells: Implications for Duchenne Muscular Dystrophy and Limb-Girdle Muscular Dystrophy-1C." *Molecular Biology of the Cell* 14 (October): 4075–88. doi:10.1091/mbc.E03.

Walton, John. 1981. *Disorders of Voluntary Muscle*. Edited by Churchill Livingstone. 4th ed.

Webster, C., and HM. Blau. 1990. "Accelerated Age-Related Decline in Replicative Life-Span of Duchenne Muscular Dystrophy Myoblasts: Implications for Cell and Gene Therapy." *Somatic Cell and Molecular Genetics* 16 (6): 557–65. doi:10.1007/BF01233096.

Welm, AL., NA. Timchenko, Y. Ono, H. Sorimachi, HS. Radomska, DG. Tenen, J. Lekstrom-Himes, and GJ. Darlington. 2002. "C/EBPalpha Is Required for Proteolytic Cleavage of Cyclin A by Calpain 3 in Myeloid Precursor Cells." *Journal of Biological Chemistry* 277 (37): 33848–56. doi:10.1074/jbc.M204096200.

Wen, Y., P. Bi, W. Liu, A. Asakura, C. Keller, and S. Kuang. 2012. "Constitutive Notch Activation Upregulates Pax7 and Promotes the Self-Renewal of Skeletal Muscle Satellite Cells." *Molecular and Cellular Biology* 32 (12): 2300–2311. doi:10.1128/MCB.06753-11.

Westerblad, H., JD. Bruton, and A. Katz. 2010. "Skeletal Muscle: Energy Metabolism, Fiber Types, Fatigue and Adaptability." *Experimental Cell Research* 316 (18). Elsevier Inc.: 3093–99. doi:10.1016/j.yexcr.2010.05.019.

Xu, C., M. Tabebordbar, S. Iovino, C. Ciarlo, J. Liu, A. Castiglioni, E. Price, et al. 2013. "XA Zebrafish Embryo Culture System Defines Factors That Promote Vertebrate Myogenesis across Species." *Cell* 155 (4). Elsevier: 909–21. doi:10.1016/j.cell.2013.10.023.

Yasuno, T., K. Osafune, H. Sakurai, I. Asaka, A. Tanaka, S. Yamaguchi, K. Yamada, et al. 2014. "Functional Analysis of iPSC-Derived Myocytes from a Patient with Carnitine Palmitoyltransferase II Deficiency." *Biochemical and Biophysical Research Communications* 448 (2). Elsevier Inc.: 175–81. doi:10.1016/j.bbrc.2014.04.084.

Yeo, S., S. Jeong, J. Kim, JS. Han, YM. Han, and YK. Kang. 2007. "Characterization of DNA Methylation Change in Stem Cell Marker Genes during Differentiation of Human Embryonic Stem Cells." *Biochemical and Biophysical Research Communications* 359 (3): 536–42. doi:10.1016/j.bbrc.2007.05.120.

Yoon, S., G. Stadler, ML. Beermann, EV. Schmidt, JA. Windelborn, P. Schneiderat, WE. Wright, and JB. Miller. 2013. "Immortalized Myogenic Cells from Congenital Muscular Dystrophy type1A Patients Recapitulate Aberrant Caspase Activation in Pathogenesis: A New Tool for MDC1A Research." *Skeletal Muscle* 3 (1): 28. doi:10.1186/2044-5040-3-28.

Zatz, M., and A. Starling. 2005. "Calpains and Disease." *N Engl J Med* 35223352: 2413–23. doi:10.1056/NEJMra043361.

Zatz, M., M. Vainzof, and MR. Passos-Bueno. 2000. "Limb-Girdle Muscular Dystrophy: One Gene with Different Phenotypes, One Phenotype with Different Genes." *Current Opinion in Neurology* 13: 511–17. doi:10.1097/00019052-200010000-00002.

Zhang, WY, PE de Almeida, and JC Wu. 2012. "Teratoma Formation: A Tool for Monitoring Pluripotency in Stem Cell Research". Cambridge (MA): Harvard Stem Cell Institute.

Zhao, XY., W. Li, Z. Lv, L. Liu, M. Tong, T. Hai, J. Hao, et al. 2009. “iPS Cells Produce Viable Mice through Tetraploid Complementation.” *Nature* 461 (7260). Nature Publishing Group: 86–90. doi:10.1038/nature08267.

Zheng, B., B. Cao, M. Crisan, B. Sun, G. Li, A. Logar, S. Yap, et al. 2007. “Prospective Identification of Myogenic Endothelial Cells in Human Skeletal Muscle.” *Nature Biotechnology* 25 (9): 1025–34. doi:10.1038/nbt1334.